DISCOVERY AND INVESTIGATION OF NOVEL RADIOSENSITISING GENES

Gaganpreet Singh Tiwana

Cancer Research UK and Medical Research Council Oxford

Institute for Radiation Oncology

and

Linacre College

A thesis submitted for the degree of Doctor of Philosophy in

the University of Oxford, Hilary term, 2015

ABSTRACT

Gaganpreet Tiwana, Linacre College

Submitted for the degree of D.Phil. at the University of Oxford, Hilary Term, 2015

Radiotherapy is second only to surgery in the curative management of patients with cancer, and yet the molecular mechanisms that determine the sensitivity of tumours to radiation remain largely unclear. A high-throughput radiosensitivity screening method based on clonogenicity was developed and a siRNA library against kinase targets was screened. The gold standard colony formation endpoint was chosen for determining reproductive cell death after radiation treatment, since effects on proliferation often do not reflect survival.

Thiamine pyrophosphokinase-1 (TPK1), a key component of Vitamin B1/thiamine metabolism, was identified as a target for radiosensitisation. TPK1 knockdown caused significant radiosensitisation in cancer but not normal tissue cell lines. Other means of blocking this pathway such as knockdown of thiamine transporter-1 (THTR1) or treatment with the thiamine analogue pyrithiamine hydrobromide (PyrH) caused significant tumour specific radiosensitisation. There was persistent DNA damage in cells irradiated after TPK1 and THTR1 knockdown or PyrH treatment. Thus this screen allowed the identification of thiamine metabolism as a novel radiosensitisation target that affects DNA repair. Short-term modulation of thiamine metabolism could be a clinically exploitable strategy to achieve tumour specific radiosensitisation.

Three additional genes, signal recognition particle-72 kDa (SRP72), glycogen synthase 3-beta (GSK3β) and MAP/Microtubule Affinity-Regulating Kinase 2 (MARK2) were also investigated. Knockdown of these genes radiosensitised both tumour and normal tissue cell lines and expression of two of them, GSK3β and SRP72 were found to be associated with poor recurrence-free survival in early breast cancer patients.

AKNOWLEDGEMENTS

First and foremost I would like to thank my supervisors, Dr Geoff Higgins and Professor Gillies McKenna, for giving me the opportunity to carry out the D.Phil in their laboratory and for their continued support, encouragement and advice throughout the past four years. I must give a special thank you to our lab manager, Remko Prevo. Without his support and guidance, this thesis and its contents would have not been realised. His knowledge and expertise are unprecedented and I am lucky to have been guided by such an exceptional individual.

I would like to thank everyone else in the McKenna lab, Tom, Giacomo, Jessica, Gonzalo, Lianne, and Martin. In addition, I would like to thank former lab members, Dorine and Patsy. I had a wonderful time working with you all and thank you for your support during my D.Phil. I would also like to thank other members of our department for their advice on methodologies, sample preparation and help with editing publications. In particular, Professor Ruth Muschel, Dr Francesca Buffa, Dr Sheng Yu, Dr Lisa Folkes, Daniel Ebner, Alison Howarth and Dr Vicenzo D'Angiolella.

I am very fortunate to have made many close friends in Oxford and would like especially thank Claire Mortimer, Rebecca Butler, Sami Jaffar and Michelle Taylor for their support and continuing friendship.

Finally, I would like to thank my parents and my brother for their support especially during the tough periods of the D.Phil. Without their help, I would not have been able to pursue an MSc at the University of Oxford which led to the D.Phil.

CONTENTS

ABSTRACT II

AKNOWLEDGEMENTS III

CONTENTS IV

ABBREVIATIONS AND ACRONYMS 1

CHAPTER 1 5

GENERAL INTRODUCTION 5

1.1 RADIOTHERAPY OVERVIEW 6

1.2 RADIOTHERAPY PHYSICS 7

1.3 TARGET OF IR: DNA 7

1.4 DNA-DAMAGE LESIONS 10

1.5 DOUBLE-STRAND BREAK REPAIR 11

1.5.1 NHEJ repair mechanism 11

1.5.1.1 Damage recognition, protein recruitment and DNA-bridging 11
1.5.1.2 DNA damage termini processing 12
1.5.1.3 Ligation 13

1.5.2 Homologous recombination 15

1.5.2.1 End resection 15
1.5.2.2 Single strand binding and nucleoprotein assembly 15
1.5.2.3 SDSA and DSBR 16

1.6 RADIOTHERAPY IN THE CLINIC 19

1.7 THERAPEUTIC WINDOW 20

1.8 HYPOXIA 22

1.9 INTRINSIC RADIOSENSITIVITY 24

1.10 MODULATING INTRINSIC RADIOSENSITIVITY 26

1.10.1 Chemoradiation 26

1.10.2 Molecular targeting 28

1.11 IDENTIFYING RADIOSENSITISERS 31

1.12 RNA INTERFERENCE (RNAI) 31

1.12.1 siRNA and miRNA targeted silencing 32

1.12.2 Off-target effects 34

1.13 HTS: ENDPOINTS 37

1.13.1 Evaluating cell death caused by IR 37

1.13.2 Surrogate markers and assays to evaluate RT 38

1.13.2.1 Cell proliferation assays 38
1.13.2.2 Micronuclei assay 39
1.13.2.3 DNA-damage foci quantification 39
1.13.2.4 Cell growth and survival assays 40
1.13.2.5 Colony formation assays 41
1.14 PROPOSED siRNA SCREEN 42
1.15 AIMS OF THESIS 43
CHAPTER 2 44
MATERIALS AND METHODS 44
2.1 CELL CULTURE 45
2.1.1 Cell line maintenance 45
2.1.2 Cell line storage and resuscitation 45
2.1.3 Passaging cell lines 46
2.1.4 Cell counting 46
2.2. CHEMICALS 46
2.3. HIGH-THROUGHPUT SCREENING 46
2.3.1 siRNA libraries 46
2.3.1.1 Primary screening library 46
2.3.1.2 Secondary screening libraries 47
2.3.2 96-well reverse transfection 47
2.3.2.1 siRNA plate preparation 47
2.3.2.2 Preparation of cell plates and cell lifting 48
2.3.2.3 siRNA complex formation and cell addition 48
2.3.2.4 Lifting and plating 49
2.3.3 Irradiation 50
2.3.4 Staining and counting 50
2.3.5 Screening statistical analyses 51
2.4 SIX-WELL siRNA TRANSFECTIONS 52
2.4.1 siRNA sequences 52
2.4.2 Reverse transfection protocol 52
2.4.3 Six-well colony formation assay 53
2.4.4 Statistical analysis for 6-well CFA 55
2.5 THIAMINE ANALOGUE TREATMENT 56
2.6 HPLC 56
2.7 SDS-PAGE AND IMMUNOBLOTTING 58
2.7.1 Buffers and reagents 58
2.7.2 Protein lysates preparation 59
2.7.3 Protein level quantification 59
2.7.4 SDS-Page 59
2.7.5 Immunoblotting 60
2.8 IMMUNOFLUORESCENCE 62
2.9 QUANTITATIVE REAL TIME PCR 63

2.9.1 Total RNA sample preparation 63
2.9.2 cDNA preparation 64
2.9.3 qRT-PCR 64
2.10 FACS 66
2.10.1 Cell cycle analysis by propidium iodide staining 66
2.10.2 Annexin-V/ Propidium iodide staining 66
2.11 CASPASE 3/7 ACTIVITY ASSAY 67
2.12 RESAZURIN ASSAY 67
2.13 STATISTICAL ANALYSIS 67
2.14 PROGNOSTIC ANALYSIS 68

CHAPTER 3 70

HIGH THROUGHPUT COLONY FORMATION ASSAY 70

3.1 INTRODUCTION 71
3.1.1 High-throughput colony formation assay 71
3.2 RESULTS 71
3.2.1 Cell line evaluation 71
3.1.1.1 Transfection optimisations 72
3.1.1.2 Optimising plating numbers and IR dose 74
3.1.2 Z-factor testing 79
3.1.3 Kinome screen 81
3.1.4 Secondary 'kinome' screen 83
3.2 DISCUSSION 87
3.2.1 Summary of findings 87
3.2.2 Limitations of the 96-well plate assay 87
3.2.1.1 HeLa cell line 87
3.2.1.2 Colony forming ability 88
3.2.1.3 Plating efficiencies 88
3.2.1.4 False negatives and positives 89
3.2.3 Future directions 90
3.2.3.1 Compound screening 90

CHAPTER 4 91

THIAMINE METABOLISM IS LINKED TO TUMOUR RADIORESISTANCE 91

4.1 INTRODUCTION 92
4.1.1 Thiamine metabolism 92
4.1.2 Thiamine metabolism in cancer 95
4.1.3 Thiamine metabolism and tumour radiosensitivity 99
4.2 RESULTS 101
4.2.1 TPK1 knockdown causes tumour specific radiosensitisation 101
4.2.2 Disrupting thiamine metabolism results in tumour specific radiosensitisation 104

4.2.3 Disrupting thiamine metabolism results in DNA-damage persistence 112
4.3 DISCUSSION 115
4.3.1 Radiosensitivity of TPK1 knockdown is linked to the pentose-phosphate pathway 115
4.3.2 Clinical feasibility of disrupting thiamine metabolism 117

CHAPTER 5 119

GSK3B, MARK2 AND SRP72 CANDIDATE GENE VALIDATION 119

5.1 INTRODUCTION 120
5.1.2 Glycogen synthase kinase- 3β (GSK-3β) 121
5.1.3 Signal recognition particle 72 kDa (SRP72) 123
5.1.4 MAP/Microtubule Affinity-Regulating Kinase 2 (MARK2) 124
5.2 RESULTS 126
5.2.1 GSK-3β, MARK2 and SRP72 are linked to tumour cell radioresistance 126
5.2.2 Knockdown of candidate genes radiosensitises normal tissue cell lines 133
5.2.3 Knockdown of GSK-3β, MARK2 and SRP72 potentiates radiation induced apoptosis 134
5.2.4 Prognostic significance of GSK3β and SRP72 expression in early breast cancer patients 138
5.3 DISCUSSION 140
5.3.1 GSK3β, MARK2 and SRP72 are linked to tumour cell radioresistance 140
5.3.2 Prognostic significance of candidate gene expression in early breast cancer patients 141
5.3.3 GSK3β, MARK2 and SRP72 expression suppresses radiation induced apoptosis 141

CHAPTER 6 143

GENERAL DISCUSSION 143

6.1 DISCUSSION 144
6.1.1 Summary of findings 144
6.1.2 Significance of findings 145
6.1.3 Concluding remarks 149

REFERENCES 150

APPENDIX 202

APPENDIX 1: SCREENING DATA TABLES 202
APPENDIX 2-MANUSCRIPT: IDENTIFICATION OF VITAMIN B1 METABOLISM AS A TUMOR-SPECIFIC RADIOSENSITIZING PATHWAY USING A HIGH-THROUGHPUT COLONY FORMATION SCREEN. 221

ABBREVIATIONS AND ACRONYMS

^{125}IUdR	iodine-125-iododeoxyuridine
3D-CRT	three-dimensional conformal radiotherapy
53BP1	p53-binding protein 1
6-PGCA	6-Phosphogluconic acid
6PGDH	6-phosphogluconate dehydrogenase
Ab	antibody
AKT	protein kinase B
APC	adenomatous polyposis coli
APLF	aprataxin- and PNK-like factor
Argo2	argonaute-2
ATCC	American Type Culture Collection
AThTP	adenosine thiamine triphosphate
ATM	ataxia telangiectasia mutated
ATP	adenosine triphosphate
ATR	ataxia telangiectasia and Rad3-related protein
BCA	bicinchoninic acid assay
BCAA	branched chain amino acid
BCKDC	branched chained α-keto acid dehydrogenase complex
bp	base pair
BRCA2	breast cancer susceptibility gene 2
BrdU	bromodeoxyuridine
BSA	bovine serum albumin
C.elegans	*Caenorhabditis elegans*
cDNA	complementary DNA
CFA	colony formation assay
CHEK1	checkpoint kinase 1
CHEK2	checkpoint kinase 2
CTIP	C-terminal binding protein interacting protein
dATP	deoxyadenosine triphosphate
dCTP	deoxycytidine triphosphate
DDR	DNA-damage response
dGTP	deoxyguanosine triphosphate
DMEM	Dulbecco's modified Eagle's medium
DMSO	dimethyl sulfoxide
DNA	deoxyribonucleic acid
DNA-PK*cs*	DNA-dependent protein kinase catalytic subunit
dNTP	deoxynucleoside triphosphate
DR4	death receptor 4
DR5	death receptor 5
drosophila	*drosophila melanogaster*
DSB	double strand break

DSBR	DSB repair
dsRNA	double stranded RNA
DTT	dithiothrietol
dTTP	deoxythymidine triphosphate
E4P	erythrose-4-phosphate
ECL	enhanced chemiluminescence
EDTA	ethylenediaminetetraacetic acid
EGFR	epidermal growth factor receptor
ER	endoplasmic reticulum
esiRNA	endoribonuclease-prepared short interfering RNAs
FACS	fluorescence activated cell sorting
FBS	fetal bovine serum
Fig	figure
Freon	1, 1, 2 trichlorotrifluorethane
G6P	glucose-6-phosphate
GEO	Gene Expression Omnibus
GPCR	G-coupled protein receptors
GSH	glutathione
GSK3β	glycogen synthase kinase 3 beta
GTP	guanosine triphosphate
h	hour
h.pylori	*helicobacter pylori*
HNSCC	head and neck squamous cell carcinoma
HPLC	high performance liquid chromatography
HR	homologous recombination
HRP	horseradish peroxidase
HTS	high-throughput screening
IMRT	intensity modulated radiotherapy
IR	Irradiation
kb	kilobase
kDa	kiloDalton
LEF	lymphoid enhancer factor
LET	linear energy transfer
MARK2	MAP/microtubule affinity-regulating kinase 2
MC	mitotic catastrophe
min	minute
mi-RNA	micro-RNA
miRNP	miRNA ribonucleoprotein complexes
MRI	magnetic resonance imaging
MRN	MRE11/RAD50/NSB1
mRNA	messenger ribonuleic acid
mTOR	mammalian target of rapamycin
MTT	3-(4,5-Dimethylthiazol-2-yl)-2,5-diphenyl tetrazolium bromide
NADPH	nicotinamide adenine dinucleotide phosphate
NCI	National Cancer Institute

ng	nanogram
NHEJ	non-homologous end joining
NSCLC	non-small-cell lung carcinoma
NT	non-targeting
nt	nucleotide
NTCP	normal tissue complication probabilities
OER	oxygen enhancement ratio
PAI	pathogenicity island
PARP	poly (ADP-ribose) polymerase
PBS	phosphate buffered saline
PCR	polymerase chain reaction
PDH	pyruvate dehydrogenase
PE	plating efficiency
Pen	penicillin
PET	positron emission tomography
PFA	paraformaldehyde
PFP	percentage of false positives
PI	propidium iodide
PI3K	phosphoinositide 3-kinase
PINK1	PTEN-induced kinase 1
PLK-1	polo-like kinase-1
PNKP	polynucleotide kinase phosphatase
PPP	pentose-phosphate pathway
PRB	protein running buffer
PTEN	phosphatase and tensin homolog
PyrH	pyrithiamine hydrobromide
R5-P	ribulose-5-phosphate
RER	rough endoplasmic reticulum
RFS	recurrence-free survival
RIPA	radioimmunoprecipitation assay
RISC	RNA-Induced Silencing Complex
RLC	RISC-loading complex
RNA	ribonucleic acid
RNAi	RNA interference
RNC	ribosome nascent chain complex
RO	reverse osmosis
ROS	reactive oxygen species
RPA	replication protein A
Rpi	ribose-5-phosphate isomerise
rpm	revolutions per minute
RPMI	Roswell Park Memorial Institute
R-score	radiosensitivity scores
RT	radiotherapy treatment
RT-PCR	reverse transcriptase PCR
Ru5P	ribulose-5-phosphate
S7P	sedoheptulose-7-phosphate

sd	standard deviation
SDS	sodium dodecyl sulfate
SDS PAGE	sodium dodecyl sulfate polyacrylamide gel electrophoresis
SDSA	synthesis dependent strand annealing
SER_{10}	survival enhancement ratio at 0.10 surviving fraction
SF	surviving fraction
siRNA	small interfering RNA
SLC	solute carrier
SRP72	signal recognition protein-72 kDa
SSB	single strand break
SSB1	single strand binding protein-1
STR	short tandem repeat
Strep	streptomycin
TALDO	transaldolase
TCA	trichloroacetic acid
TCF	T cell factor
TCP	tumour control probability
THTR1	Thiamine transporter 1
THTR2	Thiamine transporter 2
TKT	transketolase
TMP	thiamine monophosphate
TMPase	thiamine monophosphatases
TPC	thiamine pyrophosphate carrier
TPK1	thiamine pyrophosphokinase-1
TRBP	double-stranded RNA binding protein
Tris	Tris-hydroxymethylamino methane
TTP	thiamine triphosphate
TTPase	thiamine pyrophosphatases
Tween20	polyethylene glycol sorbitan monolaurate
UN	untransfected
UROD	uroporphyrinogen decarboyxlase
UTR	untranslated region
WNT	wingless signalling protein
WRNp	werners protein
XLF	XRCC4-like factor
XRCC4	X-ray repair cross-complementing protein 4
α	alpha
α-KGDH	α-ketogluturate dehydrogenase
β	beta
γ	gamma
λ	lamda

CHAPTER 1

GENERAL INTRODUCTION

1.1 Radiotherapy overview

Radiotherapy is delivered with curative intent for more than 50% of all cancer patients for localised tumours (Delaney et al., 2005).Patients which have tumours located at sites such as the central nervous system, cervix, bladder, breast, lung, prostate, oesophageal, stomach and head and neck, form the largest proportion of patients receiving radiotherapy (Delaney et al., 2005). The appropriateness of radiotherapy is based on the underlying histology and anatomical site. In breast cancer, radiotherapy is used postoperatively following mastectomy or lumpectomy to reduce the long-term risk of local re-occurrence (Fisher et al., 2002). In sites such as the lung, locally advanced stage III non-small cell lung tumours are typically inoperable, and subsequently radiotherapy and chemotherapy become the primary treatment modalities delivered concurrently (Fournel et al., 2005). In rectal cancers, neo-adjuvant chemoradiation is given to shrink the tumour before resection and neo-adjuvant RT to improve local recurrence rates (Bosset et al., 2006). Finally, radiotherapy also plays a crucial role in the treatment of incurable disease by alleviating symptoms and improving quality of life in palliative care. Palliative care is provided for patients with metastatic disease which has spread to sites such as bone (Tong et al., 1982), brain (Borgelt et al., 1980) and lung (Temel et al., 2010). Radiotherapy can only achieve its curative or palliative aims if it is able to cause damage at the cellular and atomic level.

1.2 Radiotherapy physics

Radiotherapy in the clinical setting predominantly involves delivering ionising radiation (IR) as megavoltage X-rays. Radiation is ionising if it has enough energy to displace orbiting electrons (Hall and Giaccia, 2006). In the electromagnetic spectrum, X-rays and γ-rays are the only forms of radiation that have sufficient energy to carry out such interactions. Particulate radiation such as electrons, protons, α-particles, neutrons and heavy charged particles can ionise atoms, however the main focus will be directed on the absorption and target of X-rays.

Megavoltage X-rays are principally absorbed by the Compton process (Hall and Giaccia, 2006). The Compton process involves the photon interacting with an orbital electron that has negligible binding energy, and the subsequent transfer of kinetic energy to this electron (Hall and Giaccia, 2006). The passing photon with its residual energy is deflected and the fast electron continues down the path of the incident photon. The fast electron can then carry out further interactions leading to subsequent ionisation events. During radiotherapy treatment, the Compton process produces numerous fast electrons. As the fast electrons begin to slow down, ionisations form clusters, which will cause biological damage.

1.3 Target of IR: DNA

The main target for IR that leads to cell lethality is DNA (Warters and Hofer, 1977; Warters et al., 1978). This was first identified in seminal experiments using tritiated thymidine or iodine-125-iododeoxyuridine (^{125}IUdR) labelling of DNA, and ^{125}I-concanavalin-A labelling of cell membranes/cytoplasm in Chinese hamster ovarian (CHO) cells (Warters and Hofer, 1977; Warters et al., 1978). These studies demonstrated that the irradiated nucleus caused significantly greater cell lethality

compared to irradiated cytoplasmic or cell membrane labelled compartments (Warters and Hofer, 1977).

Radiation can interact with DNA in direct or indirect action (Hall and Giaccia, 2006). Direct action involves the ionisation of the atoms of the critical target (DNA) within the cell, forming DNA radicals, and a subsequent cascade of chemical changes leading to biological change. This action is particularly abundant with particulate radiations, although does occur to a lesser extent with photons. With photons, indirect action is most common. This is the process by which radiation interacts with surrounding molecules or atoms, yielding free radicals that travel to, and then damage the DNA (Hall and Giaccia, 2006). A free radical is a molecule that has an unpaired valence electron. In a chemically stable molecule, two electrons spin in opposite directions on their axis in the outer shell. The free radical is highly reactive since the electron is without its pairing and has thus nothing to counteract the spin on its axis. Given that a large volume of the cell's content is comprised of H_2O, many of the free radicals will be derived from interactions with this molecule. The interaction of H_2O with a photon yields a positively charged ion radical, H_2O^+, and a free electron (Fig.1.1). The ion radical has a short half-life of 10^{-10} second where it will degrade to a free radical (Hall and Giaccia, 2006).

The H_2O^+ ion radical will react rapidly with a second water molecule, forming hydroxyl radicals, OH·, which are extremely chemically unstable (Halliwell and Aruoma, 1991) and the interactions with macromolecules typically last for no more than 1 ms following irradiation.

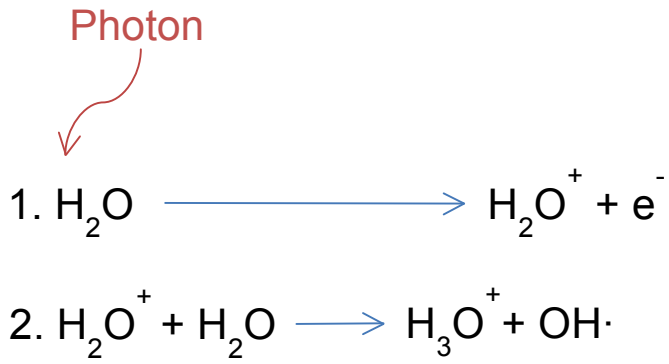

Figure 1.1. Radiolysis of water

1) The interaction of H_2O with a photon yields a positively charged ion radical (H_2O^+) and a free electron (e^-). **2)** H_2O^+ reacts with a second H_2O molecule, forming hydroxyl radicals (OH·) and hydronium ions (H_3O^+).

The traversal of a photon and initial ionisation events take roughly 10^{-18} to 10^{-15} seconds (Hall and Giaccia, 2006; Joiner and Kogel, 2009). This initial phase is known as the physical phase of the interaction. The next phase is the chemical phase, which involves the chemical interactions forming free radicals. The ion radicals produced have a lifetime of 10^{-10} seconds and the hydroxyl radicals formed from ion radical interactions with water last typically 10^{-9} seconds (Hall and Giaccia, 2006). The DNA radicals formed from the interactions between DNA and hydroxyl or ion radicals have lifetimes in the range of 10^{-5} seconds (Hall and Giaccia, 2006). The next phase is the biological phase, which typically lasts from minutes, hours, days and even years following the initial photon traversal. This phase encompasses DNA damage repair, cellular death, early/late normal tissue effects and mutagenesis.

1.4 DNA-damage lesions

A vast array of DNA lesions are induced by IR (Ward, 1988). For every 1 Gy of low LET radiation, approximately 1000 single strand breaks (SSB), 1000 base lesions (thymine damage and 8-Hydroxyadenine), 40 double strand breaks (DSB) and 150 DNA-protein cross-links are formed in a single cell (Blocher, 1982; Goodhead, 1994; Ward, 1988). DNA double strand breaks were identified as the lesion that is most deleterious to a cell. DSBs are formed when the breaks on either side of the DNA complementary strands are suitably adjacent to one another, making it problematic for base pairing and chromatin to maintain structure. This was demonstrated by experiments designed to look at SSBs and how they related to cell survival. Hydrogen peroxide (H_2O_2) which produces large quantities of OH· was administered to Chinese hamster V79-191 cells, which produced an equivalent amount of SSBs induced by 10 Gy IR alone, however these lesions did not translate to the same magnitude of cell death caused by IR (Ward et al., 1985). IR is thought to produce clustered damage compared to hydrogen peroxide. It was only after higher concentrations of hydrogen peroxide producing SSBs equivalent to 6000 Gy IR that cells underwent cell death, demonstrating that SSBs are not the most important lesion resulting in cell death. These conclusions were further confirmed by examining the repair kinetics of DSBs.

A study examining repair kinetics of double strand breaks demonstrated that the time to repair could be used to model cell survival curves (Blocher and Pohlit, 1982). These models accurately predicted experimentally derived cell survival curves suggesting that one single DSB could cause a lethal event (Blocher and Pohlit, 1982). Further evidence supporting the claim that DSBs are the most important lesion was obtained by comparing the differences of high-linear energy transfer (LET) to low-LET radiation. Compared with γ-radiation (low-LET), an equivalent dose of α-radiation (high-LET)

caused a greater number of unrepaired DSBs and increased cell death (Coquerelle et al., 1987). This is attributed to that fact that high-LET radiation causes clustered DNA damage with a higher degree of complex DSB damage compared to low-LET radiation. These combined observations demonstrate that DSBs are the most deleterious lesion for a cell and the failure or improper repair of DSBs caused by IR can have a huge detrimental effect on a cell.

1.5 Double-strand break repair

Cells have evolved two highly specialised repair mechanisms, non-homologous end joining (NHEJ) and homologous recombination (HR) to repair DSBs.

1.5.1 NHEJ repair mechanism

The NHEJ pathway aims to ligate broken strands of DNA without the need for any homology directed repair and can be broken down into three steps summarised in Figure 1.2. The first step involves recognition of the DNA-damage site and recruitment of proteins. Site recognition is then followed by DNA-termini processing to ensure that the opposing strands are ligatable. The final step involves the ligation of the DNA strands, resolving the DSB.

1.5.1.1 Damage recognition, protein recruitment and DNA-bridging

The first step in the NHEJ pathway involves recognition of the DSB by the Ku heterodimer (Ku70 and Ku 80) (Mari et al., 2006; Mimori and Hardin, 1986). The importance of the binding of the Ku heterodimer is to prevent the unspecific processing of the break and to keep the broken strands juxtaposed for ligation (Pang et al., 1997). Ku localises rapidly to DSBs because of its large abundance within a cell (400,000 to 500,000 Ku/molecules/cell) and the high affinity for DNA ends (2×10^9 M^{-1} binding constant) (Blier et al., 1993; Falzon et al., 1993; Mimori and Hardin, 1986). The purpose of the Ku toroid structure is to act as a protein scaffold enabling other proteins to

engage in protein-protein interactions (Zhang et al., 2004). This involves the recruitment of polymerases, nucleases and ligases, which begin the process of processing and resolving the DNA damage site. Following the binding of Ku heterodimer to the DNA ends, DNA-dependent protein kinase catalytic subunit (DNA-PK*cs*) (Uematsu et al., 2007), X-ray repair cross-complementing protein 4 (XRCC4) (Costantini et al., 2007; McElhinny et al., 2000), XRCC4-like factor (XLF) (Yano and Chen, 2008; Yano et al., 2008), DNA Ligase IV (Costantini et al., 2007; McElhinny et al., 2000) and aprataxin- and PNK-like factor (APLF) (Grundy et al., 2013; Iles et al., 2008; Macrae et al., 2008a; Rulten et al., 2011) assemble at the site.

The DNA-PK*cs* interaction with the Ku heterodimer is the most heavily examined. As depicted in Figure 1.2, the interaction requires the presence of DNA and the interaction translocates Ku80/70 towards the inner region of the strand break and consequently activates the kinase activity of DNA-PK*cs* (Gottlieb and Jackson, 1993). Similar to the action of Ku, DNA-PK*cs* helps to bridge the ends of DNA strands together (Cary et al., 1997). XRCC4 forms a multimeric protein complex with DNA ligase IV which directly interacts with Ku70/80 (Mari et al., 2006). Of which XRCC4 interacts with Ku70, and DNA ligase IV interacts with the entire heterodimer. XLF interacts with the Ku heterodimer using the c-terminal end of the XLF protein and interacts with XRCC4 (Yano et al., 2011). It has been suggested that XRCC4-XLF forms filaments used to help to bridge the opposing DNA-strands together (Malivert et al., 2010).

1.5.1.2 DNA damage termini processing

DNA damage processing requires the use of multiple proteins, each one carrying out a specific job in relation to the damage inferred. For the purpose of making DNA ends ligatable, blocking end groups such as 5′ hydroxyls or 3′ phosphates can be removed by polynucleotide kinase phosphatase (PNKP) (Bernstein et al., 2005). In addition, Ku can

process 5' ends of DNA by removing abasic sites using its 5′-deoxyribose-5-phosphate lyase activity (Roberts et al., 2010). Similarly, adenylate groups that are covalently bound to 5'-phosphate ends can be removed by a hydroylase known as Aprataxin (Ahel et al., 2006). After the cleaning of these 'dirty ends' of DNA, the strands may need to be resected to provide suitable overhangs for optimal ligation. Resection is carried out by specialised exo/endonucleases such as Artemis. Artemis possesses DNA-PK*cs* independent 5' to 3' exonuclease activity for 5' overhangs producing blunt ends on ssDNA, and has some exonucleolytic activity against dsDNA (Ma et al., 2002). Importantly, Artemis function is enhanced as it complexes and is phosphorylated by DNA-PK*cs* activating its endonucleolytic activity (Ma et al., 2002). Artemis having both exonuclease and endonuclease activity suggests that there is no requirement for additional nucleases for end resection. Nevertheless other proteins have been implicated in this processing. An additional protein with exonuclease activity involved in NHEJ is the Werners protein (WRNp) and defective WRNp results in Werners syndrome, which is characterised by premature ageing. WRNp directly binds to ku70/ku86 and possesses 3′ to 5′ exonuclease activity. Furthermore, APLF has been implicated in end resection of 3' overhangs through its exonuclease activity (Li et al., 2011). Upon completion of resection, DNA gaps are filled by polymerases μ and λ (Nick McElhinny et al., 2005).

1.5.1.3 Ligation

Following DNA strand break recognition and processing, DNA Ligase IV/XRCC4/XLF ligates the broken strands. The ligase activity of DNA ligase IV is stabilised and stimulated through adenylylation by XRCC4 and it is able to ligate incompatible DNA strands across gaps (Grawunder et al., 1997; Gu et al., 2007; Li et al., 1995). XLF interacts with DNA/ligase IV/XRCC4(Ahnesorg et al., 2006).

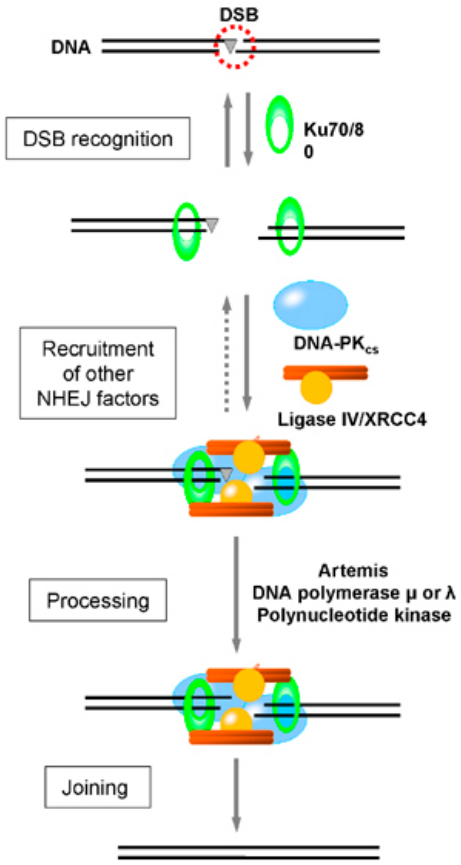

Figure 1.2. Simplistic overview of non-homologous end joining

Double strand breaks are recognised by the Ku heterodimer (Ku70 and Ku80), acting as a protein scaffold enabling other proteins to engage in protein-protein interactions. A multimeric complex of proteins then forms, which includes DNA-PK*cs*, XRCC4, XLF, DNA Ligase-V and APLF. DNA termini are processed by Artemis which complexes with DNA-PK*cs* and engages its endonucleolytic activity. DNA strands are ligated back together following termini processing by DNA Ligase IV/XRCC4/XLF complex. Adapted from van Gent and Van der Burg, 2007.

Non homologous end joining is active throughout the whole cell cycle (Rothkamm et al., 2003) and is a rapid process (Mao et al., 2008) but suffers from reduced accuracy. The repair is often error prone resulting from insertions or deletions caused by end resection and polymerisation during the above steps.

1.5.2 Homologous recombination

Homologous recombination involves the use of sister chromatid template to repair the double strand break (Richardson et al., 1998). Since the homologous sequence is available on the sister strand, the repair is error-free.

HR involves several specialised steps that result in the resolution of the DSB (Fig 1.3). The first is the recognition and coating by proteins with high affinity for ssDNA and the subsequent formation of nucleoprotein filaments. These filaments then invade the sister chromatid DNA forming a cross-over structure known as a Holliday junction. The cross-over junction is expanded by helicases thus allowing the strands to align and the polymerases to synthesise the missing DNA. The cross-over junction is then reversed, by means of nucleases that cut the DNA and subsequent ligation by ligases. This is to ensure that the chromatin structure is correctly organised.

1.5.2.1 End resection

End resection has been comprehensively studied in single cellular organisms such as *Saccharomyces cerevisiae*. The MRE11/RAD50/NSB1 (MRN) complex carries out the resection (Mimitou and Symington, 2008; Zhu et al., 2008) which leaves 3' overhangs. The MRE11 complex has exonuclease activity and leaves ssDNA required for strand invasion (Buis et al., 2008). MRN complex also interacts with C-terminal binding protein interacting protein (CTIP) (Sartori et al., 2007), and is essential for DSB resection, recruitment of replication protein A (RPA) and activation of DNA damage response checkpoint kinases. In humans, the BLM helicase interacts with Exo1 and stimulates DNA resection using its 5' to 3' exonucleolytic activity (Nimonkar et al., 2008).

1.5.2.2 Single strand binding and nucleoprotein assembly

The ssDNA left by end resection is coated by RPA and single strand binding protein-1 (SSB1) (Richard et al., 2008; Wold, 1997). These proteins are most likely required to

cap and protect the DNA from unspecific DNA-termini processing. Breast cancer susceptibility gene 2 (BRCA2) promotes the assembly and formation of RAD51 nucleoprotein filaments onto ssDNA, blocking ATP hydrolysis, and thus displacing RPA (Baumann et al., 1996; Jensen et al., 2010; Thorslund et al., 2010). The nucleoprotein filaments are required for strand invasion and homology searching of the sister chromatid DNA (Baumann et al., 1996). Several RAD51 paralogues are involved in the production of the nucleoprotein filament which includes XRCC2, XRCC3, RAD51B, RAD51C and RAD51C which forms a structure that keeps the strands separate known as the displacement loop (D-loop, Fig.1.3).

1.5.2.3 SDSA and DSBR

After the formation of the D-loop, two models have been proposed for the repair of the DNA-damage site, which are synthesis dependent strand annealing (SDSA) and DSB repair (DSBR). During SDSA, the nascent synthesised strand is annealed to the opposing complementary DNA end following strand displacement, resulting in a non-crossover (Szostak et al., 1983). DNA polymerases polymerise the missing DNA (McIlwraith et al., 2005) and next to this a Holliday junction is formed (X-shaped structure) (Holliday, 2007). The Holliday junction can be moved through the binding of certain proteins (WRNp, BLM, p53), which is known as branch migration, and this allows for the invading strand to be released. The final step involves the ligation of the nicks and gaps.

In DSBR, the D-loop strands both invade the sister chromatid DNA forming a double Holliday junction. This results in possible cross-over and non-crossover outcomes. However, in mammalian cells cross-over products are rarely visualised and this mode of cell repair has been questioned (Johnson and Jasin, 2000). Branch migration is carried out by BLM (RecQ-like helicase) in association with BLAP75 and topoisomerase

IIIalpha (Bussen et al., 2006; Wu and Hickson, 2003), plus RAD54 (Bugreev et al., 2006) to unwind the DNA and enlarge the cross over junction. The polymerases involved in HR remain uncertain. However, replication polymerases remain the best candidates since the repair is carried out in an error-free manner. The Holliday junctions are resolved by resolvases, which nick DNA. GEN1 has been implicated in this process through its endonuclease activity (Rass et al., 2010). DNA-ligase-1 ligates the cut strands and completes the DNA break repair.

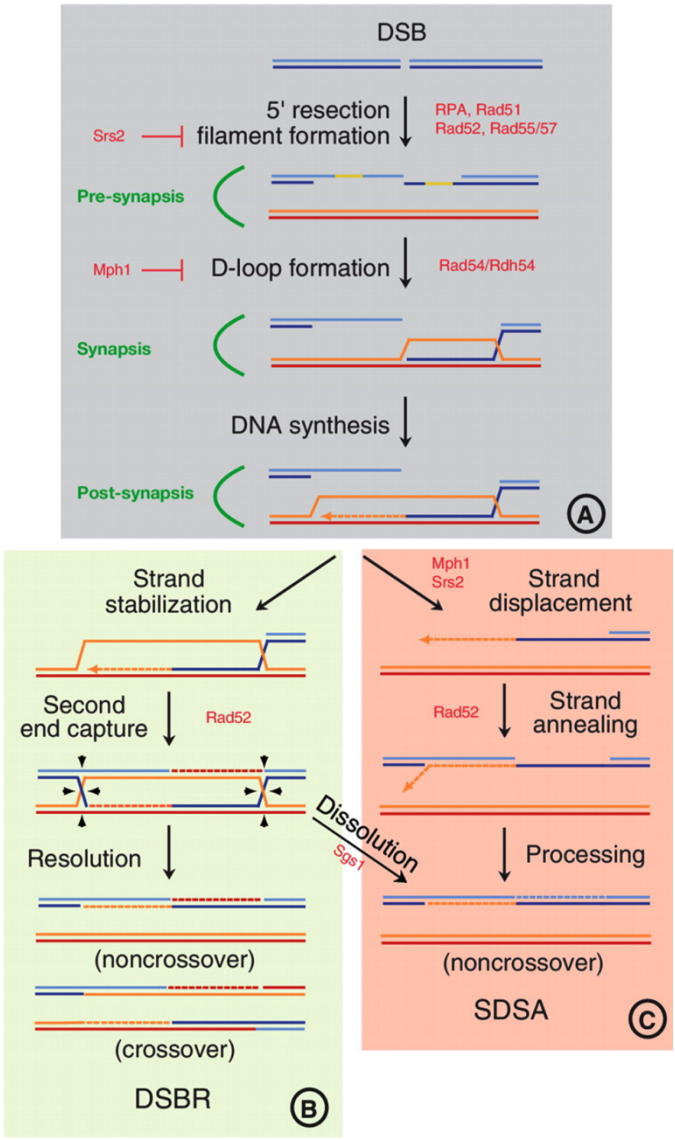

Figure 1.3. Overview of homologous recombination and its pathways.

A) All homology mediated repair begins with 5' resection and follows the recruitment of SSB proteins. RAD51 produces nucleoprotein filaments which invade the complementary sister chromatid DNA. This produces the displacement loop (D-loop) and Holliday junction. Alternative pathways can follow the D-loop to resolve the DSB. **B)** Double strand break repair (DSBR) involves the invasion of both ends of the DNA, resulting in second end capture and a double Holliday structure. This results in non-crossover and crossover outcomes. **C)** Synthesis dependent strand annealing (SDSA) is the process by which newly synthesised strand is displaced and pairs with 3' tail of the opposing DNA strand. Followed by strand annealing and branch migration, DNA nicks and gaps are ligated in final processing step. Adapted from Krejci *et al.,* 2012.

1.6 Radiotherapy in the clinic

As described previously radiation interacts with the cell at the physical, chemical and biological level leading to either repair and survival, or cell death. The aim of radiotherapy treatment is to deliver a large enough dose to tumours so they are sterilised. Providing a sufficient dose to cancer cells will cure the patient of the cancer but may leave the normal tissue surrounding the cancer functionally damaged. Therefore, radiotherapy treatment is restricted by the dose tolerances of the normal tissue (Emami et al., 1991). In order to minimise side effects, treatment is conformed around the tumour with the use of static and dynamic approaches to spare normal tissue. Advances in technology have made it possible to carry out three-dimensional conformal radiotherapy (3D-CRT) to outline and treat the tumour volume and deliver radiation treatment more precisely. 3D images are reconstructed from slices generated by computed tomography (CT), magnetic resonance imaging (MRI) or positron emission tomography (PET) imaging techniques. Accurate tumour volume determination has been complemented by improvements in radiation delivery.

Dynamic multi-leaf collimator approaches coupled with intensity modulated radiotherapy (IMRT) enables radiation dose to be mapped around tumours that are close to critical normal tissue, which could not be achieved by static 3D-CRT approaches (Tubiana and Eschwege, 2000). IMRT has shown success in reducing side effects in normal tissues surrounding prostate and cervical cancers (Chao et al., 2001; Nutting et al., 2000). Future methods taking advantage of the physical properties of proton or heavy ions may also reduce dose to surrounding normal tissue, as dose is deposited at a specific depth within the tissue (Schulz-Ertner and Tsujii, 2007). Studies on the use of heavy ions in the treatment of inaccessible radioresistant tumours show great promise (Schulz-Ertner

et al., 2004). All approaches are aimed at widening the therapeutic window in which radiotherapy treatment can be safely delivered.

Conforming the dose to the tumour volume provides the ability to dose escalate and this has its merits as demonstrated in studies showing improved clinical outcomes in specific histological sites such as prostate, but the therapeutic gain is dampened by an increase in late toxicities (Al-Mamgani et al., 2008; Pollack et al., 2000; Storey et al., 2000). In addition dose escalation for lung tumours has been shown to be potentially actively harmful and constricts the therapeutic window (Bradley et al., 2015). As a consequence, additional methods are required to widen the therapeutic window, achieving tumour control with lower doses, and avoiding increase in early and late toxicities.

1.7 Therapeutic window

Radiotherapy treatment is a balance between tumour control and normal tissue complications. As illustrated in Figure 1.4, these can be depicted as hypothetical curves for tumour control probability (TCP) and normal tissue complication probabilities (NTCP). As TCP increases with cumulative dose, the NTCP also increases. The region between these curves is the therapeutic window in which a curative dose can be delivered safely. Avoiding normal tissue complications by achieving better conformality of dose to the tumour widens this therapeutic window by shifting the NTCP curve to the right. This then provides the opportunity to dose escalate before the threshold 5% of NTCP in 5 years (TD 5/5) used in clinical practice is reached. However, technical approaches that widen the therapeutic window neglect the static TCP curve. To achieve greater widening of the therapeutic window, factors that can shift the TCP curve to the left must be determined and assessed.

One major determinant of the TCP curve is intrinsic radiosensitivity (Gerweck et al., 2006). An attractive approach would be to shift the probability of achieving tumour control towards the left, by modulating the intrinsic radiosensitivity of the tumour. Sensitising the tumour to radiation in this way would achieve the same level of TCP with lower total dose.

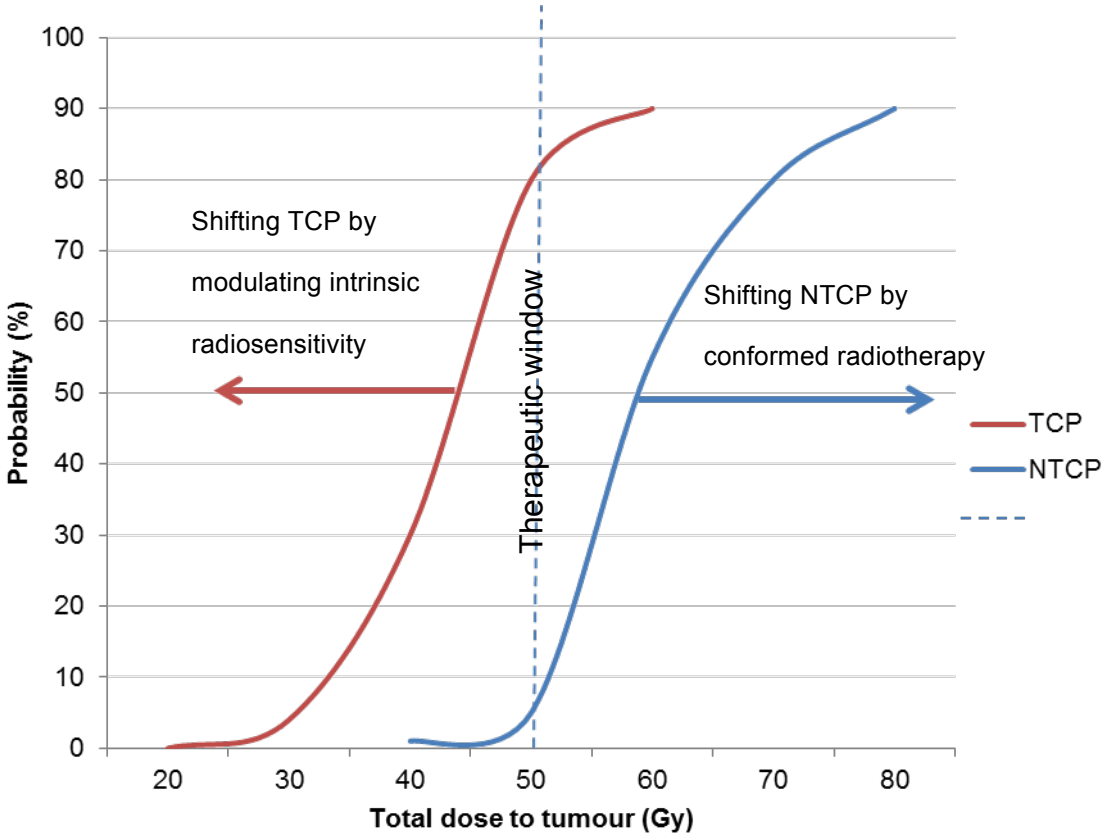

Figure 1.4. Theoretical depiction of tumour control and normal tissue control probabilities.

Tumour control and normal tissue control probability curves both rise with increasing dose. The clinical threshold of acceptable normal tissue complications is set at 5% within 5 years of treatment (TD5/5). Accurate tumour delineation delivered with conformed radiotherapy delivery can shift the NTCP curve to the right, enabling dose escalation and widening the therapeutic window. Modulation of intrinsic radiosensitivity shifts the TCP curve to the left, achieving greater tumour control at a reduced total dose.

1.8 Hypoxia

An extrinsic factor that can severely impact radiosensitivity of tumour cells and the response to IR is the availability of oxygen (Gray et al., 1953; Nordsmark et al., 1996). Solid tumours often have large regions of hypoxia and *in vitro* experiments using mammalian cells cultured under nitrogen gas demonstrated that hypoxic cells are significantly radioresistant (Gray et al., 1953). On cell survival curves, the magnitude of this oxygen effect on survival is best illustrated by the oxygen enhancement ratio (OER, Fig 1.5). The OER is the irradiation dose in hypoxic conditions over the dose in aerobic conditions that leads to the same level of survival (OER= IR dose in hypoxia/ IR dose in normoxia). The OER for megavoltage X-rays is in the region of 3.0. At clinically relevant doses, the OER is reduced which has an impact on fractionated regimens (Palcic and Skarsgard, 1984). The oxygen effect is dependent on oxygen being present at the time of irradiation (Michael et al., 1973), thus demonstrating that this effect is linked to early stages of DNA-damage in which oxygen radicals are formed.

The radioresistance caused by hypoxia is thought to be the result of inability to chemically fix into position DNA radical damage (Brown and William, 2004) (Fig.1.5B). During indirect DNA damage, the production of highly reactive oxygen radicals interacts with DNA forming DNA radicals (Fig 1.5B). In the presence of oxygen, the DNA radicals are oxidised, chemically stabilising the damage (Brown and William, 2004). Without oxygen, the DNA radical has an extended half-life, and interacts with H^+ or with reducing agents. This interaction will cause restitution of DNA radical to its original form, thus preventing the onset of downstream biological change.

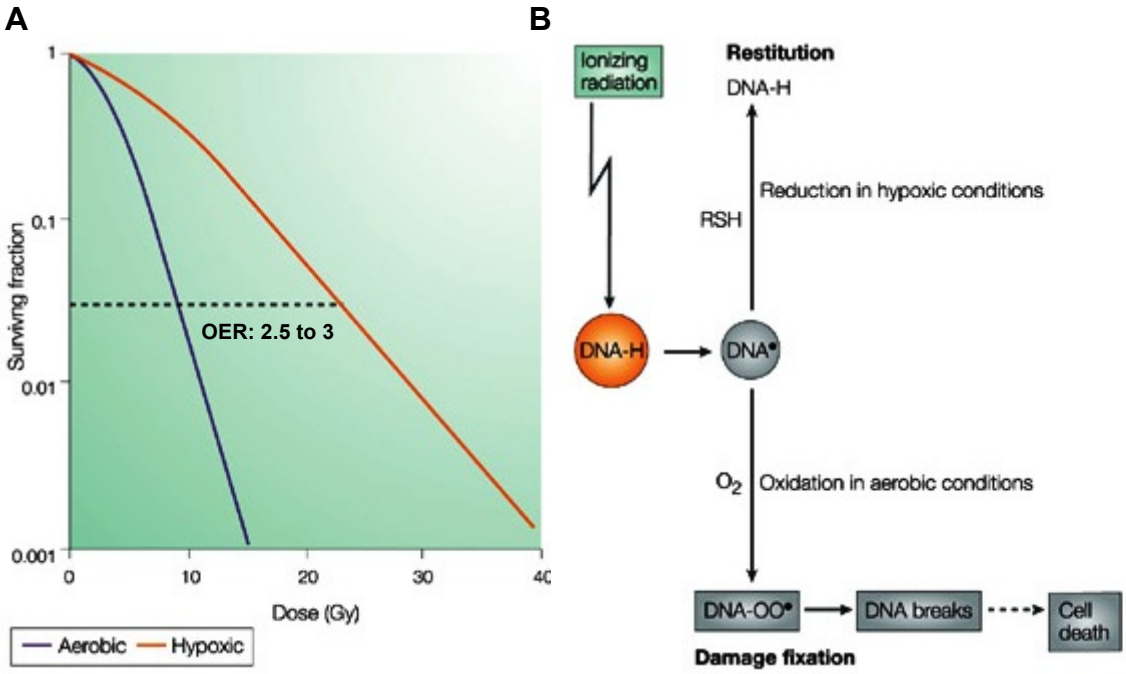

Figure 1.5. The oxygen effect and the oxygen fixation hypothesis

A) A cell survival curve illustrating the oxygen effect. Hypoxic cells are radioresistant to IR. The oxygen enhancement ratio (OER) is calculated as the dose for hypoxic cells over the dose in aerobic conditions required to produce the same level of survival. **B)** Oxygen fixation hypothesis: Indirect action of IR produces large quantities of highly reactive oxygen species. These oxygen radicals will interact with DNA to produce DNA radicals (DNA•). In hypoxic conditions, reducing agents such as –SH containing compounds (RSH) or interaction with H^+ can revert the DNA• to its original stable form (DNA-H). In aerobic conditions, oxygen oxidises the DNA• resulting in fixing of the DNA chemical modification. Thus, this leads to enzymatic activation, DNA-damage recognition and subsequent cell death. Adapted from Brown and William, 2004.

Hypoxic regions in tumours can be formed by two primary processes. The first process is known as diffusion limited chronic hypoxia and is the result of the tumour reaching a size (> 70 μM), which is greater than the diffusion distance of oxygen (Joiner and Kogel, 2009; Vaupel and Harrison, 2004). Therefore, as the tumour develops from the tumour vasculature, a hypoxic region forms in the middle. With sustained lack of nutrients and oxygen this region becomes necrotic.

The second cause is perfusion limited acute hypoxia, which arises from the premature and irregular structure of blood vessels supplying the tumour. The sudden shunting,

occlusion, incomplete endothelial layer, dilations and abnormalities of the tumour vasculature causes these acute hypoxia regions (Vaupel and Harrison, 2004). These regions of hypoxia are reversible, short-lived (acute), and thus dynamic over the growth of the tumour. In addition, tumour hypoxia can also be caused by anaemia. This is caused by the reduced transport capacity of blood haemoglobin for oxygen (Vaupel and Harrison, 2004). Another significant determinant of tumour response to radiation is intrinsic radiosensitivity.

1.9 Intrinsic radiosensitivity

Intrinsic radiosensitivity reflects the differences in susceptibility of cells, tissues, organs and organisms to the ionizing effects of radiation treatment caused by underlying genetic variations. Therefore, intrinsic radiosensitivity is typically the observation that cells have different levels of survival following a given dose of radiation and is dependent on intrinsic molecular factors. Consequently, modulation of these factors that confer a resistance phenotype (radioresistant) can shift the TCP curve to the left, thus widening the therapeutic window. The importance and impact of intrinsic radiosensitivity on tumour response was demonstrated by several key findings.

Firstly, intrinsic radiosensitivity is a principal determinant of tumour response to radiation (Gerweck et al., 2006), demonstrated by experiments transplanting tumour cell lines which were either deficient or proficient for DNA-PK*cs*, into genetically and phenotypically identical mice (Gerweck et al., 2006). These investigations demonstrated that the DNA-PK$cs^{-/-}$ cells were more radiosensitive examined by colony formation assay and there was a significant growth delay between DNA-PK$cs^{-/-}$ and DNA-PK$cs^{+/+}$ irradiated xenografts. The differences in growth delay suggested that the stroma was not a key determinant of radiosensitivity in these settings.

Secondly, it was demonstrated that tumours cells obtained from clinical samples were sensitive to radiation to the different degrees and that these differences can have an effect on the radiocurability of cancer (Fertil and Malaise, 1985). Fertil & Malaise (1985) analysed 92 different human tumour cell lines and applied parameters to assess the variation in radiosensitivity. A common parameter used to assess radiosensitivity is the surviving fraction after 2 Gy (SF_2) determined using *in vitro* colony formation assay (Deacon et al., 1984). Table 1.1 demonstrates that the SF_2 value varies substantially between radioresistant glioblastoma to radiosensitive lung carcinoma. The growing body of evidence of such findings resulted in the proposal that intrinsic radiosensitivity should be named as one of the 'Rs' of radiobiology (Steel et al., 1989).

Tumour	SF_2
Glioblastoma	0.58(0.33/0.84)
Melanomas	0.51(0.44/0.58)
Breast adenocarcinoma	0.30
Medulloblastoma	0.27
Myelomas	0.16
Lung carcinoma	0.18

Table 1.1: Variation in intrinsic radiosensitivity between tumour types

Tumour types have varying intrinsic radiosensitivity. Surviving fraction after 2 Gy (SF_2) is used as the parameter to compare radiosensitivity between tumour types. 95% confidence limits have been included where possible. Adapted from Fertil and Malaise, 1985.

The differences in intrinsic radiosensitivity of tumour lines depicted in Table 1.1 can be translated to significant changes in clinical endpoints, including survival, local control and disease free survival (West et al., 1997). SF_2 was demonstrated as a prognostic marker for local control in head and neck in a study where 84 patient tumour specimens were grown and assayed using the colony formation assay (Bjork-Eriksson et al., 2000).

These patients underwent radical treatment with neoadjuvant chemotherapy plus radiation. The median SF_2 for the 84 tumours was 0.40 and after a follow-up of 25 months, patients developing local reoccurrence had a median SF_2 of 0.53 which was significantly larger than patients with no local re-occurrences (SF_2 of 0.38, p=0.015) (Bjork-Eriksson et al., 2000). Furthermore, 88 tumour specimens derived from patients treated with radical radiotherapy for stage I to III cervical uterine carcinomas were stratified above and below a median SF_2 of 0.40 (West et al., 1993). Patients whose tumour cells had a median SF_2 >0.40 did significantly worse for 3-year survival (p = 0.002) and local recurrence rates (p =0.001) compared to the radiosensitive SF_2 <0.40 population of patients (West et al., 1993). The follow-up to this previous study with a larger set of patients also demonstrated that there is a worse prognosis in metastasis free survival for cervical patients stratified above the median SF_2 compared to the radiosensitive population (West et al., 1997).

These studies demonstrate the impact that intrinsic radiosensitivity has on clinically relevant endpoints. It is important to tackle intrinsic radiosensitivity of tumours to improve the clinical outcome for patients. This requires discovering the factors that are involved in determining intrinsic radiosensitivity and how they can be modulated to make the tumour more susceptible to radiotherapy treatment, ideally without altering the sensitivity of normal cells.

1.10 Modulating intrinsic radiosensitivity

1.10.1 Chemoradiation

Rendering tumour cells more susceptible to radiation is not a novel approach. Chemoradiation regimens have demonstrated this with improved progression free survival and local control/survival in non-small lung, glioblastoma, HNSCC and cervical

cancers (Al-Sarraf et al., 1998; Chan et al., 2005; Rose et al., 1999; Schaakekoning et al., 1992).

Cisplatin is a widely implemented chemotherapy in the clinic that radiosensitises tumour cells. The mode of action of cisplatin is still disputed but its main target is DNA (Eastman and Barry, 1987), inducing intra and inter-strand cross links that subsequently result in the induction of the DNA damage response and cell death through apoptosis (Eastman, 1987; Eastman and Barry, 1987). The mechanism behind the radiosensitisation effect is unknown but has been suggested to occur through the inhibition of DNA repair or its ability to sensitise hypoxic environments of tumours when unbound to DNA (Amorino et al., 1999; Richmond et al., 1984). Although the mechanism is disputed, the radiosensitisation seen *in vitro* translates to impressive clinical outcomes. A phase 3 clinical trial of 350 patients comparing radiotherapy alone and concurrent cisplatin with radiotherapy for nasopharyngeal carcinoma demonstrates that chemoradiation can have an improved outcome on overall survival (Chan et al., 2005). Five year overall survival in the radiotherapy alone arm was 58.6% compared to the chemoradiation arm with 70.3 % (p = 0.049, Hazard ratio: 0.71 in support of chemoradiation) (Chan et al., 2005). Combination of cisplatin and radiotherapy results in improved clinical endpoints for multiple cancers including cervical (Peters et al., 2000), nasopharyngeal (Huncharek and Kupelnick, 2002) and oesophageal (Herskovic et al., 1992) cancers. However, the key setback with chemoradiation regimens is their indiscriminate action between tumour cells and normal tissue. In a study comparing chemoradiation with RT vs. RT alone for oesophageal cancers, 64% of patients suffered either severe or life threatening side effects in the combined therapy compared to 28% in the RT alone (Herskovic et al., 1992). As a result, the benefit that is seen by radiosensitising cancer cells is dampened by an increase in normal tissue toxicity,

constraining the therapeutic window. An approach needs to be found where significant increase in tumour control can be achieved at a lower dose while normal tissue complications can be reduced or unaffected. One strategy that could achieve this aim is molecular targeting.

1.10.2 Molecular targeting

Studies have demonstrated that molecular targeting can achieve modulation of intrinsic radiosensitivity of tumour cells. Cetuximab is a monoclonal antibody and was regarded as the most successful molecular targeting agent (Bonner et al., 2006). Its mode of action is to antagonise the epidermal growth factor receptor (EGFR), which is overexpressed in several tumour types (Bonner et al., 2006). The overexpression of EGFR is commonly observed in head and neck tumours, and it is a marker for worse survival, disease free progression and increased radioresistance (Milas et al., 1999; Rubin Grandis et al., 1998; Sheridan et al., 1997). Cetuximab enhances the effect of radiotherapy *in vitro* and *in vivo* (Buchsbaum et al., 1999; Huang and Harari, 2000a; Milas et al., 2000) and inhibits the proliferation of tumours by antagonising EGFR, which is thought to drive cell cycle progression and apoptosis inhibition by activating the Ras-Pi3 pathway. The mechanism of action has also been linked to DNA-repair inhibition and these observations suggest that cetuximab causes its effects in multiple approaches (Huang and Harari, 2000a). In addition, the radiosensitisation caused by cetuximab has been attributed to the arrest of the cell cycle in radiosensitive phases (G2/M arrest), DNA repair factors sequestering to the cytosol and up-regulation of angiogenesis markers (Huang and Harari, 2000b).

Regardless of mechanism, cetuximab was shown to be a potential promising clinical drug for the use with radiotherapy. A study comparing the concomitant use of cetuximab with RT vs. RT alone in squamous cell carcinoma of the head and neck demonstrated a

survival of 45.6% in the combination arm compared to 36.4% in the RT alone with acceptable side effects (Bonner et al., 2010). While demonstrating initial promise, the drug could not compete with chemoradiation regimens established in the clinic for HNSCC, and its inclusion in these regimens did not translate to improved clinical outcomes (Ang et al., 2014).

Despite cetuximab demonstrating no significant effectiveness over the standard chemoradiation treatment in HNSCC, an array of inhibitors have been developed that target downstream of EGFR within the Phosphoinositide 3-kinase/Protein Kinase B (PI3K-AKT) or Ras-*Raf-MEK-ERK* pathways (Chung et al., 2009; Fokas et al., 2012b; Mauceri et al., 2012). The rationale is that tumour cells constitutively activate the downstream effectors of these pathways via various routes which include mutations or over-expression in Ras oncogene (Bernhard et al., 1998; Gupta et al., 2001; McKenna et al., 1990), PI3K (Gupta et al., 2001; Krasilnikov et al., 1999) and Phosphatase and tensin homologue (PTEN) deleted on chromosome 10 (Wick et al., 1999), resulting in pro-survival. The activation of these pathways through Ras and PI3K has been shown to cause tumour radioresistance (Bernhard et al., 2000; Gupta et al., 2001; Prevo et al., 2008) and inhibition of these pathways reduces tumour cell survival (Gupta et al., 2001). Drugs such as BKM120 (PI3K inhibitor, Novartis,) (Liu et al., 2014), Everolimus (mTOR inhibitor Novartis) (Mauceri et al., 2012) and AZD6244 (MEK1/2 inhibitor , AstraZeneca) (Chung et al., 2009) are now in clinical trials and may provide substantial benefit to patients with NSCLC and HNSCC tumours.

In addition to EGFR signaling, groups have focussed on understanding defective DNA repair mechanisms in tumour cells and subsequently targeting the remaining back-up pathway to induce cell death, commonly known as ‘synthetic lethality’ (Kaelin, 2005). This is true of poly (ADP-ribose) polymerase (PARP) in the base excision repair

pathway, which is involved in SSB repair, and inhibition of this pathway is synthetically lethal with breast and ovarian cancers defective in HR (Farmer et al., 2005). PARP inhibitors cause significant radiosensitisation in tumour cells and this is thought to be dependent on unrepaired SSBs being converted to DSBs during replication fork collapse in the S-phase of the cell cycle (Saleh-Gohari et al., 2005). Therefore, PARP inhibitors may yield the largest benefit in tumours that are highly proliferative. However, concerns still surround PARP inhibition for normal tissues, since not all normal tissues have low turnover.

Other molecular targeting strategies focus on DNA-damage response (DDR) pathways and may provide tumour specific radiosensitisation. DDR pathways are essential to amplify signals following DNA-damage initiation and to regulate repair to prevent tumourigenesis and maintain genome integrity (Huen and Chen, 2008). DDR pathways are complex and have been reviewed in detail by Jackson and Bartek, 2009, and Zhou and Elledge, 2000. Some of the processes that follow DDR pathways include cell cycle arrest, ceasing transcription/translation or inducing cell death mechanisms. Integral to the DDR pathways are ATM and ATR, which activate downstream effectors following DSBs and SSBs, respectively (Smith et al., 2010). Mutations of ATM are regularly seen in tumours such as lung (Ding et al., 2008), breast (Renwick et al., 2006) and ovarian (Thorstenson et al., 2003). These tumour cells then become reliant on ATR for DDR signalling. To specifically target these tumours, inhibitors have been made against ATR, such as VE-822 (Vertex), which has been shown to cause tumour specific radiosensitisation in both tumour lines *in vitro* and *in vivo* xenografts (Fokas et al., 2012a). The drug did not sensitise normal tissue lung fibroblasts cell lines to radiation (Fokas et al., 2012a). In addition, VE-822 did not cause any weight loss or physical changes to gastrointestinal tract of mice (Fokas et al., 2012a). The tumour specificity of

ATR inhibition most likely arises from the fact that normal tissues have functional ATM. Therefore, synthetic lethality only occurs in tumour cells that rely on ATR. In the context of lung tumours, 70% of tumours have ATM and p53 gene mutations, and these strategies may have great benefits for patients.

1.11 Identifying radiosensitisers

As discussed above, successful manipulation of intrinsic radiosensitivity can be achieved by modifying specific cancer biology, thus widening the therapeutic window with minimal tolerable side effects. Therefore, research into discovering new targets that can provide pronounced radiosensitivity is vital. It is likely that there are a wide range of genes that modulate intrinsic radiosensitivity but many remain unidentified. The identification of novel radiosensitisation targets requires high-throughput screening (HTS) methods that can reliably identify targets using robust endpoints (Katz et al., 2009). Small interfering RNA (siRNA) screens are commonly used to identify such targets (Echeverri and Sachse, 2004; Tuschl and Dorsett, 2004). The aim of this thesis is to find modulators of radiosensitivity using siRNA as a tool to interrogate individual genes, evaluated by an endpoint that closely reflects the true action of radiotherapy treatment. The discovery of siRNAs and their ability to silence genes is integral to the aims of this thesis and is discussed in detail below.

1.12 RNA interference (RNAi)

siRNAs and micro-RNA (mi-RNA) are short sequences of RNA that trigger the RNA interference (RNAi) pathway resulting in a sequence specific silencing or degradation of gene products at the post transcriptional level. There are subtle differences between siRNA and miRNA. siRNA are double stranded and bind to mRNA with perfect sequence complementary. miRNAs are single stranded and their binding to mRNA is imperfect resulting in broad spectrum gene silencing or degradation.

The observation that injection of double stranded RNA (dsRNA) could cause profound silencing of genes was first discovered in *Caenorhabditis elegans* (*C.elegans*) (Fire et al., 1998). This RNAi machinery has now been shown to be conserved across species including *Drosophila melanogaster* (Elbashir et al., 2001b) and humans (Elbashir et al., 2001a). Historically, siRNAs were thought be produced from exogenous dsRNA and miRNA from stem-loop structures coded from non-coding regions. In the case of siRNAs, it has emerged that they can be formed from endogenous routes such as repetitive sequences (transposons) (Lippman and Martienssen, 2004), endogenous dsRNA (Watanabe et al., 2008) and natural antisense transcripts of protein coding genes (Werner et al., 2014). The components of the RNAi pathway have largely been deciphered in *Drosophila,* with the human system being elucidated over the past decade. siRNA and miRNA mediated silencing is illustrated in Figure 1.6.

1.12.1 siRNA and miRNA targeted silencing

In the production of siRNA and miRNA, dsRNA is cleaved by the dicer protein, an endoribonuclease forming part of the RNase III superfamily, which results in 21-28 nucleotide length RNA fragments with 5'phosphate and 3'overhangs (Bernstein et al., 2001; Hutvagner et al., 2001; Zamore et al., 2000). In addition, dicer facilitates the loading of one of the RNA strand duplexes (guide strand) to the ribonucleoprotein complex known as RNA-Induced Silencing Complex (RISC) (Liu et al., 2006b).

In humans, RISC contains one strand of the siRNA duplex (Martinez et al., 2002), dicer, double-stranded RNA binding protein (TRBP), and argonaute-2 (Argo2) (Gregory et al., 2005; Maniataki and Mourelatos, 2005). These three proteins form the RISC-loading complex (RLC) and are involved in slicing of dsRNA to siRNA (dicer), Argo2 dependent siRNA loading and degradation of the remaining 'passenger strand' (MacRae et al., 2008b). In mammals it remains unclear how the siRNA strand is selected in the active

RISC complex, but it is likely determined by the thermodynamic stabilities of the siRNA duplex. Each strand of siRNA duplex in *drosophila* can trigger the RNAi machinery to target its corresponding mRNA sequence (Elbashir et al., 2001b; Elbashir et al., 2001c). The guide strand which enters the RISC complex is thought to be favoured if there is weaker binding to its complementary sequence at the 5' end (Schwarz et al., 2003), and is also selected through binding with Argo2 following unwinding of the siRNA duplex. Through the binding with Argo2, the 'passenger strand' is degraded (Leuschner et al., 2006; Matranga et al., 2005). Following the above steps, Argo2 uses its endonucleolytic activity to degrade the target mRNA by interacting with its PIWI domain, resulting in the slicing of residues 10 and 11 of the complemented siRNA/mRNA (Liu et al., 2004a; Tuschl et al., 1999). This exposes the 5-monophosphate and 3-hydroxyl termini to exonucleases which complete the degradation of the target mRNA (Orban and Izaurralde, 2005).

The process described above only forms a small portion of the complete miRNA pathway where long non-coding dsRNA is processed for gene silencing. The miRNA pathway begins in the nucleus where non-coding RNA produces long primary dsRNA transcripts known as pri-miRNAs. The pri-mRNAs are cleaved into stem-loop structures using the nuclease activity of Drosha (DGC38 protein in mammals), which is a member of the RNase III superfamily (Lee et al., 2003). These 70 nucleotide length products (pre-miRNAs) are exported into the cytoplasm by exportin-5 (Bohnsack et al., 2004; Yi et al., 2003). In the cytoplasm, the pre-miRNAs are cleaved by dicer forming the mature miRNA (Bernstein et al., 2001; Hutvagner et al., 2001; Zamore et al., 2000). These mature miRNAs then can be loaded onto complexes analogous to RISC, known as miRNA ribonucleoprotein complexes (miRNP), which target mRNA for repression or degradation.

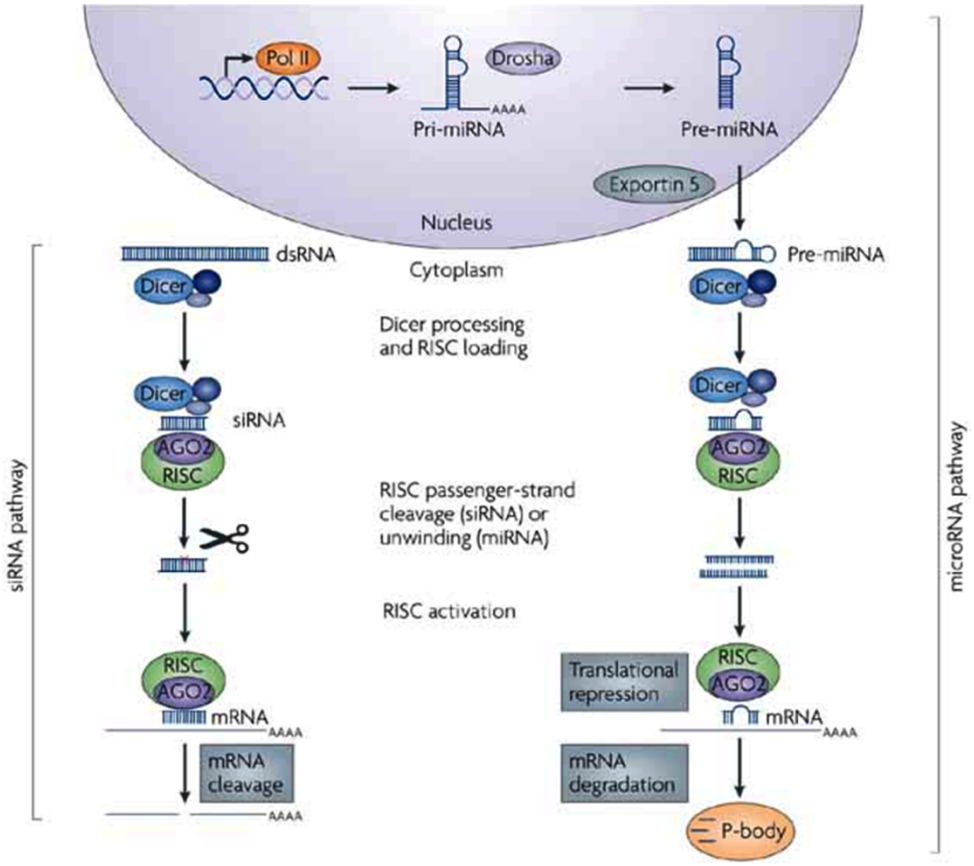

Figure 1.6. siRNA/miRNA mediated gene silencing

miRNA pathway: Immature miRNAs in stem-loop structures are processed by Drosha into pre-miRNAs. The pre-miRNAs are transported into the cytoplasm by exportin-5 and cleaved by Dicer to short 21-23 nucleotide length mature miRNAs. *siRNA pathway*: Similarly, endogenous dsRNA is cleaved by Dicer into short 21-23 nt length siRNAs. Both siRNA and miRNAs associate with a complex of proteins forming either siRISC or miRNP complexes which target mRNA for degradation or repression. Adapted from de Fougerolles *et al*.,2007.

1.12.2 Off-target effects

A major difficulty with screening with siRNA is the unintended downregulation of mRNAs that are not complementary to siRNA guide strand sequence, causing off-target effects. Unwanted outcomes from siRNAs arise from sequence dependent and independent effects (Jackson and Linsley, 2010). Sequence independent effects will not be discussed in detail as they primarily focussed on outcomes of *in vivo* utilisation of siRNAs and have been reviewed in detail by Jackson and Linsley, 2010.

Sequence dependent effects were first identified through microarray profiling of insulin growth factor receptor and mitogen-activated protein kinase 1 (Jackson et al., 2003). The authors demonstrated that different siRNAs targeted against these genes produced distinctly different expression profiles, and attributed these to the pairing of 3' untranslated region (3'UTR) of mRNA to the 5' end of the guide strand (Birmingham et al., 2006; Jackson et al., 2003). This observation was further confirmed by introducing base mismatches at the 5' end of the siRNA seed region for the above targets, resulting in changes to which 3'UTRs were targeted, and triggering altered off-target effects (Jackson et al., 2006b). This demonstrated the importance of the seed region of siRNA in determining which 3'UTRs are targeted, resulting in the undesired off-target events.

These off-target effects translate into unwanted phenotypical changes such as inhibition of cell growth (Jackson et al., 2006b), which was shown to be correlated with the matching of 3'UTRs with the seed region of the siRNA (Jackson et al., 2006a). One method of mitigating off-target effects is by manipulating the guide and passenger strands by chemical modification. A 2′-*O*-methyl ribosyl substitution in the 2nd position in the guide strand results in on average 66% less off-target effects at the transcript levels (Jackson et al., 2006a). In addition, the same substitution in the passenger strand reduces its activity and possibility of it causing off-target effects (Jackson et al., 2006a). In addition to methods aimed at chemical modification of siRNA, simpler methods are available to mitigate their effects.

Another method for reducing off-target effects is through the pooling of different siRNAs that target the same gene (Kittler et al., 2007). This strategy is typically employed when it is unknown which siRNA will provide optimal gene knockdown. The addition of multiple siRNAs introduces competition. Certain siRNAs within the pool will have higher affinity for the target mRNA, thus out-competing the others and ensuring that optimal

silencing occurs (Kittler et al., 2007). Therefore, without a pooling strategy, single siRNAs should be individually validated for their ability to cause sufficient knockdown. Furthermore, the benefit of pooling siRNAs arises from the reduction in off-target effects as the concentration of each single siRNA within the pool is reduced, which in turn decreases the number of 3‘UTRs targeted on unwanted genes (Kittler et al., 2007).

However, re-designing siRNA or pooling siRNA, resulting in less unwanted off target effects does not indicate that the phenotypical changes are genuine. In siRNA screening or target validation, the use of multiple siRNAs, resulting in the same observed phenotype, provides confidence that the effect is real (Jackson and Linsley, 2010). A second approach would be to run a rescue experiment to confirm the phenotype was caused by siRNA mediated silencing. This requires the addition of a functional target gene, introduced by molecular cloning, that has silent mutations at the binding site of the siRNA, thus making it siRNA resistant. However, the rescue experiment is challenging to implement, and the results are difficult to interpret because the level of expression of the siRNA-resistant target gene is frequently different from the endogenous gene (Jackson and Linsley, 2010). Once a method to reliably deplete target genes is identified, an appropriate phenotypical endpoint needs to be chosen which closely reflects the true action of radiotherapy.

1.13 HTS: Endpoints

Since siRNAs were established as an unbiased route to inhibit individual genes, several groups have used siRNAs for high-throughput screening to identify targets that modulate radiosensitivity. In the past, siRNA screens sought to identify radiosensitivity modulating genes using short term *in vitro* cell viability, DNA damage, loss of function and cell proliferation assays (Higgins et al., 2010; Liu et al., 2011; Sudo et al., 2007; Zheng et al., 2008). There are a number of drawbacks with the use of these assays in determining targets that modulate radiosensitivity, which will be discussed below.

1.13.1 Evaluating cell death caused by IR

A large proportion of siRNA screens evaluate short-term endpoints which are typically within minutes to hours after IR treatment. This short time scale also determines the mode of death that can be assessed. In this period the primary mode of cell death is apoptosis (programmed cell death) and the evidence of this was demonstrated by examining the kinetics of apoptosis following radiation treatment (Algan et al., 1996; Fritsch et al., 1994). Although this mode of cell death is important and prevalent in some tissues such as myeloid and lymphoid tissues (Radford et al., 1994), it is not the predominant contributor to cell death following IR in solid tumours (Eriksson and Stigbrand, 2010). Endpoints which evaluate apoptosis are best suited for assessing chemo-resistance, since chemotherapies such as tamoxifen (Zhang et al., 1999a), 5-FU (Nita et al., 1998) and taxol (Park et al., 2004) induce rapid apoptosis in cells (Weller et al., 1995).

The principal method of cell killing triggered by radiotherapy is through mitotic cell death termed mitotic catastrophe (MC) (Roninson et al., 2001). This is characterised by multiple rounds of aberrant mitoses resulting in the formation of giant multinucleated cells (Andreassen et al., 2001; Swanson et al., 1995) with micronuclei and

uncondensed chromosomes (Swanson et al., 1995). MC is brought about by DNA damage in combination with the inefficiency to induce cell cycle checkpoints in cancerous cells. Tumour cells with unrepaired DNA enter mitosis prematurely by overcoming the G2/M checkpoint, which can be in a p53 dependent or independent manner (Castedo et al., 2004). As a result, they will lose their replicative potential and may go on to die by apoptosis or become senescent. However, the key difference between MC and apoptosis is that the cells die from the aberrant mitosis rather than the initial DNA damage induced by IR. Another significant difference between MC and apoptosis is that cells can go through multiple rounds of replication over a number of days and weeks after the initial damage insult in comparison with apoptotic cell death, which typically occurs much more rapidly (Forrester et al., 1999).

1.13.2 Surrogate markers and assays to evaluate RT

Surrogate markers and viability assays evaluating tumour cell survival following radiation have previously been used in radiation sensitivity screens (Ito et al., 2011; Lally et al., 2007; Zheng et al., 2008) but have several limitations.

1.13.2.1 Cell proliferation assays

Bromodeoxyuridine (BrdU) incorporation assays have been used in siRNA screens to identify radiosensitisers (Ito et al., 2011). BrdU is a halogenated pyrimidine nucleoside analogue of thymidine that is incorporated in DNA as replication occurs. Rapidly proliferating cells will incorporate greater amounts of BrdU and this can be quantified through enzymatic or fluorescent labelled antibodies designed to bind this nucleoside analogue. Although this method has been successfully used to identify genes that specifically alter tumour radiosensitivity such as uroporphyrinogen decarboyxlase (UROD) (Ito et al., 2011), it is not examining MC caused by IR, which results in loss of replicative potential. Consequently, short-term cell proliferation assays will exclude

targets that exert their effects over protracted time periods or those that have cellular mechanisms not connected to cell cycle events.

1.13.2.2 Micronuclei assay

A surrogate marker in HTS siRNA screening requires the ability to assess the actual outcomes of IR. The quantification of micronuclei formed following MC is a possible route for determining radiosensitising targets. Micronuclei are small fragments of chromosomes separate to the main nucleus, which typically form by mis-segregation of chromosomes during anaphase. The micronuclei assay involves culturing cells in the presence of cytochalasin-B which blocks cytokinesis, forming binucleated cells, and thus allowing for the quantification of micronuclei which have arisen during mitosis (Fenech and Morley, 1985). Previous groups have demonstrated there is a correlation between radiosensitivity and micronuclei formation (Guo et al., 1999; Liu et al., 2005b; Shibamoto et al., 1991). However, studies on NSCLC cell lines demonstrated the micronuclei assay does not correlate well at clinically relevant doses of 2 Gy and may only be suitable for high dose IR (Bergqvist et al., 2001). In a separate study, cell lines exhibiting varying levels of intrinsic radiosensitivity were tested using the micronuclei assay following 2 Gy IR, and also demonstrated no correlation in the number of micronuclei and their relative intrinsic sensitivity towards radiation (Bush and Mcmillan, 1993). Furthermore, the micronucleus assay is time consuming requiring a complex scoring system (Balmus et al., 2015). Recently a 96-well HTS format of the micronuclei assay has been developed, however this adaptation is used to assess genome instability rather than the cytotoxicity of IR (Balmus et al., 2015).

1.13.2.3 DNA-damage foci quantification

Another successfully employed method of identifying radiosensitising genes is by the quantification of DNA damage foci following IR (Higgins et al., 2010). IR causes a

recruitment of proteins to the site of DSBs and this clustering of proteins can be visualised as specks when tagged by fluorescent antibodies. In the early stages of DNA-damage response, histone H2AX is phosphorylated to γ-H2AX by ataxia telangiectasia mutated (ATM) (Burma et al., 2001), ataxia telangiectasia and Rad3-related protein (ATR) (Ward and Chen, 2001) kinases or DNA-PK*cs* (Stiff et al., 2004). This initiates the recruitment of repair factors and additional effectors. Kinetic studies examining the resolution of γ-H2AX ser 139 phosphorylation following IR at clinically relevant doses demonstrated some correlation between foci number and intrinsic radiosensitivity in various tumour lines (Banath et al., 2004; Klokov et al., 2006; MacPhail et al., 2003). This was further confirmed in hypoxic cells, which demonstrated that there was a greater resolution of γ-H2AX ser 139 phosphorylation post IR compared to anoxic cells (Olive and Banath, 2004). Although this assay has been previously implemented successfully (Higgins et al., 2010), it may only be suitable for identifying targets that directly interfere with DNA repair.

1.13.2.4 Cell growth and survival assays

Short term siRNA screens have tried to find targets by observing the loss of cell viability following radiation treatment (Zheng et al., 2008). The 3-(4,5-Dimethylthiazol-2-yl)-2,5-diphenyl tetrazolium bromide (MTT) assay is typically employed to measure cell viability (Mosmann, 1983). MTT is converted by NADPH dependent oxidoreductase enzymes into insoluble purple formazan. This conversion of MTT to formazan can be measured by a spectrophotometer to determine treatment effects. This assay or its derivations have been used to screen for radiosensitising targets (Ni et al., 2011). However, this assay has technical issues surrounding solubilisation of colorimetric staining, which can introduce significant errors in absorbance readings (Joiner and Kogel, 2009). Furthermore, growth assays may be significantly influenced by external factors that

surround the maintenance of tumour cells in tissue culture environments. Since radiation induces cell cycle arrest slowing proliferation, without altering overall survival to the same extent (Bjork-Eriksson et al., 1999; McGowan et al., 2011), cells that ultimately show clonogenic failure often temporarily continue to proliferate for several generations yielding false negatives (Price and McMillan, 1990).

1.13.2.5 Colony formation assays

The most significant drawback of the above endpoints is that they do not assess the clonal inactivation that is associated with radiation treatment. The true assessment of clonal inactivation (loss of replicative potential) caused by radiation treatment can only be achieved by the colony formation assay and therefore this is the gold standard (Franken et al., 2006). The clonogenic assay is a survival assay that measures whether a single cell can replicate into a colony of cells. A collection of cells is termed a colony if there are greater than 50 cells within the group. Using this technique, all cells can be assayed for mitotic catastrophe. CFAs are often laborious and are carried out in 6-well plates, reducing their appeal for high-throughput screening. However, preliminary work in our lab leading up to this thesis has demonstrated that the colony formation assay can be carried out in a 96-well format, enabling its use for high-throughput assays.

1.14 Proposed siRNA screen

The inhibition of kinases such as DNA-PK*cs* (Gerweck et al., 2006), ATM (Sarkaria et al., 1999), ATR (Sarkaria et al., 1999), CHEK1 (Morgan et al., 2010), CHEK2 (Morgan et al., 2010) and PLK-1 (Lund-Andersen et al., 2014) have been shown to cause increased radiosensitivity in cancer. Many of the kinases are involved in DNA repair or cell cycle signalling. Although pronounced radiosensitisation can be achieved following the inhibition of such targets, the effects on normal tissue dampen the benefits, thus constraining the therapeutic window for radiotherapy delivery. As a consequence, novel targets are required that modulate tumour radioresistance and do not affect normal tissue intrinsic radiosensitivity. As explained previously, our lab had recently developed a 96-well version of the colony formation assay, enabling us to screen for novel radiosensitising targets in a high-throughput approach using the gold standard endpoint for assessing the effects of radiotherapy (Franken et al., 2006). This thesis will discuss the use of a high-throughput CFA screen using siRNA targeted against 709 kinases (‘kinome’).

1.15 Aims of thesis

The main aim of this thesis is to discover and investigate novel molecular determinants of tumour radiosensitivity, which have the potential to be clinically exploitable or provide prognostic information. The objectives are outlined as follows:

1) Perform a high-throughput siRNA screen targeted against 709 kinases with colony formation as an endpoint to discover novel radiosensitising genes.
2) Investigate the targets from the siRNA screening for tumour specific effects using conventional CFAs and to investigate the molecular mechanisms behind the radiosensitisation.
3) Investigate if over-expression of the targets results in worse clinical outcomes in cancer patients.

CHAPTER 2

MATERIALS AND METHODS

2.1 Cell culture

2.1.1 Cell line maintenance

HeLa (cervical), MRC5 (lung fibroblast), HFL-1, (lung fibroblast), T24 (bladder), PSN-1 (pancreatic), PANC-1 (pancreatic), MCF-7 (breast), H460 (lung), CAL51 (breast), BT-549 (breast) cell lines were purchased from American Type Culture Collection (ATCC). SQ2OB (head and neck) cells were provided by Dr. Ralph Weichselbaum (University of Chicago, Chicago, IL). HeLa, PSN-1, MCF7, CAL51, BT-549 and PANC-1 cells were maintained in Dulbecco's modified Eagle's medium (DMEM, Sigma) supplemented with 10 % foetal bovine serum (FBS). T24 and H460 cell line was maintained in Roswell Park Memorial Institute (RPMI)-1640 (Sigma) media supplemented with 10% FBS. MRC5 cells were maintained in minimum essential medium (MEM, Sigma) supplemented with 10% FBS. HFL-1 cells were maintained in DMEM/F-12 Ham media supplemented with 10% FBS. Cell lines were never grown beyond four months after purchase. The HeLa cell line, which had been cultured for a longer period, was authenticated by LGC standards (ATCC) by short tandem repeat (STR) profiling. The SQ20B cell line was authenticated by Professor Ruth Muschel using STR profiling and has not varied over time. All cell lines were tested for mycoplasma using MycoAlert (Lonza).

2.1.2 Cell line storage and resuscitation

Cells were kept in cryovials stored in liquid nitrogen vapour phase. Cells were thawed rapidly in a water bath at 37^0C. Cells were immediately diluted in 10 mL of media in a 50 mL falcon tube and centrifuged at 240 x *g* for 5 minutes. Media was removed and re-suspended in 10 mL of media and seeded into a T75 flask. MRC5, HFL-1 and IMR-90 were initially seeded into T25 flasks.

2.1.3 Passaging cell lines

Media was removed from cells cultured in T75 flasks. Cells were washed in 5-10 mL of phosphate buffered saline (PBS) and 3 mL of trypsin-ethylenediaminetetraacetic acid (EDTA) was added to the flask as a wash and 2.5 mL of trypsin-EDTA removed immediately. Cells were returned to the 37^0C incubator for 5-10 minutes. Medium was added after cells had lifted, and the cell suspension was diluted appropriately in medium (Typically: 1:10, 1:12 or 1:20 dilutions) and returned to the incubator. Cell lines were passaged for a maximum of 3 weeks (passaged when cells reached ~60-80 % confluence). Cells were cultured in incubators at 37°C supplied with 5% CO_2.

2.1.4 Cell counting

Cells were trypsinised as described above. A 50 µL cell suspension was diluted 1:10 in DMEM within a microcentrifuge tube and counted using the Scepter 2.0 (Millipore) hand held automated cell counter.

2.2. Chemicals

All chemicals were purchased from Sigma, unless stated otherwise. Solutions were prepared using reverse osmosis (RO) water.

2.3. High-throughput screening

2.3.1 siRNA libraries

2.3.1.1 Primary screening library

The 96-well colony formation assay (CFA) described below utilised a commercially available ‘kinome’ siRNA library. The ‘kinome’ library contained 709 ON-TARGET*plus* (Dharmacon) pooled siRNAs (4 strands per gene) against protein kinases (641 siRNAs) and other targets which include enzymatic processes, transmembrane receptors, transcription factors/regulators, regulatory subunits,

ligands, potassium channels, ER associated proteins, chromatin remodelling, pseudokinases, scaffold/tight junctions, nucleoporins and uncharacterised proteins.

2.3.1.2 Secondary screening libraries

A secondary screen was carried out for the 'kinome' siRNA library eliminating the chances of discovering false positives resulting from off-target effects of the siRNA. A custom-made secondary kinome library was created by 'cherry picking' from an in-house siGENOME kinome library (Dharmacon). The top-76 siRNA from the primary kinome screen runs were chosen for the custom library based on the lowest radiosensitivity scores (R-scores) ordered by rank-product analysis (see screening statistical analysis).

2.3.2 96-well reverse transfection

HeLa cells were reverse transfected with ON-TARGET*plus* or siGENOME library plates at 20 nM final concentration using Dharmafect1 (Dharmacon) transfection reagent at a final concentration of 0.1 µL/well.

2.3.2.1 siRNA plate preparation

Transfections were carried out in weekly batches consisting of twelve siRNA library plates. First, 10 µL of 0.4 µM siRNA from library plates was transferred using the 96-tip pipetting unit from the Janus automated workstation (PerkinElmer) into empty V-bottom plates. Control siRNAs were added manually to V-bottom plates in columns 1 and 12 as illustrated in the plate map shown in Figure 2.1. Control siRNA consisted of non-targeting (NT), untransfected (UN), DNA-dependent protein kinase catalytic subunit (DNA-PK*cs*) and polo-like kinase-1 (PLK-1).

	1	2	3	4	5	6	7	8	9	10	11	12
A	PLK	LIBRARY	LIBRARY	LIBRARY	LIBRARY	LIBRARY	LIBRARY	LIBRARY	LIBRARY	LIBRARY	LIBRARY	DNA-PK*cs*
B	NT	LIBRARY	LIBRARY	LIBRARY	LIBRARY	LIBRARY	LIBRARY	LIBRARY	LIBRARY	LIBRARY	LIBRARY	UN
C	NT	LIBRARY	LIBRARY	LIBRARY	LIBRARY	LIBRARY	LIBRARY	LIBRARY	LIBRARY	LIBRARY	LIBRARY	UN
D	NT	LIBRARY	LIBRARY	LIBRARY	LIBRARY	LIBRARY	LIBRARY	LIBRARY	LIBRARY	LIBRARY	LIBRARY	NT
E	NT	LIBRARY	LIBRARY	LIBRARY	LIBRARY	LIBRARY	LIBRARY	LIBRARY	LIBRARY	LIBRARY	LIBRARY	NT
F	UN	LIBRARY	LIBRARY	LIBRARY	LIBRARY	LIBRARY	LIBRARY	LIBRARY	LIBRARY	LIBRARY	LIBRARY	NT
G	UN	LIBRARY	LIBRARY	LIBRARY	LIBRARY	LIBRARY	LIBRARY	LIBRARY	LIBRARY	LIBRARY	LIBRARY	NT
H	DNA-PK*cs*	LIBRARY	LIBRARY	LIBRARY	LIBRARY	LIBRARY	LIBRARY	LIBRARY	LIBRARY	LIBRARY	LIBRARY	DNA-PK*cs*

Figure 2.1. siRNA library plate layout.
Controls are located on the edge columns 1 and 12. A total of eight non-targeting (NT), one PLK1 siRNA (transfection control), three DNA-PK*cs* siRNA (DNA-PK*cs*; positive radiosensitisation control), and four untransfected (UN) wells are found in columns 1 and 12. Library siRNA are located on columns 2 through 11.

2.3.2.2 Preparation of cell plates and cell lifting

Twelve flat bottom 96-well plates were filled with 30 µL of DMEM 10% FBS Pen/Strep using the FlexDrop (PerkinElmer) 8-channel precision reagent dispenser. Three T75 flasks containing HeLa cells (70-80% confluent) were trypsinised and counted. Next, 300 mL of HeLa cells at a concentration of 80,000 cells/mL was prepared in a sterile glass bottle with stirrer and was connected to the FlexDrop.

2.3.2.3 siRNA complex formation and cell addition

A working stock of DharmaFECT-1 transfection reagent was prepared, by adding 420 µL DharmaFECT-1 to 42 mL of DMEM serum free medium, which was then added to deep-well plates (2 mL volume 96-well plates) at 420 µL of DharmaFECT-1 dilution per well.

For each library plate transfection, 30 µL of the DharmaFECT-1 dilution was transferred from the deep-well plate using the Janus 96-tip pipetting unit to the V-bottom siRNA plates containing 10 µL siRNA and mixed. The siRNA and transfection reagent mix was left for 20 minutes at room temperature to allow for siRNA complex formation. Next, 20 µL of the transfection mix from the V-bottom siRNA plates was

transferred using the Janus 96-tip pipetting unit to the cell plates containing 30 µL DMEM medium. Then, 50 µL of HeLa cell suspension (4000 cells total from 80,000/mL) was added to the cell plates using the FlexDrop. Plates were incubated at room temperature for 20 minutes before incubating at 37°C (5 % CO_2). Plates were left in the incubator for 72-hours at 37°C (5 % CO_2).

2.3.2.4 Lifting and plating

At 72 hrs post transfection, cells were lifted and plated for irradiation. To ensure correct cell plating numbers, a single non-targeting siRNA well from a transfection plate was washed with PBS, lifted using trypsin-EDTA and counted to calculate the volume of cell suspension that provided 9600 cells (for the siNT wells). In preparation for the high throughput lifting procedure, 48 x 96-well flat bottom plates were filled using the FlexDrop with 176 µL DMEM Pen/Strep and 12 x 2 mL deep-well plates were filled with 1350 µL DMEM Pen/strep minus the volume required for 9600 cells.

The 12 siRNA transfection plates were lifted in a staggered approach with 10 minutes between each plate. Each transfection plate was manually aspirated, washed with 50 µL trypsin-EDTA and incubated with 50 µL trypsin-EDTA per well for 10 minutes at 37°C (5 % CO_2). Using the Janus 96-tip unit, 150 µL of DMEM Pen/Strep was transferred from a deep-well plate to each well of the transfection plate. The cells were re-suspended with multiple mixing steps and the volume containing for 9600 cells was transferred from each well to the corresponding well of the deep-well plate using the Janus 96-tip unit producing a 1.2 mL 8000 cells/mL working cell stock for each well. After thorough mixing the deep-well plate at different depths, 24 µL (approximating 192 cells for siNT wells) of the working cell stock was transferred to four flat bottom 96-well plates containing 176 µL DMEM Pen/Strep

prepared previously. Next, 200 µL (approximating 1600 cells for siNT wells) of the working cell stock was transferred to four empty flat bottom 96-well plates. Plates were left at room temperature for 20 minutes to reduce the risk of edge effects. At this stage the next transfection plate would be ready for plating procedure, having started incubation in trypsin-EDTA 10 min earlier. Plates were returned to the incubator for 4-hours at 37°C to allow for cell adherence. In summary, all twelve transfection plates were lifted and plated out into quadruplicate repeat 96-well plates, either containing 192 (untreated plates) or 1600 (irradiated plates) cells.

2.3.3 Irradiation

Treatment plates were irradiated in batches of 24 within a 2 cm thick tissue-equivalent Perspex phantom. The phantom was irradiated with 6 MV photons at a dose rate of 600 MU/min delivered using a Varian IX linear accelerator at gantry angles of 0 and 180 degrees to a total dose of 7 Gy. Cross-sectional film dosimetry tests confirmed the accuracy of this technique to +/- 3 % of intended dose for each well of the 96-well plate. Following irradiation, treatment plates were returned to the incubator to allow for colony formation.

2.3.4 Staining and counting

Plates were taken out of the incubator either at day 6 (untreated) or day 8 (treatment) post IR. Media was aspirated using the BioTek ELx405 microplate washer. Next 20 µL of 0.5% crystal violet stain (10% ethanol, 50% Methanol and 40 % H_20) was added per well using the MultiDrop 8-channel automated dispenser (Thermofisher) and left at room temperature for 2 minutes. Plates were washed three times with H_20 using the microplate washer to remove staining solution. Colonies were counted using the GelCount colony counter (Oxford Optronix).

2.3.5 Screening statistical analyses

Plates were analysed by averaging the colony counts for the quadruplicate repeats for both untreated and treated plate wells. Plating efficiencies (PE) for the untreated and treated plates were calculated:

$$PE = Average\ Colony\ Number / Cells\ plated$$

siRNA knockdowns that had $PE_{untreated} < 0.05$ were excluded from the analyses. Surviving fractions (SF) were calculated for all remaining siRNA knockdowns:

$$SF = (\mathrm{PE})_{treated} / (\mathrm{PE})_{untreated}$$

The SF for each target siRNA were normalised to the median non-targeting (NT) SF on each library plate. A radiosensitisation score (R-score), comparing each library siRNA to the median of the NT wells across all library plates, was calculated from the normalised SF:

$$R-score = \left(Normalised\ SF - 1\right) / \left(Mean\ absolute\ deviation\ of\ normalised\ NT\ SF\right)$$

R-scores were ranked in ascending order and a rank product analysis carried out for the replicate runs for primary and secondary siRNA libraries (Birmingham et al., 2009). The rank product and the estimate percentage of false positives (pfp) were obtained using the method described by Breitling and collegues (Breitling et al., 2004). The rank product was calculated by multiplying the rank value of each siRNA from the screening runs, and dividing this by the total number of siRNA to the square of the number of replicates. Dr Sheng Yu, working in the Computational Biology and Integrated Genomics group, has implemented this algorithm in Python modifying the original *rankprod* package in R (http://www.cran.org), and run the analysis for us. Briefly, this method computes the pfp using permutation (here N=100); it estimates the significance of observing a rank product based on combined probability from all repeated runs and establishes rank value orientations that are unlikely.

The likelihood of observing the rank product for a siRNA is then calculated by running 100 permutations of the possible rank values and converting this to an Expect (E) value. Z-factors were calculated to assess the robustness of the screening data using the formula (Zhang et al., 1999b):

$$\text{Z-Factor} = 1 - \frac{3(\sigma_{SF_{NT}} + \sigma_{SF_{DNA-PKcs}})}{|\mu_{SF_{NT}} - \mu_{SF_{DNA-PKcs}}|}$$

μ=Mean σ= Standard deviation

Heat-maps were produced to visualise the reproducibility between runs.

2.4 Six-well siRNA transfections

2.4.1 siRNA sequences

Validation and mechanistic studies used Ambion Silencer Select siRNA (Life Technologies). The sense strand sequences for the individual genes were as follows: **TPK1** (TPK1-1) GGAGACUUUGAUUCUAUUA, (TPK1-2) GCCUUUGGACAACUAUUUU, **THTR1** GCCUUAUUGUUACAUGGUU, **TPC** GACCAUGUAUAGGAGCGAA, **PLK-1** CCAUUAACGAGCUGCUUAA, **SRP72** GGACAAGUGUUAUACCGUU, **MARK2** GCCUAGGAGUUAUCCUCUA and **GSK3β** CUCAAGAACUGUCAAGUAA.

2.4.2 Reverse transfection protocol

Validation studies used a reverse transfection protocol with a final siRNA concentration of 20 or 40 nM depending on cell line. INTERFERin-HTS (Polyplus) or lipofectamine 2000 (Life technologies) transfection reagent concentrations were optimised for each cell line. Typically, transfections in 6-well plates were carried out in duplicate wells, subsequently enabling knockdown confirmation by western blot or RT-PCR.

Transfection reagent complexes were formed in 1.5 mL microcentrifuge tubes using conditions stated in Table 2.1. Tubes were incubated at room temperature for 20 minutes for complex formation. Complexes were transferred to 6-well plates. Then 2 mL of cell stock/well was added to the transfection mix and returned to the incubator. At 72-hours post-transfection, transfected cells were re-plated for clonogenic assays, immunofluorescence and knockdown confirmation by Western blotting or qRT-PCR.

Cell line	siRNA final concentration (nM)	INTERFERin concentration (µL/well)	Lipofectamine 2000 concentration (µL/well)	Final cell concentration
HeLa	20/40	1.0	-	$1.8*10^5$
PSN-1	20	1.6	-	$1.6*10^5$
SQ20B	20	1.2	-	$1.6*10^5$
T24	20	1.4	-	$1.2*10^5$
BT-549	40	2		$2*10^5$
CAL51	40		5	$2*10^5$
MCF-7	40	2		$2*10^5$

Table 2.1 Six-well siRNA complex formation.
List of reagents prepared for each cell line for a single well siRNA transfection

2.4.3 Six-well colony formation assay

At 72-hours post siRNA transfection, cells were lifted using trypsin-EDTA and re-suspended in 2 mL of the appropriate media. Cells were counted and 4 mL of working cell suspension prepared. The working stock was plated in triplicate wells of 6-well plates containing 2 mL of media at cell densities for the required radiation

dose. Table 2.2 shows the cell number added in triplicate for the different radiation doses.

Cell line	Number of cells plated/well			
	0 Gy	**2 Gy**	**4 Gy**	**6 Gy**
HeLa	200	400	800	1600
PSN-1	200	400	800	1600
SQ20B	400	800	1600	3200
T24	200	400	800	1600
CAL51	750	1500	3000	7500
MCF-7	1000	2000	4000	10,000
BT-549	750	1500	3000	7500

Table 2.2 Plating numbers at different radiation doses

List of cell lines and the number of cells plated at each radiation dose to be used in 6-well plate colony formation assays

Plates were returned to the incubator for 4 hours to allow for cell adherence prior to irradiation. Plates were irradiated at 2, 4 and 6 Gy by caesium-137 irradiator, Gamma Service: GSR D1; dose rate 1.938 Gy/min. Plates were incubated for 7-18 days (cell line dependent) at 37°C for colony formation and cells were stained with crystal violet. Plates were counted using the GelCount colony counter (Oxford Optronix).

2.4.4 Statistical analysis for 6-well CFA

The effect of siRNA knockdown or inhibitor on the dose survival curves were estimated by two methods.

1. Initially the survival data was curve fitted using GraphPad Prism by non-linear regression of the linear quadratic equation:

$$S = \exp^{-(\alpha D + \beta D^2)};$$

S denoting survival probability, D (Gy) is radiation dose and *α* (Gy^{-1}) and *β* (Gy^{-2}) are parameter constants. The magnitude of the siRNA/inhibitor effect was determined by calculating the sensitisation enhancement ratio at 10% surviving fraction (SER_{10}) using α (Gy^{-1}) and *β* (Gy^{-2}) estimated coefficients:

$$SER_{10} : \mathrm{D}_{untreated} / \mathrm{D}_{treated}$$

$D_{untreated}$ and $D_{treated}$ values were calculated using α (Gy^{-1}) and *β* (Gy^{-2}) coefficients that yielded 10% survival by solving the quadratic equation below:

$$\beta D^2 + \alpha D - 2.3026 = 0$$

2. To demonstrate if the siRNA knockdown or inhibitor was having a statistically significant effect, an indicator variable was introduced to specify targeting and non-targeting condition as described previously (Chalmers et al., 2007). A factorial 2-way ANOVA was performed with survival as the dependent variable and dose levels (2, 4 and 6 Gy) and treatment (control, siRNA/DMSO) as the two factors; interaction between dose and treatment was estimated. *P*-values produced are for interaction between drug and dose.

2.5 Thiamine analogue treatment

HeLa cells were seeded at 2 x 10^5 per well of 6-well plates and incubated for 96 hours in 10 μM pyrithiamine hydrobromide (PyrH, SIGMA) in low thiamine medium (M199; SIGMA) supplemented with 10 % FBS. Plates were then irradiated as described above. At 4 hours post irradiation, cells were trypsinised and re-plated for CFA or immunofluorescence.

2.6 HPLC

HeLa cells were seeded for high performance liquid chromatography (HPLC) in 15 cm dishes at concentration of 1 x 10^6. Cells were incubated with 10 μM PyrH in M199 media 10 % FBS for 96 hours. Treated cells were trypsinised, re-suspended, counted and pelleted by centrifugation at 200 x *g* for 5 minutes. The cells were washed with PBS and centrifuged for a further 5 minutes at 200 x *g* for 5 minutes. Cells were lysed in 6 % Trichloroacetic acid (TCA) and stored at -80°C until dinucleotide triphosphate (dNTPs) extraction. Samples were thawed and diluted to a final concentration of 2.6 % TCA using Milli-Q water. Freon (1, 1, 2 trichlorotrifluorethane): trioctylamine at a ratio of 4:1 was used to neutralise the samples and 40 μL of the aqueous supernatant was injected for chromatography. The chromatography was performed on a Waters 2695 system with a monitoring wavelength of 254 nM. The Ace (3 μM, 3 × 125 mm) chromatography column was sustained at 30°C and samples kept at 10°C. The separation of the sample was carried out with Waters Acc-Q Tag Ultra eluent A (10 mM potassium dihydrogen phosphate, 10 mM tetrabutylammonium hydroxide, 10 % methanol at pH 6.9) and eluent B (50 mM potassium dihydrogen phosphate, 6 mM tetrabutylammonium hydroxide, 30 % methanol at pH 7). A flow rate of 600 μL/minute with a gradient of 25%–80% was utilised over 20 minutes. Quantification of dNTPs was carried out

using commercially available nucleotides as standards. The HPLC procedure was carried out by Dr Lisa Folkes within the department.

2.7 SDS-Page and Immunoblotting

2.7.1 Buffers and reagents

Buffers	Formulation and preparation
10 x Protein running buffer (PRB)	0.2 M Tris base with 0.09 M glycine in dH_20
Western transfer buffer	200 mL Methanol, 100 mL 10x running buffer (PRB), made up to 1 L with dH2O
Stripping buffer purchased from Millipore Cat No. 2502	ReBlot Plus Mild Antibody Stripping Solution, 1:10 dilution with H2O
LDS Sample Loading Buffer *(4X)* purchased from Expedeon Cat No. NXB31010 Supplemented with 50 mM of Dithiothreitol (DTT) reducing agent	40 % glycerol, 4 % lithium dodecyl sulfate (LDS), 4 % Ficoll*- 400, 0.8 M triethanolamine-Cl pH 7.6, 0.025% phenol red, 0.025% coomassie G250, 2mM EDTA disodium
Lysis buffer: RIPA Lysis buffer purchased from Thermoscientific Cat No. 89900 supplemented with protease inhibitor Roche Cat No.11836153001	1 mL of RIPA lysis buffer: 25 mM Tris-HCl (pH7.6), 150 mM NaCl, 1 % NP-40, 1 % sodium deoxycholate, 0.1% SDS 143 µL of 7x protease inhibitor

Table 2.3. Buffers for western blotting

List of buffers and their composition

Reagents and materials	Formulation/Preparation
TBS-T	100 mL 10xTBS, 1 mL Tween to 1 L with H2O
Blocking Reagent	TBST-Marvel (10 % w/v Marvel in TBST
Immobilon Western Chemiluminescent HRP Substrate. Millipore, Catalogue Number : WBKLS0500	
SuperSignal West Pico Chemiluminescent Substrate Thermoscientific Cat No. 34080	
Nitrocellulose	
PVDF	
TBS-T-BSA	TBS-T + 5 % w/v BSA
TBS-T-Marvel	TBS-T + 5 % w/v Marvel
RunBlue® pre-cast gels	
BCA protein assay kit Thermoscientific- Product code: 23225	Reagent A- sodium carbonate, sodium bicarbonate, bicinchoninic acid and sodium tartrate in 0.1 M sodium hydroxide Reagent B- 4 % cupric sulfate

Table 2.4. Reagents and materials for western blotting

List of materials and reagents and their composition

2.7.2 Protein lysates preparation

Cells were lysed in RIPA lysis buffer (100 µL per well of a 6-well plate) using a cell scraper. Cell lysates were transferred to 1.5 mL microcentrifuge tubes and incubated on ice for 5 minutes and sonicated for 10 seconds. Lysates were spun down at 28, 620 x g in a 4°C centrifuge for 10 minutes. Supernatants were transferred to fresh microcentrifuge tubes and stored a -20°C until further use.

2.7.3 Protein level quantification

Protein extracts were checked for total cellular protein levels using a bicinchoninic acid assay (BCA) kit (Thermoscientific) according to the manufacturer's instructions. Briefly, 2 µL of protein lysates was pipetted in duplicate into a 96-well plate. A standard curve of concentrations was produced using bovine serum albumin (BSA); concentrations ranged between 0 µg/mL to 2000 µg/mL. Reagent A and B from the kit was combined with a 50:1 ratio. Then 200 µL of the reagent mixture was added to each well containing sample or standard and incubated at 37ºC for 30 minutes. The absorbance was read at a wavelength of 562 nM using the POLARstar Omega (BMG Labtech). Protein concentrations for samples were calculated using the standard curve.

2.7.4 SDS-Page

RunBlue pre-cast 4-12% gradient SDS-PAGE gels together with RunBlue running and loading buffer were purchased from Expedeon. Loading buffer (1/4 volume) was added to protein extracts and denatured for 10 minutes at 72°C in a heat block prior to loading and 15-30 µg of protein sample was loaded per lane of a SDS-PAGE gel. Precision plus protein standards (dual colour standards) purchased from Bio-Rad were run alongside all samples. Gels were run for 1 hour at 180 V.

2.7.5 Immunoblotting

The XCell II™ Blot Module (Invitrogen) was used to set up the transfer. Hybond nitrocellulose transfer membrane (GE-healthcare) and SDS gel were sandwiched between two sheets of Whatman paper and compressed with sponges. Protein was transferred onto the nitrocellulose membrane in Tris Glycine transfer buffer at 30 V for 1 hour. Next, membranes were blocked in 5 % Marvel diluted in Tris buffered saline with 1 % Tween (TBS-T) for 1 hour at room temperature. Primary antibodies were diluted to manufacturer's recommendations in 5 % BSA/TBS-T or 5 % Marvel/TBS-T. A list of all antibodies and their working concentrations can be found in Table 2.5.

Gene	Protein description	Western blot dilution	Protein Size kDa	Host	Cat #
DNA-PK$_{cs}$	Purified Mouse anti human DNA-PKcs antibody	1:500	450-465	Mouse	BD Pharmingen Cat No.556456
β-Actin	β-Actin antibody	1:10000	45	Mouse	Sigma A1978
Anti-rabbit secondary antibody	ImmunoPure Goat Anti-Rabbit IgG (H L), peroxidase conjugated	1:10000		Rabbit	Thermoscientific 31460
Anti-mouse secondary antibody	ImmunoPure Rabbit Anti-mouse IgG (H L)	1:10000		Mouse	Thermoscientific 31335
TPK1	Anti thiamine pyrophosphokinase-1 rabbit Polyclonal	1:1000	28	Rabbit	ProteinTech 10942-1-AP
SRP72	Anti- signal recognition protein-72 kDa	1:1000	72	Rabbit	Epitomics, T1841
MARK2	Anti rabbit polyclonal	1:500	78,82	Rabbit	Cell signaling #9118
GSK3β (27c10)	Anti rabbit monoclonal	1:10000	46	Rabbit	Cell signaling #9315s
PARP-1 (F-2)	Anti mouse monoclonal	1:2500	116	Mouse	Santa Cruz, sc-8007

Table 2.5 Antibody list.

Details of antibodies and the recommended western blot dilutions

Primary antibody incubations were performed overnight at 4°C. Three washes with TBS-T were carried out between primary and secondary antibody incubation. Secondary HRP-conjugated anti-mouse and anti-rabbit antibodies (Thermofisher) were diluted to a concentration of 1:10,000 in 5 % Marvel/TBS-T apart from β-actin

probed membranes, which were probed with a secondary anti-mouse concentration of 1:50,000. Membranes were washed 3 times in TBS-T and incubated with Immobilon Western Chemiluminescent HRP Substrate *(*Millipore*)*. Membranes were visualised using photographic film.

2.7.6 Stripping and re-probing

Blots were stripped in 10 mL stripping buffer (Millipore) for 15 minutes at room temperature. The membrane was washed in TBS-T for 5 minutes. The blots were re-blocked in 5 % Marvel/TBS-T and incubated with desired antibodies.

2.7.7 Densitometry

Semi-quantitative protein densitometry was conducted in ImageJ software. Protein bands were segmented using equal size rectangles and intensity profiles produced. The area under each intensity peak was calculated using the wand tool and normalised to actin. The fold change in protein levels for treated vs. control samples was calculated by dividing the normalised peak areas.

2.8 Immunofluorescence

For DNA damage foci analysis, siRNA-transfected or thiamine analogue-treated HeLa cells were re-plated in 96-well plates. At various time-points following IR treatment, cells were washed with 200 µL PBS and fixed with 100 µL 3 % paraformaldehyde (in PBS) for 10 minutes. After washing with 200 µL PBS cells were blocked and permeabilised in 100 µL PBS with 0.1 % Triton, 1 % BSA and 1 % Goat serum at room temperature for at least 1 hour. Blocking buffer was removed and cells were probed for γH2AX Ser139 (Upstate/Millipore, #05-636) and 53BP1 (Cell Signaling Technology, #4937S) antibodies at a concentration of 1/1500 and 1/800, respectively diluted in 1 % BSA, 1 % Goat serum (in PBS) overnight at 4°C. Plates were washed thrice with 200 µL PBS with the second wash lasting 10

minutes. Alexa Flour 488 goat anti-mouse (Invitrogen # A11001, 1:2000), Alexa Fluor 568 Goat Anti-Rabbit (Invitrogen # A11011, 1:2000) conjugated secondary antibodies and 6-diamidino-2-phenylindole (DAPI, 0.5 µg/mL) were incubated for at least 1 hour in the dark. Once more, plates were washed thrice with 200 µL PBS. Foci were detected using the IN Cell Analyzer 1000 automated epifluorescence microscope (GE Healthcare). Foci were quantified using the IN Cell Analyzer Workstation software (v3.5). A minimum of 500 cells per well were counted.

2.9 Quantitative real time PCR

2.9.1 Total RNA sample preparation

Cells grown in 6-well plates had their medium aspirated and were frozen and stored at -80°C. Total RNA was extracted using GenElute kit (Sigma) according to the manufacturer's instructions. Briefly, plates were thawed and lysed in 250 µL of lysis buffer. Lysates were cleared on a filtration column, mixed with 1 volume of 70 % ethanol and transferred to the GenElute binding column. Following three washes, RNA was eluted from the column with 40 µL of elution buffer. RNA concentration was determined by A260 measurement (Nanodrop). The 260/280 ratio was around 1.9 - 2.1; the 260/230 ratio between 2 and 2.2.

2.9.2 cDNA preparation

Following RNA extraction, cDNA was prepared from 500 ng total RNA using Affinity script cDNA synthesis system for RT-PCR (Agilent Technologies) according to the manufacturer's instructions. Each cDNA reaction was prepared as follows:

1. 10 µL of 2x first strand master mix
2. 3 µL of oligo (dT) and random primers (0.1 µg/µL)
3. X- volume of 500 ng RNA
4. 1.0 µL of AffinityScript RT/ RNase Block enzyme mixture

   Made up to 20 µL with RNAse free H_20

The samples were then incubated for 25°C for 5 minutes and 42°C for 5 minutes to enable primer annealing followed by cDNA synthesis at 55°C for 45 minutes. The reaction was terminated by incubation at 95°C for 5 minutes.

2.9.3 qRT-PCR

Following cDNA synthesis, qPCR was carried out using Brilliant II SYBR Green (Agilent Technologies) on a MX3005P qPCR machine (Agilent Technologies). A final primer concentration of 0.2 µM and 2 µL cDNA template in 20 µL reaction volume was used. GAPDH amplification was used as a normalising control. Primer sequences were designed using NCBI Primer-BLAST/Primer3 software and always spanned exon-exon junctions. HPLC-purified primers were ordered from Eurofins MWG Operon. Amplifications were conducted as follows: 95°C for 30 s, 58°C for 30 s, and 72°C for 60 s for 40 cycles, followed by a melting curve analysis cycle.

Primer forward (F) and reverse(R) sequences 5' to 3' were:

GAPDH-F	CCGCATCTTCTTTTGCGTCGC
GAPDH-R	AAATGAGCCCCAGCCTTCTCCATG
TPK1-F	TCGTGACACTGGGAGGCCTTG
TPK1-R:	ACCTGTGCTTTCCTGGTTGGAGC
THTR1-F:	ACCGAGAGGGAGGTCTTCAA
THTR1-R	AGCCCCTGCAGTAGAACAAC
TPC-F:	GGAGCTAGAGAGAGCGGAGA
TPC-R	CATCAGTATCAAGATACGGTCTGT

Ct values were converted into relative copy number and normalised to GAPDH control.

2.10 FACS

2.10.1 Cell cycle analysis by propidium iodide staining

Cells were lifted using Trypsin-EDTA, re-suspended in medium, transferred to fluorescence-activated cell sorting (FACS) tubes and pelleted by centrifugation at 200 x g for 5 minutes. Media was aspirated and cells were fixed in ice-cold 70% Ethanol. Samples were stored at 4^{o}C until ready for analysis. Samples were then centrifuged at 400 x g for 5 minutes and ethanol removed. After a PBS wash to remove all ethanol, 300 µL propidium iodide (PI) staining solution (50 µg/mL PI, 200 µg/mL RNase) was added. Cells were vortexed briefly and incubated at room temperature in the dark for 30 minutes. Stained cells were analysed using the BD FACS scan flow cytometer. Histogram plots were fitted with ModFit software.

2.10.2 Annexin-V/ Propidium iodide staining

Cells were stained with annexin-V/ propidium iodide using the Annexin-V-FLUOS staining kit (Roche) as follows. Cells were lifted and re-plated into 12-well plates at a concentration of 1x10^{5} and left to adhere for 4 hours at 37^{o}C prior to irradiation. Cells were irradiated at 6 Gy and left for 24, 48 or 72 hours at 37^{o}C until staining was carried out. Cells were washed with PBS, lifted in trypsin-EDTA, re-suspended in medium and transferred to FACS tubes and spun down at 200 x g for 5 minutes. The pellet was washed with 1 mL PBS and re-suspended in 100 µL of Annexin-V staining solution (2 µL Annexin-V and 2 µL propidium iodide diluted in 100 µL incubation buffer per sample). FACS tubes were vortexed briefly and placed in the dark at room temperature for 15 minutes. Samples were run on the CyAn ADP Analyzer (Beckman Coulter).

2.11 Caspase 3/7 activity assay

Cells were plated at 3000 per well (4000 for irradiated plates) into 96-well plates and left to adhere for 4 hours at 37 ^{o}C prior to irradiation. Cells were irradiated at 6 Gy and left for 72 hours at 37 ^{o}C and assayed using the Caspase Glo 3/7 assay (Promega). Prior to caspase activity measurement, cells were first incubated with 10 µg/mL resazurin (Sigma) in medium for 1 hour to measure the number of viable cells and fluorescence 560Ex/590Em was measured on a POLARstar Omega plate reader. Subsequently, one volume of Caspase Glo solution was added, plates were left for 1 hour at room temperature and luminescence was read using a POLARstar Omega plate reader. Luminescence values were normalised to cell viability fluorescence values to account for cell number differences between wells.

2.12 Resazurin assay

Viability of HeLa cells following treatment was measured by the conversion of resazurin sodium salt (Sigma) to fluorescent resorufin. A working stock of 10 µg/mL resazurin diluted in PBS was made. The working stock was added to cells in a 1/10 ratio (e.g. 10 µL working stock to 100 µL medium). Cells were incubated for 1 hour at 37°C and fluorescence measured on a POLARstar Omega plate reader at 560Ex/590.

2.13 Statistical analysis

Unpaired two-sided students t-tests comparing treatment to control were carried out in GraphPad Prism (v5).

2.14 Prognostic analysis

Prognostic meta-analysis was carried out by Dr. Francesca Buffa. The methods, selection and curation of datasets for the meta-analysis based on GEO cohorts have been described previously (Buffa et al., 2010) . Briefly, the prognostic meta-analysis was carried out using the *rmeta* R package (http://cran.r-project.org/). A fixed-effect model was used. The log hazard ratios and standard errors were obtained for each study from Cox proportional hazards regression, study results were combined using the generic inverse-variance method. The variance was estimated as the square of the standard errors; this follows a Chi-Squared distribution with approximately k-1 degrees of freedom (k=number of studies). The collation and curation of the data sets has been described previously (Buffa et al., 2011). In summary, the patient numbers and treatment information for the data sets are as follow:

- GSE6532: Early stage breast cancer patients given adjuvant tamoxifen (Loi et al., 2008). GSE6532Oxf, GSE6532KI, GSE6532GUY datasets contain 98,136 and 87 patients, respectively.
- GSE2034: 286 patients with early breast cancer not receiving either adjuvant or neoadjuvant therapy. 219 patients received breast conserving surgery and 67 were given radical mastectomy. 248 patients received radiotherapy (Wang et al., 2005).
- GSE9195: 77 early stage breast cancer patients which were treated with adjuvant tamoxifen monotherapy (Loi et al., 2008).
- GSE1456: 159 patients early breast cancer patients. 104 receiving adjuvant tamoxifen or chemotherapy (Pawitan et al., 2005).

- GSE22219: 207 primary breast cancer patients. Patients received adjuvant chemotherapy, and/or adjuvant hormone therapy or no adjuvant treatment. 184 patients received radiotherapy.

CHAPTER 3

HIGH THROUGHPUT COLONY FORMATION ASSAY

3.1 Introduction

3.1.1 High-throughput colony formation assay

One of the aims of this thesis was to develop a robust colony formation screening protocol that enables sensitive and selective identification of radiosensitising targets in a high-throughput manner. Short-term endpoints evaluating IR damage such as γ-H2AX quantification, micronuclei and viability assays all have several weaknesses (discussed in detail in the general introduction). The most significant drawback of short-term assays is their inability to assess mitotic catastrophe, the predominant method of cell death following IR treatment, resulting in a loss of replicative potential. The only assay which is able to truly assess this clonal inactivation is the gold standard colony formation assay (CFA) (Franken et al., 2006). The CFA is routinely used in the assessment of radiation treatment. However, it is considered laborious and cumbersome, and rarely implemented in a high-throughput manner. To identify novel genes that are linked to tumour radiosensitivity, this assay was miniaturised to fit a 96-well plate format, making it feasible to implement for high-throughput screening. The standard siRNA 6-well CFA has a transfection and plating step which required adaptation to fit a 96-well format. Consequently, the conditions for transfection and plating required optimisation.

3.2 Results

3.2.1 Cell line evaluation

HeLa cells were chosen because they form discrete, tight and countable colonies in both untreated and irradiated conditions (Figure 3.1). Cell seeding densities and IR dose were optimised, so that large enough colonies could be obtained to accurately assess clonogenic survival. The siRNA transfection, seeding and irradiation optimisations are discussed.

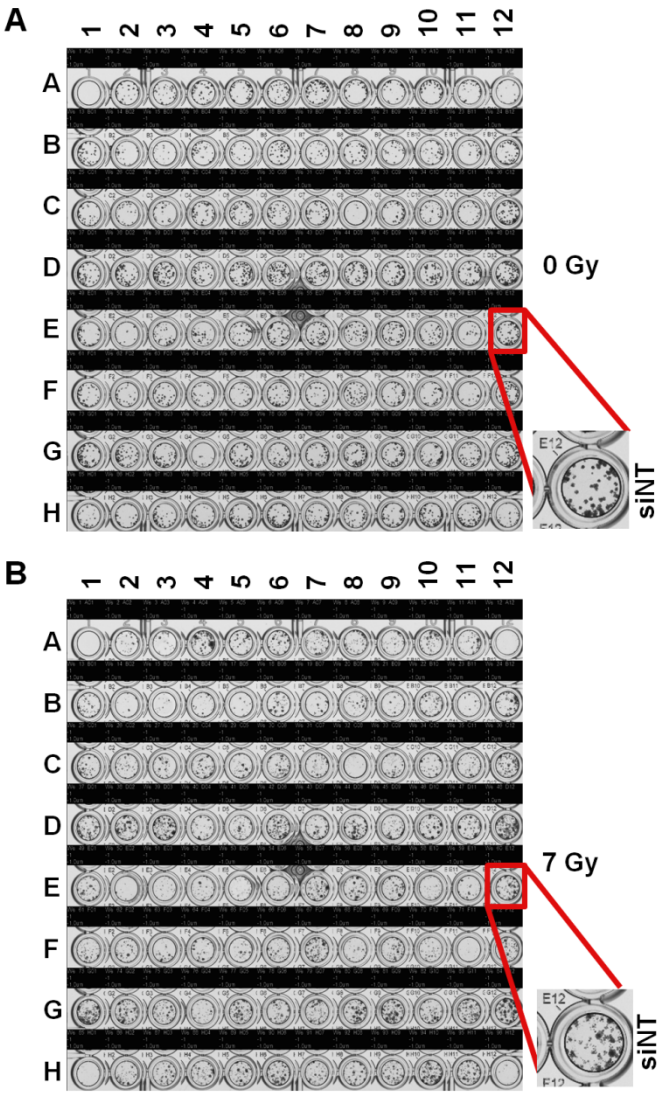

Figure 3.1 HeLa cell line colony formation assay in 96-well plates

Crystal violet stained 96-well plates following **A)** 0 Gy and **B)** 7 Gy irradiation. Non-targeting siRNA (siNT) containing well is indicated. Representative plates of quadruplicate repeats are shown. Plate layout can be found in Figure 2.1.

3.1.1.1 Transfection optimisations

Dharmacon ON-TARGET*plus* siRNA was chosen for the screen for its reduced off-target effects. These siRNAs have modifications on the antisense strand that reduce off-targets effects. In addition, there is an inactivating chemical modification on the sense strand to prevent interaction with RISC, so that only the antisense strand is utilised. (Jackson et al., 2006a). The transfection reagent chosen for this assay was

DharmaFECT-,1 previously shown to transfect well with ON-TARGET*plus* siRNA at 20 nM concentration in 6-well CFA. The concentration of DharmaFECT-1 required per well of a 96-well plate was unknown. As the screen would be carried out in 'semi-sterile' conditions inside the Janus liquid handling workstation ScanLaf Class 1 cabinet, the culture media needed to be supplemented with penicillin-streptomycin (Pen-Strep) at 100 µg/mL concentration to prevent bacterial infections. Hence it was evaluated whether Pen-Strep supplementation to media had an adverse effect on siRNA transfection. To evaluate transfection efficiency, polo-like kinase-1 (PLK-1) was used, as successfully transfected cells die readily after PLK-1 knockdown, due to mitotic spindle disassembly and subsequent onset of apoptosis (Spankuch-Schmitt et al., 2002). The transfection efficiency of siPLK-1 and non-targeting siNT control was tested with increasing amounts of DharmaFECT-1 in media with or without Pen-Strep (Fig.3.2). Increasing amounts of DharmaFECT-1 caused toxicity in siNT survival but Pen-Strep did not cause a significant additive reduction in survival (Fig.3.2). The optimal conditions for transfection in the presence of Pen/Strep was 0.1 µL/well DharmaFECT-1, which reduced survival of cells to 0.20 (+/-0.026) for siPLK-1, while siNT survival remained at 1.0 (+/-0.028) compared to untransfected cells.

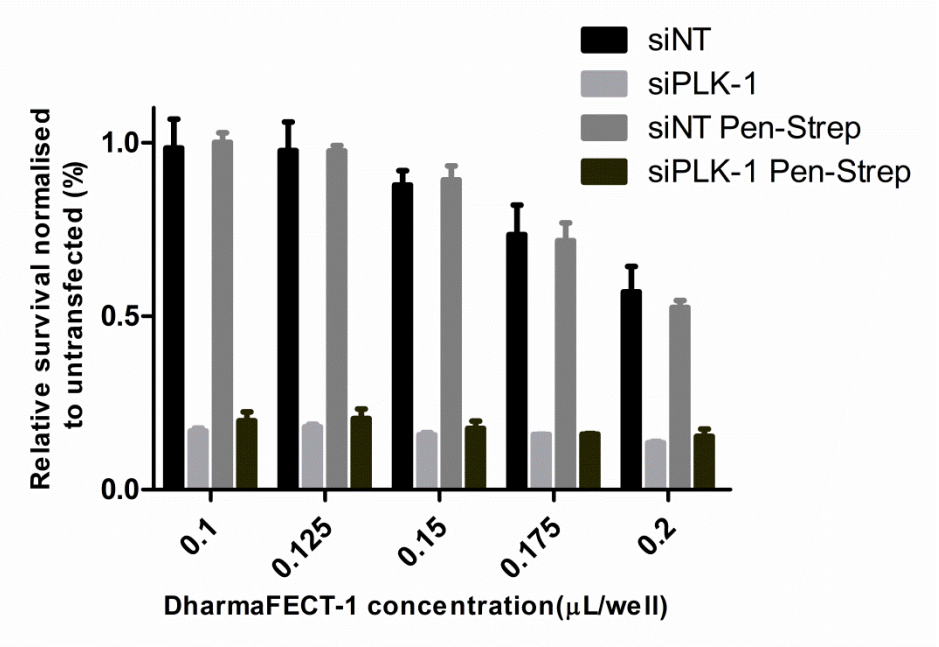

Figure 3.2. Transfection optimisation with DharmaFECT-1

HeLa cells transfected in a 96-well plate with 20 nM Ambion siNT and siPLK-1 supplemented with varying concentrations of DharmaFECT-1 transfection reagent. siRNA complexes were added to cells maintained in growth medium supplemented with +/- 100 µg/mL Pen-Strep. After 72 hours transfection, cell viability was determined using 1 hour of incubation with Resazurin substrate. Resazurin assay: representative of three independent experiments, data points presented as mean +/- SD from triplicate wells.

3.1.1.2 Optimising plating numbers and IR dose

Next, plating densities and radiation dose were evaluated. The importance of optimising cell seeding densities and irradiation doses was to ensure accurate assessment of clonogenic survival where SF could be reproducibly calculated. In these optimisations, DNA-PK*cs* and polymerase theta (POLQ) were utilised as positive controls to assess radiosensitivity. Knockdown of DNA-PK*cs* causes pronounced radiosensitisation and was included as the main positive control (Gerweck et al., 2006; Zhuang et al., 2011). Knockdown of POLQ has been shown previously to radiosensitise HeLa cells with a comparatively smaller magnitude of effect than observed with knockdown of DNA-PK*cs*, ATM or ATR (Higgins et al., 2010). It was included as a second positive control to

assess whether the assay could identify siRNAs that only cause a relatively small increase in radiosensitivity.

First the cell plating numbers were assessed for the unirradiated plates. Transfected cells were tested for their colony forming ability in 96-well plates following re-plating in a dilution series (Fig.3.3). The highest PE in 0 Gy control plates was observed with seeding concentrations of 165 to 229 cells per well (Fig.3.3). The 190 cells/well seeding density with a PE of 38.68% (+/- 4) for siNT was chosen as the optimal concentration for unirradiated plates, as this yielded the most consistent and optimal colony density.

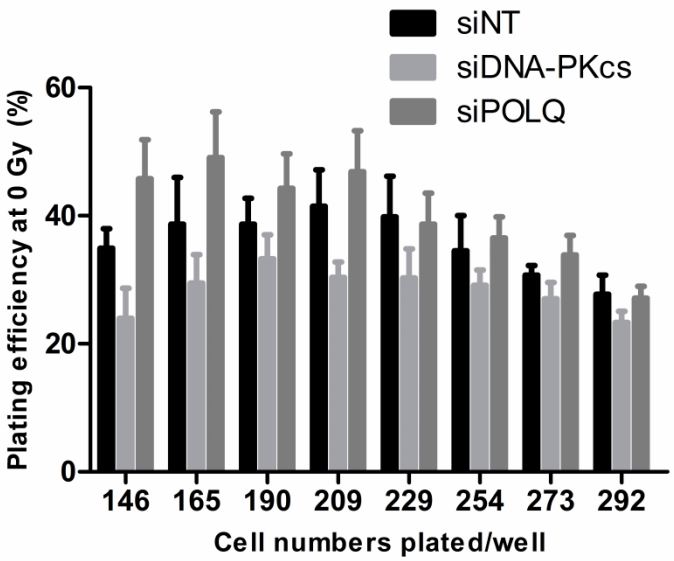

Figure 3.3. Cell density optimisation of un-irradiated (0 Gy) 96-well colony formation plates

Plating efficiencies in 96-well CFA of HeLa cells transfected with 20 nM Dharmacon siNT, siDNA-PK*cs* and siPOLQ siRNA. After 72-hours of transfection, cells were split into 96-well plates at different cell densities and left for 6 days at 37°C (5%CO_2) to allow for colony formation. Cells were stained with crystal violet and counted using the GelCount colony counter. CFA: representative of three independent experiments, data points presented as mean +/- SD from quadruplicate repeats.

The optimal radiation dose and seeding density was identified from assessing three radiation doses: 6, 7 and 8 Gy (Fig.3.4). The aim of this optimisation was to identify a radiation dose and seeding density that provided the greatest dynamic range between negative and positive controls with acceptable standard deviation between replicates.

The 8 Gy radiation dose was associated with a very low SF for siNT, and a high degree of variability resulting in a poor dynamic range between the positive and negative controls (Fig.3.4C). These results closely reflected previous findings from groups that radiation doses >8 Gy compromise the dynamic range between controls due to the difficulties in counting colonies containing radiation-induced giant cells (Katz et al., 2008). The high variability observed during the 8 Gy optimisations may be the result of the difficulty for the GelCount automated colony counter to identify true colonies rather than intensely stained giant cells. Variability was less in the 6 and 7 Gy irradiated plates, with the 1959 and 1561 seeding densities for 7 Gy yielding the best dynamic range. The Z-factor, a measurement of dynamic range between negative and positive controls, was 0.8 and 0.76 for the 1959 and 1561 seeding densities at 7 Gy, respectively. The Z-factor is measured between 0 and 1, with 1 indicating an ideal screen with no standard deviation between replicates with a limitless dynamic range:

$$\text{Z-Factor} = 1 - \frac{3(\sigma_{SF_{NT}} + \sigma_{SF_{DNA-PKcs}})}{|\mu_{SF_{NT}} - \mu_{SF_{DNA-PKcs}}|}.$$

Biochemical assays have Z-factors which are typically greater than 0.5 (D'Agostino et al., 2013; Poe et al., 2014) and cell based screening is generally in the range of 0 to 0.5 (Iversen et al., 2006). Therefore Z-factors for the seeding optimisations at 7 Gy indicate excellent dynamic range between positive and negative controls with minimal standard deviation between replicates. Based on these results it was decided to run the screen with a 7 Gy radiation dose and plating density of 1600 cells per well.

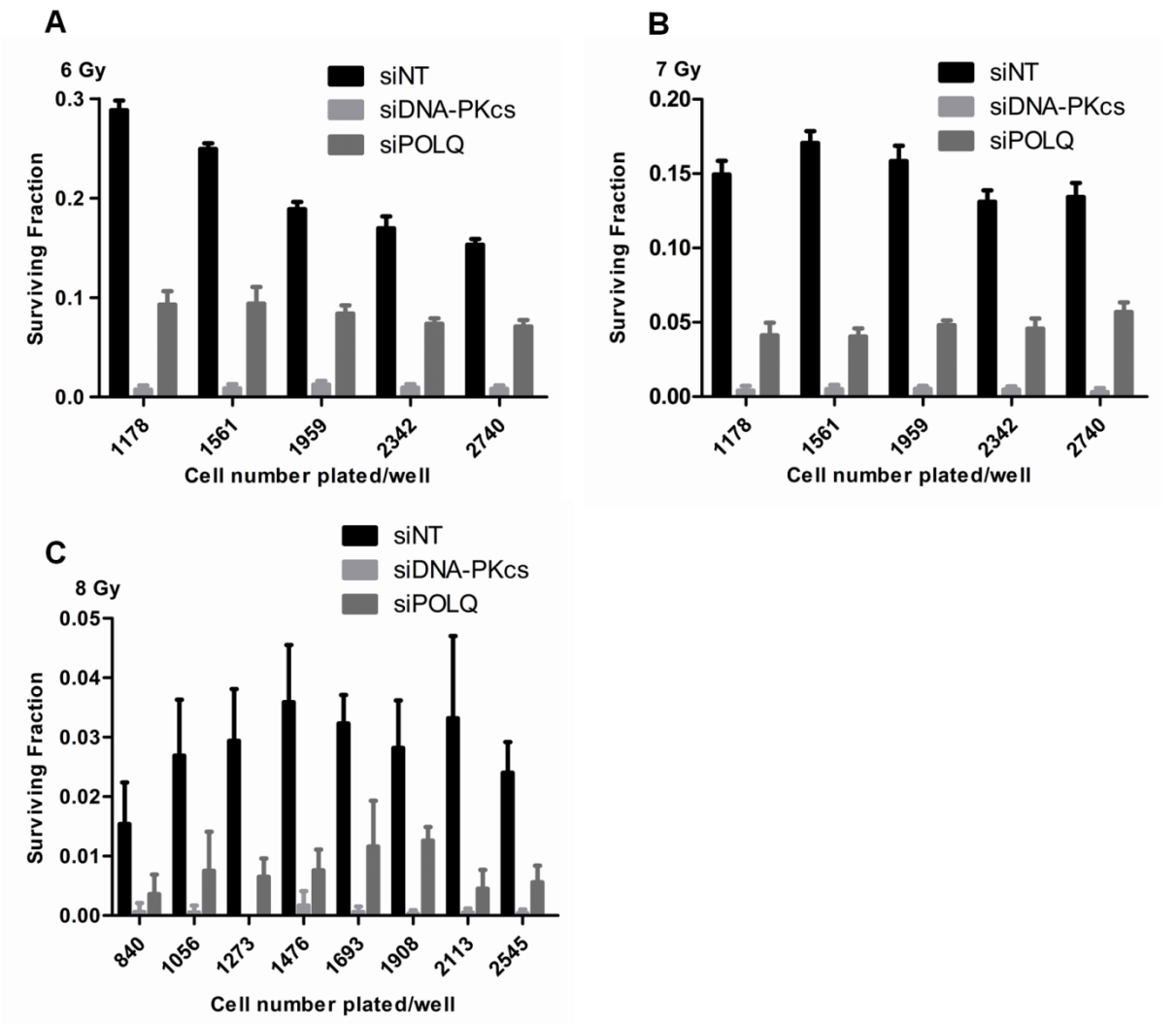

Figure 3.4. Cell density optimisation for irradiated plates using 96-well colony formation assay

The 96-well colony formation assay was conducted for HeLa cells transfected with 20 nM Ambion siNT, siDNA-PK*cs* and siPOLQ siRNAs. After, 72-hours of transfection, cells were split into 96-well plates at different cell densities and incubated for 4 hours at 37°C (5%CO_2). Plates were irradiated at 6 (**A**), 7(**B**), or 8 (**C**) Gy, and returned to the incubator for 8 days to allow for colony formation. Cells were stained with crystal violet and colonies counted using the GelCount colony counter. CFA: representative of three independent experiments, data points presented as mean +/- SD from quadruplicate repeats.

A screening protocol was devised and shown below in Figure 3.5.

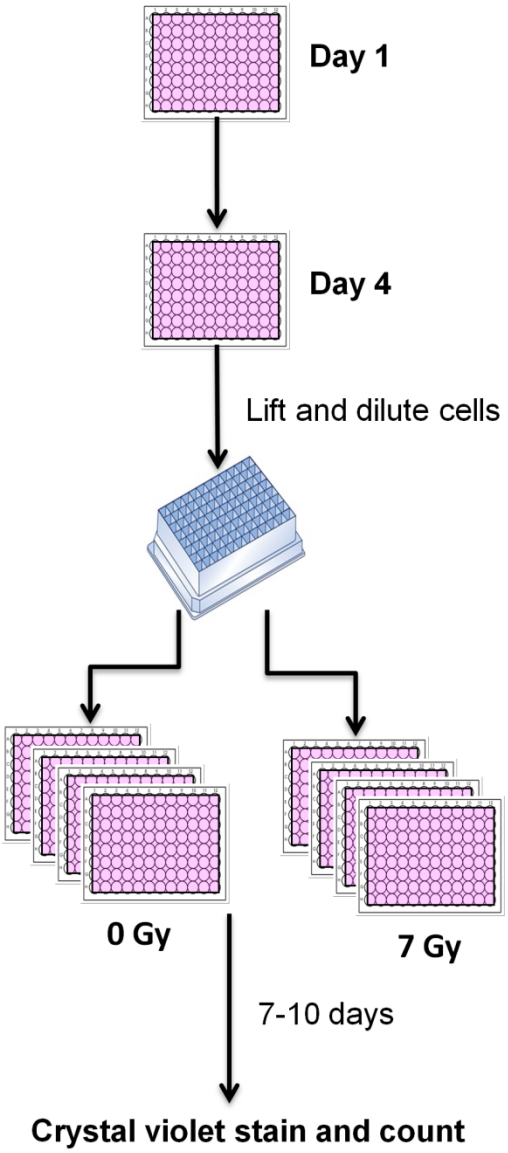

Figure 3.5. Screening protocol using the 96-well colony formation assay

Day 1) Library plates are transfected using reverse transfection of 20 nM ON-TARGET*plus* siRNA supplemented with 1 µL/well DharmaFECT-1 transfection reagent. **Day 4**. Transfected cells are lifted with trypsin-EDTA. Part of cell suspension is transferred to a 96-deep well plate containing 1.2 ml medium per well. Cells are transferred from deep well plate to 4 x 0 Gy plates (192 cells/well) and 4 x 7 Gy plates (1600 cells/well). 7 Gy plates are irradiated. **Day 10** 0 Gy plates were stained and counted **Day 12**. 7 Gy plates were stained and counted.

3.1.2 Z-factor testing

Having established the optimal conditions for siRNA transfection, radiation dose and cell seeding densities, it was important to confirm that these conditions were robust enough for a high-throughput screen. To this end, established conditions were combined to carry out the 96-well CFA protocol (Fig.3.5) with a large number of control siRNAs. A 96-well plate was produced containing 32 siNT, 32 siDNA-PKcs, 8 siPOLQ and 16 untransfected control siRNA wells. The 0 Gy PE for siNT was 37.1 % (+/- 7.6 %). The average SF at 7 Gy for siNT across the plate was 0.058 (+/-0.013) and mean SF for DNA-PKcs across the plate was 0.0016 (+/-0.0012) (Fig.3.6). This provided a Z-factor of 0.23 demonstrating a high dynamic range between the negative and positive controls with acceptable variability between replicates.

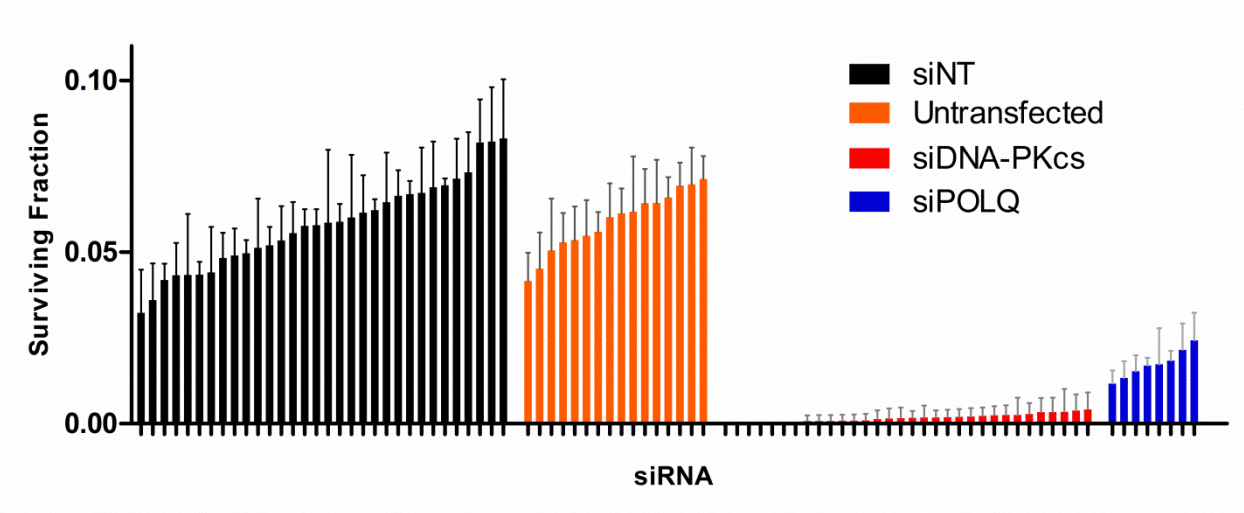

Figure 3.6 Optimisation of 96-well colony formation with manual plating

The 96-well colony formation assay conducted with HeLa cells transfected with 20 nM ON-TARGET*plus* siNT, siDNA-PK*cs* and siPOLQ. After 72-hours of transfection, cells were manually split into quadruplicate repeat control (192 cells/well) and treatment (1600 cells/well) plates. Plates were left in the incubator for 4 hours. Treatment plates were irradiated at 7 Gy and returned to the incubator. Control (6 days post IR) and treatment plates (8 days post IR) were stained with crystal violet and counted using the GelCount. CFA: representative of three independent experiments, data points presented as mean +/- SD from quadruplicate repeats.

Thus far all optimisations were carried out manually. The screening protocol was still to be implemented in a high-throughput manner using the Janus automated liquid handling workstation to carry out transfection and plating steps. Therefore, the experiment described above (Fig.3.6) was repeated using the Janus (Fig.3.7). This was to determine if the automated liquid handling would have any effect on the reproducibility and robustness of the assay. The 0 Gy PE for siNT was 27.7 % (+/- 3.97%). The average SF of siNT across the plate was 0.0688 (+/-0.007) and mean SF for DNA-PKcs across the plate was 0.0045 (+/-0.003) (Fig.3.6), producing a Z-factor of 0.54.

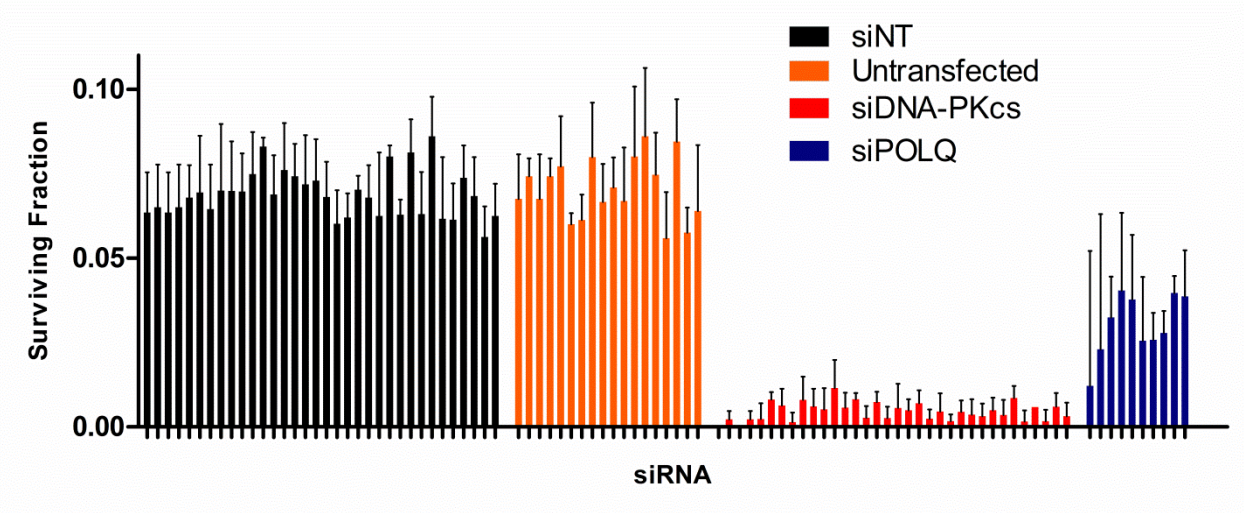

Figure 3.7. High-throughput 96-well colony formation test

The 96-well colony formation assay was conducted with HeLa cells transfected with 20 nM ON-TARGET*plus* siNT, siDNA-PK*cs* and siPOLQ siRNAs using the Janus workstation. After 72-hours of transfection, cells were split using the Janus workstation into quadruplicate repeat control (192 cells/well) and treatment (1600 cells/well) plates and left in the incubator for 4 hours. Treatment plates were irradiated at 7 Gy and returned to the incubator. Control (6 days post IR) and treatment plates (8 days post IR) were stained with crystal violet and counted using the GelCount. CFA: representative of three independent experiments, data points presented as mean +/- SD from quadruplicate repeats.

3.1.3 Kinome screen

Having successfully adapted the CFA for a high-throughput screen, this assay was used to screen a siRNA library containing 709 siRNAs against protein kinases. The library was screened on two separate occasions. The average plating efficiency for NT siRNA treated wells was 28% (+/- 9.45 %) with an average SF at 7 Gy of 0.084 (+/- 0.019). Knockdown of DNA-PK*cs* was used as positive control and had a SF of 0.0038 (+/- 0.003) at 7 Gy. This yielded a Z-factor of 0.13 for the first run and 0.46 for the second run. A radiosensitisation score, R-score, was calculated for each target, with negative values indicating greater radiosensitisation compared to the siNT control. The coefficient of determination (R^2), a measurement for inter-assay variability, comparing the R-score values between the two runs was 0.38. Targets from the primary screen were ordered using rank-product analysis, minimising variability in R-scores between screening runs. The identification of known modulators of radiosensitivity including CHEK1, ATM, ATR and DNA-PK*cs* (Fig.3.8A) confirmed the validity of the screening protocol.

Figure 3.8A shows the R-score distributions of the two runs of the primary kinome screen. The R-score distributions are not negatively or positively skewed for the siRNAs suggesting the screening protocol does not add a bias in either direction and that the siRNA library is not enriched for siRNAs that are linked to radioresistance. The 25 lowest rank-product R-scores (most sensitising) and the 25 highest ranked (least sensitising) are shown in Figure 3.8B. A complete list of the targets and their R-scores can be found in Table A1 in the Appendix.

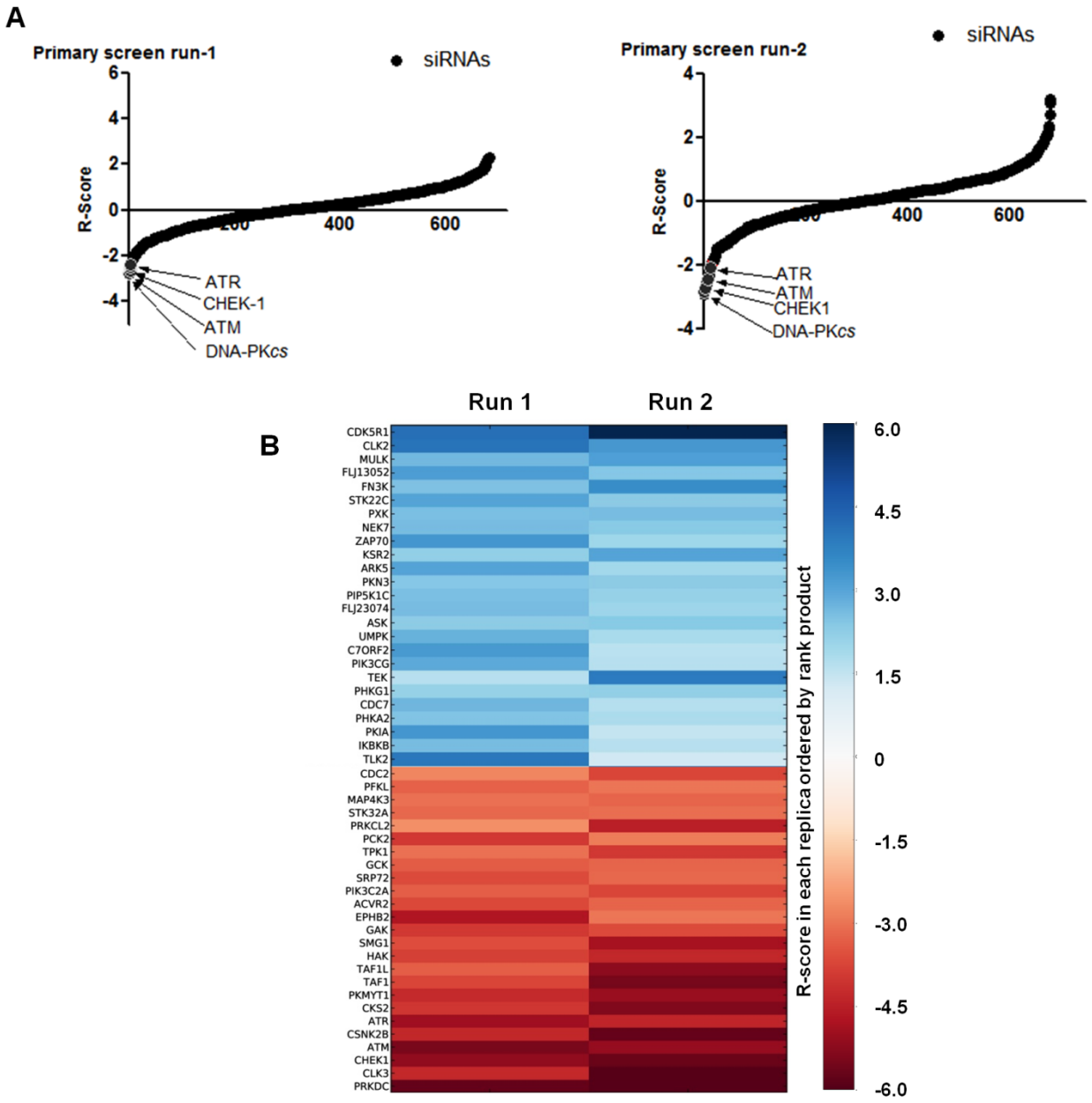

Figure 3.8. R-score distribution and rank-product analysis of primary kinome screen

A) R-score distributions for the two runs of the 709 Dharmacon Kinome ON-TARGET*plus* siRNA library CFAs. Radiosensitising siRNAs have R-scores <0. siRNAs that reduced PE < 5% were excluded from the analysis. **B)** Heatmap of the R-scores from the primary screen calculated from rank-product analysis of the two runs. Top 25 lowest and highest ranked R-scores are shown. Radiosensitising siRNAs are shown by R-scores <0. Adapted and permission gained from Tiwana *et al*.,2015.

3.1.4 Secondary 'kinome' screen

The top-76 targets based on rank-product of primary screening runs were re-screened using siGENOME SMARTpool siRNA in place of ON-TARGET*plus* siRNA, thus reducing the risk of identifying targets due to off-target effects (Fig.3.9A). This number of siRNAs was chosen because they created a single 96-well siRNA custom library plate together with control wells. The R-score distributions are negatively skewed for siRNAs in this library, as would be anticipated for a secondary screening library enriched for siRNAs that modulate tumour radiosensitivity. The secondary screening protocol was again validated by the identification of known modulators of radiosensitivity that included ATM and DNA-PK*cs* (Fig.3.9A). The Z-factor of the secondary screen was 0.55 for the first and 0.62 for the second run. The R^2 coefficient comparing the R-scores between the two runs was 0.58. Of the chosen targets from the primary screen, 89% had R-scores< 0 in the secondary screen, indicating high reproducibility. Coefficients of variation (CV), a measurement for intra-assay variability, for siNT SF_{7Gy}, across the library siRNA plates for the primary and secondary screen can be found within Table A2 of the appendix.

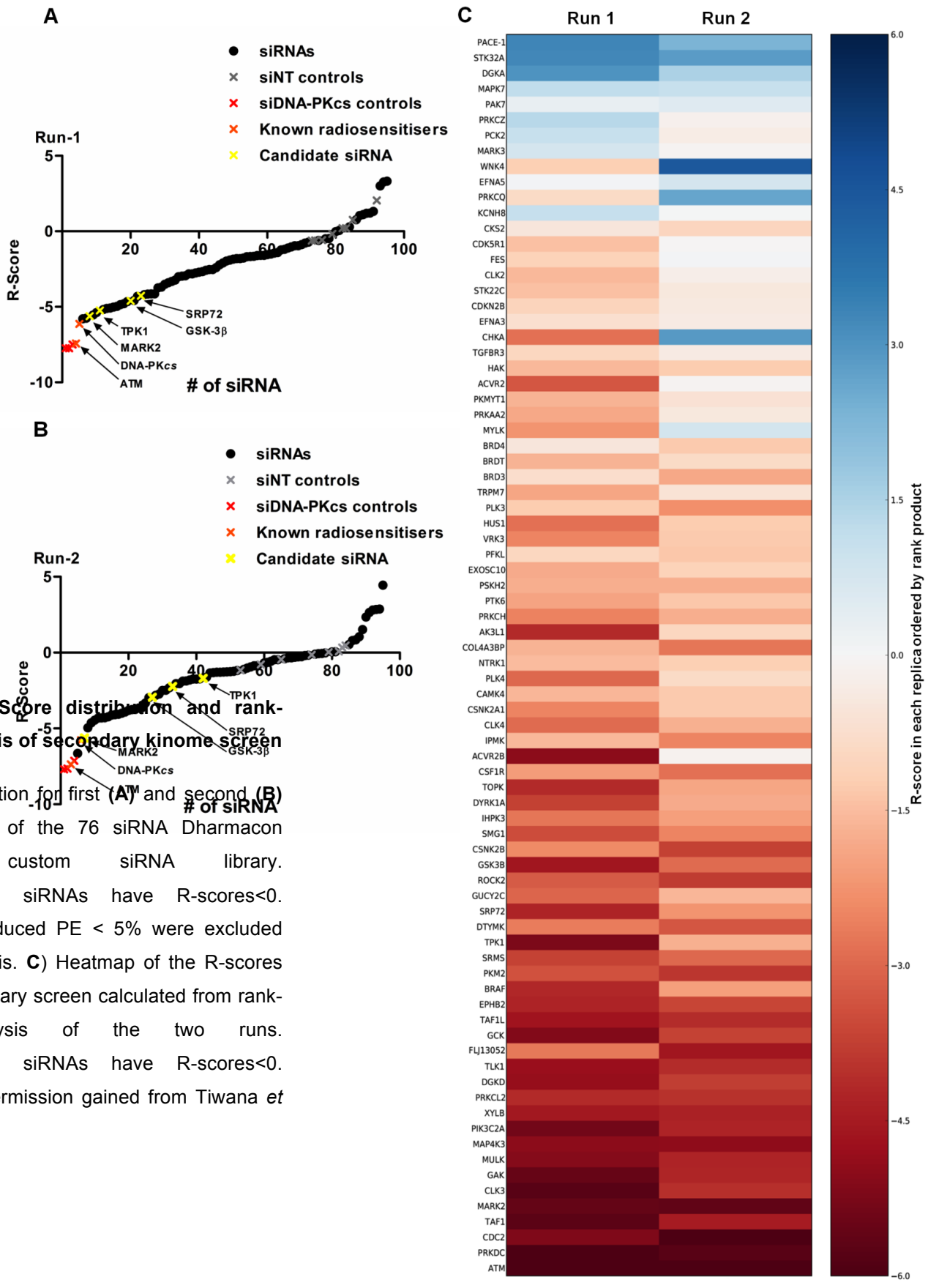

gure 3.9. R-Score distribution and rank-oduct analysis of secondary kinome screen

score distribution for first (**A**) and second (**B**) reening runs of the 76 siRNA Dharmacon GENOME custom siRNA library. idiosensitising siRNAs have R-scores<0. RNAs that reduced PE < 5% were excluded m the analysis. **C**) Heatmap of the R-scores m the secondary screen calculated from rank-oduct analysis of the two runs. idiosensitising siRNAs have R-scores<0. apted and permission gained from Tiwana *et* ,2015.

Targets from the secondary screen were ordered by rank-product. Targets ranked within the top 40 from the secondary screen (Appendix, Table A3) were selected for further evaluation based on the following criteria: novelty in the context of radiosensitivity, differential expression in tumour cells compared to normal tissue based on Oncomine data (Rhodes et al., 2007), and availability of reagents for expanded study. Based on this, four targets were chosen: MARK2, TPK1, GSK3β and SRP72. The evaluation of TPK1 is described in the Chapter 4, and Chapter 5 describes the remaining genes.

Candidate	Full name	Role/function	Reason for choice
TPK1	Thiamine pyrophosphokinase 1	Converts thiamine to thiamine pyrophosphate (Nosaka et al., 2001).	No radiosensitivity link Overexpressed in esophageal and kidney cancers (Rhodes et al., 2007).
GSK3β	Glycogen synthase kinase 3 beta	Involved in multiple pathways including WNT signalling (Liu et al., 2005a). Phosphorylates multiple targets involved in survival, microtubule regulation and cell proliferation (Hoeflich et al., 2000; Wagner et al., 1996).	One of the top hits in original screen and is an attractive clinical target. Inhibitors of GSK3β are radiosensitising and chemosensitising in glioma cells (Miyashita et al., 2009). Overexpressed in bladder, brain, breast and cervical cancers (Rhodes et al., 2007).
SRP72	Signal recognition protein 72 kDa	Ribonucleoprotein involved in processing and secretion of polypeptides from the ribosome (Iakhiaeva et al., 2010; Iakhiaeva et al., 2005).	No radiosensitivity link. Overexpressed in breast, kidney and head and neck cancers (Rhodes et al., 2007).
MARK2	MAP/microtubule affinity-regulating kinase 2	Involved in cascade of microtubule processes including regulation of cell polarity and cell migration (Nishimura et al., 2012).	No radiosensitivity link. Overexpressed in prostate, breast and bladder cancers (Rhodes et al., 2007).

Table 3.1 Kinome targets chosen for further investigation

Targets were chosen based on novelty, over expression in clinically relevant cancer histologies treated with radical radiotherapy and position within original screen or custom secondary kinome library screens.

3.2 Discussion

3.2.1 Summary of findings

The CFA is the gold standard for determining survival following irradiation (Franken et al., 2006) as it assesses the true replicative potential of a single cell. This chapter described the successful adaptation of the traditional CFA to a 96-well screening protocol. The 96-well CFA has been previously demonstrated as a feasible approach for examining drug combination therapies, however it has not been utilised with siRNA for target identification (Lin et al., 2014). Optimising the conditions for siRNA transfection and subsequent plating for colony formation posed significant challenges in developing this assay.

Transfection conditions were adapted from 6-well CFAs that used siRNA transfection and irradiation steps. Optimal conditions for siRNA transfection using DharmaFECT-1 were established (Fig.3.2). Cell seeding was optimised for the 7 Gy radiation dose and the screening protocol was devised (Fig.3.5). Z-factors demonstrated excellent dynamic range between positive and negative controls taking into account the standard deviation (Zhang et al., 1999b) in subsequent HTS optimisations (Fig.3.6 & Fig.3.7). Dharmacon-ON-TARGET*plus* 'kinome' was screened with the HTS protocol. The Z-factors for the kinome primary and secondary screens ranged from 0.1 to 0.5 indicating excellent quality metrics.

3.2.2 Limitations of the 96-well plate assay

3.2.1.1 HeLa cell line

This assay was optimised for the HeLa cell line. Despite being the optimal cell line in our investigations for forming countable colonies in the 96-well plate format, these cells are not the perfect cancer model. Deep DNA and RNA sequencing of the HeLa genome, revealed anticipated findings that there are significant aberrant differences in

copy number, single-nucleotide variants, structural variants (translocations) compared to normal tissue data gathered from the Illumina Human BodyMap 2.0 (RNA Seq) (Landry et al., 2013). It is highly likely that some of these differences have developed during *in vitro* cell culture and this cell line is characteristically dissimilar from its original isolation in the 1950's, and therefore not a true reflection of cancer in patients. Therefore, the experimental results derived from the HeLa cell line should be tested across additional cell lines to ensure their validity. As discussed chapter 4 and 5, candidate gene validation was carried out across a number of cell lines derived from cancer histologies routinely treated with radical radiotherapy, to overcome this limitation of the HeLa cell line.

3.2.1.2 Colony forming ability

The feasibility of the CFA in the HTS format was largely dependent on the ability of HeLa cells to form discrete countable colonies in 96-well plates. This assay can be adapted for other cancer cell lines but this will require them to be able to produce colonies which are discrete, compact and that produce PEs that are large enough to reliable calculate SF.

3.2.1.3 Plating efficiencies

Furthermore, there is a measurable drop to in 0 Gy PEs in the 96-well format. A 0 Gy PE for siNT is typically observed between ~25 to 35 % in HTS format, compared to ~40-50 % for the traditional 6-well plate CFA. A group which conducted a feasibility study for compound screening using a 96-well CFA, also noticed a significant drop of 40 % in PE compared to the traditional 6-well method (Lin et al., 2014). These reductions in PE may be caused by robot automation introducing errors during cell seeding during transfection and plating steps. Furthermore, manual pipetting may be gentler on cells reducing the probability of cell shearing compared with automated methods. Consequently, if the 96-

well CFA method is adapted for other cells lines, the cells must be sufficiently robust to withstand automated handling and dispensing, so that SFs can be accurately and reproducibly calculated.

3.2.1.4 False negatives and positives

False negatives can be introduced during colony counting. If intensely stained giant cells are abundant in a well of a 96-well plate, the colony counter marks them as true colonies. Groups that have successfully shown the feasibility of using high content CFAs, employed fluorescent dyes to label the nucleus to distinguish between giant single cells and real colonies (Katz et al., 2008; Lin et al., 2014). The future adaptation of the HTS screening protocol may require the addition of labelling dyes to diminish false negatives caused by inaccurate counting of colonies.

Furthermore, false positives are caused by the off-target effects of siRNA. This was largely circumvented by the chemical modifications on the Dharmacon ON-TARGET*plus* siRNA used in the screening protocol. However, future strategies may look to employ the 96-well CFA protocol with endoribonuclease-prepared short interfering RNAs (esiRNAs) produced from enzymatic degradation of dsRNA, which results in a 12 fold reduction in off-target effects compared to siRNA (Kittler et al., 2007). Thus, these strategies may reduce the chances of selecting false positive targets from screening that are result of off-target effects. False negatives may also arise from low PE. siRNAs which were toxic were removed from screening analysis with the implementation of a 5% 0 Gy PE cut off. This cut-off may have caused the loss of potential genes that are involved in tumour radioresistance. However, without this cut-off, gene knockdowns that were toxic to cells may have been followed-up and most likely would cause similar phenotypes in normal tissues.

3.2.3 Future directions

3.2.3.1 Compound screening

The 96-well CFA screening protocol can also be adapted for use with compounds to investigate drug radiotherapy combinations. The feasibility of compound screening with high content CFA has been established previously (Lin et al., 2014). However, novel targets and pathways linked to tumour radioresistance have not been identified with such feasibility studies as of yet. Furthermore, the 96-well CFA screen may be an excellent method for combining drugs with radiotherapy for cancers that have developed resistance mechanisms to established treatments, or to identify synthetic lethality interactions in the absence of irradiation.

CHAPTER 4

THIAMINE METABOLISM IS LINKED TO TUMOUR RADIORESISTANCE

4.1 Introduction

The first candidate gene investigated from the radiosensitivity screen was thiamine pyrophosphokinase-1 (TPK1). TPK1 is an essential kinase involved in thiamine metabolism. Particular attention will be focussed on thiamine metabolism and how this pathway provides a growth advantage for numerous tumour types. Finally, thiamine metabolism and its role in intrinsic radiosensitivity will be explored.

4.1.1 Thiamine metabolism

Thiamine/ Vitamin B1 is an essential water soluble micronutrient produced by plants, bacteria and fungi (Kawasi et al., 1969; Kong et al., 2008; Tatum and Bell, 1946). Mammals receive thiamine from dietary intake which broadly includes meat, fish, breads and legumes. The vitamin has a pyrimidine group and thiazole ring, and is an essential co-factor for enzymes within the tricarboxylic acid cycle (TCA cycle) for the overall goal of converting glucose to adenosine triphosphate (ATP), and in the pentose-phosphate pathway (PPP) for the production of nucleotides (Zastre et al., 2013b).

Thiamine does not readily diffuse into a cell, unless at high concentrations, and therefore requires active transport using transmembrane proteins (Zielinska-Dawidziak et al., 2008). Thiamine is transported into the cell by the proteins encoded by solute carrier (SLC)-19 transporter family, SLC19A2/THTR1 and SLC19A3/THTR2, which also belong to the major facilitator superfamily (Ganapathy et al., 2004; Hawkins et al., 1989). The third member of the family, SLC19A1/RFC1, transports negatively charged folate. THTR1 and THTR2 have 64% amino acid similarity, (Eudy et al., 2000) and RCF1 has 55% and 56% amino acid similarity to THTR1 and THTR2, respectively (Dutta et al., 1999).

THTR1 and THTR2 have a binding affinity for thiamine measured by the influx constant K_t = 2.5 μM (Dutta et al., 1999) and 27.1 nM (Said et al., 2004), respectively. THTR1

expression is highest in skeletal muscles followed by heart, kidney and liver (Dutta et al., 1999). THTR2 is highly expressed within the intestines and given that it is direct contact with dietary supply, it is logical that it would have higher affinity for thiamine (Dutta et al., 1999). As depicted in Figure 4.1, thiamine is transported into the cells where it is converted to thiamine pyrophosphate (TPP) by TPK1. TPK1 is the only known kinase which can facilitate conversion to the thiamine derivatives. There are three forms of thiamine which are measurable; thiamine monophosphate (TMP), thiamine triphosphate (TTP) and adenosine thiamine triphosphate (AThTP) (Bettendorff et al., 2007; Gangolf et al., 2010). Unlike other thiamine derivatives, TPP is the only known prosthetic group which is able to bind to the enzymes to carry out cellular functions. TPP is transported into the mitochondria by thiamine pyrophosphate carrier (TPC) and used as co-factor for the TCA cycle enzymes which include α-ketogluturate dehydrogenase (α-KGDH) and pyruvate dehydrogenase (PDH) complex (Danner et al., 1978; Hawkins et al., 1989). These two enzymes are essential in the TCA cycle for the extraction of energy from glucose. Pyruvate is converted to acetyl-CoA by PDH through pyruvate decarboxylation which is dependent on TPP. Further into the steps within the TCA cycle, α-KGDH requires TPP to convert α-ketogluturate to succinyl-CoA. TPP is also essential for energy release associated with branched chain amino acid (BCAA) catabolism (Chuang et al., 1982). This process involves the conversion of BCAAs to α-keto acid by transamination (Mitch and Chan, 1978). Branched chained α-keto acid dehydrogenase complex (BCKDC) then carries out a decarboxylation step which converts alpha-keto acid to acetyl-CoA or succinyl-CoA (Epstein et al., 1980; Parker and Randle, 1978). Subsequently, these metabolites can be used by the TCA cycle to create further ATP. TPP is also a co-factor for transketolase (TKT) in the non-oxidative arm of the pentose phosphate pathway (PPP), for the production of nucleotides. A

detailed illustration of thiamine transport and utilisation by the cell is depicted in Figure 4.1.

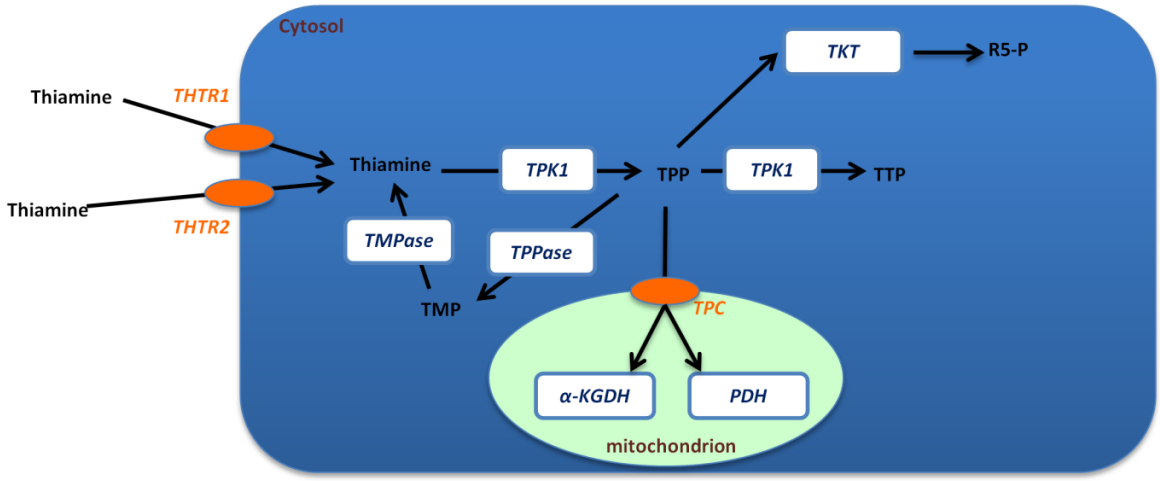

Figure 4.1 Thiamine transport and utilisation

Thiamine enters the cells by thiamine transporters, THTR1 or THTR2, and readily converted to TPP by TPK1 (Nosaka et al., 2001; Yoshioka, 1984). The pyrophosphorylation can be reversed from TPP to TMP by thiamine pyrophosphatases (TTPase) (Goldfischer et al., 1971; Sano et al., 1988). Additionally, TMP can be converted back to thiamine by thiamine monophosphatases (TMPase). TPP is transported into the mitochondria by thiamine pyrophosphate carrier (TPC) and used as co-factor for the TCA cycle enzymes which include α-ketogluturate dehydrogenase (α-KGDH) and pyruvate dehydrogenase (PDH) complex (Danner et al., 1978; Hawkins et al., 1989). TPP is also a co-factor for the transketolase (TKT) required for the production of ribose-5 phosphate (R5-P) in the non-oxidative arm of the pentose phosphate pathway (PPP). Finally TPP is essential for energy release associated with branched chain amino acid (BCAA) catabolism (Chuang et al., 1982).

4.1.2 Thiamine metabolism in cancer

Altered metabolism is a hallmark of cancer cells which under-go increased glycolysis for the conversion of glucose to lactate, termed the Warburg Effect (Racker, 1972). The Warburg effect provides a growth advantage for cancer cells as it results in increased nucleotide synthesis and overall biomass production driven by oncogenic signals (Koppenol et al., 2011). Since TPP produced by TPK1 is essential for general metabolism to drive growth through energy and nucleotide production, it can be postulated that a growth advantage may be provided for cancer cells utilising this pathway.

When glucose intake is increased by high carbohydrate diets, thiamine levels in plasma, faeces and urine decrease (Elmadfa et al., 2001). This demonstrates the integral link between glucose and thiamine utilisation. Patients with early breast (Basu and Dickerson, 1976), bronchial carcinomas (Basu and Dickerson, 1976) and B-chronic lymphocytic leukaemia (Seligmann et al., 2001) that are typically associated with high levels of glucose metabolism also have reduced levels of thiamine. The global depletion in thiamine in patients with cancer suggests either a global impairment for the conversion of thiamine to TPP, or that cancer cells are turning over thiamine more rapidly. The increased aerobic glycolysis observed in cancer cells and subsequent reduction in thiamine, means that cancer cells must increase thiamine uptake.

SLC19A2/THTR1 and SLC25A19/TPC have been shown to be up-regulated in breast cancer in both patients and cell lines (Zastre et al., 2013a). The authors also show that TPK1 is overexpressed in breast cancer samples, suggesting that thiamine uptake, TPP formation and mitochondrial transport are increased to support the demand for thiamine dependent cellular processes. Conversely, THTR2 has been shown to be down-regulated in a panel of breast cancer lines determined by cDNA micro-arrays compared

to normal tissues levels (Liu et al., 2003). The authors also demonstrated that increasing expression of THTR2 by 2.5 fold in ZR75 cells caused sensitivity towards radiation which was associated with an increase in TUNEL staining (Liu et al., 2003). Therefore, THTR2 may have an additional undiscovered role which impacts survival. In gastric carcinoma, the down-regulation of THTR2 was caused by a hypermethylation of the SCL19A3 gene and by demethylating its promoter, expression was restored (Liu et al., 2009). This is further complicated as down-regulation of THTR1 and THTR2 has been observed in lung tumours (Liu et al., 2004b). Therefore, it remains unclear how thiamine transporters are regulated and if this is dependent on the histological subtype of the tumour.

Other means of understanding how cancer cells utilise thiamine metabolism is by looking at enzymes that active TPP binds to. Cancer cells are reliant on the pentose phosphate pathway for the production of ribulose-5-phosphate (R5-P) used in the formation of nucleotides to maintain sustained cell division (Boros et al., 1997; Boros et al., 2000). The production of R5-P in normal tissues is predominantly brought about through the action of the oxidative branch of PPP (Fig.4.2). This is an irreversible branch of the pathway which yields NADPH and ribonucleotides. The pathway comprises of G6P being dehydrogenated by G6P dehydrogenase to yield NADPH and 6-phosphogluconalactone (G6PL) (Glock and Mclean, 1953; Lienhard and Rose, 1964; Rippa et al., 1998). NADPH is required for the production of glutathione (GSH) and is an important scavenger of reactive oxygen species (ROS) (Winkler et al., 1986). Subsequently, the oxidative arm of PPP serves as a vital pathway to deal with oxidative stress. The next reaction in the oxidative PPP is G6PL being hydrolysed by 6-phosphogluconolactonase (6PGL) forming 6-Phosphogluconic acid (6-PGCA) (Miclet et al., 2001). 6-PGCA undergoes oxidative carboxylation by 6-phosphogluconate

dehydrogenase (6PGDH), which forms ribulose-5-phosphate (Ru5P) (Horecker et al., 1951; Tedokon et al., 1992). Finally, isomerases then convert the Ru5P to R5P.

However, in cancer there is a shift in R5-P production to the thiamine dependent non-oxidative branch. For example, pancreatic adenocarcinoma cancer cells shift 85% of all ribose production to this pathway (Boros et al., 1997). This is further supported by evidence that H441 lung adenocarcinoma cells are 98% reliant on the non-oxidative PPP branch for the production of ribose molecules (Boros et al., 2000). It is the reversible nature of this branch of the pathway which allows cancer to shift the demand for nucleotide production and put more reliance on the TPP dependent TKT enzyme. Figure 4.2 illustrates in detail how TPP is utilised in the thiamine metabolism pathway.

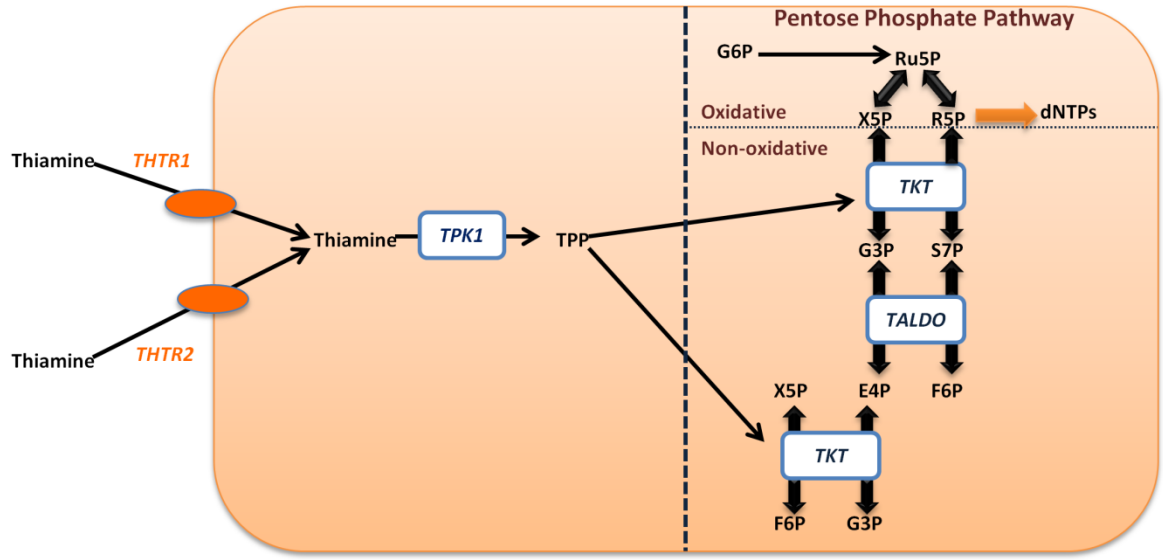

Figure 4.2. The role of thiamine in the pentose phosphate pathway

In the oxidative arm, glucose-6-phosphate (G6P) which is produced by the Embden-Meyerof pathway (glycolysis) is converted to R5-P (Horecker et al., 1951). Ru5P is converted to ribose-5-phosphate (R5-P) by ribose-5-phosphate isomerise (Rpi) (Kirk, 1959; Novello and McLean, 1968). R5-P is exploited for *de novo* nucleotide synthesis or unutilised R5-P is shunted into the non-oxidative arm of PPP. The non-oxidative branch of the PPP pathway is reversible and links carbohydrate metabolism providing flexibility in the way it responds to its metabolic requirements. This branch has 3 reversible steps which are catalyzed by TPP dependent TKT and transaldolase (TALDO). First, TKT converts R5P and xylulose 5-phosphate (Xu5P) to G3P and sedoheptulose-7-phosphate (S7P) (Horecker et al., 1963; Horecker et al., 1956; Pontremoli et al., 1960). The second step is carried out by TALDO which produces F6P and erythrose-4-phosphate (E4P) (Gunsalus et al., 1955; Horecker and Smyrniotis, 1953). The third step involves TKT converting the previous products to generate F6P and G3P, which can be shunted back to glycolysis to maintain the production of NADPH.

Cancer cells can also regulate TPP dependent enzymes such as TKT to ensure sustained growth and division. TKT expression has been shown to be higher in lung cancer lines and clinical samples compared to normal bronchial tissue (Lin et al., 2011). Additionally, there are two further isoforms of TKT, TKT-like 1 (TKTL1) and TKT-like 2 (TKTL2). TKTL1 is overexpressed in a number of carcinomas which include gastric (Langbein et al., 2006), non-small-cell lung carcinomas (Langbein et al., 2006; Schultz et al., 2008), breast (Foldi et al., 2007; Langbein et al., 2006), thyroid (Langbein et al., 2006), prostate (Langbein et al., 2006), pancreas (Langbein et al., 2006), ovarian

(Langbein et al., 2006), cervical (Chen et al., 2009; Langbein et al., 2006), rectal (Langbein et al., 2006) and kidney (Langbein et al., 2006). TKTL1 expression is also correlated with worse overall survival (Kayser et al., 2011; Langbein et al., 2006) and disease free survival (Schwaab et al., 2011) in patients. Although, TKTL1 has been shown to be TPP independent and does not function like TKT, it is unclear if other forms of thiamine can bind to this isoform or its function altered in dimerisation with other isoforms of the protein (Meshalkina et al., 2013).

In addition to cancer cells driving nucleotide synthesis through the PPP pathway, tumour cells can support TPP dependent enzymes in the TCA cycle by increasing glutamine metabolism. Glutamine catabolism produces α-ketogluturate which then is utilised by the thiamine dependent branch chain α-KGDH to produce succinyl-CoA. In cancer cells in general, glutamine catabolism is increased beyond the requirement for fatty acid synthesis, driving the production of oxaloacetate required to maintain the TCA cycle (DeBerardinis et al., 2007). Glutamine catabolism also supports the formation of nucleotides as malate from the TCA cycle is used to produce aspartate and reduces NADP to NADPH.

Cumulatively, it is a combination of increased activity of thiamine dependent enzymes through the TCA cycle, PPP and glutamine catabolism that drives the growth of cancer cells. Each pathway delivering metabolic precursors required for ATP production and nucleotide synthesis.

4.1.3 Thiamine metabolism and tumour radiosensitivity

The focus of this investigation is to discover novel genes involved in radiosensitivity. TPK1 has not previously been linked to radiosensitivity. Thiamine metabolism remains relatively unexplored in relation to radiation treatment. There is some tentative evidence suggesting a link between high THTR2 expression and increased radiosensitivity in

breast cancer cells (Liu et al., 2003). In this study THTR2 expression was found to be downregulated in a panel of breast cancer cell lines and this was associated with apoptosis resistance. When THTR2 expression was restored by cloning and transfecting into ZRF5 cells, they became radiosensitive in colony formation assays. Other than this study, proteins involved in thiamine metabolism have not been studied with regard to tumour radioresistance.

4.2 Results

4.2.1 TPK1 knockdown causes tumour specific radiosensitisation

The identification of TPK1 was not the result of off-target effects of the library siRNA, confirmed by means of depleting TPK1 using two sequence specific siRNAs from a third vendor. TPK1 knockdown with the two sequence specific Ambion siRNA resulted in significant radiosensitisation of HeLa cells (Fig.4.3A). The survival enhancement ratio at 0.10 surviving fraction (SER_{10}) for siTPK1-1 and siTPK1-2 was 1.33 and 1.30, respectively. Furthermore, this radiosensitisation effect was not exclusive to HeLa cells. The highly radioresistant SQ20B head and neck tumour line was radiosensitised by TPK1 knockdown (SER_{10} of 1.14; p <0.001, Fig.4.3B). A similar magnitude of radiosensitisation was observed with breast ductal carcinoma cell line BT-549 (SER_{10} of 1.19; p<0.001; Fig. 4.3C) following TPK1 knockdown. TPK1 knockdowns were confirmed by immunoblotting (Fig.4.3).

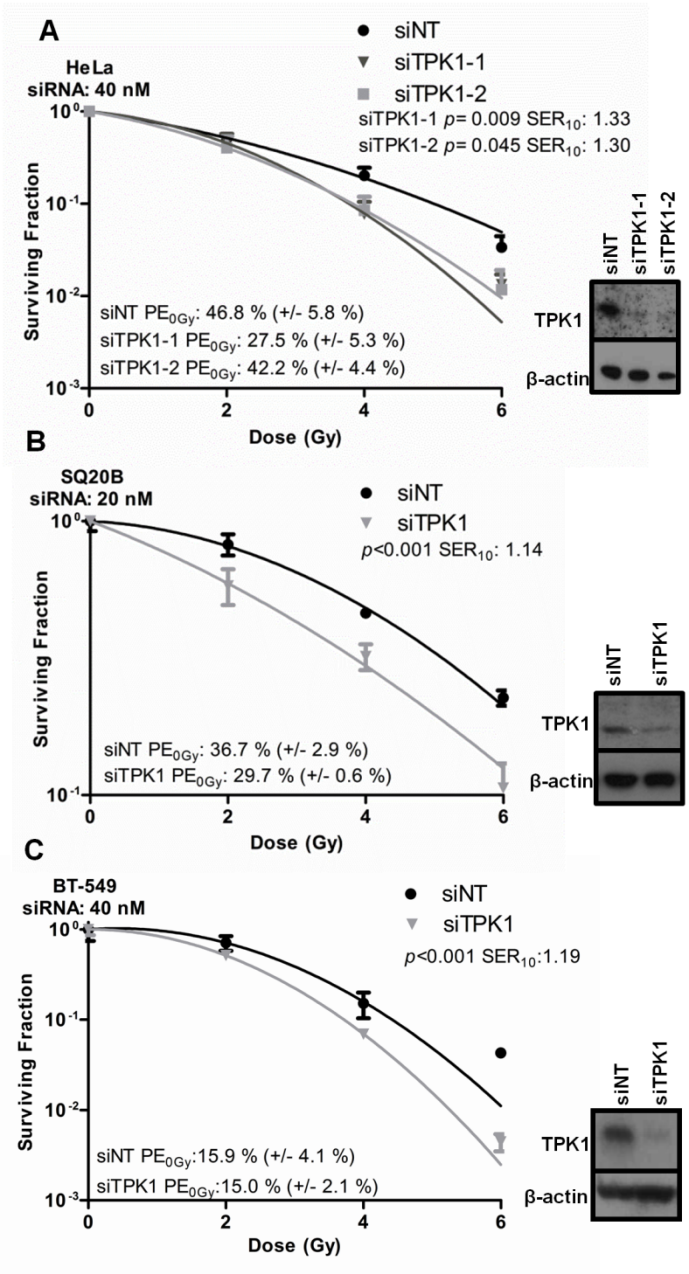

Figure 4.3. TPK1 knockdown causes tumour radiosensitisation

A) Colony formation assay (CFA) of HeLa cells irradiated following 72-hour Ambion siRNA transfection with non-targeting (siNT) and two sequence specific TPK1 siRNAs: TPK1-1 and siTPK1-2. TPK1 knockdown was confirmed by immunoblotting (inset) **B)** CFA of SQ20B cells irradiated following 72-hour Ambion siRNA transfection with siNT and siTPK1 at 20 nM final siRNA concentration. TPK1 knockdown was confirmed by immunoblotting (inset). **C)** CFA of BT-549 cells irradiated following 72-hour Ambion siRNA transfection with siNT and siTPK1 at 40 nM final siRNA concentration. TPK1 knockdown was confirmed by immunoblotting (inset).

CFA: representative of three independent experiments, data points and plating efficiencies at 0 Gy (PE_{0Gy}) presented as mean +/- SD from triplicate wells, *p*-values generated by factorial 2-way ANOVA. Sensitisation enhancement ratio at 0.10 surviving fraction (SER_{10}) calculated from non-linear regression of linear quadratic model. Adapted and permission gained for use of figure from Tiwana *et al.*,2015.

However, the knockdown of TPK1 in normal tissue lung fibroblasts cell lines MRC5 and HFL-1 did not result in significant radiosensitisation in standard CFAs (MRC5: *p*=0.337, HFL-1: *p*=0.747 Fig.4.4). Knockdown of TPK1 for MRC5 and HFL-1 cell lines was confirmed by immunoblotting (Fig.4.4). The lack of radiosensitivity observed with depleting TPK1 protein levels in normal tissue compared to tumour cell lines, indicates TPK1 could be a candidate for tumour specific radiosensitisation.

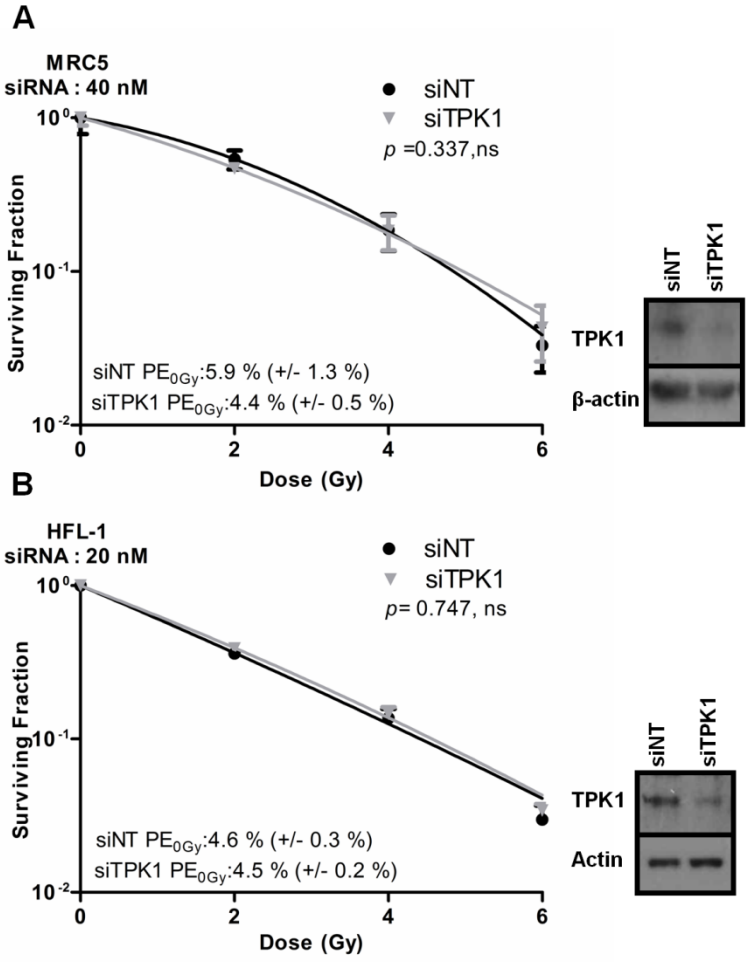

Figure 4.4. TPK1 knockdown does not radiosensitise normal tissue cell lines

A) CFA of MRC5 cells irradiated following 72-hour Ambion siRNA transfection with siNT and TPK1 siRNA at 40 nM final siRNA concentration. TPK1 knockdown was confirmed by immunoblotting (inset) **B)** CFA of HFL-1 cells irradiated following 72-hour Ambion siRNA transfection with siNT and siTPK1 at 20 nM final siRNA concentration. TPK1 knockdown was confirmed by immunoblotting (inset). CFA: representative of three independent experiments, data points and plating efficiencies at 0 Gy (PE_{0Gy}) presented as mean +/- SD from triplicate wells, *p*-values generated by factorial 2-way ANOVA. Sensitisation enhancement ratio at 0.10 surviving fraction (SER_{10}) calculated from non-linear regression of linear quadratic model. Adapted and permission gained for use of figure from Tiwana *et al*.,2015.

4.2.2 Disrupting thiamine metabolism results in tumour specific radiosensitisation

Since TPK1 plays an essential role in thiamine metabolism by converting thiamine to thiamine pyrophosphate (TPP), we investigated whether depletion of other proteins radiosensitised tumour lines. Attention was focussed on the transporters involved in transporting thiamine into the cell, and transporting TPP into the mitochondrion. The knockdown of one of the main transporters for thiamine, THTR1, caused significant radiosensitisation of HeLa cells (SER_{10} of 1.24; p =0.001, Fig.4.5A). The magnitude of this effect was similar to the knockdown of TPK1 (SER_{10} of 1.26; p <0.001, Fig.4.5A). The combined knockdown of TPK1 and THTR1 in HeLa cells caused comparable SER_{10} values (SER_{10} of 1.25; p <0.001, Fig.4.5A) to the individually knocked down targets described above. This is indicative of the same pathway being affected following knockdown of TPK1 and THTR1. siRNA knockdowns for TPK1 and THTR1 in HeLa cells were confirmed by qRT-PCR (Fig.4.5B).

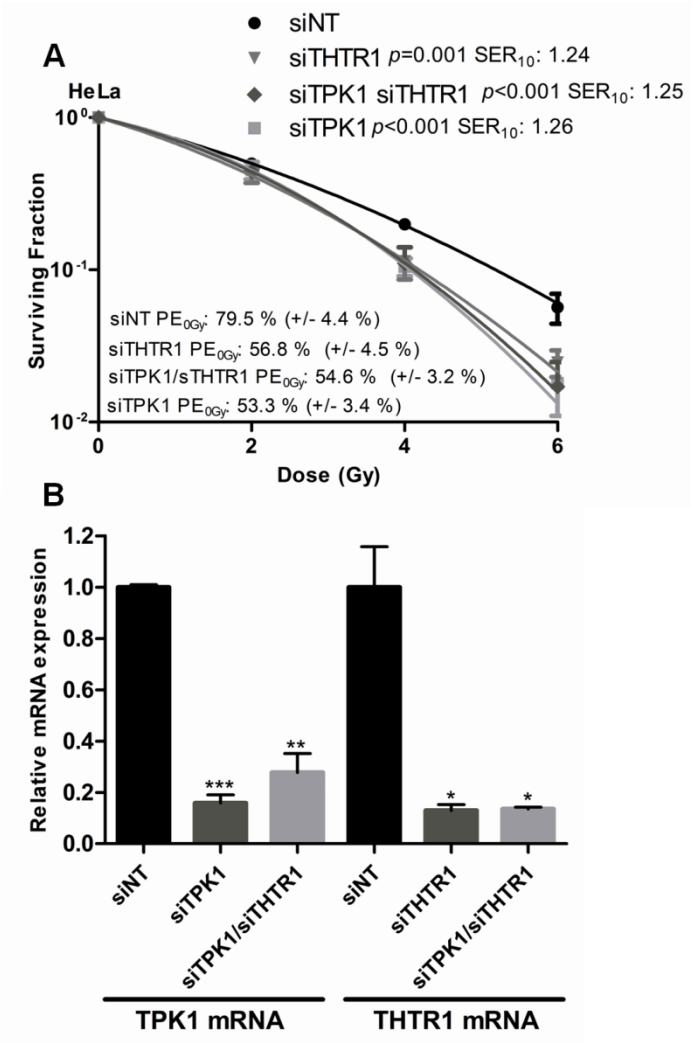

Figure 4.5. TPK1 and THTR1 knockdown has similar magnitude of radiosensitivity

A) CFA of HeLa cells irradiated following 72-hour Ambion siRNA transfection at a final concentration of 40 nM with siNT, siTPK1, siTHTR1 and siTPK1/THTR1. **B)** Single and double knockdowns confirmed by qRT-PCR. CFA: Representative of three independent experiments, data points and plating efficiencies at 0 Gy (PE_{0Gy}) presented as mean +/- SD from triplicate wells, *p*-values generated by factorial 2-way ANOVA. Sensitisation enhancement ratio at 0.10 surviving fraction (SER_{10}) calculated from non-linear regression of linear quadratic model. qRT-PCR: Unpaired two-sided students t-test comparing siNT to candidate knockdown t-tests *p<0.05, **p<0.01, ***p<0.001. Adapted and permission gained for use of figure from Tiwana *et al*.,2015.

The next step was to investigate if members of the thiamine metabolism pathway involved in transporting the active form of thiamine, TPP, were implicated in tumour radiosensitivity. Mitochondrial pyrophosphate carrier (TPC) is involved in transporting TPP across the mitochondrial membrane, for enzymes involved within TCA cycle. The

knockdown of TPC compared to siNT in HeLa cells did not cause radiosensitisation (*p*=0.688, Fig.4.6). TPC knockdown was confirmed by qRT-PCR (Fig.4.6B).

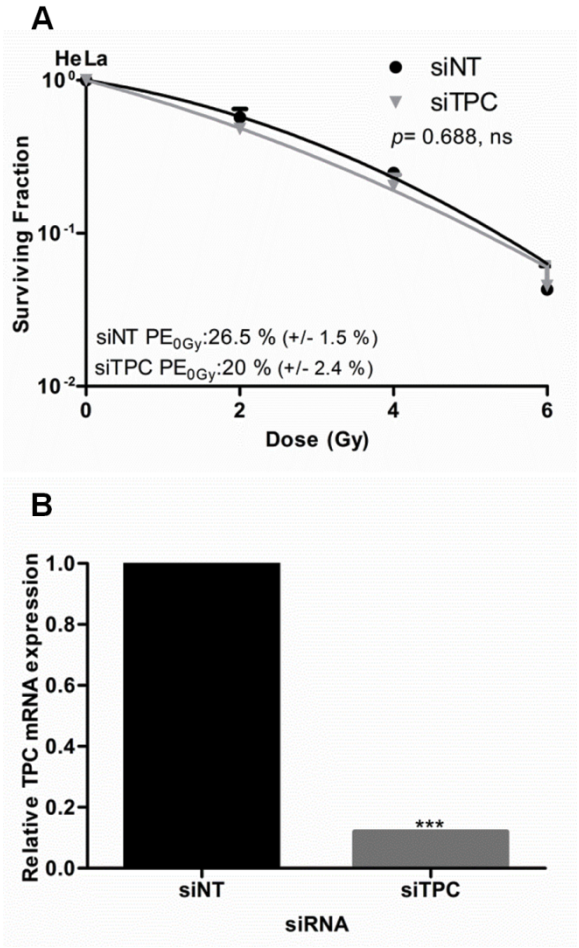

Figure 4.6. TPC knockdown does not radiosensitise HeLa cells

A) CFA of HeLa cells irradiated following 72-hour Ambion siRNA transfection at a final concentration of 20 nM with siNT and siTPK1 **B)** TPC knockdown confirmed by qRT-PCR.

CFA: Representative of three independent experiments, data points and plating efficiencies at 0 Gy (PE_{0Gy}) presented as mean +/- SD from triplicate wells, *p*-values generated by factorial 2-way ANOVA. Sensitisation enhancement ratio at 0.10 surviving fraction (SER_{10}) calculated from non-linear regression of linear quadratic model. qRT-PCR: Unpaired two-sided students t-test comparing siNT to candidate knockdown t-tests ***p<0.001. Adapted and permission gained for use of figure from Tiwana *et al*.,2015.

To add further confidence that thiamine metabolism is involved in tumour radioresistance, a pharmacological inhibitor of TPK1, pyrithiamine hydrobromide (PyrH), which competes for the active site of TPK1 (Liu et al., 2006a) was tested for its radiosensitisation capabilities. PyrH treated HeLa cells were significantly radiosensitised compared to DMSO treated cells (SER_{10}: 1.3, $p<0.001$, Fig.4.7A). In addition, a representative panel of cell lines derived from histological sites typically treated with radiotherapy was assembled and treated with PyrH. Following treatment with PyrH, significant radiosensitisation was observed with H460 lung carcinoma (SER_{10} of 2.09; $p<0.0001$, Fig.4.7B), CAL-51 breast carcinoma (SER_{10} of 1.76; $p<0.001$, Fig.4.7C), HCT-116 colorectal carcinoma (SER_{10} of 1.64; $p<0.00001$, Fig.4.7D), BT-549 breast carcinoma (SER_{10} of 1.24; $p<0.0001$, Fig.4.7E) and PSN-1 pancreatic adenocarcinoma (SER_{10} of 1.19; $p<0.0001$, Fig.4.7F) cell lines.

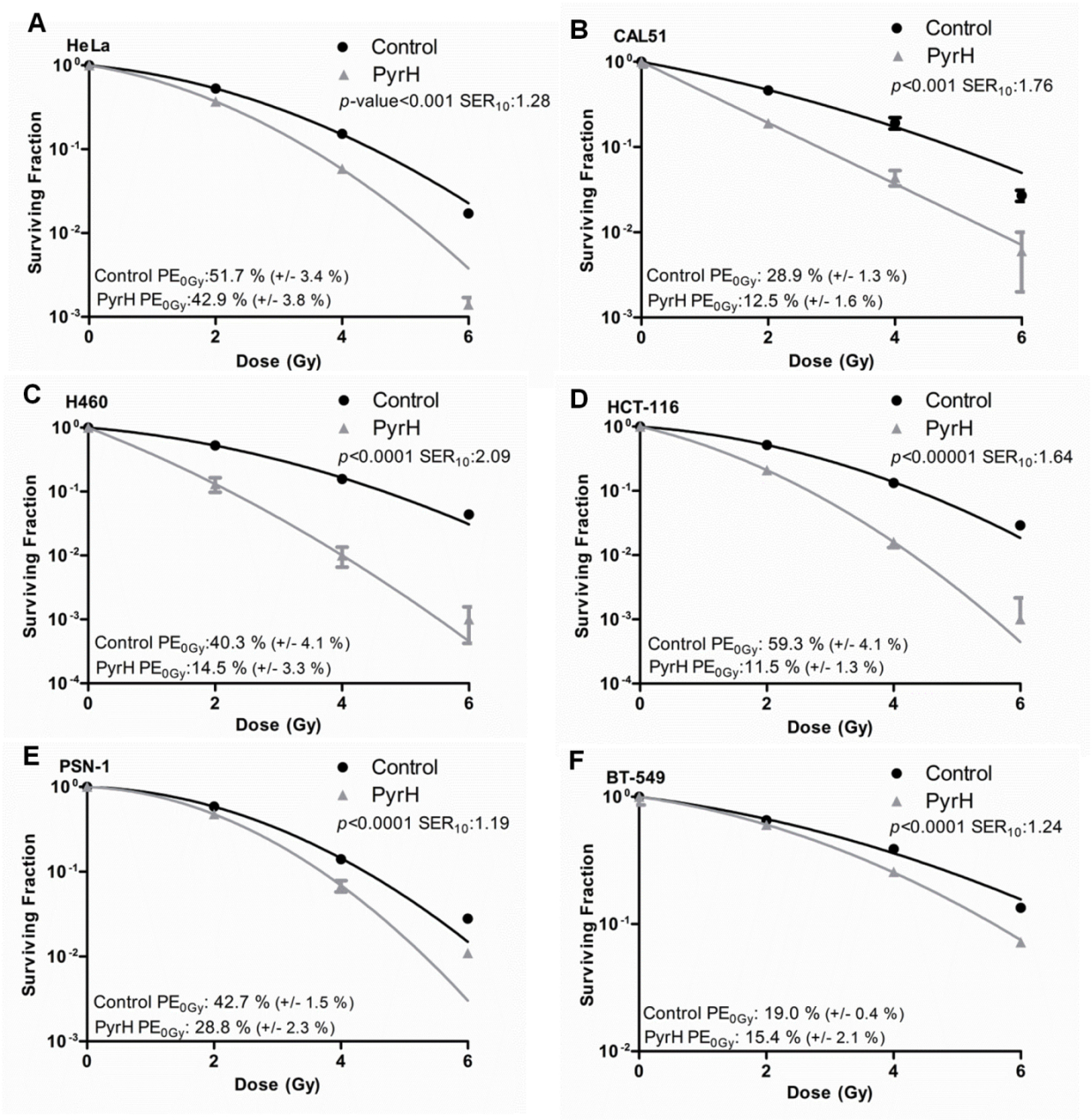

Figure 4.7. Tumour cell lines are radiosensitised by pharmacological inhibition of TPK1 by PyrH

CFA of tumour lines **A)** HeLa, **B)** H460, **C)** CAL51, **D)** HCT-116, **E)** BT-549 and **F)** PSN-1 irradiated following four days incubation with 10 μM Pyrithiamine Hydrobromide (PyrH) and DMSO (control). Cells were maintained in low thiamine M199 media supplemented with 10% FBS. CFA: representative of three independent experiments, data points and plating efficiencies at 0 Gy (PE_{0Gy}) presented as mean +/- SD from triplicate wells, *p*-values generated by factorial 2-way ANOVA. Sensitisation enhancement ratio at 0.10 surviving fraction (SER_{10}) calculated from non-linear regression of linear quadratic model. Permission received for re-print of figure from Tiwana *et al*.,2015.

Comparable to TPK1 knockdown, no significant radiosensitisation was observed with PyrH treatment with the normal tissue lung fibroblast HFL-1 (p=0.676, Fig.4.8A) and MRC5 cell lines (p=0.303, Fig.4.8B). This suggests that thiamine metabolism pathway either disrupted by siRNA or pharmacological inhibition results in tumour specific radiosensitisation.

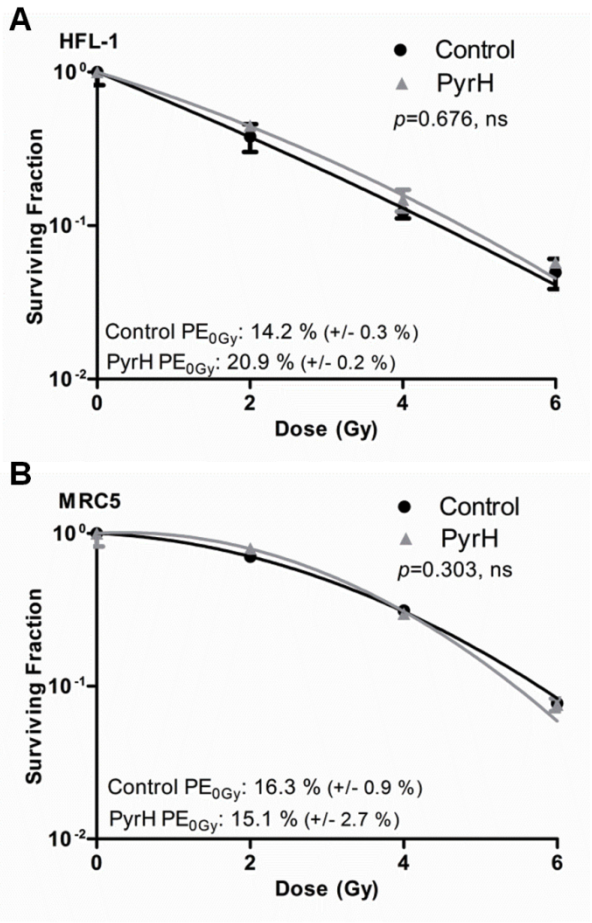

Figure 4.8. PyrH does not radiosensitise normal tissue fibroblast cell line

A) CFA of HFL-1 cells irradiated following four days incubation with 10 μM PyrH or DMSO (control). Cells were maintained in low thiamine M199 media supplemented with 10% FBS **B)** CFA of MRC5 cells irradiated following four days incubation with 10 μM PyrH or DMSO (control). Cells were maintained in low thiamine M199 media supplemented with 10% FBS

CFA: representative of three independent experiments, data points and plating efficiencies at 0 Gy (PE_{0Gy}) presented as mean +/- SD from triplicate wells, p-values generated by factorial 2-way ANOVA. Sensitisation enhancement ratio at 0.10 surviving fraction (SER_{10}) calculated from non-linear regression of linear quadratic model. Adapted and permission gained for use of figure from Tiwana *et al*., 2015.

Curative radiotherapy is typically delivered in a fractionated regimen delivered with 2 Gy single fractions. To demonstrate that the radiosensitisation observed in Figure 4.5A and 4.7A could be achieved at clinically relevant doses, a fractionated regimen of 3 x 2 Gy was delivered following either PyrH or siRNA treatment. Significant radiosensitisation was observed with siTPK1 (p<0.01, Fig.4.9A) and siTHTR1 (p<0.01, Fig.4.9A) compared with the fractionated regimen for siNT. In addition, radiosensitisation was observed with the fractionated regimen delivered for PyrH treatment HeLa cells compared to DMSO control (p<0.001, Fig.4.9B).

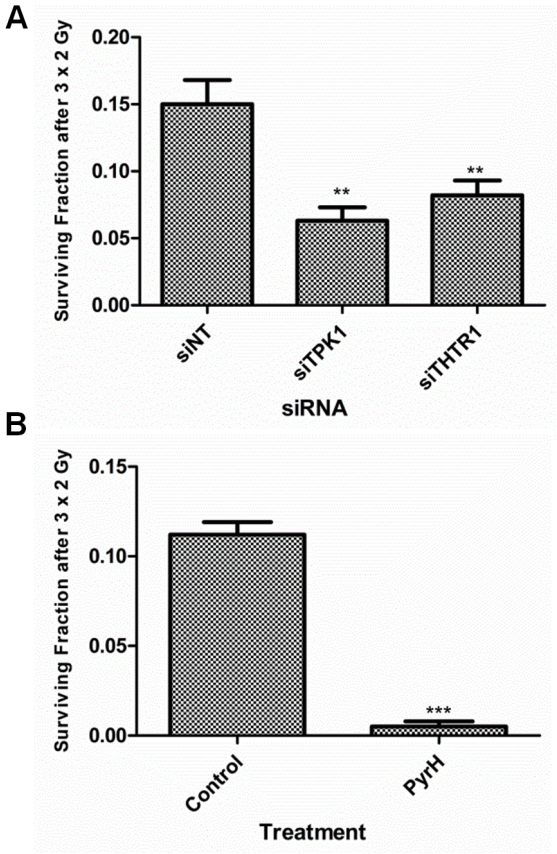

Figure 4.9. HeLa cells radiosensitised with fractionated radiotherapy regimen following thiamine metabolism perturbation

A) CFA of HeLa cells irradiated with fractionated regimen of 3 single treatments of 2 Gy provided over 3 consecutive days, commenced after 48 hours transfection with 40 nM Ambion siRNA for siNT, siTPK1 and siTHTR1. **B)** CFA of HeLa cells irradiated with fractionated regimen of 3 single treatments of 2 Gy provided over 3 consecutive days, commenced after 72 hours incubation with DMSO (control) or 10 μM PyrH. Cells were maintained in low thiamine M199 media supplemented with 10% FBS

Colony formation assay: representative of three independent experiments, data points presented as mean +/- SD from triplicate wells. Unpaired two-sided students t-tests comparing siNT/control to candidate knockdown/treatment $^{**}p<0.01$, $^{***}p<0.001$. Permission gained for use of figure from Tiwana *et al.*, 2015.

Collectively these data suggests that thiamine metabolism is a novel pathway involved in tumour radioresistance, and its disruption by either siRNA silencing or PyrH treatment may result in potentially clinically exploitable tumour specific radiosensitisation.

4.2.3 Disrupting thiamine metabolism results in DNA-damage persistence

To investigate whether the increased radiosensitivity was due to alterations in DNA repair, the level of DNA damage foci after radiation was assessed. Knockdown of TPK1 and THTR1 in HeLa cells caused significant elevation in γ-H2AX and 53BP1 foci in irradiated cells (Fig. 4.10A, B). Similarly, cells pre-treated with PyrH prior to irradiation showed significantly more unresolved 53BP1 and γ-H2AX foci at 24 hrs post 6 Gy irradiation (Fig. 4.10A, C). Together these findings suggest that depleting cells of thiamine pyrophosphate inhibits their ability to repair DNA DSBs.

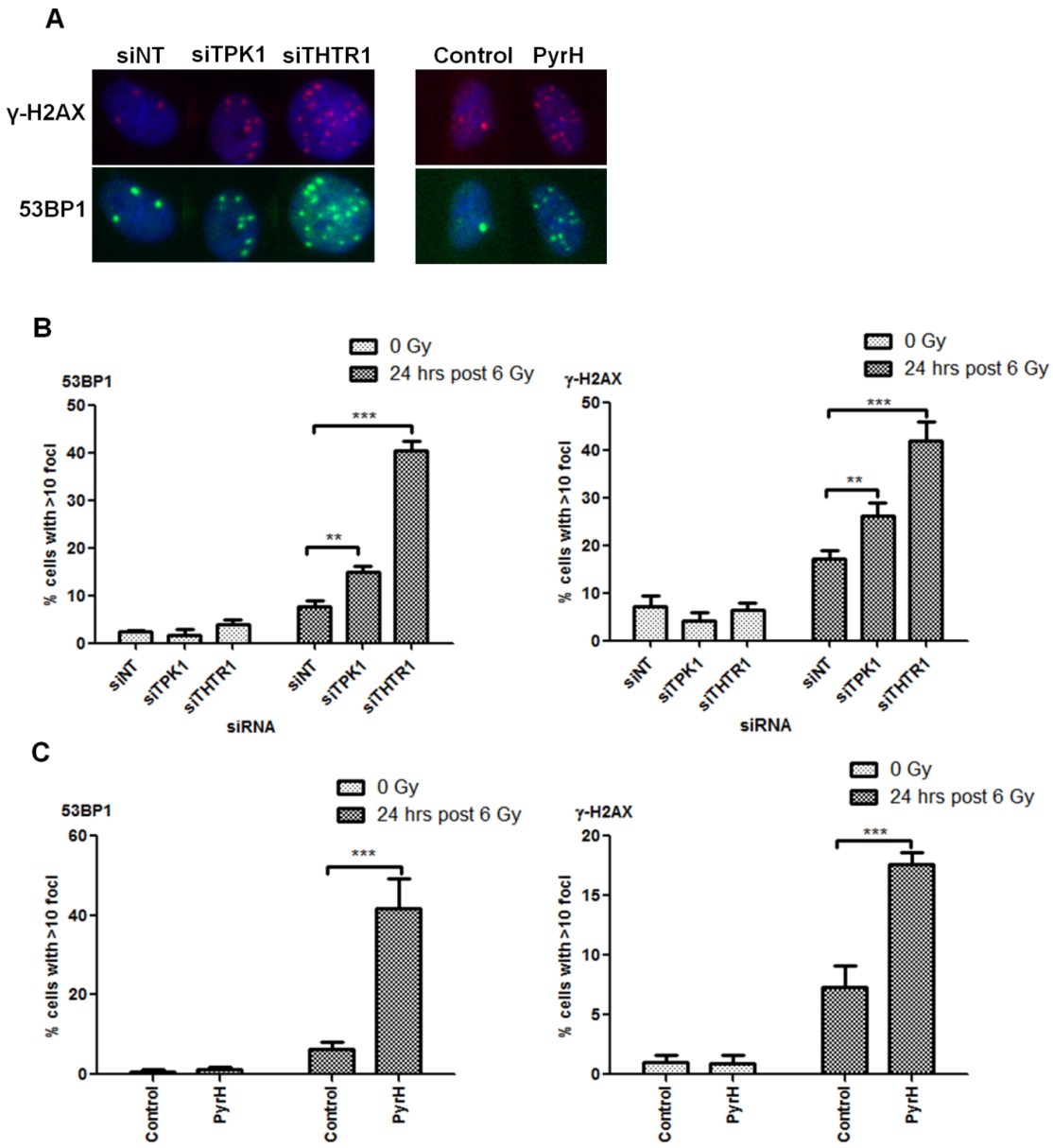

Figure 4.10. Persistent DNA-damage is observed following disruption of thiamine metabolism pathway

A) Immunofluorescence microscopy of HeLa cells irradiated with 6 Gy following treatment with either DMSO or 10 μM PyrH, or transfected with 40 nM Ambion siRNA (siNT, siTPK1 and siTHTR1). Cells were fixed 24 hours post irradiation, and probed for 53BP1 (green), γ-H2AX (red) and nuclei (blue). Images were captured on IN Cell Analyzer 1000 (GE Healthcare). Images are representative of irradiated and stained cells. **B)** DNA-damage foci quantification of HeLa cells irradiated following 72-hour transfection with 40 nM Ambion siNT, siTPK1 and siTHTR1. Cells were fixed 24 hours post irradiation, and probed for 53BP1 and γ-H2AX. Images were captured on IN Cell Analyzer 1000 (GE Healthcare) and quantified on IN Cell Analyzer workstation (GE Healthcare). **C)** DNA-damage foci quantification of HeLa cells irradiated following 4 days incubation with DMSO (control) or 10 μM PyrH. Cell staining and quantification as described in B. DNA-damage foci: Representative of three independent experiments, data represented as mean +/- SD from triplicate wells. Unpaired two-sided students t-tests comparing siNT to candidate knockdown $^{**}p<0.01$, $^{***}p<0.001$. Permission gained for use of figure from Tiwana *et al.*,2015.

As thiamine pyrophosphate is required as a cofactor for transketolase in the pentose-phosphate pathway for the production of ribose-5-phosphate, utilised in the production of nucleotides, we tested whether cells treated with the thiamine analogue had reduced levels of cellular nucleotides. High performance liquid chromatography (HPLC) analysis confirmed that dATP, dCTP, dGTP and dTTP were all reduced in cells treated with PyrH (Fig. 4.11).

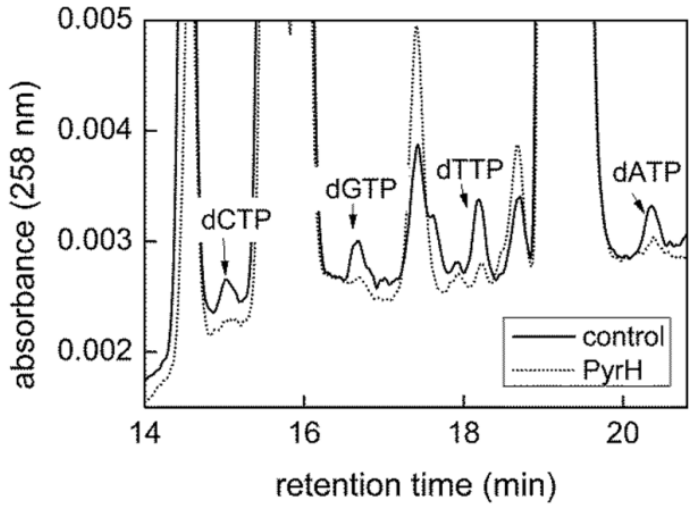

Figure 4.11. Pyrithiamine hydrobromide (PyrH) causes a reduction in deoxynucleotide triphosphates (dNTPs)

High performance liquid chromatography: HeLa cells were incubated with DMSO (control) or 10 μM PyrH for 4 days in M199 media. Representative of three independent experiments. Adapted and permission gained from Tiwana *et al*.,2015.

4.3 Discussion

To identify novel modulators of tumour radiosensitivity, the colony formation assay (CFA) was adapted for high-throughput screening. Although the adaptation of the CFA for screening purposes has been trialled by others (Katz et al., 2008; Lin et al., 2014) , this is the first implementation of CFA for a siRNA screen, which led to the identification of TPK1 as a potential radiosensitisation target. In this study, TPK1 and thiamine metabolism were shown to be linked to tumour radioresistance.

4.3.1 Radiosensitivity of TPK1 knockdown is linked to the pentose-phosphate pathway

Thiamine is transported and then converted by TPK1 into its active form, thiamine pyrophosphate (TPP), which can then be transported into the mitochondria by TPC and used as co-factor for the citric acid cycle enzymes α-ketogluturate dehydrogenase and pyruvate dehydrogenase complex (Danner et al., 1978; Hawkins et al., 1989). TPP is also a co-factor for the transketolase enzyme required for the production of ribose-5 phosphate (R5-P) in the non-oxidative arm of the pentose phosphate pathway.

Unlike TPK1 and THTR1 knockdown, TPC knockdown did not cause an increase in radiosensitivity (Fig. 4.6A), suggesting that TPK1 depletion-induced radiosensitivity is primarily brought about through the activity of TPP in the pentose phosphate pathway. Since the non-oxidative arm of this pathway is used to produce the backbone of nucleotides, R-5P (Usmanov et al., 1985), it could be postulated that inhibition of thiamine metabolism would result in reduction in nucleotide pools. This was indeed found to occur when cells were treated with PyrH (Fig.4.11). This model fits with observations that inhibition of the transketolase enzyme by oxythiamine caused a reduction in R-5P, nucleotide acid synthesis and a subsequent tumour proliferation delay (Boros et al., 1997; Rais et al., 1999).

The radiosensitisation seen with PyrH treatment, TPK1 and THTR1 knockdown was accompanied by a persistence of DSB foci after irradiation (Fig. 4.10A, B, C). THTR1 knockdown was associated with a greater number of residual 53BP1 and γ-H2AX foci compared to siTPK1, but interestingly this did not translate to increased radiosensitisation, which was similar for TPK1 and THTR1 knockdown (Fig. 4.5A). These observations could be explained by different effects on DNA repair kinetics or additional unknown roles for thiamine metabolism that contribute to tumour radioresistance.

It could be hypothesised that the increased unresolved DNA-damage breaks seen after thiamine metabolism inhibition may occur due to the low levels of nucleotides reducing the efficiency of DNA-repair leading to increased radiosensitivity. A model of radiosensitisation by inhibition of thiamine metabolism has been depicted in Figure 4.12.

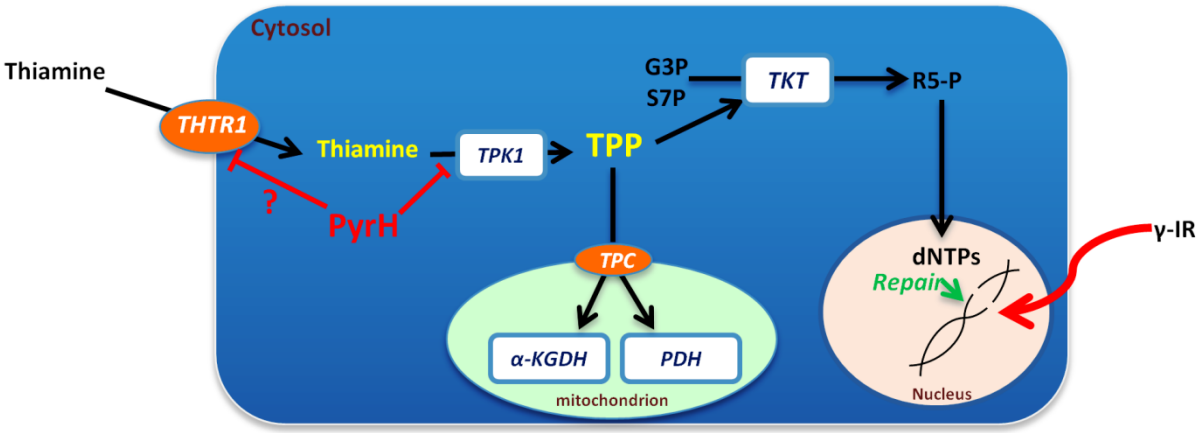

Figure 4.12. Possible model of radiosensitisation by thiamine metabolism inhibition.
Thiamine enters the cell via the THTR1 transporter where it is readily converted to TPP by TPK1. TPP is a co-factor for TKT in the non-oxidative PPP which catalyses from G3P and S7P the production of R5-P, the sugar phosphate backbone of dNTPs. TPP can also be transported into the mitochondria by TPC and used as a prosthetic group for PDH and α-KGDH. Thiamine metabolism can be perturbed by THTR1 and TPK1 knockdown, reducing thiamine uptake and production of TPP, respectively. In addition, disruption of thiamine metabolism can be achieved by the thiamine analogue PyrH, reducing TPP levels and possibly also thiamine uptake directly. As less TPP is available as a co-factor for TKT, the production of R5-P is decreased. This results in an inhibition of nucleotide production, reducing the cell's capability to repair DNA after irradiation and increasing cell death. The mitochondrial functions of TPP do not appear to be linked with radiosensitivity as knockdown of the mitochondrial transporter, TPC did not affect radiosurvival. Permission gained for use of figure from Tiwana *et al*.,2015.

4.3.2 Clinical feasibility of disrupting thiamine metabolism

The finding that TPK1 depletion or inhibition caused radiosensitisation in tumour but not normal tissue cells suggests that inhibiting TPK1 may be a potentially useful clinical strategy to cause tumour-specific radiosensitisation. The main obstacle to such an approach lies in the complications associated with thiamine deprivation. The most common clinical manifestation of thiamine deficiency is Wernicke's encephalopathy, which results from long-standing, severe alcohol abuse and can be reversed by prompt administration of parenteral thiamine following signs of initial clinical symptoms (Blass and Gibson, 1977). Individuals with autosomal mutations in the TPK1 gene exhibit

features of dystonia, lactic acidosis and retardation symptoms, typically after age one (Mayr et al., 2011).

Long-term thiamine depletion is thus not a viable clinical option. However, conventional radiotherapy is typically delivered over a duration of several weeks, stereotactic ablative body radiotherapy over a period of days and brachytherapy over a few hours. It is therefore possible that temporary inhibition of thiamine metabolism may improve the efficacy of radiotherapy before clinical symptoms of thiamine deficiency become apparent. Such a rationale is similar to the use of the folic acid antagonist methotrexate in acute lymphocytic leukemia and osteosarcoma (Cohen and Wolff, 2014), which is administered at high-doses that might otherwise be fatal, but this outcome is avoided by reversal with folinic acid before folic acid deficiency results in clinically apparent symptoms.

Future work will require the *in vivo* validation of the *in vitro* findings described in this chapter. The use of compounds such as oxythiamine, a competitive analogue of thiamine that unlike PyrH does not cross the blood brain barrier (Greenwood and Pratt, 1985), may circumvent the neurotoxicity associated with thiamine depletion.

CHAPTER 5

GSK3β, MARK2 AND SRP72

CANDIDATE GENE VALIDATION

5.1 Introduction

Following the successful validation of thiamine metabolism as a potentially clinically exploitable tumour specific radiosensitisation pathway, additional candidate genes from the kinome screening were evaluated for their potential as radiosensitisation targets.

Glycogen synthase kinase-3 beta (GSK-3β), MAP/microtubule affinity regulating kinase 2 (MARK2) and signal recognition protein 72 (SRP72) were investigated in further detail. GSK-3β was chosen because of recent studies suggesting that inhibition of GSK-3β is radioprotecting in normal tissue such as small intestine (Thotala et al., 2008), bone marrow (Thotala et al., 2008) and hippocampal neurones (Thotala et al., 2012; Yang et al., 2011). In cancer cells such as neuroblastoma, there is decreased viability and tumour growth delay observed with inhibition of GSK-3β (Dickey et al., 2011). This suggests that there is a potential therapeutic window for GSK-3β modulation in radiotherapy that warrants further investigation. MARK2 and SRP72 have not been implicated in radioresistance and were investigated because of their novelty in modulating tumour intrinsic radiosensitivity. Further justifications for candidate gene choices can be found in Table 3.1 (Chapter 3), which includes cancer over-expression data. The rank product scores of the chosen candidate siRNAs from the secondary kinome screen with ATM selected as a positive control are shown below in Table 5.1.

Ranked	siRNA	Rank product score	R-score Run1	R-score Run2
1	ATM	3.30	-7.43	-7.37
5	MARK2	7.96	-5.62	-5.63
25	SRP72	28.96	-4.27	-2.23
27	GSK-3β	31.34	-4.60	-2.95

Table 5.1 Rank-product analysis of the MARK2, SRP72 and GSK-3β

Selected candidate siRNAs ordered by rank product by analysing the secondary kinome screen runs. Rank product scores were calculated based on R-score. Radiosensitising siRNAs shown by R-scores <0.

The most relevant cellular functions and their involvement in tumour growth of these three genes are summarised below.

5.1.2 Glycogen synthase kinase- 3β (GSK-3β)

GSK-3β and GSK-3α are isoforms of the ubiquitously expressed GSK-3 protein kinase (Woodgett, 1990). The protein function of GSK-3 was originally isolated from rat skeletal muscles and its function placed within the glycogen biosynthesis pathway, where an inhibitory phosphorylation inactivates glycogen synthase (Embi et al., 1980; Parker et al., 1983). It has since been found to be involved in a myriad of cellular processes which include growth signalling (Pap and Cooper, 2002), insulin response (Mussmann et al., 2007; Welsh and Proud, 1993), cell structure (Culbert et al., 2001), apoptosis (Hoeflich et al., 2000; Pap and Cooper, 1998), differentiation (Esfandiari et al., 2012) and cell cycle regulation (Wakefield et al., 2003).

GSK-3β has a controversial and complicated role in cancer as both a tumour suppressor and promoter, and the genetic background of the tumour cell plays a significant role in determining its response to modulation of GSK-3β. In COS-1 prostate cancer cells, expression of GSK-3β was able to repress androgen-mediated transactivation, demonstrating the ability to act as tumour suppressor (Wang et al., 2004). Conversely, inhibition of GSK-3β in colon cancer cells resulted in a reduction in

proliferation and induction of apoptosis, illustrating that it can act as a tumour promoter (Grassilli et al., 2013; Shakoori et al., 2007).

Signals directed towards GSK-3β arrive from several pathways, however wingless signalling protein (Wnt)/ β-Catenin and PI-3K signalling play the predominant part. Under physiological conditions, GSK-3β is constitutively active following phosphorylation at tyrosine 216 (Hughes et al., 1993). In this 'resting state', GSK-3β acts as a functional repressor of many of its substrates. One major substrate of GSK-3β is β-Catenin. GSK-3β is kept in a complex of proteins which includes β-Catenin, axins and adenomatous polyposis coli (APC) (Behrens et al., 1998; Ikeda et al., 1998). Within this complex, GSK-3β is able to phosphorylate β-Catenin, which marks it for degradation by the proteosome, mediated by ubquitin (Aberle et al., 1997). External stimuli such as insulin signalling through protein kinase B (AKT) (Cross et al., 1995) or Wnt (Inoki et al., 2006), result in inhibitory phosphorylation at serine 9 of GSK-3β (Sutherland et al., 1993). This leads to an accumulation of β-Catenin in the nucleus and cytoplasm. β-Catenin complexes with T cell factor (TCF) / lymphoid enhancer factor (LEF) proteins within the nucleus (Behrens et al., 1996; Molenaar et al., 1996). These complexes bind to TCF/LEF promoter binding sites of target gene sequences, initiating expression of genes such as Cyclin D1 and promoting tumour growth.

In addition to the transcriptional changes brought about by β-Catenin accumulation, GSK-3β is able to directly influence many other transcription factors which include c-myc (Gregory et al., 2003), snail1 (Yook et al., 2006), nuclear factor-KB (Demarchi et al., 2003), p53 (Turenne and Price, 2001), PTEN (Al-Khouri et al., 2005) and c-Jun (Wei et al., 2005). Hence, this protein can affect tumour growth and differentiation through a number of cellular pathways and processes. Although GSK-3β has been

heavily investigated in cancer, there remain unanswered questions surrounding its impact on tumour radioresistance.

5.1.3 Signal recognition particle 72 kDa (SRP72)

SRP72 is part of a ribonucleoprotein complex, known as the signal recognition particle (SRP), that includes 7S RNA and several protein subunits. SRP72 was first purified from canine pancreas by blocking proteins from leaving the cell membrane using high ionic salt concentrations (Walter and Blobel, 1980; Walter and Blobel, 1982; Walter et al., 1981). SRP function is highly conserved, however the component composition varies across species. In mammalian cells, the components include SRP9, SRP14, SRP19, SRP54, SRP68, and SRP72.

SRP is involved in translocation of ribosome bound nascent pre-secretory proteins to the rough endoplasmic reticulum (RER), ahead of being integrated as trans-membrane or secreted proteins (Lutcke, 1995). The importance of this is to help secretory proteins to travel across the hydrophobic lipid bi-layers, and preventing the proteins from obtaining unfavourable structural confirmations (Lutcke, 1995). The SRP achieves this by first recognising the hydrophobic ends of the nascent protein using the methionine rich end of the SRP54 subunit, forming a complex known as ribosome nascent chain complex (RNC) (Lutcke et al., 1992; Zopf et al., 1990). The next step is to prevent further elongation of the translating mRNA which is most likely achieved by SRP9/14-RNA domains of the SRP complex known as Alu domains (Thomas et al., 1997). The RNC binds to the RER membrane following interaction with the SRP receptor in a guanosine triphosphate (GTP) dependent manner (Fulga et al., 2001; Gilmore et al., 1982; Jiang et al., 2008; Rapiejko and Gilmore, 1997). When the SRP complex disassociates from the ER, elongation and translocation commences. SRP72 has been the least characterised subunit of the SRP ribonucleoprotein complex. SRP72 has a

RNA binding domain and directly interacts with SRP68 and is thought to be involved in the recognition of nascent protein (Iakhiaeva et al., 2005; Yin et al., 2007).

Familial mutations in SRP72 have been associated with bone marrow failure and deafness in patients attributed to this functional loss (Kirwan et al., 2012). However, the literature surrounding SRP72 involvement in cancer growth or progression is nominal. One study exploring the differences between how death receptor 4 and 5 (DR4 & DR5) are regulated in response to TRAIL mediated apoptosis identified SRP72 as a regulator of this response (Ren et al., 2004). The authors found that depleting SRP72 in HCT15 cells conferred resistance against DR4 dependent apoptosis (Ren et al., 2004). However, depletion of SRP54 gave similar results, suggesting that this is not solely dependent on SRP72 function (Ren et al., 2004). Furthermore, a cDNA study carried out in gastric cancer cells looking at genes associated with 5-flourouracil-resistance identified SRP72 expression as part of a resistance signature, yet no experimental work was carried out to support this claim (Park et al., 2002). Cumulatively, very little is known about SRP72, its role in cancer and in tumour cell radioresistance.

5.1.4 MAP/Microtubule Affinity-Regulating Kinase 2 (MARK2)

MARK2 also known as partitioning defective-1b (PAR1b) and EFKL motif kinase 1(EMK1), is a highly conserved serine/threonine kinase. MARK2 is part of a family of four kinases in mammalian cells, which comprises PAR1c (MARK1), PAR1a (MARK3) and PAR1d (MARK4). MARK2 was originally isolated from mouse embryos using degenerate PCR techniques (Inglis et al., 1993). The first known functional role of MARK2 was discovered in a study to identify mammalian homologs to the partition deficient kinases (PAR-1) in *C.elegans* (Bohm et al., 1997). Screening of *C.elegans* had identified the importance of these PAR genes in polarisation of epithelial cells at the apico-basal membrane. Polarisation is fundamental as it enables the cell to break its

isotropic morphology to carry out division, differentiation and various cell death fates (Macara, 2004). This is achieved by regulating the tubulin and actin filaments that are asymmetrically organised in the cell.

MARK2 affects cell polarity by regulating tau and other microtubule associated proteins (MAP) such as MAP2c and MAP4 (Drewes et al., 1997). Its importance in cell polarity was demonstrated by the almost complete microtubule disassembly and subsequent rounding in MARK2 over-expressing CHO cells (Drewes et al., 1997). MARK2 is localised with atypical protein kinase C (aPKC) at the lateral membrane tight junctions of epithelial cells and it is directly phosphorylated by aPKC at threonine 595 (Suzuki et al., 2004). This phosphorylation results in the binding of MARK2 to 14-3-3 proteins and causes MARK2 to disassociate from the lateral membrane. MARK2 then goes on to form membrane domains which effect the epithelial polarity (Suzuki et al., 2004). The molecular mechanisms behind polarity regulation by MARK2 have not been completely elucidated in mammalian cells. However, it is important to note that MARK2 has other functions, demonstrated by knockout mice studies demonstrating dysregulation in the immune system, glucose metabolism, and adiposity regulation (Hurov et al., 2007; Hurov et al., 2001).

In cancer, MARK2 was first identified as a tumour suppressor, preventing the transformation of canine MDCK epithelial cells (Elbert et al., 2006). siRNA mediated depletion of MARK2 in these cells resulted in a reduction in E-cadherin dependent cell-cell adhesion. Additionally, MARK2 has also been implicated in gastric carcinogenesis caused by cytotoxin-associated gene A (cagA) positive *Helicobacter pylori* (*h.pylori*) infection. *H.pylori* introduces cagA into the cytoplasm of gastric cells by a type IV secretion system which resembles a syringe like complex encoded by the genes located on its pathogenicity island (PAI) (Backert et al., 2000; Tegtmeyer et al., 2014).

CagA causes the loss of polarity in apical-basolateral membranes of epithelial cells by disturbing the tight junctions, by interaction with the kinase domain of MARK2 and inhibiting its activity (Nesic et al., 2010; Saadat et al., 2007). This causes defects in the epithelial polarisation and allows the oncogenic phosphatase SHP-2 to bind to multimirised cagA, thus promoting transformation of the gastric cells (Saadat et al., 2007). SHP-2 promotes cell transformation through the ras-MAP pathway and induces a phenotype known as hummingbird (Higashi et al., 2004). Hummingbird phenotype is caused by a drastic change in cytoskeletal organisation, increased cellular motility and an elongation of the epithelial cells. MARK2 involvement in cancer has predominantly focused around its role in tumour cell transformation and no information is available on its role in tumour radioresistance.

GSK-3β, MARK2 and SRP72 have clear merits as outlined previously for further investigation as genes associated with tumour cell radioresistance.

5.2 Results

5.2.1 GSK-3β, MARK2 and SRP72 are linked to tumour cell radioresistance

Following the identification of GSK-3β, MARK2 and SRP72 from the high throughput screen described in chapter 3, we confirmed that the identification of the candidate genes were not due to off-target effects of the library siRNA by conducting a standard clonogenic assay using two separate siRNA strands obtained from a different vendor (Ambion) than the one used in the screen (Dharmacon ON-TARGETplus). Knockdown of GSK-3β using either of two Ambion Silencer Select siRNA strands radiosensitised HeLa cells in colony-forming assays (Fig.5.1A). The SER_{10} for siGSK-3β-1 and siGSK-3β-2 was 1.35 and 1.21, respectively. Knockdown of MARK2 significantly radiosensitised HeLa cells yielding SER_{10} values of 1.2 and 1.375 for siMARK2-1 and siMARK2-2, respectively (Fig.5.1B). Similarly, knockdown of SRP72 significantly

radiosensitised HeLa cells producing SER_{10} values of 1.32 and 1.24 for siSRP72-1 and siSRP72-2, respectively (Fig.5.1C). Knockdown of the gene products were confirmed by immunoblotting. The 0 Gy plating efficiencies (PE) for target genes were lower than siNT for all gene knockdowns, suggesting some degree of toxicity caused by gene knockdown itself.

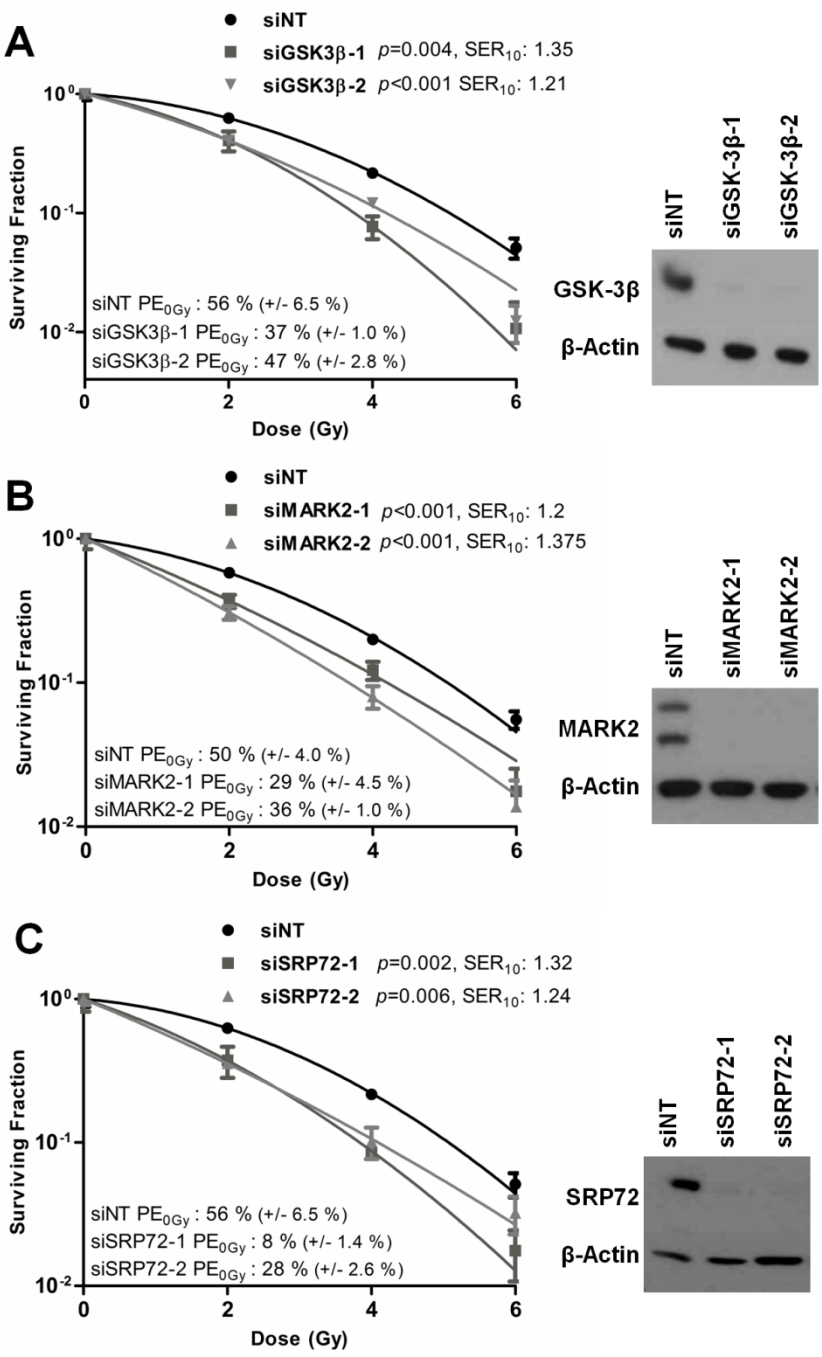

Figure 5.1. Validation of radiosensitisation by target gene knockdown.

A) CFA of HeLa cells irradiated following 20 nM Ambion siRNA transfection with non-targeting (siNT), siGSK-3β1 and siGSK-3β2. Knockdown was confirmed by immunoblotting (insets). **B**) CFA of HeLa cells irradiated following 20 nM Ambion siRNA transfection with siNT, siMARK2-1 and siMARK2-2. Knockdown was confirmed by immunoblotting (inset). **C**) CFA of HeLa cells irradiated following 20 nM Ambion siRNA transfection siNT, siSRP72-1 and siSRP72-2. Knockdown was confirmed by immunoblotting (inset).

CFA: representative of three independent experiments, data points and plating efficiencies at 0 Gy (PE_{0Gy}) represented as mean +/- SD from triplicate wells, *p*-values generated by factorial 2-way ANOVA. Sensitisation enhancement ratio at 10% surviving fraction (SER_{10}) calculated from non-linear regression of linear quadratic model.

To demonstrate that the observed radiosensitivity was not restricted to HeLa cells, colony formation assays were conducted in cancer cell lines derived from tumour types typically treated with radical radiotherapy. Knockdown of GSK-3β significantly radiosensitised the SQ20B head and neck squamous cell carcinoma cell line (SER_{10} of 1.06; p <0.001, Fig.5.2). Knockdown of GSK-3β also reduced the PE_{0Gy} to 13% compared to 37% for siNT. MARK2 and SRP72 knockdown were lethal in the SQ20B cell line.

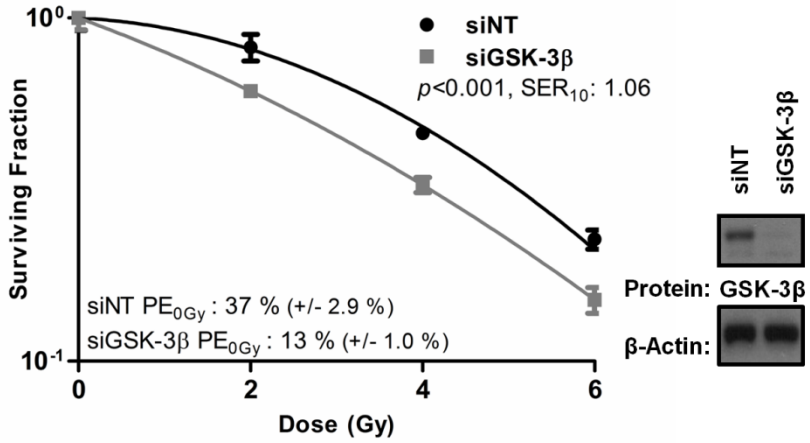

Figure 5.2. GSK-3β knockdown radiosensitises the SQ20B cell line

A) CFA of SQ20B cells irradiated following 20 nM Ambion siRNA transfection with siNT and siGSK-3β. Knockdown was confirmed by immunoblotting (Inset; knockdown of MARK2 and SRP72 was lethal)**.** Representative of three independent experiments, data points and plating efficiencies at 0 Gy (PE_{0Gy}) represented as mean +/- SD from triplicate wells, *p*-values generated by factorial 2-way ANOVA. Sensitisation enhancement ratio at 10% surviving fraction (SER_{10}) calculated from non-linear regression of linear quadratic model.

The T24 bladder carcinoma cell line was also radiosensitised following knockdown of GSK-3β (SER_{10} of 1.187; p =0.001, Fig.5.3A), MARK2 (SER_{10} of 1.52; p <0.001, Fig.5.3B) and SRP72 (SER_{10} of 1.307; p <0.001, Fig.5.3C). Knockdown of SRP72 and GSK-3β reduced the PE_{0Gy} in the T24 cell line in the absence of radiation (Fig.5.3).

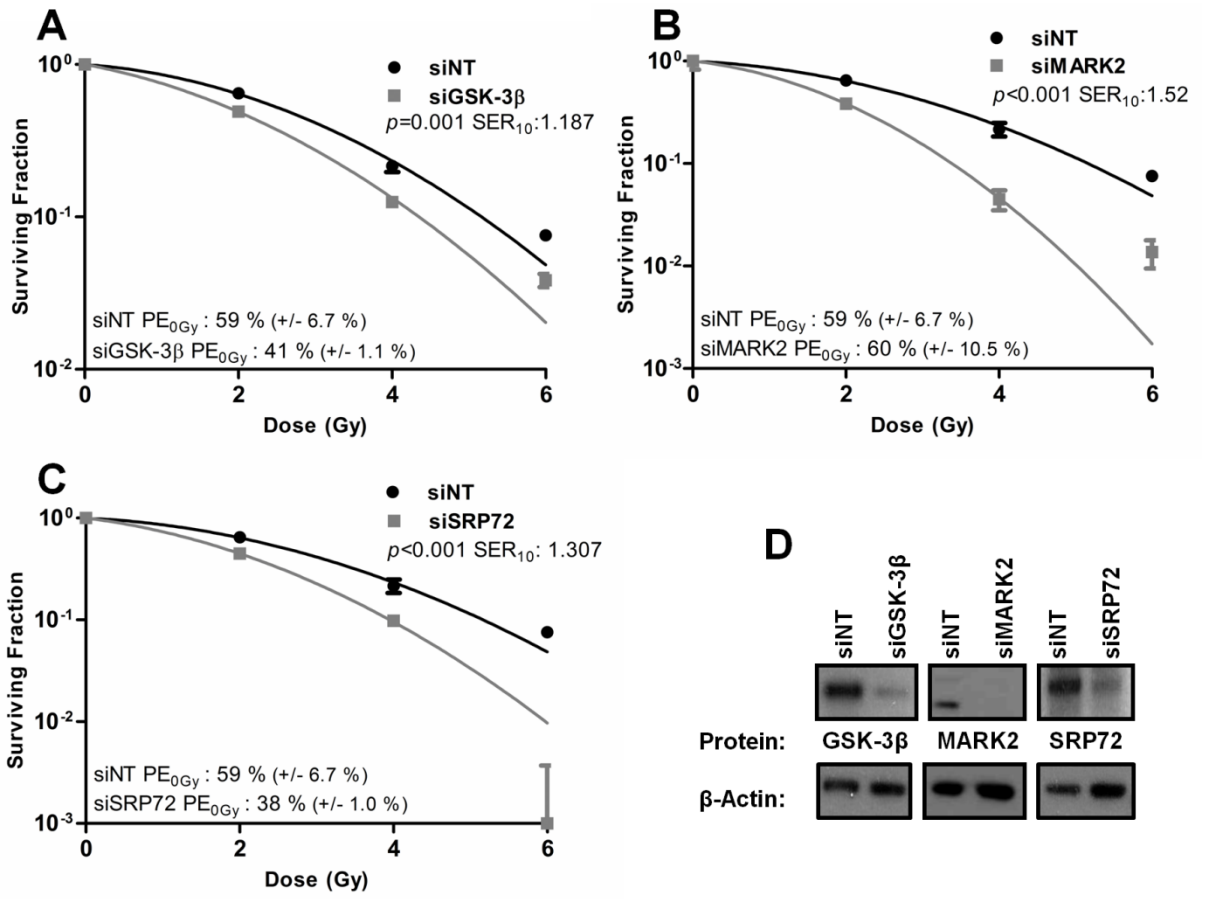

Figure 5.3. GSK-3β, MARK2 and SRP72 knockdown radiosensitises the T24 bladder carcinoma line

CFA of T24 cells irradiated following 20 nM Ambion siRNA transfection with siNT, siGSK-3β **(A),** siMARK2 **(B)**, and siSRP72 **(C). D)** Knockdown was confirmed for A-C by immunoblotting. CFA: representative of three independent experiments, data points and plating efficiencies at 0 Gy (PE_{0Gy}) represented as mean +/- SD from triplicate wells, *p*-values generated by factorial 2-way ANOVA. Sensitisation enhancement ratio at 10% surviving fraction (SER_{10}) calculated from non-linear regression of linear quadratic model.

In addition, the PSN1 pancreatic adenocarcinoma cell line was significantly radiosensitised following the knockdown of MARK2 (SER_{10} of 1.468; p <0.001, Fig.5.4B) and SRP72 (SER_{10} of 1.15; p=0.003, Fig.5.4C). However, GSK-3β knockdown had no effect on radiosensitisation, but there was still a reduction in PE_{0Gy} as seen with the previous cell lines.

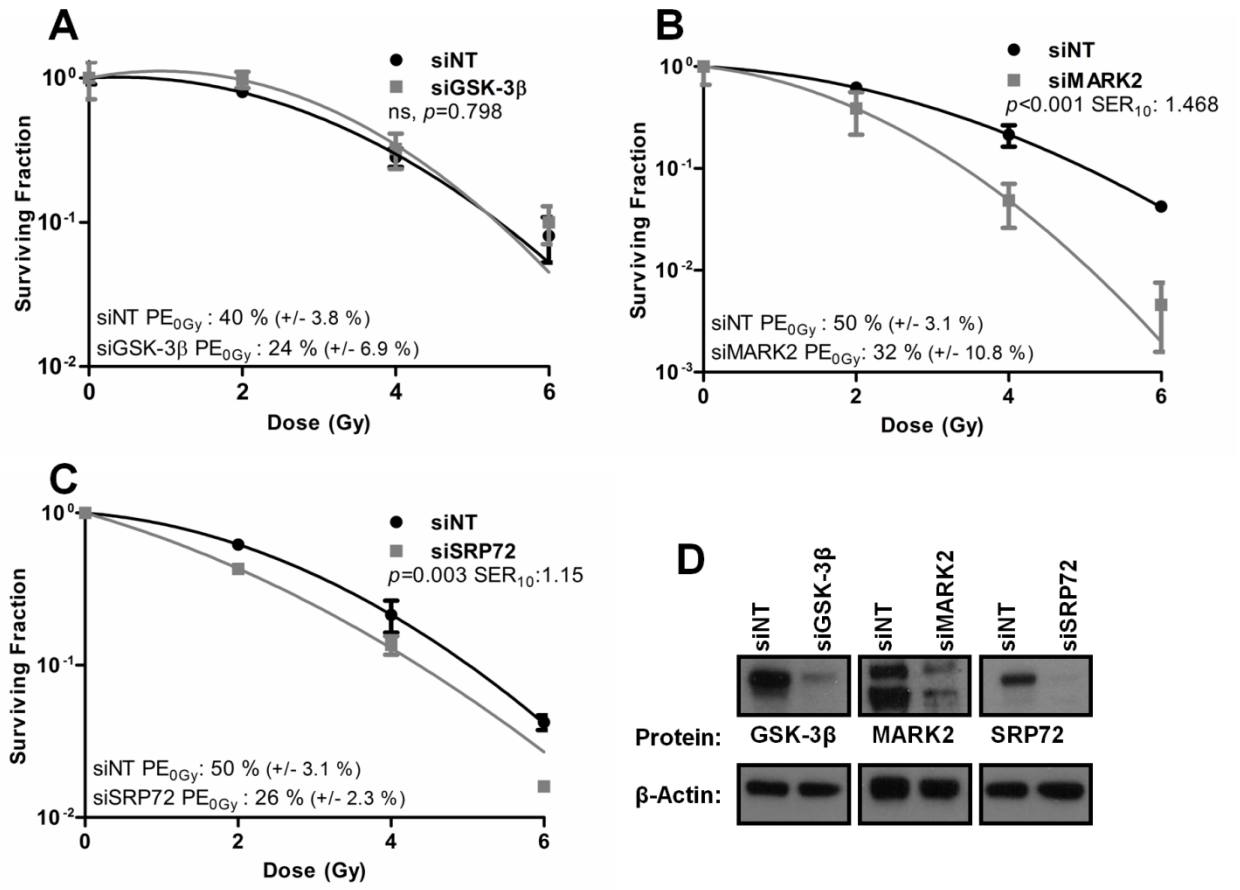

Figure 5.4. Effect of GSK-3β, MARK2 and SRP72 knockdown on radiosensitivity in the PSN-1 pancreatic adenocarcinoma line

CFA of PSN-1 cells irradiated following 20 nM Ambion siRNA transfection with siNT, siGSK-3β **(A),** siMARK2 **(B)**, and siSRP72 **(C). D)** Knockdown was confirmed for A-C by immunoblotting. CFA: representative of three independent experiments, data points and plating efficiencies at 0 Gy (PE_{0Gy}) represented as mean +/- SD from triplicate wells, *p*-values generated by factorial 2-way ANOVA. Sensitisation enhancement ratio at 10% surviving fraction (SER_{10}) calculated from non-linear regression of linear quadratic model.

In the MCF7 breast ductal carcinoma cell line there was some sensitisation following the knockdown of GSK-3β but this was not significant, although the factorial 2-way ANOVA suggested there was significant difference in SER_{10} between siNT and siGSK-3β curves. The knockdown of GSK3β was toxic, causing a significant drop in PE_{0Gy} compared with siNT, subsequently making it difficult to produce reliable survival curves. However, the MCF7 cells were radiosensitised following the knockdown of MARK2

(SER_{10} of 1.61; p<0.0001, Fig.5.5B) and SRP72 (SER_{10} of 1.56; p=0.011, Fig.5.5C). As seen with siGSK-3β, a drop in PE_{0Gy} was observed with siSRP72 compared with siNT.

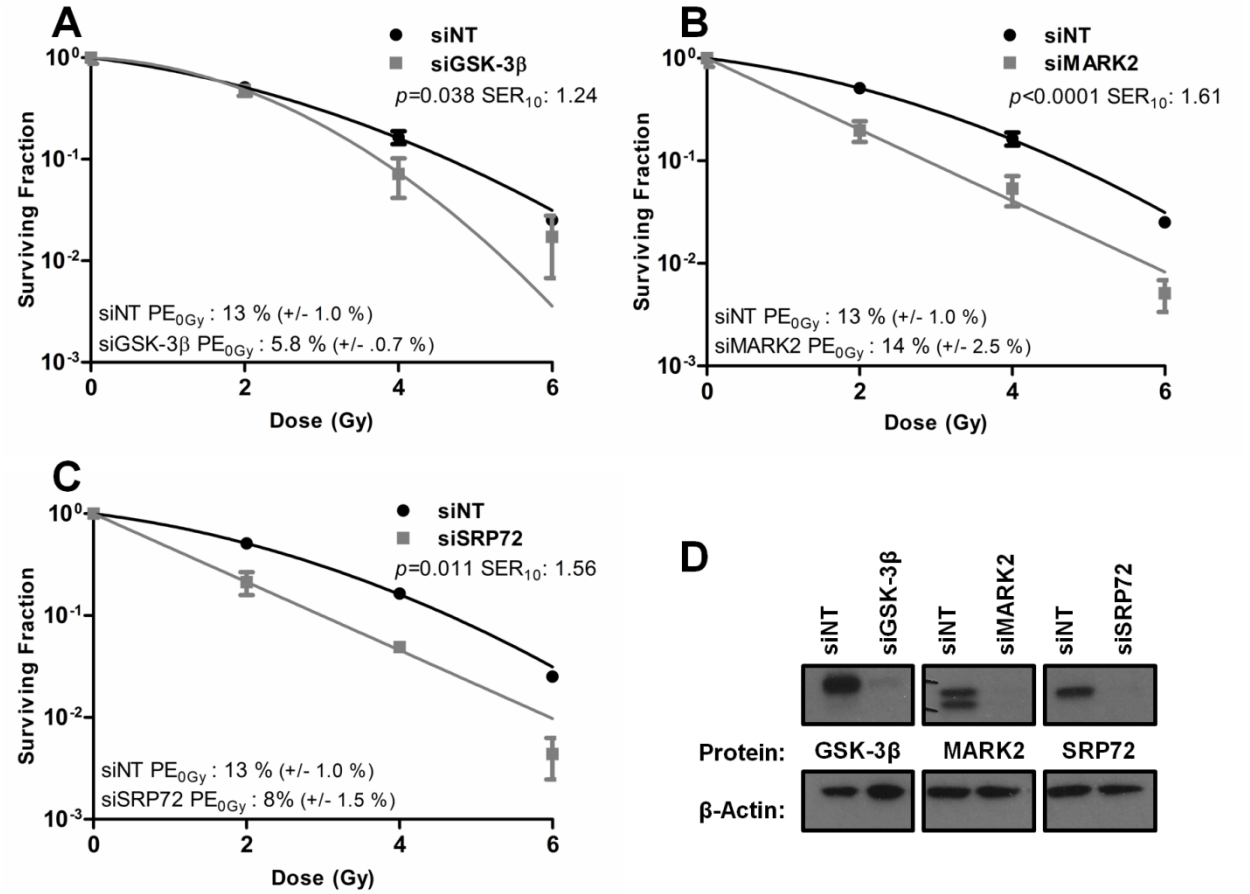

Figure 5.5. Effect of GSK-3β, MARK2 and SRP72 knockdown on radiosensitivity of the MCF7 breast adenocarcinoma line

CFA of MCF-7 cells irradiated following 20 nM Ambion siRNA transfection with siNT, siGSK-3β **(A),** siMARK2 **(B)**, and siSRP72 **(C). D)** Knockdown was confirmed for A-C by immunoblotting. CFA: representative of three independent experiments, data points and plating efficiencies at 0 Gy (PE_{0Gy}) represented as mean +/- SD from triplicate wells, p-values generated by factorial 2-way ANOVA. Sensitisation enhancement ratio at 10% surviving fraction (SER_{10}) calculated from non-linear regression of linear quadratic model.

5.2.2 Knockdown of candidate genes radiosensitises normal tissue cell lines

After determining that depletion of the candidate genes radiosensitised tumour lines, normal tissue fibroblasts were investigated. MRC5 lung fibroblast cells were radiosensitised following the knockdown of GSK-3β (SER_{10} of 1.48; p=0.006, Fig.5.6A), MARK2 (SER_{10} of 1.72; p <0.01, Fig.5.6B) and SRP72 (SER_{10} of 1.23; p =0.001, Fig.5.6C). The knockdown of all three genes caused a drop in PE_{0Gy}.

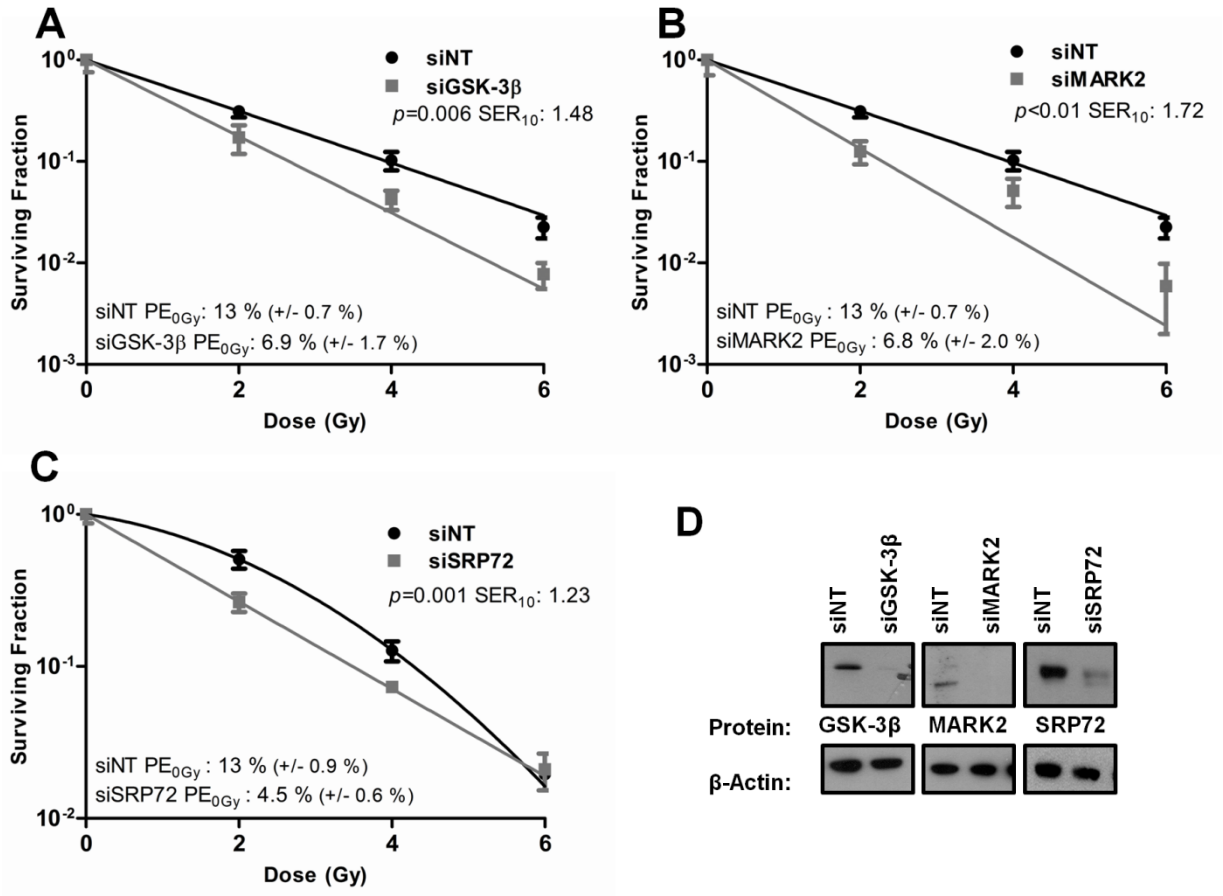

Figure 5.6. GSK-3β, MARK2 and SRP72 depletion radiosensitises the MRC5 lung fibroblast cell line

CFA of MRC5 cells irradiated following 20 nM Ambion siRNA transfection with siNT, siGSK-3β **(A),** siMARK2 **(B)**, and siSRP72 **(C). D)** Knockdown was confirmed for A-C by immunoblotting. CFA: representative of three independent experiments, data points and plating efficiencies at 0 Gy (PE_{0Gy}) represented as mean +/- SD from triplicate wells, p-values generated by factorial 2-way ANOVA. Sensitisation enhancement ratio at 10% surviving fraction (SER_{10}) calculated from non-linear regression of linear quadratic model.

5.2.3 Knockdown of GSK-3β, MARK2 and SRP72 potentiates radiation induced apoptosis

Next the mechanism behind the radiosensitisation effect was investigated. Initially, differences in DNA-repair were assessed following IR treatment by quantifying DNA damage foci. GSK-3β knockdown caused significant elevation in 53BP1 foci (p<0.01, Fig.5.7A) 24-hours post-irradiation. Cell cycle analysis showed that this coincided with a G2/M arrest (Fig.5.7B). siSRP72 did not cause an elevation of DNA-damage foci but did cause a marginal increase in G2/M. siMARK2 had no effect on DNA-damage foci or cell cycle arrest compared with siNT (Fig.5.7A, B).

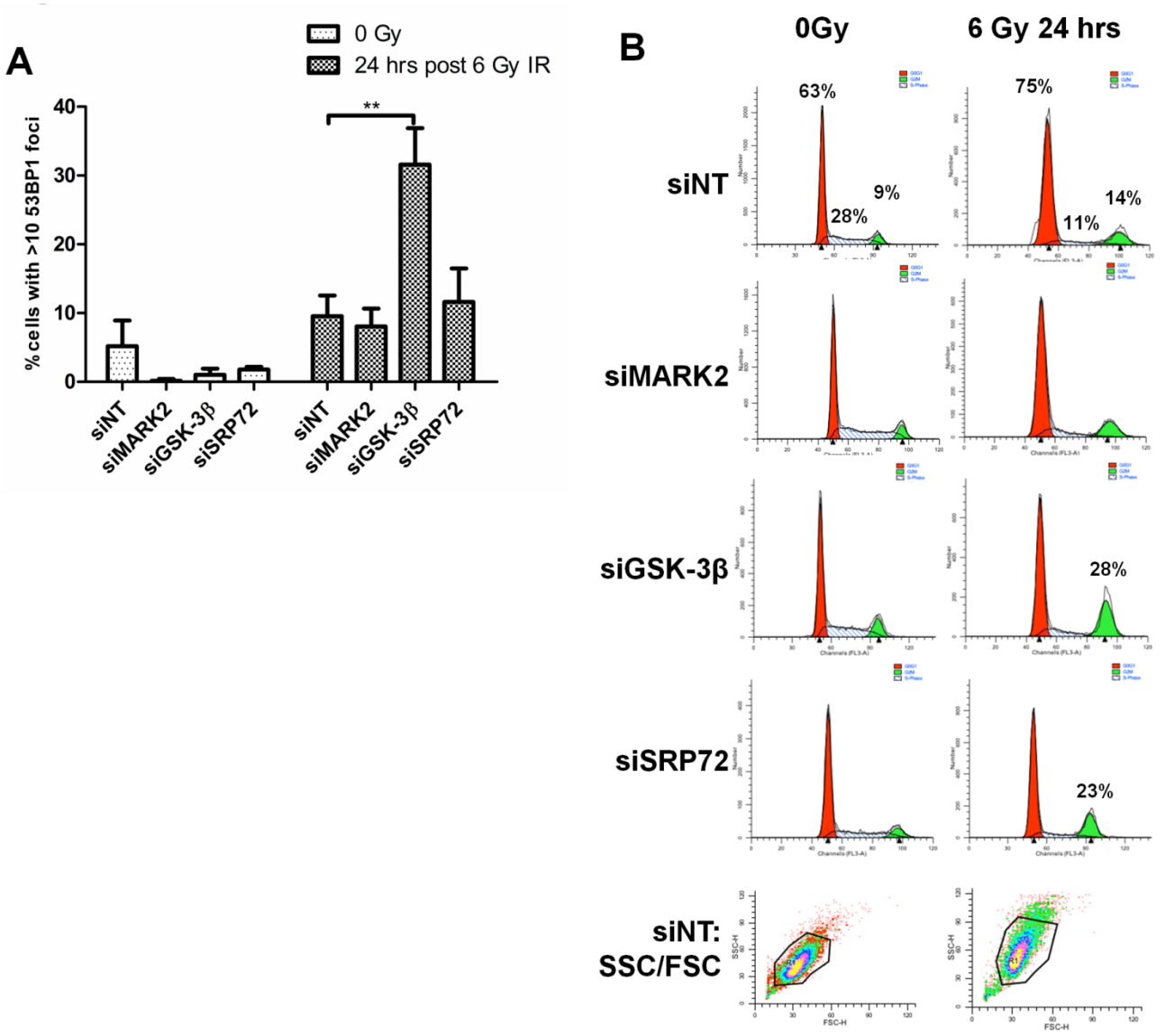

Figure 5.7. GSK-3β knockdown enhances IR induced DNA damage and causes cell cycle arrest

A) HeLa cells were irradiated following 20 nM Ambion siRNA transfection with siNT, siGSK-3β, siMARK2 and siSRP72. Cells were fixed 24 hrs post-irradiation and probed for 53BP1. DNA damage foci were imaged and quantified using the IN Cell Analyzer. Representative experiment of n=3 is shown, data represented as mean +/- SD from triplicate wells. Unpaired two-sided student's t-tests comparing siNT to target knockdown $^{**}p<0.01$. **B)** HeLa cells were irradiated following 20 nM Ambion siRNA transfection with siNT, siGSK-3β, siMARK2 and siSRP72. Cells were fixed 24 hrs post-irradiation and stained with propidium iodide. Total DNA quantification carried out by FACS and cell cycle phase proportions were calculated following curve fitting with ModFit software (red: G1, white: S; green: G2/M)

Subsequently, endpoints evaluating cell fate were investigated. GSK-3β inhibition or depletion has been previously demonstrated to enhance apoptosis in the absence of irradiation (Liao et al., 2003). In addition, SRP72 has been implicated in the post-translational modification events during apoptosis (Utz et al., 1998). Therefore, it was investigated whether knockdown of these genes potentiated apoptosis following irradiation. Poly ADP ribose polymerase (PARP) cleavage was measured by immunoblotting following 6 Gy IR. Cleaved PARP showed fold changes of 1.94, 2.08 and 1.63 for siMARK2, siGSK-3b and siSRP72 compared with 6 Gy siNT, respectively (Fig.5.8A). The elevation in apoptosis following knockdown of the three genes after IR was further confirmed by Annexin-V PI staining and caspase activity assays (Fig.5.8B, C). Knockdown of SRP72 also caused an increase in caspase 3/7 activity in the absence of IR.

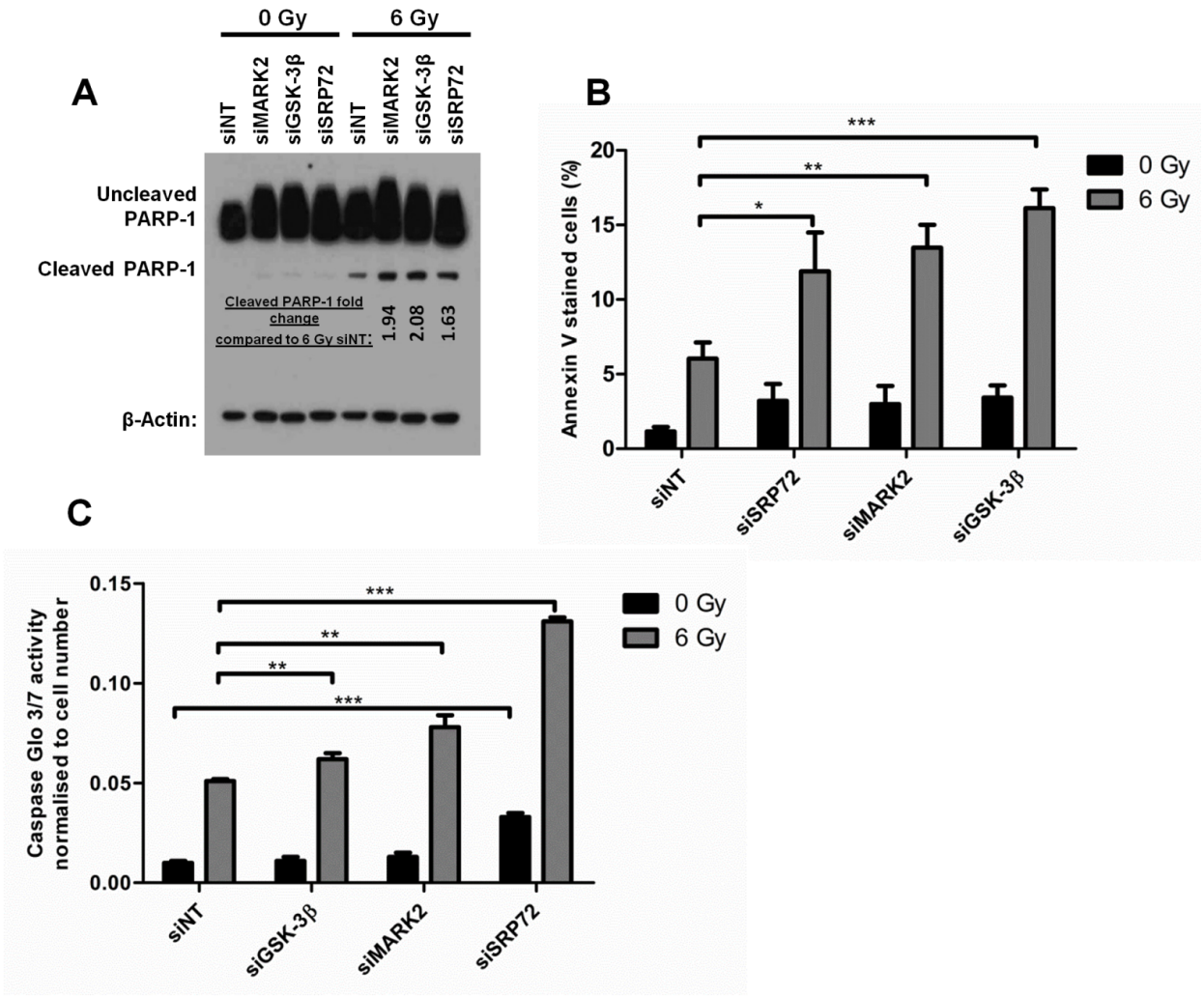

Figure 5.8. GSK-3β, MARK2 and SRP72 knockdown potentiates apoptosis following IR

HeLa cells were irradiated with 6 Gy IR following a 20 nM Ambion siRNA transfection with siNT, siGSK3β, siMARK2 and siSRP72. Apoptosis was assessed by: **A)** Immunoblotting with PARP-1 antibody carried out 72-hours post-irradiation. Cleaved PARP-1 fold changes were calculated by comparing the area under each intensity peak normalised to actin, produced by rectangle segmentation of protein bands in ImageJ software. **B)** FACS: Annexin-V/PI staining carried out 72 hours post-irradiation and samples run on BD FACS, data represented as mean +/- SD from triplicate repeats. Unpaired two-sided student's t-tests comparing siNT to target knockdown, **p*<0.05 ***p*<0.01 ****p*<0.001. **C)** Caspase assay: Caspase 3/7 activity was read on plate reader (Polstar Omega) 72 hours post irradiation. Representative experiment of n=3 is shown, data represented as mean +/- SD from triplicate wells. Unpaired two-sided student's t-tests comparing siNT to target knockdown, ***p*<0.01 ****p*<0.001.

5.2.4 Prognostic significance of GSK3β and SRP72 expression in early breast cancer patients

It was explored if expression levels of these three genes in tumour samples are associated with worse outcomes in early breast cancer patients. Early breast cancer patient cohorts were chosen because access to this data was publicly available. Meta-analysis on cohorts of early breast cancer patients was conducted to determine if these genes predicted a worse prognosis for recurrence-free survival (RFS). Forest plots demonstrated that for both SRP72 and GSK-3β individual cohorts demonstrated a trend towards worse prognosis for RFS (Fig 5.9A, B). The overall meta-analysis showed a significant worse prognosis for RFS for GSK-3β (Summary effect= 1.752, 95% CI: 1.160/2.646, Fig.5.9A) and SRP72 (Summary effect=1.751, 95% CI: 1.156/ 2.651, Fig.5.9B). The estimated heterogeneity variance for GSK-3β (p=0.22) and SRP72 (p=0.953) are non-significant, illustrating that the prognostic effects are not the result of large variances and biases in the probe-sets. In contrast, we found that MARK2 expression levels were not associated with outcome (data not shown).

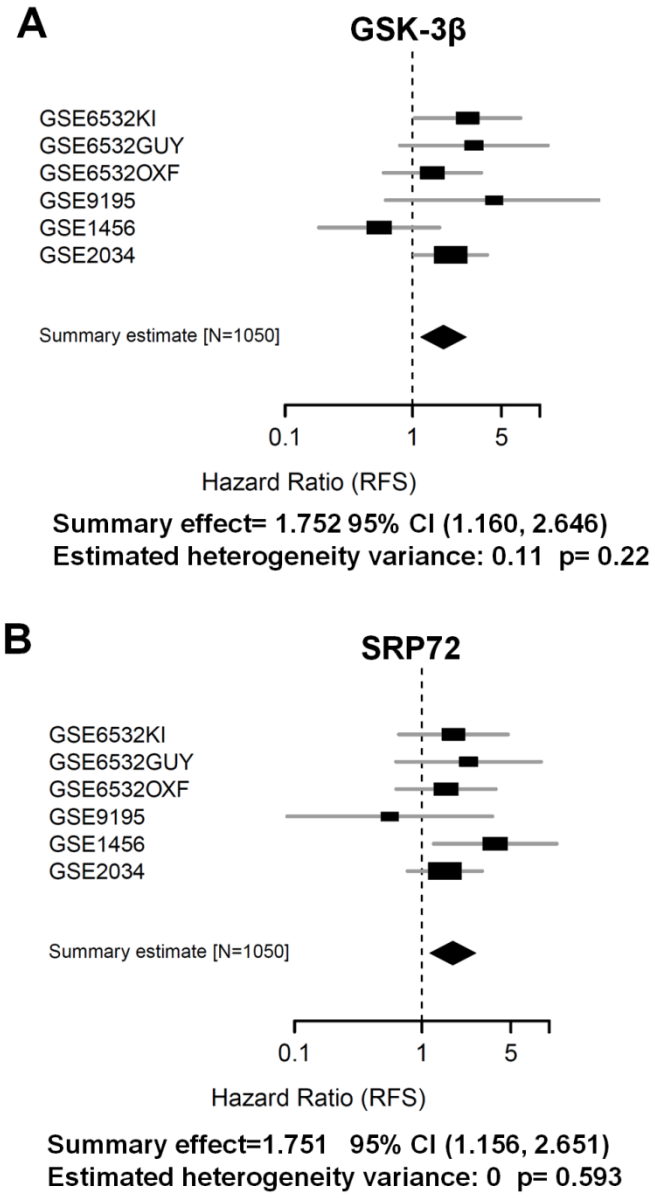

Figure 5.9. GSK-3β and SRP72 expression associated with worse recurrence-free survival

A Forest plot showing meta-analysis on 6 curated retrospective breast cancer datasets on **(A)** GSK3β and **(B)** SRP72. Hazard-ratio (HR) for recurrence-free survival (RFS) (high expression levels associated with good prognosis if HR<1, worse prognosis if HR>1), with 95% confidence interval, is shown for each datasets and for the summary effect on the 1050 samples.

5.3 Discussion

5.3.1 GSK3β, MARK2 and SRP72 are linked to tumour cell radioresistance

Genes that are linked to radiation resistance need to be identified for a number of fundamental reasons. Principally these genes could make good clinical targets for the modulation of intrinsic radiosensitivity of tumour cells to increase the efficacy of radiotherapy. Ideally they would act specifically on tumour cells without increasing normal tissue damage by targeting the unique genetic, metabolic or physiological differences (angiogenesis) underlying the disease. However, in many cases radiation modulators also sensitise normal tissue, which does not widen the therapeutic window. Although these targets may not be ideal clinical targets, they may still provide valuable prognostic information, and indications of molecular pathways that lead to radiation resistance.

GSK-3β, MARK2 and SRP72 were identified as potential modulators of radiosensitivity from the high-throughput colony formation screen described in chapter 3. In this chapter it was shown that depletion of these genes radiosensitised several tumour lines, HeLa, T24, SQ20B, PSN1 and MCF-7. Regrettably, depleting these genes in MRC5 normal tissue fibroblasts cells also caused significant radiosensitisation, suggesting that these effects are not tumour specific. Consequently, these genes may not prove to be favourable targets for expanded study with clinical endpoints in mind but they can still provide valuable prognostic information.

Knockdown of MARK2 and SRP72 in the SQ20B head and neck cancer cell line was lethal, suggesting that their depletion is synthetically lethal with the genetic makeup of SQ20B cells. GSK-3β knockdown was unable to sensitise the PSN1 pancreatic cancer cell line (Fig.5.4). It has been established previously that knocking down, inhibiting or forming a kinase dead version of GSK-3β in Panc1 and BxPC3 pancreatic cells results

in radioprotection (Watson et al., 2010). Conversely, a separate study carried out with the same cell lines demonstrated a modest radiosensitising effect following inhibition of GSK-3β (Kitano et al., 2013). Therefore, the effects on tumour survival following modulation of intrinsic radiosensitivity by perturbing GSK-3β in pancreatic cells remain ambiguous.

5.3.2 Prognostic significance of candidate gene expression in early breast cancer patients

Genes that are involved in radioresistance are typically overexpressed and associated with worse prognosis for patients. High tumour expression levels of SRP72 and GSK-3β were associated with a significantly worse recurrence free survival (RFS) in early breast cancer patients (Fig.5.9). GSK-3β over-expression has previously been implicated in worse prognosis for different clinical endpoints and histological sites (Quintayo et al., 2012; Zeng et al., 2014b). Overexpression of SRP72 has not been previously been shown to be associated with a worse prognosis in clinical samples and further work to determine if this holds true for other histological sites and clinical endpoints would be useful.

5.3.3 GSK3β, MARK2 and SRP72 expression suppresses radiation induced apoptosis

Depleting HeLa cells of GSK3β, MARK2 and SRP72 caused a significant elevation in radiation induced apoptosis. This was confirmed by PARP cleavage, Annexin-V/PI staining and caspase activity assays (Fig.5.8A, B, and C). MARK2 is primarily involved in the stability of microtubules by phosphorylating tau and its involvement in apoptosis may be linked to PTEN-induced kinase 1 (PINK1). In normal neuronal cells PINK1 knockout causes increased apoptosis as assessed by Annexin-V/PI staining (Matenia et al., 2012; Requejo-Aguilar et al., 2014). However, until now a link with increased

radiosensitivity and increased apoptosis following MARK2 knockdown had not been shown. The same holds true for SRP72 depletion. A previous study has shown that SRP72 is involved in regulating TRAIL-mediated apoptosis through the death receptor DR4 (Ren et al., 2004). Interestingly, the authors did not see a drop in cell viability or growth arrest with SRP72 knockdown. We clearly show that knockdown of SRP72 causes growth inhibition in cancer and normal cells as demonstrated by a reduction in 0 Gy plating efficiencies in colony formation assays, and an elevation of apoptosis following IR (Fig.5.1, Fig.5.6 and Fig.5.8).

Similarly, GSK-3β depletion was accompanied by an increase in radiation-induced apoptosis in HeLa cells. Studies have demonstrated previously that GSK-3β inhibition causes an induction of apoptosis without irradiation (Marchand et al., 2012; Zeng et al., 2014a). Radiosensitisation in pancreatic cells was observed, however a mechanism was not elucidated (Kitano et al., 2013). We demonstrate that GSK-3β is linked to radioresistance by suppressing apoptosis induction. Since GSK-3β receives signals via the pro-survival Ras/AKT/PI-3K pathway, the finding that it is linked to radioresistance by repressing apoptosis may be logical. Future mechanistic clarification to identify the pathways that lead to induction of apoptosis would be scientifically interesting.

In summary, this chapter describes how MARK2, SRP72 and GSK-3β are linked to tumour cell radioresistance by suppressing radiation-induced apoptosis. These genes may not be clinically exploitable drug targets due to normal tissue radiosensitisation that was seen for all three genes. However, SRP72 and GSK-3β may be used as prognostic markers in breast cancer and included as part of genetic signature from future screening results that can be prospectively tested in patient samples.

CHAPTER 6

GENERAL DISCUSSION

6.1 Discussion

6.1.1 Summary of findings

The aim of this thesis was to discover and investigate novel molecular determinants of tumour radiosensitivity, which could have potential clinical use or provide prognostic information. A high-throughput colony formation screen was successfully developed which demonstrated excellent quality metrics (Z-factors, intra-inter assay variability parameters, Chapter 3). Although other groups have shown the feasibility using high-throughput colony formation assay with compounds in the past (Katz et al., 2008; Lin et al., 2014), they did not identify novel radiosensitisers. To our knowledge, this is first documented HTS siRNA screen using the colony formation endpoint that has identified novel determinants of tumour radioresistance. The screen was performed with a 'kinome' siRNA library containing 709 siRNAs targeting kinases.

Apart from a number of known radiosensitivity modulating genes such as DNA-PK*cs*, ATR, and ATM, the 'kinome' screen identified several genes not previously associated with radiosensitivity. Based on certain criteria (novelty in the context of radiosensitivity, differential expression in tumour cells compared to normal tissue based on Oncomine data (Rhodes et al., 2007), and availability of reagents for expanded study), a number were selected for further investigation. This led to the identification of thiamine pyrophosphokinase-1 (TPK1) as a tumour specific radiosensitisation target (Chapter 4). TPK1 is involved in vitamin B1/thiamine metabolism where it converts thiamine to thiamine pyrophosphate. It was demonstrated that siRNA mediated depletion or pharmacological inhibition (PyrH) of TPK1 resulted in tumour specific radiosensitisation (Chapter 4, Fig.4.3 and Fig.4.7). Furthermore, depletion of thiamine transporter-1 (THTR1) also caused pronounced radiosensitisation (Chapter 5, Fig.5.4) and these combined observations indicated that the Vitamin B1 metabolism pathway is linked to

tumour radioresistance. The observed radiosensitivity was attributed to persistence in DNA-damage quantified by DNA-damage foci following siRNA or PyrH treatment.

The three other genes that were selected for further investigation were signal recognition particle-72 kDa (SRP72), glycogen synthase 3-beta (GSK3β) and MAP/Microtubule Affinity-Regulating Kinase 2 (MARK2) (Chapter 5). It was confirmed that knockdown of all three genes caused significant tumour radiosensitisation in a standard colony formation assay. However, it was found that knockdown of these genes in normal fibroblasts also caused radiosensitisation. Although these genes are not tumour specific radiosensitisation targets, SRP72 and GSK3β tumour expression appears to provide valuable prognostic information in early breast cancer patients with over-expression of SRP72 and GSK3β being associated with significantly worse recurrence-free survival rates (Chapter 5, Fig 5.9).

6.1.2 Significance of findings

The principal undertaking in this thesis was the development of the 96-well CFA assay and to use it to screen a kinome siRNA library. The significance of the assay lies in its ability to assess the replicative potential of tumour cells in a high throughput manner. Thus, it is the closest *in vitro* equivalent to the clinical use of radiation.

This assay has now been modified for compound or siRNA screening with tumour lines with different genetic backgrounds (not in this thesis). However, this does rely on the tumour lines achieving appropriate transfection efficiency, forming distinct countable colonies and having sufficient plating efficiency in the 96-well format. Furthermore, this assay can be used in combination with chemotherapies typically employed in chemoradiation regimens in the clinic to improve established protocols.

The identification of TPK1, a tumour specific radiosensitising target, demonstrates that there may be a wealth of potentially undiscovered tumour specific radiosensitising

genes. TPK1 inhibition may be viable clinical option, however caution should be taken since long-term thiamine deficiency causes Wernicke's encephalopathy and results in severe neurological disorders. Since radiotherapy is typically delivered over a short course, it may be possible to inhibit TPK1 during radiotherapy treatment before the onset of adverse outcomes. Furthermore, TPK1 inhibitors such as oxythiamine may circumvent neurological disorders associated with thiamine deprivation as it is suggested that this compound does not cross the blood-brain barrier. The effectiveness of TPK1 inhibition will require testing using *in vivo* pre-clinical models with RT.

Aside from potential toxicity issues, successful clinical application of TPK1 inhibition may only be achieved if biomarkers are developed that correctly identify which patients will benefit from treatment and the subsequent TPK1 activity can be measured. One method to assess the activity of TPK1 is to determine the activity of transketolase in erythrocytes (Brin, 1962), which requires the TPK1 product, TPP, as a co-factor. Samples are given excess ribose-5-phosphate and TPP, and the amount of these substrates that are utilised *in vitro* by the erythrocytes is symptomatic of the magnitude of thiamine deprivation. This is known as the 'TPP effect' (Brin, 1962). This may be a simple way of determining if TPK1 inhibitors are working and if the levels of thiamine are reaching levels that could cause significant adverse events in patients. Since certain cancers such as breast over-express TPK1, it is reasonable that there may be elevated levels of TPP. Patients could be chosen based on identifying the levels of TPP in biopsies using methods designed to quantify TPP levels from extracts (Deus and Blum, 1974; Deus et al., 1969). From our studies we have identified that TPK1 inhibition radiosensitises a range of cell lines demonstrating the broad spectrum of cancers this strategy could be beneficial for, unlike some inhibitors which rely of specific oncogenic signals. Therefore it will be valuable to test levels of TPP across a broad range of

cancer cell lines *in vitro* to decipher which tumours types would benefit the greatest and to see if there is a correlation between TPP levels and radiosensitivity. However, since inhibition of TPK1 could have a broad impact, adverse events could pose a problem and this should be evaluated with *in vivo* models.

In addition to the biomarkers required to determine which patients are likely to benefit and if treatment is working, it is important to demonstrate that TPK1 inhibition is superior to the established treatments within the clinic. The discovery of cetuximab highlighted how molecular targeted agents may not hold superior benefit over established chemoradiation regimens. Early clinical trials in head and neck cancers suggested that compared with radiotherapy alone, cetuximab in combination with radiotherapy yielded superior clinical outcome without additional side effects (Bonner et al., 2010; Bonner et al., 2006). Shortly after however, it was shown that concurrent chemoradiation had improved outcomes over RT alone in head and neck, and the addition of cetuximab to chemoradiation showed no significant improvements, demonstrating that this novel compound had no longer a clinical benefit (Ang et al., 2014).The cetuximab account demonstrates that inhibitors targeting TPK1 or any other molecular targeted therapies must show significant improvements compared to the most recently established treatment methodologies.

Furthermore, the potential future of TPK1 inhibition also relies on the identification of potential resistance mechanisms. Molecular targeting using BRAF inhibitors in melanoma (Sun et al., 2014) and tyrosine kinase inhibitors in chronic myeloid leukaemia (Shah et al., 2002) are examples of cases where resistance mechanisms have developed resulting in the relapse of the tumour. It is therefore essential that TPK1 inhibitors are thoroughly tested *in vitro* for potential resistance mechanisms by culturing tumour lines with inhibitors over long periods of time. The resistant cell lines can be

sequenced to determine what has changed at the genomic level or evaluated at the biochemical level for changes in metabolism.

In addition to the modulation of intrinsic radiosensitivity of tumour cells, extrinsic factors that infer radioresistance should be evaluated. Radiosensitivity is severely affected by the level of hypoxia in a tumour (Conger, 1956; Gray et al., 1953). Tumours exhibiting hypoxic regions are radioresistant with the oxygen enhancement ratio (OER) potentially being as high as 2.7-2.8 in hypoxic/anoxic compared to normoxia areas (Gray et al., 1953). It has been demonstrated that thiamine transporter-2 (THTR2) is up-regulated in breast cancer lines in hypoxic environments (Sweet et al., 2010). In hypoxia, there was a 2-fold increase in thiamine uptake in BT474 cells (Sweet et al., 2010). This suggests that radiosensitisation by thiamine inhibition could be higher under hypoxic conditions, as hypoxic cells are more dependent on thiamine. Therefore, future work will require the investigation of PyrH under hypoxia to evaluate the radiosensitisation by thiamine metabolism inhibition under these conditions.

This thesis also led to the identification of radiosensitisation targets that were not tumour specific. Although these targets may not have any therapeutic potential, the identification of such genes can provide potentially valuable prognostic information. This work has demonstrated prognostic data in early breast cancer patients for GSK3β and SRP72. Future work will require the investigation of candidate genes and their gene expression data in cohorts of patients treated with RT. Currently, there are no reliable gene expression data corresponding to patient cohorts treated with RT in the public domain. Therefore, our lab plans to prospectively bank tissues from patients treated with RT, so that detailed RT related queries can be posed. A genetic radioresistance signature will be developed from future screening and tested prospectively in patients.

6.1.3 Concluding remarks

Many potential genes that are linked to tumour radioresistance remain undiscovered. To solve this problem, a high-throughput colony formation screen has been developed. This strategy led to the discovery that Vitamin B1 metabolism is linked with radiation sensitivity and identified three novel genes that are linked with tumour radioresistance. This thesis thus showed this assay can be used successfully to identify novel tumour specific radiosensitisation targets or genes that can provide prognostic information. This assay can be modified to interrogate tumour lines using compound libraries or in combination with chemotherapies. By using colony formation as an endpoint, which is the gold standard method in assessing loss of replicative potential caused by IR, this strategy may ultimately reduce the time spent investigating and validating false positives in the hunt for radiosensitising targets.

REFERENCES

Aberle, H., A. Bauer, J. Stappert, A. Kispert, and R. Kemler. 1997. beta-catenin is a target for the ubiquitin-proteasome pathway. *Embo J*. 16:3797-3804.

Ahel, I., U. Rass, S.F. El-Khamisy, S. Katyal, P.M. Clements, P.J. McKinnon, K.W. Caldecott, and S.C. West. 2006. The neurodegenerative disease protein aprataxin resolves abortive DNA ligation intermediates. *Nature*. 443:713-716.

Ahnesorg, P., P. Smith, and S.P. Jackson. 2006. XLF interacts with the XRCC4-DNA ligase IV complex to promote DNA nonhomologous end-joining. *Cell*. 124:301-313.

Al-Khouri, A.M., Y. Ma, S.H. Togo, S. Williams, and T. Mustelin. 2005. Cooperative phosphorylation of the tumor suppressor phosphatase and tensin homologue (PTEN) by casein kinases and glycogen synthase kinase 3beta. *J Biol Chem*. 280:35195-35202.

Al-Mamgani, A., W.L.J. van Putten, W.D. Heemsbergen, G.J.L.H. van Leenders, A. Slot, M.F.H. Dielwart, L. Incrocci, and J.V. Lebesque. 2008. Update of Dutch Multicenter Dose-Escalation Trial of Radiotherapy for Localized Prostate Cancer. *Int J Radiat Oncol*. 72:980-988.

Al-Sarraf, M., M. LeBlanc, P.G. Giri, K.K. Fu, J. Cooper, T. Vuong, A.A. Forastiere, G. Adams, W.A. Sakr, D.E. Schuller, and J.F. Ensley. 1998. Chemoradiotherapy versus radiotherapy in patients with advanced nasopharyngeal cancer: phase III randomized Intergroup study 0099. *J Clin Oncol*. 16:1310-1317.

Algan, O., C.C. Stobbe, A.M. Helt, G.E. Hanks, and J.D. Chapman. 1996. Radiation inactivation of human prostate cancer cells: The role of apoptosis. *Radiat Res*. 146:267-275.

Amorino, G.P., M.L. Freeman, D.P. Carbone, D.E. Lebwohl, and H. Choy. 1999. Radiopotentiation by the oral platinum agent, JM216: Role of repair inhibition. *International Journal of Radiation Oncology Biology Physics*. 44:399-405.

Andreassen, P.R., F.B. Lacroix, O.D. Lohez, and R.L. Margolis. 2001. Neither p21WAF1 nor 14-3-3sigma prevents G2 progression to mitotic catastrophe in human colon carcinoma cells after DNA damage, but p21WAF1 induces stable G1 arrest in resulting tetraploid cells. *Cancer research*. 61:7660-7668.

Ang, K.K., Q. Zhang, D.I. Rosenthal, P.F. Nguyen-Tan, E.J. Sherman, R.S. Weber, J.M. Galvin, J.A. Bonner, J. Harris, A.K. El-Naggar, M.L. Gillison, R.C. Jordan, A.A. Konski, W.L. Thorstad, A. Trotti, J.J. Beitler, A.S. Garden, W.J. Spanos, S.S. Yom, and R.S. Axelrod. 2014. Randomized phase III trial of concurrent accelerated radiation plus cisplatin with or without cetuximab for stage III to IV head and neck carcinoma: RTOG 0522. *Journal of clinical oncology : official journal of the American Society of Clinical Oncology*. 32:2940-2950.

Backert, S., E. Ziska, V. Brinkmann, U. Zimny-Arndt, A. Fauconnier, P.R. Jungblut, M. Naumann, and T.F. Meyer. 2000. Translocation of the Helicobacter pylori CagA protein in gastric epithelial cells by a type IV secretion apparatus. *Cell Microbiol*. 2:155-164.

Balmus, G., N.A. Karp, B.L. Ng, S.P. Jackson, D.J. Adams, and R.E. McIntyre. 2015. A high-throughput in vivo micronucleus assay for genome instability screening in mice. *Nature protocols*. 10:205-215.

Banath, J.P., S.H. MacPhail, and P.L. Olive. 2004. Radiation sensitivity, H2AX phosphorylation, and kinetics of repair of DNA strand breaks in irradiated cervical cancer cell lines. *Cancer research*. 64:7144-7149.

Basu, T.K., and J.W. Dickerson. 1976. The thiamin status of early cancer patients with particular reference to those with breast and bronchial carcinomas. *Oncology*. 33:250-252.

Baumann, P., F.E. Benson, and S.C. West. 1996. Human Rad51 protein promotes ATP-dependent homologous pairing and strand transfer reactions in vitro. *Cell*. 87:757-766.

Behrens, J., B.A. Jerchow, M. Wurtele, J. Grimm, C. Asbrand, R. Wirtz, M. Kuhl, D. Wedlich, and W. Birchmeier. 1998. Functional interaction of an axin homolog, conductin, with beta-catenin, APC, and GSK3 beta. *Science*. 280:596-599.

Behrens, J., J.P. von Kries, M. Kuhl, L. Bruhn, D. Wedlich, R. Grosschedl, and W. Birchmeier. 1996. Functional interaction of beta-catenin with the transcription factor LEF-1. *Nature*. 382:638-642.

Bergqvist, A.S., D. Brattstrom, M. Bergqvist, O. Brodin, G. Wagenius, and L.A. Zetterberg. 2001. The frequency of micronuclei in lung cancer cell lines and their correlation to intrinsic radiation sensitivity. *Anticancer Res*. 21:3853-3856.

Bernhard, E.J., W.G. McKenna, A.D. Hamilton, S.M. Sebti, Y. Qian, J.M. Wu, and R.J. Muschel. 1998. Inhibiting Ras prenylation increases the radiosensitivity of human tumor cell lines with activating mutations of ras oncogenes. *Cancer research*. 58:1754-1761.

Bernhard, E.J., E.J. Stanbridge, S. Gupta, A.K. Gupta, D. Soto, V.J. Bakanauskas, G.J. Cerniglia, R.J. Muschel, and W.G. McKenna. 2000. Direct evidence for the contribution of activated N-ras and K-ras oncogenes to increased intrinsic radiation resistance in human tumor cell lines. *Cancer research*. 60:6597-6600.

Bernstein, E., A.A. Caudy, S.M. Hammond, and G.J. Hannon. 2001. Role for a bidentate ribonuclease in the initiation step of RNA interference. *Nature*. 409:363-366.

Bernstein, N.K., R.S. Williams, M.L. Rakovszky, D. Cui, R. Green, F. Karimi-Busheri, R.S. Mani, S. Galicia, C.A. Koch, C.E. Cass, D. Durocher, M. Weinfeld, and J.N. Glover. 2005. The molecular architecture of the mammalian DNA repair enzyme, polynucleotide kinase. *Mol Cell*. 17:657-670.

Bettendorff, L., B. Wirtzfeld, A.F. Makarchikov, G. Mazzucchelli, M. Frederich, T. Gigliobianco, M. Gangolf, E. De Pauw, L. Angenot, and P. Wins. 2007. Discovery of a natural thiamine adenine nucleotide. *Nature chemical biology*. 3:211-212.

Birmingham, A., E.M. Anderson, A. Reynolds, D. Ilsley-Tyree, D. Leake, Y. Fedorov, S. Baskerville, E. Maksimova, K. Robinson, J. Karpilow, W.S. Marshall, and A. Khvorova. 2006. 3' UTR seed matches, but not overall identity, are associated with RNAi off-targets. *Nature methods*. 3:199-204.

Bjork-Eriksson, T., C. West, E. Karlsson, and C. Mercke. 2000. Tumor radiosensitivity (SF2) is a prognostic factor for local control in head and neck cancers. *International journal of radiation oncology, biology, physics*. 46:13-19.

Bjork-Eriksson, T., C.M.L. West, E. Cvetskovska, M. Svensson, E. Karlsson, B. Magnusson, N.J. Slevin, S. Edstrom, and C. Mercke. 1999. The lack of correlation between proliferation (Ki-67, PCNA, LI, Tpot), p53 expression and radiosensitivity for head and neck cancers. *Brit J Cancer*. 80:1400-1404.

Blass, J.P., and G.E. Gibson. 1977. Abnormality of a thiamine-requiring enzyme in patients with Wernicke-Korsakoff syndrome. *The New England journal of medicine*. 297:1367-1370.

Blier, P.R., A.J. Griffith, J. Craft, and J.A. Hardin. 1993. Binding of Ku Protein to DNA - Measurement of Affinity for Ends and Demonstration of Binding to Nicks. *J Biol Chem*. 268:7594-7601.

Blocher, D. 1982. DNA Double Strand Breaks in Ehrlich Ascites Tumor-Cells at Low-Doses of X-Rays .1. Determination of Induced Breaks by Centrifugation at Reduced Speed. *Int J Radiat Biol*. 42:317-328.

Blocher, D., and W. Pohlit. 1982. DNA Double Strand Breaks in Ehrlich Ascites Tumor-Cells at Low-Doses of X-Rays .2. Can Cell-Death Be Attributed to Double Strand Breaks. *Int J Radiat Biol*. 42:329-338.

Bohm, H., V. Brinkmann, M. Drab, A. Henske, and T.V. Kurzchalia. 1997. Mammalian homologues of C-elegans PAR-1 are asymmetrically localized in epithelial cells and may influence their polarity. *Current Biology*. 7:603-606.

Bohnsack, M.T., K. Czaplinski, and D. Gorlich. 2004. Exportin 5 is a RanGTP-dependent dsRNA-binding protein that mediates nuclear export of pre-miRNAs. *RNA*. 10:185-191.

Bonner, J.A., P.M. Harari, and J. Giralt. 2010. Radiotherapy plus cetuximab for locoregionally advanced head and neck cancer: 5-year survival data from a phase 3 randomised trial, and relation between cetuximab-induced rash and survival (vol 11, pg 21, 2010). *Lancet Oncology*. 11:14-14.

Bonner, J.A., P.M. Harari, J. Giralt, N. Azarnia, D.M. Shin, R.B. Cohen, C.U. Jones, R. Sur, D. Raben, J. Jassem, R. Ove, M.S. Kies, J. Baselga, H. Youssoufian, N. Amellal, E.K. Rowinsky, and K.K. Ang. 2006. Radiotherapy plus cetuximab for squamous-cell carcinoma of the head and neck. *The New England journal of medicine*. 354:567-578.

Borgelt, B., R. Gelber, S. Kramer, L.W. Brady, C.H. Chang, L.W. Davis, C.A. Perez, and F.R. Hendrickson. 1980. Palliation of Brain Metastases - Final Results of the 1st 2 Studies by the Radiation-Therapy-Oncology-Group. *Int J Radiat Oncol*. 6:1-9.

Boros, L.G., J. Puigjaner, M. Cascante, W.N. Lee, J.L. Brandes, S. Bassilian, F.I. Yusuf, R.D. Williams, P. Muscarella, W.S. Melvin, and W.J. Schirmer. 1997. Oxythiamine and dehydroepiandrosterone inhibit the nonoxidative synthesis of ribose and tumor cell proliferation. *Cancer research*. 57:4242-4248.

Boros, L.G., J.S. Torday, S. Lim, S. Bassilian, M. Cascante, and W.N.P. Lee. 2000. Transforming growth factor beta(2) promotes glucose carbon incorporation into nucleic acid ribose through the nonoxidative pentose cycle in lung epithelial carcinoma cells. *Cancer research*. 60:1183-1185.

Bosset, J.F., L. Collette, G. Calais, L. Mineur, P. Maingon, L. Radosevic-Jelic, A. Daban, E. Bardet, A. Beny, and J.C. Ollier. 2006. Chemotherapy with preoperative radiotherapy in rectal cancer. *The New England journal of medicine*. 355:1114-1123.

Bradley, J.D., R. Paulus, R. Komaki, G. Masters, G. Blumenschein, S. Schild, J. Bogart, C. Hu, K. Forster, A. Magliocco, V. Kavadi, Y.I. Garces, S. Narayan, P. Iyengar, C. Robinson, R.B. Wynn, C. Koprowski, J. Meng, J. Beitler, R. Gaur, W. Curran, Jr., and H. Choy. 2015. Standard-dose versus high-dose conformal radiotherapy with concurrent and consolidation carboplatin plus paclitaxel with or without cetuximab for patients with stage IIIA or IIIB non-small-cell lung cancer (RTOG 0617): a randomised, two-by-two factorial phase 3 study. *The lancet oncology*. 16:187-199.

Brin, M. 1962. Erythrocyte transketolase in early thiamine deficiency. *Annals of the New York Academy of Sciences*. 98:528-541.

Brown, J.M., and W.R. William. 2004. Exploiting tumour hypoxia in cancer treatment. *Nature Reviews Cancer*. 4:437-447.

Buchsbaum, D.J., M.N. Saleh, K.P. Raisch, M.A. Stackhouse, W.E. Grizzle, J.A. Bonner, M.S. Mayo, H.G. Kim, R.F. Meredith, and R.H. Wheeler. 1999. Combined modality therapy of A431 human epidermoid cancer using anti-EGFr antibody C225 and radiation. *Cancer Biotherapy and Radiopharmaceuticals*. 14:451-463.

Buffa, F.M., C. Camps, L. Winchester, C.E. Snell, H.E. Gee, H. Sheldon, M. Taylor, A.L. Harris, and J. Ragoussis. 2011. microRNA-associated progression pathways and potential therapeutic targets identified by integrated mRNA and microRNA expression profiling in breast cancer. *Cancer research*. 71:5635-5645.

Buffa, F.M., A.L. Harris, C.M. West, and C.J. Miller. 2010. Large meta-analysis of multiple cancers reveals a common, compact and highly prognostic hypoxia metagene. *Br J Cancer*. 102:428-435.

Bugreev, D.V., O.M. Mazina, and A.V. Mazin. 2006. Rad54 protein promotes branch migration of Holliday junctions. *Nature*. 442:590-593.

Buis, J., Y.P. Wu, Y.B. Deng, J. Leddon, G. Westfield, M. Eckersdorff, J.M. Sekiguchi, S. Chang, and D.O. Ferguson. 2008. Mre11 nuclease activity has essential roles in DNA repair and genomic stability distinct from ATM activation. *Cell*. 135:85-96.

Burma, S., B.P. Chen, M. Murphy, A. Kurimasa, and D.J. Chen. 2001. ATM phosphorylates histone H2AX in response to DNA double-strand breaks. *J Biol Chem*. 276:42462-42467.

Bush, C., and T.J. Mcmillan. 1993. Micronucleus Formation in Human Tumor-Cells - Lack of Correlation with Radiosensitivity. *Brit J Cancer*. 67:102-106.

Bussen, W.L., S.J. Raynard, and P. Sung. 2006. A double-holliday junction dissolvasome comprising BLM, topoisomerase IIIalpha, and BLAP75. *Environ Mol Mutagen*. 47:423-423.

Cary, R.B., S.R. Peterson, J. Wang, D.G. Bear, E.M. Bradbury, and D.J. Chen. 1997. DNA looping by Ku and the DNA-dependent protein kinase. *Proc Natl Acad Sci U S A*. 94:4267-4272.

Castedo, M., J.L. Perfettini, T. Roumier, A. Valent, H. Raslova, K. Yakushijin, D. Horne, J. Feunteun, G. Lenoir, R. Medema, W. Vainchenker, and G. Kroemer. 2004. Mitotic catastrophe constitutes a special case of apoptosis whose suppression entails aneuploidy. *Oncogene*. 23:4362-4370.

Chalmers, A.J., S.M. Bentzen, and F.M. Buffa. 2007. A general framework for quantifying the effects of DNA repair inhibitors on radiation sensitivity as a function of dose. *Theor Biol Med Model*. 4.

Chan, A.T.C., S.F. Leung, R.K.C. Ngan, P.M.L. Teo, W.H. Lau, W.H. Kwan, E.P. Hui, H.Y. Yiu, W. Yeo, F.Y. Cheung, K.H. Yu, K.W. Chiu, D.T. Chan, T.S.K. Mok, S. Yau, K.T. Yuen, F.K.F. Mo, M.M.P. Lai, B.B.Y. Ma, M.K.M. Kam, T.W.T. Leung, P.J. Johnson, P.H.K. Choi, and B.C.Y. Zee. 2005. Overall survival after concurrent cisplatin-radiotherapy compared with radiotherapy alone in locoregionally advanced nasopharyngeal carcinoma. *Journal of the National Cancer Institute*. 97:536-539.

Chao, K.S.C., L. Portelance, P.W. Grigsby, H. Bennet, and D. Low. 2001. Intensity-modulated radiation therapy (IMRT) reduces small bowel, rectum, and bladder doses in patients with cervical cancer receiving pelvic and para-aortic irradiation. *International Journal of Radiation Oncology Biology Physics*. 51:261-266.

Chen, H., J.X. Yue, S.H. Yang, H. Ding, R.W. Zhao, and S. Zhang. 2009. Overexpression of transketolase-like gene 1 is associated with cell proliferation in uterine cervix cancer. *J Exp Clin Canc Res*. 28.

Chuang, D.T., L.S. Ku, and R.P. Cox. 1982. Thiamin-Responsive Maple-Syrup-Urine Disease - Decreased Affinity of the Mutant Branched-Chain Alpha-Keto Acid Dehydrogenase for Alpha-Ketoisovalerate and Thiamin Pyrophosphate. *P Natl Acad Sci-Biol*. 79:3300-3304.

Chung, E.J., A.P. Brown, H. Asano, M. Mandler, W.E. Burgan, D. Carter, K. Camphausen, and D. Citrin. 2009. In vitro and in vivo radiosensitization with AZD6244 (ARRY-142886), an inhibitor of mitogen-activated protein kinase/extracellular signal-regulated kinase 1/2 kinase. *Clin Cancer Res*. 15:3050-3057.

Cohen, I.J., and J.E. Wolff. 2014. How Long Can Folinic Acid Rescue Be Delayed After High-Dose Methotrexate Without Toxicity? *Pediatr Blood Cancer*. 61:7-10.

Conger, A.D. 1956. The effect of oxygen on the radiosensitivity of mammalian cells. *Radiology*. 66:63-69.

Coquerelle, T.M., K.F. Weibezahn, and C. Luckehuhle. 1987. Rejoining of Double Strand Breaks in Normal Human and Ataxia-Telangiectasia Fibroblasts after Exposure to Co-60 Gamma-Rays, Am-241 Alpha-Particles or Bleomycin. *Int J Radiat Biol*. 51:209-218.

Costantini, S., L. Woodbine, L. Andreoli, P.A. Jeggo, and A. Vindigni. 2007. Interaction of the Ku heterodimer with the DNA ligase IV/Xrcc4 complex and its regulation by DNA-PK. *DNA Repair*. 6:712-722.

Cross, D.A., D.R. Alessi, P. Cohen, M. Andjelkovich, and B.A. Hemmings. 1995. Inhibition of glycogen synthase kinase-3 by insulin mediated by protein kinase B. *Nature*. 378:785-789.

Culbert, A.A., M.J. Brown, S. Frame, T. Hagen, D.A.E. Cross, B. Bax, and A.D. Reith. 2001. GSK-3 inhibition by adenoviral FRAT1 overexpression is neuroprotective and induces Tau dephosphorylation and beta-catenin stabilisation without elevation of glycogen synthase activity. *FEBS letters*. 507:288-294.

D'Agostino, V.G., V. Adami, and A. Provenzani. 2013. A Novel High Throughput Biochemical Assay to Evaluate the HuR Protein-RNA Complex Formation. *Plos One*. 8.

Danner, D.J., F.B. Wheeler, S.K. Lemmon, and L.J. Elsas, 2nd. 1978. In vivo and in vitro response of human branched chain alpha-ketoacid dehydrogenase to thiamine and thiamine pyrophosphate. *Pediatric research*. 12:235-238.

de Fougerolles, A., H.P. Vornlocher, J. Maraganore, and J. Lieberman. 2007. Interfering with disease: a progress report on siRNA-based therapeutics. *Nat Rev Drug Discov*. 6:443-453.

Deacon, J., M.J. Peckham, and G.G. Steel. 1984. The radioresponsiveness of human tumours and the initial slope of the cell survival curve. *Radiother Oncol*. 2:317-323.

DeBerardinis, R.J., A. Mancuso, E. Daikhin, I. Nissim, M. Yudkoff, S. Wehrli, and C.B. Thompson. 2007. Beyond aerobic glycolysis: Transformed cells can engage in glutamine metabolism that exceeds the requirement for protein and nucleotide synthesis. *P Natl Acad Sci USA*. 104:19345-19350.

Delaney, G., S. Jacob, C. Featherstone, and M. Barton. 2005. The role of radiotherapy in cancer treatment - Estimating optimal utilization from a review of evidence-based clinical guidelines. *Cancer-Am Cancer Soc*. 104:1129-1137.

Demarchi, F., C. Bertoli, P. Sandy, and C. Schneider. 2003. Glycogen synthase kinase-3 beta regulates NF-kappa B1/p105 stability. *J Biol Chem*. 278:39583-39590.

Deus, B., and H.E. Blum. 1974. A rapid and sensitive radiometric assay procedure for thiamine pyrophosphokinase activity using anion-exchange paper discs. *Analytical biochemistry*. 57:614-617.

Deus, B., H.E. Blum, and H. Holzer. 1969. Radiometric assay procedure for thiamine pyrophosphokinase activity. *Analytical biochemistry*. 27:492-501.

Dickey, A., S. Schleicher, K. Leahy, R. Hu, D. Hallahan, and D.K. Thotala. 2011. GSK-3 beta inhibition promotes cell death, apoptosis, and in vivo tumor growth delay in neuroblastoma Neuro-2A cell line. *J Neuro-Oncol*. 104:145-153.

Ding, L., G. Getz, D.A. Wheeler, E.R. Mardis, M.D. McLellan, K. Cibulskis, C. Sougnez, H. Greulich, D.M. Muzny, M.B. Morgan, L. Fulton, R.S. Fulton, Q.Y. Zhang, M.C. Wendl, M.S. Lawrence, D.E. Larson, K. Chen, D.J. Dooling, A. Sabo, A.C. Hawes, H. Shen, S.N. Jhangiani, L.R. Lewis, O. Hall, Y.M. Zhu, T. Mathew, Y.R. Ren, J.Q. Yao, S.E. Scherer, K. Clerc, G.A. Metcalf, B. Ng, A. Milosavljevic, M.L. Gonzalez-Garay, J.R. Osborne, R. Meyer, X.Q. Shi, Y.Z. Tang, D.C. Koboldt, L. Lin, R. Abbott, T.L. Miner, C. Pohl, G. Fewell, C. Haipek, H. Schmidt, B.H. Dunford-Shore, A. Kraja, S.D. Crosby, C.S. Sawyer, T. Vickery, S. Sander, J. Robinson, W. Winckler, J. Baldwin, L.R. Chirieac, A. Dutt, T. Fennell, M. Hanna, B.E. Johnson, R.C. Onofrio, R.K. Thomas, G. Tonon, B.A. Weir, X.J. Zhao, L. Ziaugra, M.C. Zody, T. Giordano, M.B. Orringer, J.A. Roth, M.R. Spitz, I.I. Wistuba, B. Ozenberger, P.J. Good, A.C. Chang, D.G. Beer, M.A. Watson, M.

Ladanyi, S. Broderick, A. Yoshizawa, W.D. Travis, W. Pao, M.A. Province, G.M. Weinstock, H.E. Varmus, S.B. Gabriel, E.S. Lander, R.A. Gibbs, M. Meyerson, and R.K. Wilson. 2008. Somatic mutations affect key pathways in lung adenocarcinoma. *Nature*. 455:1069-1075.

Drewes, G., A. Ebneth, U. Preuss, E.M. Mandelkow, and E. Mandelkow. 1997. MARK, a novel family of protein kinases that phosphorylate microtubule-associated proteins and trigger microtubule disruption. *Cell*. 89:297-308.

Dutta, B., W. Huang, M. Molero, R. Kekuda, F.H. Leibach, L.D. Devoe, V. Ganapathy, and P.D. Prasad. 1999. Cloning of the human thiamine transporter, a member of the folate transporter family. *J Biol Chem*. 274:31925-31929.

Eastman, A. 1987. The Formation, Isolation and Characterization of DNA Adducts Produced by Anticancer Platinum Complexes. *Pharmacol Therapeut*. 34:155-166.

Eastman, A., and M.A. Barry. 1987. Interaction of Trans-Diamminedichloroplatinum(Ii) with DNA - Formation of Monofunctional Adducts and Their Reaction with Glutathione. *Biochemistry-Us*. 26:3303-3307.

Echeverri, C.J., and C. Sachse. 2004. Oncology studies using siRNA libraries: the dawn of RNAi-based genomics. *Oncogene*. 23:8384-8391.

Elbashir, S.M., J. Harborth, W. Lendeckel, A. Yalcin, K. Weber, and T. Tuschl. 2001a. Duplexes of 21-nucleotide RNAs mediate RNA interference in cultured mammalian cells. *Nature*. 411:494-498.

Elbashir, S.M., W. Lendeckel, and T. Tuschl. 2001b. RNA interference is mediated by 21-and 22-nucleotide RNAs. *Gene Dev*. 15:188-200.

Elbashir, S.M., J. Martinez, A. Patkaniowska, W. Lendeckel, and T. Tuschl. 2001c. Functional anatomy of siRNAs for mediating efficient RNAi in Drosophila melanogaster embryo lysate. *Embo J*. 20:6877-6888.

Elbert, M., D. Cohen, and A. Musch. 2006. PAR1b promotes cell-cell adhesion and inhibits dishevelled-mediated transformation of Madin-Darby canine kidney cells. *Mol Biol Cell*. 17:3345-3355.

Elmadfa, I., D. Majchrzak, P. Rust, and D. Genser. 2001. The thiamine status of adult humans depends on carbohydrate intake. *International journal for vitamin and nutrition research. Internationale Zeitschrift fur Vitamin- und Ernahrungsforschung. Journal international de vitaminologie et de nutrition*. 71:217-221.

Emami, B., J. Lyman, A. Brown, L. Coia, M. Goitein, J.E. Munzenrider, B. Shank, L.J. Solin, and M. Wesson. 1991. Tolerance of normal tissue to therapeutic irradiation. *International journal of radiation oncology, biology, physics*. 21:109-122.

Embi, N., D.B. Rylatt, and P. Cohen. 1980. Glycogen-Synthase Kinase-3 from Rabbit Skeletal-Muscle - Separation from Cyclic-Amp-Dependent Protein-Kinase and Phosphorylase-Kinase. *European Journal of Biochemistry*. 107:519-527.

Epstein, C.M., R.K. Chawla, A. Wadsworth, and D. Rudman. 1980. Decarboxylation of Alpha-Ketoisovaleric Acid after Oral-Administration in Man. *American Journal of Clinical Nutrition*. 33:1968-1974.

Eriksson, D., and T. Stigbrand. 2010. Radiation-induced cell death mechanisms. *Tumor Biol*. 31:363-372.

Esfandiari, F., A. Fathi, H. Gourabi, S. Kiani, S. Nemati, and H. Baharvand. 2012. Glycogen synthase kinase-3 inhibition promotes proliferation and neuronal

differentiation of human-induced pluripotent stem cell-derived neural progenitors. *Stem cells and development*. 21:3233-3243.

Eudy, J.D., O. Spiegelstein, R.C. Barber, B.J. Wlodarczyk, J. Talbot, and R.H. Finnell. 2000. Identification and characterization of the human and mouse SLC19A3 gene: a novel member of the reduced folate family of micronutrient transporter genes. *Molecular genetics and metabolism*. 71:581-590.

Falzon, M., J.W. Fewell, and E.L. Kuff. 1993. Ebp-80, a Transcription Factor Closely Resembling the Human Autoantigen Ku, Recognizes Single-Strand to Double-Strand Transitions in DNA. *J Biol Chem*. 268:10546-10552.

Farmer, H., N. McCabe, C.J. Lord, A.N.J. Tutt, D.A. Johnson, T.B. Richardson, M. Santarosa, K.J. Dillon, I. Hickson, C. Knights, N.M.B. Martin, S.P. Jackson, G.C.M. Smith, and A. Ashworth. 2005. Targeting the DNA repair defect in BRCA mutant cells as a therapeutic strategy. *Nature*. 434:917-921.

Fenech, M., and A.A. Morley. 1985. Measurement of Micronuclei in Lymphocytes. *Mutat Res*. 147:29-36.

Fertil, B., and E.P. Malaise. 1985. Intrinsic Radiosensitivity of Human Cell-Lines Is Correlated with Radioresponsiveness of Human-Tumors - Analysis of 101 Published Survival Curves. *Int J Radiat Oncol*. 11:1699-1707.

Fire, A., S.Q. Xu, M.K. Montgomery, S.A. Kostas, S.E. Driver, and C.C. Mello. 1998. Potent and specific genetic interference by double-stranded RNA in Caenorhabditis elegans. *Nature*. 391:806-811.

Fisher, B., S. Anderson, J. Bryant, R.G. Margolese, M. Deutsch, E.R. Fisher, J.H. Jeong, and N. Wolmark. 2002. Twenty-year follow-up of a randomized trial comparing total mastectomy, lumpectomy, and lumpectomy plus irradiation for

the treatment of invasive breast cancer. *The New England journal of medicine*. 347:1233-1241.

Fokas, E., R. Prevo, J.R. Pollard, P.M. Reaper, P.A. Charlton, B. Cornelissen, K.A. Vallis, E.M. Hammond, M.M. Olcina, W.G. McKenna, R.J. Muschel, and T.B. Brunner. 2012a. Targeting ATR in vivo using the novel inhibitor VE-822 results in selective sensitization of pancreatic tumors to radiation. *Cell Death Dis*. 3.

Fokas, E., M. Yoshimura, R. Prevo, G. Higgins, W. Hackl, S.M. Maira, E.J. Bernhard, W.G. McKenna, and R.J. Muschel. 2012b. NVP-BEZ235 and NVP-BGT226, dual phosphatidylinositol 3-kinase/mammalian target of rapamycin inhibitors, enhance tumor and endothelial cell radiosensitivity. *Radiat Oncol*. 7:48.

Foldi, M., E. Stickeler, L. Bau, O. Kretz, D. Watermann, G. Gitsch, G. Kayser, A. zur Hausen, and J.F. Coy. 2007. Transketolase protein TKTL1 overexpression: A potential biomarker and therapeutic target in breast cancer. *Oncol Rep*. 17:841-845.

Forrester, H.B., C.A. Vidair, N. Albright, C.C. Ling, and W.C. Dewey. 1999. Using computerized video time lapse for quantifying cell death of X-irradiated rat embryo cells transfected with c-myc or c-Ha-ras. *Cancer research*. 59:931-939.

Fournel, P., G. Robinet, P. Thomas, P.J. Souquet, H. Lena, A. Vergnenegre, J.Y. Delhoume, J. Le Treut, J.A. Silvani, E. Dansin, M.C. Bozonnat, J.P. Daures, F. Mornex, and M. Perol. 2005. Randomized phase III trial of sequential chemoradiotherapy compared with concurrent chemoradiotherapy in locally advanced non-small-cell lung cancer: Groupe Lyon-Saint-Etienne d'Oncologie Thoracique-Groupe Francais de Pneumo-Cancerologie NPC 95-01 Study. *Journal of clinical oncology : official journal of the American Society of Clinical Oncology*. 23:5910-5917.

Franken, N.A., H.M. Rodermond, J. Stap, J. Haveman, and C. van Bree. 2006. Clonogenic assay of cells in vitro. *Nature protocols*. 1:2315-2319.

Fritsch, P., H. Richard-Le Naour, S. Denis, and F. Menetrier. 1994. Kinetics of radiation-induced apoptosis in the cerebellum of 14-day-old rats after acute or during continuous exposure. *Int J Radiat Biol*. 66:111-117.

Fulga, T.A., I. Sinning, B. Dobberstein, and M.R. Pool. 2001. SRbeta coordinates signal sequence release from SRP with ribosome binding to the translocon. *Embo J*. 20:2338-2347.

Ganapathy, V., S.B. Smith, and P.D. Prasad. 2004. SLC19: the folate/thiamine transporter family. *Pflugers Archiv : European journal of physiology*. 447:641-646.

Gangolf, M., J. Czerniecki, M. Radermecker, O. Detry, M. Nisolle, C. Jouan, D. Martin, F. Chantraine, B. Lakaye, P. Wins, T. Grisar, and L. Bettendorff. 2010. Thiamine status in humans and content of phosphorylated thiamine derivatives in biopsies and cultured cells. *Plos One*. 5:e13616.

Gerweck, L.E., S. Vijayappa, A. Kurimasa, K. Ogawa, and D.J. Chen. 2006. Tumor cell radiosensitivity is a major determinant of tumor response to radiation. *Cancer research*. 66:8352-8355.

Gilmore, R., P. Walter, and G. Blobel. 1982. Protein translocation across the endoplasmic reticulum. II. Isolation and characterization of the signal recognition particle receptor. *J Cell Biol*. 95:470-477.

Glock, G.E., and P. Mclean. 1953. Further Studies on the Properties and Assay of Glucose 6-Phosphate Dehydrogenase and 6-Phosphogluconate Dehydrogenase of Rat Liver. *Biochem J*. 55:400-408.

Goldfischer, S., E. Essner, and B. Schiller. 1971. Nucleoside diphosphatase and thiamine pyrophosphatase activities in the endoplasmic reticulum and golgi apparatus. *The journal of histochemistry and cytochemistry : official journal of the Histochemistry Society*. 19:349-360.

Goodhead, D.T. 1994. Initial Events in the Cellular Effects of Ionizing-Radiations - Clustered Damage in DNA. *Int J Radiat Biol*. 65:7-17.

Gottlieb, T.M., and S.P. Jackson. 1993. The DNA-dependent protein kinase: requirement for DNA ends and association with Ku antigen. *Cell*. 72:131-142.

Grassilli, E., R. Narloch, E. Federzoni, L. Ianzano, F. Pisano, R. Giovannoni, G. Romano, L. Masiero, B.E. Leone, S. Bonin, M. Donada, G. Stanta, K. Helin, and M. Lavitrano. 2013. Inhibition of GSK3B bypass drug resistance of p53-null colon carcinomas by enabling necroptosis in response to chemotherapy. *Clin Cancer Res*. 19:3820-3831.

Grawunder, U., M. Wilm, X. Wu, P. Kulesza, T.E. Wilson, M. Mann, and M.R. Lieber. 1997. Activity of DNA ligase IV stimulated by complex formation with XRCC4 protein in mammalian cells. *Nature*. 388:492-495.

Gray, L.H., A.D. Conger, M. Ebert, S. Hornsey, and O.C.A. Scott. 1953. The Concentration of Oxygen Dissolved in Tissues at the Time of Irradiation as a Factor in Radiotherapy. *Brit J Radiol*. 26:638-648.

Greenwood, J., and O.E. Pratt. 1985. Comparison of the effects of some thiamine analogues upon thiamine transport across the blood-brain barrier of the rat. *The Journal of physiology*. 369:79-91.

Gregory, M.A., Y. Qi, and S.R. Hann. 2003. Phosphorylation by glycogen synthase kinase-3 controls c-myc proteolysis and subnuclear localization. *J Biol Chem*. 278:51606-51612.

Gregory, R.I., T.P. Chendrimada, N. Cooch, and R. Shiekhattar. 2005. Human RISC couples microRNA biogenesis and posttranscriptional gene silencing. *Cell*. 123:631-640.

Grundy, G.J., S.L. Rulten, Z.H. Zeng, R. Arribas-Bosacoma, N. Iles, K. Manley, A. Oliver, and K.W. Caldecott. 2013. APLF promotes the assembly and activity of non-homologous end joining protein complexes. *Embo J*. 32:112-125.

Gu, J., H. Lu, B. Tippin, N. Shimazaki, M.F. Goodman, and M.R. Lieber. 2007. XRCC4:DNA ligase IV can ligate incompatible DNA ends and can ligate across gaps. *Embo J*. 26:1010-1023.

Gunsalus, I.C., B.L. Horecker, and W.A. Wood. 1955. Pathways of carbohydrate metabolism in microorganisms. *Bacteriological reviews*. 19:79-128.

Guo, G.Z., K. Sasai, N. Oya, T. Shibata, K. Shibuya, and M. Hiraoka. 1999. A significant correlation between clonogenic radiosensitivity and the simultaneous assessment of micronucleus and apoptotic cell frequencies. *Int J Radiat Biol*. 75:857-864.

Gupta, A.K., V.J. Bakanauskas, G.J. Cerniglia, Y. Cheng, E.J. Bernhard, R.J. Muschel, and W.G. McKenna. 2001. The Ras radiation resistance pathway. *Cancer research*. 61:4278-4282.

Hall, E.J., and A.J. Giaccia. 2006. Radiobiology for the radiologist. Lippincott Williams & Wilkins, Philadelphia. ix, 546 p. pp.

Halliwell, B., and O.I. Aruoma. 1991. DNA damage by oxygen-derived species. Its mechanism and measurement in mammalian systems. *FEBS letters*. 281:9-19.

Hawkins, C.F., A. Borges, and R.N. Perham. 1989. A common structural motif in thiamin pyrophosphate-binding enzymes. *FEBS letters*. 255:77-82.

Herskovic, A., K. Martz, M. Alsarraf, L. Leichman, J. Brindle, V. Vaitkevicius, J. Cooper, R. Byhardt, L. Davis, and B. Emami. 1992. Combined Chemotherapy and Radiotherapy Compared with Radiotherapy Alone in Patients with Cancer of the Esophagus. *New Engl J Med*. 326:1593-1598.

Higashi, H., A. Nakaya, R. Tsutsumi, K. Yokoyama, Y. Fujii, S. Ishikawa, M. Higuchi, A. Takahashi, Y. Kurashima, Y. Teishikata, S. Tanaka, T. Azuma, and M. Hatakeyama. 2004. Helicobacter pylori CagA induces Ras-independent morphogenetic response through SHP-2 recruitment and activation. *J Biol Chem*. 279:17205-17216.

Higgins, G.S., R. Prevo, Y.F. Lee, T. Helleday, R.J. Muschel, S. Taylor, M. Yoshimura, I.D. Hickson, E.J. Bernhard, and W.G. McKenna. 2010. A small interfering RNA screen of genes involved in DNA repair identifies tumor-specific radiosensitization by POLQ knockdown. *Cancer research*. 70:2984-2993.

Hoeflich, K.P., J. Luo, E.A. Rubie, M.S. Tsao, O. Jin, and J.R. Woodgett. 2000. Requirement for glycogen synthase kinase-3beta in cell survival and NF-kappaB activation. *Nature*. 406:86-90.

Holliday, R. 2007. A mechanism for gene conversion in fungi (Reprinted). *Genetics Research*. 89:285-307.

Horecker, B.L., T. Cheng, and S. Pontremoli. 1963. The Coupled Reaction Catalyzed by the Enzymes Transketolase and Transaldolase. Ii. Reaction of Erythrose 4-Phosphate and the Transaldolase-Dihydroxyacetone Complex. *J Biol Chem*. 238:3428-3431.

Horecker, B.L., J. Hurwitz, and P.Z. Smyrniotis. 1956. The role of xylulose 5-phosphate in the transketolase reaction. *J Biol Chem*. 223:1009-1019.

Horecker, B.L., and P.Z. Smyrniotis. 1953. Transaldolase - the Formation of Fructose-6-Phosphate from Sedoheptulose-7-Phosphate. *J Am Chem Soc*. 75:2021-2022.

Horecker, B.L., P.Z. Smyrniotis, and J.E. Seegmiller. 1951. The enzymatic conversion of 6-phosphogluconate to ribulose-5-phosphate and ribose-5-phosphate. *J Biol Chem*. 193:383-396.

Huang, S.M., and P.M. Harari. 2000a. Modulation of radiation response after epidermal growth factor receptor blockade in squamous cell carcinomas: inhibition of damage repair, cell cycle kinetics, and tumor angiogenesis. *Clin Cancer Res*. 6:2166-2174.

Huang, S.M., and P.M. Harari. 2000b. Modulation of radiation response after epidermal growth factor receptor blockade in squamous cell carcinomas: Inhibition of damage repair, cell cycle kinetics, and tumor angiogenesis. *Clin Cancer Res*. 6:2166-2174.

Huen, M.S., and J. Chen. 2008. The DNA damage response pathways: at the crossroad of protein modifications. *Cell research*. 18:8-16.

Hughes, K., E. Nikolakaki, S.E. Plyte, N.F. Totty, and J.R. Woodgett. 1993. Modulation of the Glycogen-Synthase Kinase-3 Family by Tyrosine Phosphorylation. *Embo J*. 12:803-808.

Huncharek, M., and B. Kupelnick. 2002. Combined chemoradiation versus radiation therapy alone in locally advanced nasopharyngeal carcinoma - Results of a meta-analysis of 1,528 patients from six randomized trials. *Am J Clin Oncol-Canc*. 25:219-223.

Hurov, J.B., M. Huang, L.S. White, J. Lennerz, C.S. Choi, Y.R. Cho, H.J. Kim, J.L. Priori, D. Piwnica-Worms, L.C. Cantley, J.K. Kim, G.I. Shulman, and H. Piwnica-Worms. 2007. Loss of the Par-1b/MARK2 polarity kinase leads to increased

metabolic rate, decreased adiposity, and insulin hypersensitivity in vivo. *P Natl Acad Sci USA*. 104:5680-5685.

Hurov, J.B., T.S. Stappenbeck, C.M. Zmasek, L.S. White, S.H. Ranganath, J.H. Russell, A.C. Chan, K.M. Murphy, and H. Piwnica-Worms. 2001. Immune system dysfunction and autoimmune disease in mice lacking Emk (Par-1) protein kinase. *Molecular and cellular biology*. 21:3206-3219.

Hutvagner, G., J. McLachlan, A.E. Pasquinelli, E. Balint, T. Tuschl, and P.D. Zamore. 2001. A cellular function for the RNA-interference enzyme Dicer in the maturation of the let-7 small temporal RNA. *Science*. 293:834-838.

Iakhiaeva, E., A. Iakhiaev, and C. Zwieb. 2010. Identification of amino acid residues in protein SRP72 required for binding to a kinked 5e motif of the human signal recognition particle RNA. *BMC molecular biology*. 11:83.

Iakhiaeva, E., J. Yin, and C. Zwieb. 2005. Identification of an RNA-binding domain in human SRP72. *Journal of molecular biology*. 345:659-666.

Ikeda, S., S. Kishida, H. Yamamoto, H. Murai, S. Koyama, and A. Kikuchi. 1998. Axin, a negative regulator of the Wnt signaling pathway, forms a complex with GSK-3beta and beta-catenin and promotes GSK-3beta-dependent phosphorylation of beta-catenin. *Embo J*. 17:1371-1384.

Iles, N., S. Rulten, S.F. El-Khamisy, and K.W. Caldecott. 2008. APLF (C2orf13) is a novel human protein involved in the cellular response to chromosomal DNA strand breaks (vol 27, pg 3793, 2007). *Molecular and cellular biology*. 28:3561-3561.

Inglis, J.D., M. Lee, and R.E. Hill. 1993. Emk, a protein kinase with homologs in yeast maps to mouse chromosome 19. *Mammalian genome : official journal of the International Mammalian Genome Society*. 4:401-403.

Inoki, K., H. Ouyang, T. Zhu, C. Lindvall, Y. Wang, X. Zhang, Q. Yang, C. Bennett, Y. Harada, K. Stankunas, C.Y. Wang, X. He, O.A. MacDougald, M. You, B.O. Williams, and K.L. Guan. 2006. TSC2 integrates Wnt and energy signals via a coordinated phosphorylation by AMPK and GSK3 to regulate cell growth. *Cell*. 126:955-968.

Ito, E., S.J. Yue, E.H. Moriyama, A.B. Hui, I. Kim, W. Shi, N.M. Alajez, N. Bhogal, G.H. Li, A. Datti, A.D. Schimmer, B.C. Wilson, P.P. Liu, D. Durocher, B.G. Neel, B. O'Sullivan, B. Cummings, R. Bristow, J. Wrana, and F.F. Liu. 2011. Uroporphyrinogen Decarboxylase Is a Radiosensitizing Target for Head and Neck Cancer. *Sci Transl Med*. 3.

Iversen, P.W., B.J. Eastwood, G.S. Sittampalam, and K.L. Cox. 2006. A comparison of assay performance measures in screening assays: signal window, Z' factor, and assay variability ratio. *J Biomol Screen*. 11:247-252.

Jackson, A.L., S.R. Bartz, J. Schelter, S.V. Kobayashi, J. Burchard, M. Mao, B. Li, G. Cavet, and P.S. Linsley. 2003. Expression profiling reveals off-target gene regulation by RNAi. *Nature biotechnology*. 21:635-637.

Jackson, A.L., J. Burchard, D. Leake, A. Reynolds, J. Schelter, J. Guo, J.M. Johnson, L. Lim, J. Karpilow, K. Nichols, W. Marshall, A. Khvorova, and P.S. Linsley. 2006a. Position-specific chemical modification of siRNAs reduces "off-target" transcript silencing. *RNA*. 12:1197-1205.

Jackson, A.L., J. Burchard, J. Schelter, B.N. Chau, M. Cleary, L. Lim, and P.S. Linsley. 2006b. Widespread siRNA "off-target" transcript silencing mediated by seed region sequence complementarity. *RNA*. 12:1179-1187.

Jackson, A.L., and P.S. Linsley. 2010. Recognizing and avoiding siRNA off-target effects for target identification and therapeutic application. *Nat Rev Drug Discov*. 9:57-67.

Jensen, R.B., A. Carreira, and S.C. Kowalczykowski. 2010. Purified human BRCA2 stimulates RAD51-mediated recombination. *Nature*. 467:678-U662.

Jiang, Y., Z.L. Cheng, E.C. Mandon, and R. Gilmore. 2008. An interaction between the SRP receptor and the translocon is critical during cotranslational protein translocation. *J Cell Biol*. 180:1149-1161.

Johnson, R.D., and M. Jasin. 2000. Sister chromatid gene conversion is a prominent double-strand break repair pathway in mammalian cells. *Embo J*. 19:3398-3407.

Joiner, M., and A.v.d. Kogel. 2009. Basic clinical radiobiology. Hodder Arnold ;, London. vi, 375 p. pp.

Kaelin, W.G., Jr. 2005. The concept of synthetic lethality in the context of anticancer therapy. *Nature reviews. Cancer*. 5:689-698.

Katz, D., E. Ito, K.S. Lau, J.D. Mocanu, C. Bastianutto, A.D. Schimmer, and F.F. Liu. 2008. Increased efficiency for performing colony formation assays in 96-well plates: novel applications to combination therapies and high-throughput screening. *Biotechniques*. 44:ix-xiv.

Katz, D., E. Ito, and F.F. Liu. 2009. On the path to seeking novel radiosensitizers. *Int J Radiat Oncol Biol Phys*. 73:988-996.

Kawasi, T., A. Iwashima, and Y. Nose. 1969. Regulation of thiamine biosynthesis in Escherichia coli. *Journal of biochemistry*. 65:407-416.

Kayser, G., W. Sienel, B. Kubitz, D. Mattern, E. Stickeler, B. Passlick, M. Werner, and A. zur Hausen. 2011. Poor outcome in primary non-small cell lung cancers is predicted by transketolase TKTL1 expression. *Pathology*. 43:719-724.

Kirk, J.E. 1959. The ribose-5-phosphate isomerase activity of arterial tissue in individuals of various ages. *Journal of gerontology*. 14:447-449.

Kirwan, M., A.J. Walne, V. Plagnol, M. Velangi, A. Ho, U. Hossain, T. Vulliamy, and I. Dokal. 2012. Exome Sequencing Identifies Autosomal-Dominant SRP72 Mutations Associated with Familial Aplasia and Myelodysplasia. *American journal of human genetics*. 90:888-892.

Kitano, A., T. Shimasaki, Y. Chikano, M. Nakada, M. Hirose, T. Higashi, Y. Ishigaki, Y. Endo, T. Takino, H. Sato, Y. Sai, K. Miyamoto, Y. Motoo, K. Kawakami, and T. Minamoto. 2013. Aberrant Glycogen Synthase Kinase 3 beta Is Involved in Pancreatic Cancer Cell Invasion and Resistance to Therapy. *Plos One*. 8.

Kittler, R., V. Surendranath, A.K. Heninger, M. Slabicki, M. Theis, G. Putz, K. Franke, A. Caldarelli, H. Grabner, K. Kozak, J. Wagner, E. Rees, B. Korn, C. Frenzel, C. Sachse, B. Sonnichsen, J. Guo, J. Schelter, J. Burchard, P.S. Linsley, A.L. Jackson, B. Habermann, and F. Buchholz. 2007. Genome-wide resources of endoribonuclease-prepared short interfering RNAs for specific loss-of-function studies. *Nature methods*. 4:337-344.

Klokov, D., S.M. MacPhail, J.P. Banath, J.P. Byrne, and P.L. Olive. 2006. Phosphorylated histone H2AX in relation to cell survival in tumor cells and xenografts exposed to single and fractionated doses of X-rays. *Radiotherapy and Oncology*. 80:223-229.

Kong, D., Y. Zhu, H. Wu, X. Cheng, H. Liang, and H.Q. Ling. 2008. AtTHIC, a gene involved in thiamine biosynthesis in Arabidopsis thaliana. *Cell research*. 18:566-576.

Koppenol, W.H., P.L. Bounds, and C.V. Dang. 2011. Otto Warburg's contributions to current concepts of cancer metabolism. *Nature reviews. Cancer*. 11:325-337.

Krasilnikov, M., V. Adler, S.Y. Fuchs, Z. Dong, A. Haimovitz-Friedman, M. Herlyn, and Z. Ronai. 1999. Contribution of phosphatidylinositol 3-kinase to radiation resistance in human melanoma cells. *Molecular carcinogenesis*. 24:64-69.

Krejci, L., V. Altmannova, M. Spirek, and X.L. Zhao. 2012. Homologous recombination and its regulation. *Nucleic acids research*. 40:5795-5818.

Lally, B.E., G.A. Geiger, S. Kridel, A.E. Arcury-Quandt, N.E. Robbins, N.D. Kock, K. Wheeler, P. Peddi, A. Georgakilas, G.D. Kao, and C. Koumenis. 2007. Identification and biological evaluation of a novel and potent small molecule radiation sensitizer via an unbiased screen of a chemical library. *Cancer research*. 67:8791-8799.

Landry, J.J., P.T. Pyl, T. Rausch, T. Zichner, M.M. Tekkedil, A.M. Stutz, A. Jauch, R.S. Aiyar, G. Pau, N. Delhomme, J. Gagneur, J.O. Korbel, W. Huber, and L.M. Steinmetz. 2013. The genomic and transcriptomic landscape of a HeLa cell line. *G3 (Bethesda)*. 3:1213-1224.

Langbein, S., M. Zerilli, A. zur Hausen, W. Staiger, K. Rensch-Boschert, N. Lukan, J. Popa, M.P. Ternullo, A. Steidler, C. Weiss, R. Grobholz, F. Willeke, P. Alken, G. Stassi, P. Schubert, and J.F. Coy. 2006. Expression of transketolase TKTL1 predicts colon and urothelial cancer patient survival: Warburg effect reinterpreted. *Brit J Cancer*. 94:578-585.

Lee, Y., C. Ahn, J. Han, H. Choi, J. Kim, J. Yim, J. Lee, P. Provost, O. Radmark, S. Kim, and V.N. Kim. 2003. The nuclear RNase III Drosha initiates microRNA processing. *Nature*. 425:415-419.

Leuschner, P.J., S.L. Ameres, S. Kueng, and J. Martinez. 2006. Cleavage of the siRNA passenger strand during RISC assembly in human cells. *Embo Rep*. 7:314-320.

Li, S., S. Kanno, R. Watanabe, H. Ogiwara, T. Kohno, G. Watanabe, A. Yasui, and M.R. Lieber. 2011. Polynucleotide kinase and aprataxin-like forkhead-associated protein (PALF) acts as both a single-stranded DNA endonuclease and a single-stranded DNA 3' exonuclease and can participate in DNA end joining in a biochemical system. *J Biol Chem*. 286:36368-36377.

Li, Z., T. Otevrel, Y. Gao, H.L. Cheng, B. Seed, T.D. Stamato, G.E. Taccioli, and F.W. Alt. 1995. The XRCC4 gene encodes a novel protein involved in DNA double-strand break repair and V(D)J recombination. *Cell*. 83:1079-1089.

Liao, X., L. Zhang, J.B. Thrasher, J. Du, and B. Li. 2003. Glycogen synthase kinase-3beta suppression eliminates tumor necrosis factor-related apoptosis-inducing ligand resistance in prostate cancer. *Molecular cancer therapeutics*. 2:1215-1222.

Lienhard, G.E., and I.A. Rose. 1964. The Mechanism of Action of 6-Phosphogluconate Dehydrogenase. *Biochemistry-Us*. 3:190-195.

Lin, C.C., L.C. Chen, V.S. Tseng, J.J. Yan, W.W. Lai, W.P. Su, C.H. Lin, C.Y.F. Huang, and W.C. Su. 2011. Malignant pleural effusion cells show aberrant glucose metabolism gene expression. *Eur Respir J*. 37:1453-1465.

Lin, S.H., J. Zhang, U. Giri, C. Stephan, M. Sobieski, L. Zhong, K.A. Mason, J. Molkentine, H.D. Thames, S.S. Yoo, and J.V. Heymach. 2014. A high content clonogenic survival drug screen identifies mek inhibitors as potent radiation sensitizers for KRAS mutant non-small-cell lung cancer. *Journal of thoracic oncology : official publication of the International Association for the Study of Lung Cancer*. 9:965-973.

Lippman, Z., and R. Martienssen. 2004. The role of RNA interference in heterochromatic silencing. *Nature*. 431:364-370.

Liu, F.F., E. Ito, S.J. Yue, E.H. Moriyama, A.B. Hui, I. Kim, W. Shi, N.M. Alajez, N. Bhogal, G.H. Li, A. Datti, A.D. Schimmer, B.C. Wilson, P.P. Liu, D. Durocher, B.G. Neel, B. O'Sullivan, B. Cummings, R. Bristow, and J. Wrana. 2011. Uroporphyrinogen Decarboxylase Is a Radiosensitizing Target for Head and Neck Cancer. *Science Translational Medicine*. 3.

Liu, J., M.A. Carmell, F.V. Rivas, C.G. Marsden, J.M. Thomson, J.J. Song, S.M. Hammond, L. Joshua-Tor, and G.J. Hannon. 2004a. Argonaute2 is the catalytic engine of mammalian RNAi. *Science*. 305:1437-1441.

Liu, J.Y., D.E. Timm, and T.D. Hurley. 2006a. Pyrithiamine as a substrate for thiamine pyrophosphokinase. *J Biol Chem*. 281:6601-6607.

Liu, S., H. Huang, X. Lu, M. Golinski, S. Comesse, D. Watt, R.B. Grossman, and J.A. Moscow. 2003. Down-regulation of thiamine transporter THTR2 gene expression in breast cancer and its association with resistance to apoptosis. *Molecular cancer research : MCR*. 1:665-673.

Liu, S., A. Stromberg, H.H. Tai, and J.A. Moscow. 2004b. Thiamine transporter gene expression and exogenous thiamine modulate the expression of genes involved in drug and prostaglandin metabolism in breast cancer cells. *Molecular cancer research : MCR*. 2:477-487.

Liu, W.L., M. Gao, K.Y. Tzen, C.L. Tsai, F.M. Hsu, A.L. Cheng, and J.C. Cheng. 2014. Targeting Phosphatidylinositide3-Kinase/Akt pathway by BKM120 for radiosensitization in hepatocellular carcinoma. *Oncotarget*. 5:3662-3672.

Liu, X., F. Jiang, S. Kalidas, D. Smith, and Q. Liu. 2006b. Dicer-2 and R2D2 coordinately bind siRNA to promote assembly of the siRISC complexes. *RNA*. 12:1514-1520.

Liu, X., E.K. Lam, X. Wang, J. Zhang, Y.Y. Cheng, Y.W. Lam, E.K. Ng, J. Yu, F.K. Chan, H. Jin, and J.J. Sung. 2009. Promoter hypermethylation mediates downregulation of thiamine receptor SLC19A3 in gastric cancer. *Tumour biology : the journal of the International Society for Oncodevelopmental Biology and Medicine*. 30:242-248.

Liu, X., J.S. Rubin, and A.R. Kimmel. 2005a. Rapid, Wnt-induced changes in GSK3beta associations that regulate beta-catenin stabilization are mediated by Galpha proteins. *Current biology : CB*. 15:1989-1997.

Liu, Z.Z., W.Y. Huang, X.S. Li, J.S. Lin, X.K. Cai, K.H. Lian, and H.J. Zhou. 2005b. Prediction value of radiosensitivity of hepatocarcinoma cells for apoptosis and micronucleus assay. *World J Gastroentero*. 11:7036-7039.

Loi, S., B. Haibe-Kains, C. Desmedt, P. Wirapati, F. Lallemand, A.M. Tutt, C. Gillet, P. Ellis, K. Ryder, J.F. Reid, M.G. Daidone, M.A. Pierotti, E.M. Berns, M.P. Jansen, J.A. Foekens, M. Delorenzi, G. Bontempi, M.J. Piccart, and C. Sotiriou. 2008. Predicting prognosis using molecular profiling in estrogen receptor-positive breast cancer treated with tamoxifen. *BMC genomics*. 9:239.

Lund-Andersen, C., S. Patzke, V. Nahse-Kumpf, and R.G. Syljuasen. 2014. PLK1-inhibition can cause radiosensitization or radioresistance dependent on the treatment schedule. *Radiotherapy and oncology : journal of the European Society for Therapeutic Radiology and Oncology*. 110:355-361.

Lutcke, H. 1995. Signal recognition particle (SRP), a ubiquitous initiator of protein translocation. *European journal of biochemistry / FEBS*. 228:531-550.

Lutcke, H., S. High, K. Romisch, A.J. Ashford, and B. Dobberstein. 1992. The Methionine-Rich Domain of the 54 Kda Subunit of Signal Recognition Particle Is Sufficient for the Interaction with Signal Sequences. *Embo J*. 11:1543-1551.

Ma, Y., U. Pannicke, K. Schwarz, and M.R. Lieber. 2002. Hairpin opening and overhang processing by an Artemis/DNA-dependent protein kinase complex in nonhomologous end joining and V(D)J recombination. *Cell*. 108:781-794.

Macara, I.G. 2004. Parsing the polarity code. *Nat Rev Mol Cell Bio*. 5:220-231.

MacPhail, S.H., J.P. Banath, T.Y. Yu, E.H.M. Chu, H. Lambur, and P.L. Olive. 2003. Expression of phosphorylated histone H2AX in cultured cell lines following exposure to X-rays. *Int J Radiat Biol*. 79:351-358.

Macrae, C.J., R.D. McCulloch, J. Ylanko, D. Durocher, and C.A. Koch. 2008a. APLF (C2orf13) facilitates nonhomologous end-joining and undergoes ATM-dependent hyperphosphorylation following ionizing radiation. *DNA Repair*. 7:292-302.

MacRae, I.J., E. Ma, M. Zhou, C.V. Robinson, and J.A. Doudna. 2008b. In vitro reconstitution of the human RISC-loading complex. *Proc Natl Acad Sci U S A*. 105:512-517.

Malivert, L., V. Ropars, M. Nunez, P. Drevet, S. Miron, G. Faure, R. Guerois, J.P. Mornon, P. Revy, J.B. Charbonnier, I. Callebaut, and J.P. de Villartay. 2010. Delineation of the Xrcc4-interacting region in the globular head domain of cernunnos/XLF. *J Biol Chem*. 285:26475-26483.

Maniataki, E., and Z. Mourelatos. 2005. A human, ATP-independent, RISC assembly machine fueled by pre-miRNA. *Genes Dev*. 19:2979-2990.

Mao, Z., M. Bozzella, A. Seluanov, and V. Gorbunova. 2008. Comparison of nonhomologous end joining and homologous recombination in human cells. *DNA Repair (Amst)*. 7:1765-1771.

Marchand, B., I. Tremblay, S. Cagnol, and M.J. Boucher. 2012. Inhibition of glycogen synthase kinase-3 activity triggers an apoptotic response in pancreatic cancer cells through JNK-dependent mechanisms. *Carcinogenesis*. 33:529-537.

Mari, P.O., B.I. Florea, S.P. Persengiev, N.S. Verkaik, H.T. Bruggenwirth, M. Modesti, G. Giglia-Mari, K. Bezstarosti, J.A. Demmers, T.M. Luider, A.B. Houtsmuller, and D.C. van Gent. 2006. Dynamic assembly of end-joining complexes requires interaction between Ku70/80 and XRCC4. *Proc Natl Acad Sci U S A*. 103:18597-18602.

Martinez, J., A. Patkaniowska, H. Urlaub, R. Luhrmann, and T. Tuschl. 2002. Single-stranded antisense siRNAs guide target RNA cleavage in RNAi. *Cell*. 110:563-574.

Matenia, D., C. Hempp, T. Timm, A. Eikhof, and E.M. Mandelkow. 2012. Microtubule Affinity-regulating Kinase 2 (MARK2) Turns on Phosphatase and Tensin Homolog (PTEN)-induced Kinase 1 (PINK1) at Thr-313, a Mutation Site in Parkinson Disease EFFECTS ON MITOCHONDRIAL TRANSPORT. *J Biol Chem*. 287:8174-8186.

Matranga, C., Y. Tomari, C. Shin, D.P. Bartel, and P.D. Zamore. 2005. Passenger-strand cleavage facilitates assembly of siRNA into Ago2-containing RNAi enzyme complexes. *Cell*. 123:607-620.

Mauceri, H.J., H.G. Sutton, T.E. Darga, M. Kocherginsky, J. Kochanski, R.R. Weichselbaum, and E.E. Vokes. 2012. Everolimus exhibits efficacy as a radiosensitizer in a model of non-small cell lung cancer. *Oncol Rep*. 27:1625-1629.

Mayr, J.A., P. Freisinger, K. Schlachter, B. Rolinski, F.A. Zimmermann, T. Scheffner, T.B. Haack, J. Koch, U. Ahting, H. Prokisch, and W. Sperl. 2011. Thiamine pyrophosphokinase deficiency in encephalopathic children with defects in the pyruvate oxidation pathway. *American journal of human genetics*. 89:806-812.

McElhinny, S.A.N., C.M. Snowden, J. McCarville, and D.A. Ramsden. 2000. Ku recruits the XRCC4-ligase IV complex to DNA ends. *Molecular and cellular biology*. 20:2996-3003.

McGowan, E.M., N. Alling, E.A. Jackson, D. Yagoub, N.K. Haass, J.D. Allen, and R. Martinello-Wilks. 2011. Evaluation of Cell Cycle Arrest in Estrogen Responsive MCF-7 Breast Cancer Cells: Pitfalls of the MTS Assay. *Plos One*. 6.

McIlwraith, M.J., A. Vaisman, Y. Liu, E. Fanning, R. Woodgate, and S.C. West. 2005. Human DNA polymerase eta promotes DNA synthesis from strand invasion intermediates of homologous recombination. *Mol Cell*. 20:783-792.

McKenna, W.G., M.C. Weiss, V.J. Bakanauskas, H. Sandler, M.L. Kelsten, J. Biaglow, S.W. Tuttle, B. Endlich, C.C. Ling, and R.J. Muschel. 1990. The role of the H-ras oncogene in radiation resistance and metastasis. *International journal of radiation oncology, biology, physics*. 18:849-859.

Meshalkina, L.E., V.L. Drutsa, O.N. Koroleva, O.N. Solovjeva, and G.A. Kochetov. 2013. Is transketolase-like protein, TKTL1, transketolase? *Bba-Mol Basis Dis*. 1832:387-390.

Michael, B.D., G.E. Adams, H.B. Hewitt, W.B. Jones, and M.E. Watts. 1973. A posteffect of oxygen in irradiated bacteria: a submillisecond fast mixing study. *Radiat Res*. 54:239-251.

Miclet, E., V. Stoven, P.A. Michels, F.R. Opperdoes, J.Y. Lallemand, and F. Duffieux. 2001. NMR spectroscopic analysis of the first two steps of the pentose-phosphate pathway elucidates the role of 6-phosphogluconolactonase. *J Biol Chem*. 276:34840-34846.

Milas, L., T. Akimoto, N.R. Hunter, L. Buchmiller, K. Mason, and K.K. Ang. 1999. Inverse relationship between epidermal growth factor receptor expression and radiocurability of murine carcinomas. *Clinical Cancer Research*. 5:2884-2890.

Milas, L., K. Mason, N. Hunter, S. Petersen, M. Yamakawa, K. Ang, J. Mendelsohn, and Z. Fan. 2000. In vivo enhancement of tumor radioresponse by C225 antiepidermal growth factor receptor antibody. *Clinical Cancer Research*. 6:701-708.

Mimitou, E.P., and L.S. Symington. 2008. Sae2, Exo1 and Sgs1 collaborate in DNA double-strand break processing. *Nature*. 455:770-774.

Mimori, T., and J.A. Hardin. 1986. Mechanism of interaction between Ku protein and DNA. *J Biol Chem*. 261:10375-10379.

Mitch, W.E., and W. Chan. 1978. Transamination of Branched-Chain Keto Acids by Isolated Perfused Rat-Kidney. *Am J Physiol*. 235:E47-E52.

Miyashita, K., K. Kawakami, M. Nakada, W. Mai, A. Shakoori, H. Fujisawa, Y. Hayashi, J. Hamada, and T. Minamoto. 2009. Potential therapeutic effect of glycogen synthase kinase 3beta inhibition against human glioblastoma. *Clin Cancer Res*. 15:887-897.

Molenaar, M., M. van de Wetering, M. Oosterwegel, J. Peterson-Maduro, S. Godsave, V. Korinek, J. Roose, O. Destree, and H. Clevers. 1996. XTcf-3 transcription factor mediates beta-catenin-induced axis formation in Xenopus embryos. *Cell*. 86:391-399.

Morgan, M.A., L.A. Parsels, L. Zhao, J.D. Parsels, M.A. Davis, M.C. Hassan, S. Arumugarajah, L. Hylander-Gans, D. Morosini, D.M. Simeone, C.E. Canman, D.P. Normolle, S.D. Zabludoff, J. Maybaum, and T.S. Lawrence. 2010. Mechanism of radiosensitization by the Chk1/2 inhibitor AZD7762 involves

abrogation of the G2 checkpoint and inhibition of homologous recombinational DNA repair. *Cancer research*. 70:4972-4981.

Mosmann, T. 1983. Rapid colorimetric assay for cellular growth and survival: application to proliferation and cytotoxicity assays. *Journal of immunological methods*. 65:55-63.

Mussmann, R., M. Geese, F. Harder, S. Kegel, U. Andag, A. Lomow, U. Burk, D. Onichtchouk, C. Dohrmann, and M. Austen. 2007. Inhibition of GSK3 promotes replication and survival of pancreatic beta cells. *J Biol Chem*. 282:12030-12037.

Nesic, D., M.C. Miller, Z.T. Quinkert, M. Stein, B.T. Chait, and C.E. Stebbins. 2010. Helicobacter pylori CagA inhibits PAR1-MARK family kinases by mimicking host substrates. *Nature structural & molecular biology*. 17:130-132.

Ni, X., Y. Zhang, J. Ribas, W.H. Chowdhury, M. Castanares, Z. Zhang, M. Laiho, T.L. DeWeese, and S.E. Lupold. 2011. Prostate-targeted radiosensitization via aptamer-shRNA chimeras in human tumor xenografts. *J Clin Invest*. 121:2383-2390.

Nick McElhinny, S.A., J.M. Havener, M. Garcia-Diaz, R. Juarez, K. Bebenek, B.L. Kee, L. Blanco, T.A. Kunkel, and D.A. Ramsden. 2005. A gradient of template dependence defines distinct biological roles for family X polymerases in nonhomologous end joining. *Mol Cell*. 19:357-366.

Nimonkar, A.V., A.Z. Ozsoy, J. Genschel, P. Modrich, and S.C. Kowalczykowski. 2008. Human exonuclease 1 and BLM helicase interact to resect DNA and initiate DNA repair. *P Natl Acad Sci USA*. 105:16906-16911.

Nishimura, Y., K. Applegate, M.W. Davidson, G. Danuser, and C.M. Waterman. 2012. Automated screening of microtubule growth dynamics identifies MARK2 as a

regulator of leading edge microtubules downstream of Rac1 in migrating cells. *Plos One*. 7:e41413.

Nita, M.E., H. Nagawa, O. Tominaga, N. Tsuno, S. Fujii, S. Sasaki, C.G. Fu, T. Takenoue, T. Tsuruo, and T. Muto. 1998. 5-Fluorouracil induces apoptosis in human colon cancer cell lines with modulation of Bcl-2 family proteins. *Br J Cancer*. 78:986-992.

Nordsmark, M., M. Overgaard, and J. Overgaard. 1996. Pretreatment oxygenation predicts radiation response in advanced squamous cell carcinoma of the head and neck. *Radiotherapy and Oncology*. 41:31-39.

Nosaka, K., M. Onozuka, N. Kakazu, S. Hibi, H. Nishimura, H. Nishino, and T. Abe. 2001. Isolation and characterization of a human thiamine pyrophosphokinase cDNA. *Biochimica et biophysica acta*. 1517:293-297.

Novello, F., and P. McLean. 1968. The pentose phosphate pathway of glucose metabolism. Measurement of the non-oxidative reactions of the cycle. *Biochem J*. 107:775-791.

Nutting, C.M., D.J. Convery, V.P. Cosgrove, C. Rowbottom, A.R. Padhani, S. Webb, and D.P. Dearnaley. 2000. Reduction of small and large bowel irradiation using an optimized intensity-modulated pelvic radiotherapy technique in patients with prostate cancer. *International Journal of Radiation Oncology Biology Physics*. 48:649-656.

Olive, P.L., and J.P. Banath. 2004. Phosphorylation of histone H2AX as a measure of radiosensitivity. *Int J Radiat Oncol*. 58:331-335.

Orban, T.I., and E. Izaurralde. 2005. Decay of mRNAs targeted by RISC requires XRN1, the Ski complex, and the exosome. *RNA*. 11:459-469.

Palcic, B., and L.D. Skarsgard. 1984. Reduced Oxygen Enhancement Ratio at Low-Doses of Ionizing-Radiation. *Radiat Res*. 100:328-339.

Pang, D., S. Yoo, W.S. Dynan, M. Jung, and A. Dritschilo. 1997. Ku proteins join DNA fragments as shown by atomic force microscopy. *Cancer research*. 57:1412-1415.

Pap, M., and G.M. Cooper. 1998. Role of glycogen synthase kinase-3 in the phosphatidylinositol 3-Kinase/Akt cell survival pathway. *J Biol Chem*. 273:19929-19932.

Pap, M., and G.M. Cooper. 2002. Role of translation initiation factor 2B in control of cell survival by the phosphatidylinositol 3-kinase/Akt/glycogen synthase kinase 3beta signaling pathway. *Molecular and cellular biology*. 22:578-586.

Park, S., M. Lee, H. Lee, H.Y. Kim, Y.S. Lee, S.W. Jeong, and D. Jeoung. 2002. Identification of signature genes associated with 5-fluorouracil-resistance in human gastric cancer cells. *Biotechnol Lett*. 24:1651-1657.

Park, S.J., C.H. Wu, J.D. Gordon, X. Zhong, A. Emami, and A.R. Safa. 2004. Taxol induces caspase-10-dependent apoptosis. *J Biol Chem*. 279:51057-51067.

Parker, P.J., F.B. Caudwell, and P. Cohen. 1983. Glycogen synthase from rabbit skeletal muscle; effect of insulin on the state of phosphorylation of the seven phosphoserine residues in vivo. *European journal of biochemistry / FEBS*. 130:227-234.

Parker, P.J., and P.J. Randle. 1978. Partial-Purification and Properties of Branched-Chain 2-Oxo Acid Dehydrogenase of Ox Liver. *Biochem J*. 171:751-757.

Pawitan, Y., J. Bjohle, L. Amler, A.L. Borg, S. Egyhazi, P. Hall, X. Han, L. Holmberg, F. Huang, S. Klaar, E.T. Liu, L. Miller, H. Nordgren, A. Ploner, K. Sandelin, P.M. Shaw, J. Smeds, L. Skoog, S. Wedren, and J. Bergh. 2005. Gene expression

profiling spares early breast cancer patients from adjuvant therapy: derived and validated in two population-based cohorts. *Breast cancer research : BCR*. 7:R953-964.

Peters, W.A., P.Y. Liu, R.J. Barrett, R.J. Stock, B.J. Monk, J.S. Berek, L. Souhami, P. Grigsby, W. Gordon, and D.S. Alberts. 2000. Concurrent chemotherapy and pelvic radiation therapy compared with pelvic radiation therapy alone as adjuvant therapy after radical surgery in high-risk early-stage cancer of the cervix. *Journal of Clinical Oncology*. 18:1606-1613.

Poe, J.A., L. Vollmer, A. Vogt, and T.E. Smithgall. 2014. Development and Validation of a High-Content Bimolecular Fluorescence Complementation Assay for Small-Molecule Inhibitors of HIV-1 Nef Dimerization. *J Biomol Screen*. 19:556-565.

Pollack, A., G.K. Zagars, L.G. Smith, J.J. Lee, A.C. von Eschenbach, J.A. Antolak, G. Starkschall, and I. Rosen. 2000. Preliminary results of a randomized radiotherapy dose-escalation study comparing 70 Gy with 78 Gy for prostate cancer. *Journal of Clinical Oncology*. 18:3904-3911.

Pontremoli, S., A. Bonsignore, E. Grazi, and B.L. Horecker. 1960. A coupled reaction catalyzed by the enzymes transketolase and transaldolase. *J Biol Chem*. 235:1881-1887.

Prevo, R., E. Deutsch, O. Sampson, J. Diplexcito, K. Cengel, J. Harper, P. O'Neill, W.G. McKenna, S. Patel, and E.J. Bernhard. 2008. Class I PI3 kinase inhibition by the pyridinylfuranopyrimidine inhibitor PI-103 enhances tumor radiosensitivity. *Cancer research*. 68:5915-5923.

Price, P., and T.J. McMillan. 1990. Use of the tetrazolium assay in measuring the response of human tumor cells to ionizing radiation. *Cancer research*. 50:1392-1396.

Quintayo, M.A., A.F. Munro, J. Thomas, I.H. Kunkler, W. Jack, G.R. Kerr, J.M. Dixon, U. Chetty, and J.M.S. Bartlett. 2012. GSK3 beta and cyclin D1 expression predicts outcome in early breast cancer patients. *Breast Cancer Res Tr*. 136:161-168.

Racker, E. 1972. Bioenergetics and the problem of tumor growth. *American scientist*. 60:56-63.

Radford, I.R., T.K. Murphy, J.M. Radley, and S.L. Ellis. 1994. Radiation Response of Mouse Lymphoid and Myeloid Cell-Lines .2. Apoptotic Death Is Shown by All Lines Examined. *Int J Radiat Biol*. 65:217-227.

Rais, B., B. Comin, J. Puigjaner, J.L. Brandes, E. Creppy, D. Saboureau, R. Ennamany, W.N. Lee, L.G. Boros, and M. Cascante. 1999. Oxythiamine and dehydroepiandrosterone induce a G1 phase cycle arrest in Ehrlich's tumor cells through inhibition of the pentose cycle. *FEBS letters*. 456:113-118.

Rapiejko, P.J., and R. Gilmore. 1997. Empty site forms of the SRP54 and SR alpha GTPases mediate targeting of ribosome-nascent chain complexes to the endoplasmic reticulum. *Cell*. 89:703-713.

Rass, U., S.A. Compton, J. Matos, M.R. Singleton, S.C.Y. Ip, M.G. Blanco, J.D. Griffith, and S.C. West. 2010. Mechanism of Holliday junction resolution by the human GEN1 protein. *Gene Dev*. 24:1559-1569.

Ren, Y.G., K.W. Wagner, D.A. Knee, P. Aza-Blanc, M. Nasoff, and Q.L. Deveraux. 2004. Differential regulation of the TRAIL death receptors DR4 and DR5 by the signal recognition particle. *Mol Biol Cell*. 15:5064-5074.

Renwick, A., D. Thompson, S. Seal, P. Kelly, T. Chagtai, M. Ahmed, B. North, H. Jayatilake, R. Barfoot, K. Spanova, L. McGuffog, D.G. Evans, D. Eccles, D.F. Easton, M.R. Stratton, N. Rahman, and B.C. Susceptibility. 2006. ATM mutations

that cause ataxia-telangiectasia are breast cancer susceptibility alleles. *Nat Genet*. 38:873-875.

Requejo-Aguilar, R., I. Lopez-Fabuel, E. Fernandez, L.M. Martins, A. Almeida, and J.P. Bolanos. 2014. PINK1 deficiency sustains cell proliferation by reprogramming glucose metabolism through HIF1. *Nature communications*. 5:4514.

Rhodes, D.R., S. Kalyana-Sundaram, V. Mahavisno, R. Varambally, J. Yu, B.B. Briggs, T.R. Barrette, M.J. Anstet, C. Kincead-Beal, P. Kulkarni, S. Varambally, D. Ghosh, and A.M. Chinnaiyan. 2007. Oncomine 3.0: genes, pathways, and networks in a collection of 18,000 cancer gene expression profiles. *Neoplasia*. 9:166-180.

Richard, D.J., E. Bolderson, L. Cubeddu, R.I.M. Wadsworth, K. Savage, G.G. Sharma, M.L. Nicolette, S. Tsvetanov, M.J. McIlwraith, R.K. Pandita, S. Takeda, R.T. Hay, J. Gautier, S.C. West, T.T. Paull, T.K. Pandita, M.F. White, and K.K. Khanna. 2008. Single-stranded DNA-binding protein hSSB1 is critical for genomic stability. *Nature*. 453:677-U613.

Richardson, C., M.E. Moynahan, and M. Jasin. 1998. Double-strand break repair by interchromosomal recombination: suppression of chromosomal translocations. *Genes Dev*. 12:3831-3842.

Richmond, R.C., A.R. Khokhar, B.A. Teicher, and E.B. Douple. 1984. Toxic Variability and Radiation Sensitization by Pt(Ii) Analogs in Salmonella-Typhimurium Cells. *Radiation Research*. 99:609-626.

Rippa, M., P.P. Giovannini, M.P. Barrett, F. Dallocchio, and S. Hanau. 1998. 6-Phosphogluconate dehydrogenase: the mechanism of action investigated by a comparison of the enzyme from different species. *Biochimica et biophysica acta*. 1429:83-92.

Roberts, S.A., N. Strande, M.D. Burkhalter, C. Strom, J.M. Havener, P. Hasty, and D.A. Ramsden. 2010. Ku is a 5'-dRP/AP lyase that excises nucleotide damage near broken ends. *Nature*. 464:1214-1217.

Roninson, I.B., E.V. Broude, and B.D. Chang. 2001. If not apoptosis, then what? - Treatment-induced senescence and mitotic catastrophe in tumor cells. *Drug Resist Update*. 4:303-313.

Rose, P.G., B.N. Bundy, E.B. Watkins, J.T. Thigpen, G. Deppe, M.A. Maiman, D.L. Clarke-Pearson, and S. Insalaco. 1999. Concurrent cisplatin-based radiotherapy and chemotherapy for locally advanced cervical cancer. *N Engl J Med*. 340:1144-1153.

Rothkamm, K., I. Kruger, L.H. Thompson, and M. Lobrich. 2003. Pathways of DNA double-strand break repair during the mammalian cell cycle. *Molecular and cellular biology*. 23:5706-5715.

Rubin Grandis, J., M.F. Melhem, W.E. Gooding, R. Day, V.A. Holst, M.M. Wagener, S.D. Drenning, and D.J. Tweardy. 1998. Levels of TGF-alpha and EGFR protein in head and neck squamous cell carcinoma and patient survival. *J Natl Cancer Inst*. 90:824-832.

Rulten, S.L., A.E.O. Fisher, I. Robert, M.C. Zuma, M. Rouleau, L.M. Ju, G. Poirier, B. Reina-San-Martin, and K.W. Caldecott. 2011. PARP-3 and APLF Function Together to Accelerate Nonhomologous End-Joining. *Mol Cell*. 41:33-45.

Saadat, I., H. Higashi, C. Obuse, M. Umeda, N. Murata-Kamiya, Y. Saito, H. Lu, N. Ohnishi, T. Azuma, A. Suzuki, S. Ohno, and M. Hatakeyama. 2007. Helicobacter pylori CagA targets PAR1/MARK kinase to disrupt epithelial cell polarity. *Nature*. 447:330-333.

Said, H.M., K. Balamurugan, V.S. Subramanian, and J.S. Marchant. 2004. Expression and functional contribution of hTHTR-2 in thiamin absorption in human intestine. *Am J Physiol-Gastr L*. 286:G491-G498.

Saleh-Gohari, N., H.E. Bryant, N. Schultz, K.A. Parker, T.N. Cassel, and T. Helleday. 2005. Spontaneous homologous recombination is induced by collapsed replication forks that are caused by endogenous DNA single-strand breaks. *Molecular and cellular biology*. 25:7158-7169.

Sano, S., Y. Matsuda, and H. Nakagawa. 1988. Thiamine pyrophosphatase (nucleoside diphosphatase) in the Golgi apparatus is distinct from microsomal nucleoside diphosphatase. *Journal of biochemistry*. 103:678-681.

Sarkaria, J.N., E.C. Busby, R.S. Tibbetts, P. Roos, Y. Taya, L.M. Karnitz, and R.T. Abraham. 1999. Inhibition of ATM and ATR kinase activities by the radiosensitizing agent, caffeine. *Cancer research*. 59:4375-4382.

Sartori, A.A., C. Lukas, J. Coates, M. Mistrik, S. Fu, J. Bartek, R. Baer, J. Lukas, and S.P. Jackson. 2007. Human CtIP promotes DNA end resection. *Nature*. 450:509-514.

Schaakekoning, C., W. Vandenbogaert, O. Dalesio, J. Festen, J. Hoogenhout, P. Vanhoutte, A. Kirkpatrick, M. Koolen, B. Maat, A. Nijs, A. Renaud, P. Rodrigus, L. Schusteruitterhoeve, J.P. Sculier, N. Vanzandwijk, and H. Bartelink. 1992. Effects of Concomitant Cisplatin and Radiotherapy on Inoperable Non-Small-Cell Lung-Cancer. *New England Journal of Medicine*. 326:524-530.

Schultz, H., D. Kahler, D. Branscheid, E. Vollmer, P. Zabel, and T. Goldmann. 2008. TKTL1 is overexpressed in a large portion of non-small cell lung cancer specimens. *Diagn Pathol*. 3.

Schulz-Ertner, D., A. Nikoghosyan, C. Thilmann, T. Haberer, O. Jakel, C. Karger, G. Kraft, M. Wannenmacher, and J. Debus. 2004. Results of carbon ion radiotherapy in 152 patients. *International Journal of Radiation Oncology Biology Physics*. 58:631-640.

Schulz-Ertner, D., and H. Tsujii. 2007. Particle radiation therapy using proton and heavier ion beams. *J Clin Oncol*. 25:953-964.

Schwaab, J., K. Horisberger, P. Strobel, B. Bohn, D. Gencer, G. Kahler, P. Kienle, S. Post, F. Wenz, W.K. Hofmann, R.D. Hofheinz, and P. Erben. 2011. Expression of Transketolase like gene 1 (TKTL1) predicts disease-free survival in patients with locally advanced rectal cancer receiving neoadjuvant chemoradiotherapy. *Bmc Cancer*. 11.

Schwarz, D.S., G. Hutvagner, T. Du, Z.S. Xu, N. Aronin, and P.D. Zamore. 2003. Asymmetry in the assembly of the RNAi enzyme complex. *Cell*. 115:199-208.

Seligmann, H., R. Levi, A.M. Konijn, and M. Prokocimer. 2001. Thiamine deficiency in patients with B-chronic lymphocytic leukaemia: a pilot study. *Postgraduate medical journal*. 77:582-585.

Shah, N.P., J.M. Nicoll, B. Nagar, M.E. Gorre, R.L. Paquette, J. Kuriyan, and C.L. Sawyers. 2002. Multiple BCR-ABL kinase domain mutations confer polyclonal resistance to the tyrosine kinase inhibitor imatinib (STI571) in chronic phase and blast crisis chronic myeloid leukemia. *Cancer cell*. 2:117-125.

Shakoori, A., W. Mai, K. Miyashita, K. Yasumoto, Y. Takahashi, A. Ooi, K. Kawakami, and T. Minamoto. 2007. Inhibition of GSK-3 beta activity attenuates proliferation of human colon cancer cells in rodents. *Cancer Sci*. 98:1388-1393.

Sheridan, M.T., T. O'Dwyer, C.B. Seymour, and C.E. Mothersill. 1997. Potential indicators of radiosensitivity in squamous cell carcinoma of the head and neck. *Radiat Oncol Investig*. 5:180-186.

Shibamoto, Y., C. Streffer, C. Fuhrmann, and V. Budach. 1991. Tumor Radiosensitivity Prediction by the Cytokinesis-Block Micronucleus Assay. *Radiat Res*. 128:293-300.

Smith, J., L.M. Tho, N.H. Xu, and D.A. Gillespie. 2010. The ATM-Chk2 and ATR-Chk1 Pathways in DNA Damage Signaling and Cancer. *Adv Cancer Res*. 108:73-112.

Spankuch-Schmitt, B., J. Bereiter-Hahn, M. Kaufmann, and K. Strebhardt. 2002. Effect of RNA silencing of polo-like kinase-1 (PLK1) on apoptosis and spindle formation in human cancer cells. *Journal of the National Cancer Institute*. 94:1863-1877.

Steel, G., T.J. McMillan, and J.H. Peacock. 1989. The 5R's of radiobiology. *Int J Radiat Biol*. 56

1045-1048.

Stiff, T., M. O'Driscoll, N. Rief, K. Iwabuchi, M. Lobrich, and P.A. Jeggo. 2004. ATM and DNA-PK function redundantly to phosphorylate H2AX after exposure to ionizing radiation. *Cancer research*. 64:2390-2396.

Storey, M.R., A. Pollack, G. Zagars, L. Smith, J. Antolak, and I. Rosen. 2000. Complications from radiotherapy dose escalation in prostate cancer: Preliminary results of a randomized trial. *Int J Radiat Oncol*. 48:635-642.

Sudo, H., A.B. Tsuji, A. Sugyo, T. Imai, T. Saga, and Y.N. Harada. 2007. A loss of function screen identifies nine new radiation susceptibility genes. *Biochem Biophys Res Commun*. 364:695-701.

Sun, C., L. Wang, S. Huang, G.J. Heynen, A. Prahallad, C. Robert, J. Haanen, C. Blank, J. Wesseling, S.M. Willems, D. Zecchin, S. Hobor, P.K. Bajpe, C. Lieftink,

C. Mateus, S. Vagner, W. Grernrum, I. Hofland, A. Schlicker, L.F. Wessels, R.L. Beijersbergen, A. Bardelli, F. Di Nicolantonio, A.M. Eggermont, and R. Bernards. 2014. Reversible and adaptive resistance to BRAF(V600E) inhibition in melanoma. *Nature*. 508:118-122.

Sutherland, C., I.A. Leighton, and P. Cohen. 1993. Inactivation of Glycogen-Synthase Kinase-3-Beta by Phosphorylation - New Kinase Connections in Insulin and Growth-Factor Signaling. *Biochem J*. 296:15-19.

Suzuki, A., M. Hirata, K. Kamimura, R. Maniwa, T. Yamanaka, K. Mizuno, M. Kishikawa, H. Hirose, Y. Amano, N. Izumi, Y. Miwa, and S. Ohno. 2004. aPKC acts upstream of PAR-1b in both the establishment and maintenance of mammalian epithelial polarity. *Current Biology*. 14:1425-1435.

Swanson, P.E., S.B. Carrol, X.F. Zhang, and M.A. Mackey. 1995. Spontaneous Premature Chromosome Condensation, Micronucleus Formation, and Non-Apoptotic Cell-Death in Heated Hela S3 Cells - Ultrastructural Observations. *Am J Pathol*. 146:963-971.

Sweet, R., A. Paul, and J. Zastre. 2010. Hypoxia induced upregulation and function of the thiamine transporter, SLC19A3 in a breast cancer cell line. *Cancer Biol Ther*. 10:1101-1111.

Szostak, J.W., T.L. Orr-Weaver, R.J. Rothstein, and F.W. Stahl. 1983. The double-strand-break repair model for recombination. *Cell*. 33:25-35.

Tatum, E.L., and T.T. Bell. 1946. Neurospora: biosynthesis of thiamin. *American journal of botany*. 33:15-20.

Tedokon, M., K. Suzuki, Y. Kayamori, S. Fujita, and Y. Katayama. 1992. Enzymatic Assay of Inorganic-Phosphate with Use of Sucrose Phosphorylase and Phosphoglucomutase. *Clin Chem*. 38:512-515.

Tegtmeyer, N., J. Lind, B. Schmid, and S. Backert. 2014. Helicobacter pylori CagL Y58/E59 Mutation Turns-Off Type IV Secretion-Dependent Delivery of CagA into Host Cells. *Plos One*. 9.

Temel, J.S., J.A. Greer, A. Muzikansky, E.R. Gallagher, S. Admane, V.A. Jackson, C.M. Dahlin, C.D. Blinderman, J. Jacobsen, W.F. Pirl, J.A. Billings, and T.J. Lynch. 2010. Early palliative care for patients with metastatic non-small-cell lung cancer. *The New England journal of medicine*. 363:733-742.

Thomas, Y., N. Bui, and K. Strub. 1997. A truncation in the 14 kDa protein of the signal recognition particle leads to tertiary structure changes in the RNA and abolishes the elongation arrest activity of the particle. *Nucleic acids research*. 25:1920-1929.

Thorslund, T., M.J. McIlwraith, S.A. Compton, S. Lekomtsev, M. Petronczki, J.D. Griffith, and S.C. West. 2010. The breast cancer tumor suppressor BRCA2 promotes the specific targeting of RAD51 to single-stranded DNA. *Nature structural & molecular biology*. 17:1263-1265.

Thorstenson, Y.R., A. Roxas, R. Kroiss, M.A. Jenkins, K.M. Yu, T. Bachrich, D. Muhr, T.L. Wayne, G. Chu, R.W. Davis, T.M.U. Wagner, and P.J. Oefner. 2003. Contributions of ATM mutations to familial breast and ovarian cancer. *Cancer research*. 63:3325-3333.

Thotala, D., D. Hallahan, and E. Yazlovitskaya. 2008. Radioprotection of small intestines and bone marrow by inhibition of Glycogen Synthase Kinase-3 beta (GSK-30). *Int J Radiat Oncol*. 72:S698-S698.

Thotala, D.K., D.E. Hallahan, and E.M. Yazlovitskaya. 2012. Glycogen synthase kinase 3beta inhibitors protect hippocampal neurons from radiation-induced apoptosis by regulating MDM2-p53 pathway. *Cell death and differentiation*. 19:387-396.

Tiwana, G.S., R. Prevo, F.M. Buffa, S. Yu, D.V. Ebner, A. Howarth, L.K. Folkes, B. Budwal, K.Y. Chu, L. Durrant, R.J. Muschel, W.G. McKenna, and G.S. Higgins. 2015. Identification of vitamin B1 metabolism as a tumor-specific radiosensitizing pathway using a high-throughput colony formation screen. *Oncotarget*.

Tong, D., L. Gillick, and F.R. Hendrickson. 1982. The Palliation of Symptomatic Osseous Metastases - Final Results of the Study by the Radiation-Therapy Oncology Group. *Cancer-Am Cancer Soc*. 50:893-899.

Tubiana, M., and F. Eschwege. 2000. Conformal radiotherapy and intensity-modulated radiotherapy--clinical data. *Acta Oncol*. 39:555-567.

Turenne, G.A., and B.D. Price. 2001. Glycogen synthase kinase3 beta phosphorylates serine 33 of p53 and activates p53's transcriptional activity. *BMC cell biology*. 2:12.

Tuschl, T., and Y. Dorsett. 2004. siRNAs: Applications in functional genomics and potential as therapeutics. *Nat Rev Drug Discov*. 3:318-329.

Tuschl, T., P.D. Zamore, R. Lehmann, D.P. Bartel, and P.A. Sharp. 1999. Targeted mRNA degradation by double-stranded RNA in vitro. *Gene Dev*. 13:3191-3197.

Uematsu, N., E. Weterings, K. Yano, K. Morotomi-Yano, B. Jakob, G. Taucher-Scholz, P.O. Mari, D.C. van Gent, B.P.C. Chen, and D.J. Chen. 2007. Autophosphorylation of DNA-PKCS regulates its dynamics at DNA double-strand breaks. *J Cell Biol*. 177:219-229.

Usmanov, R.A., H. Neef, M.G. Pustynnikov, A. Schellenberger, and G.A. Kochetov. 1985. The effect of thiamine pyrophosphate modification on its coenzyme function in a transketolase-catalyzed reaction. *Biochemistry international*. 10:479-486.

Utz, P.J., M. Hottelet, T.M. Le, S.J. Kim, M.E. Geiger, W.J. van Venrooij, and P. Anderson. 1998. The 72-kDa component of signal recognition particle is cleaved during apoptosis. *J Biol Chem*. 273:35362-35370.

van Gent, D.C., and M. van der Burg. 2007. Non-homologous end-joining, a sticky affair. *Oncogene*. 26:7731-7740.

Vaupel, P., and L. Harrison. 2004. Tumor hypoxia: Causative factors, compensatory mechanisms, and cellular response. *Oncologist*. 9:4-9.

Wagner, U., M. Utton, J.M. Gallo, and C.C. Miller. 1996. Cellular phosphorylation of tau by GSK-3 beta influences tau binding to microtubules and microtubule organisation. *Journal of cell science*. 109 (Pt 6):1537-1543.

Wakefield, J.G., D.J. Stephens, and J.M. Tavare. 2003. A role for glycogen synthase kinase-3 in mitotic spindle dynamics and chromosome alignment. *Journal of cell science*. 116:637-646.

Walter, P., and G. Blobel. 1980. Purification of a Membrane-Associated Protein Complex Required for Protein Translocation across the Endoplasmic-Reticulum. *P Natl Acad Sci-Biol*. 77:7112-7116.

Walter, P., and G. Blobel. 1982. Signal recognition particle contains a 7S RNA essential for protein translocation across the endoplasmic reticulum. *Nature*. 299:691-698.

Walter, P., I. Ibrahimi, and G. Blobel. 1981. Translocation of Proteins across the Endoplasmic-Reticulum .1. Signal Recognition Protein (Srp) Binds to Invitro-Assembled Polysomes Synthesizing Secretory Protein. *J Cell Biol*. 91:545-550.

Wang, L., H.K. Lin, Y.C. Hu, S. Xie, L. Yang, and C. Chang. 2004. Suppression of androgen receptor-mediated transactivation and cell growth by the glycogen synthase kinase 3 beta in prostate cells. *J Biol Chem*. 279:32444-32452.

Wang, Y., J.G. Klijn, Y. Zhang, A.M. Sieuwerts, M.P. Look, F. Yang, D. Talantov, M. Timmermans, M.E. Meijer-van Gelder, J. Yu, T. Jatkoe, E.M. Berns, D. Atkins, and J.A. Foekens. 2005. Gene-expression profiles to predict distant metastasis of lymph-node-negative primary breast cancer. *Lancet*. 365:671-679.

Ward, I.M., and J.J. Chen. 2001. Histone H2AX is phosphorylated in an ATR-dependent manner in response to replicational stress. *J Biol Chem*. 276:47759-47762.

Ward, J.F. 1988. DNA Damage Produced by Ionizing-Radiation in Mammalian-Cells - Identities, Mechanisms of Formation, and Reparability. *Prog Nucleic Acid Re*. 35:95-125.

Ward, J.F., W.F. Blakely, and E.I. Joner. 1985. Mammalian-Cells Are Not Killed by DNA Single-Strand Breaks Caused by Hydroxyl Radicals from Hydrogen-Peroxide. *Radiat Res*. 103:383-392.

Warters, R.L., and K.G. Hofer. 1977. Radionuclide toxicity in cultured mammalian cells. Elucidation of the primary site for radiation-induced division delay. *Radiat Res*. 69:348-358.

Warters, R.L., K.G. Hofer, C.R. Harris, and J.M. Smith. 1978. Radionuclide toxicity in cultured mammalian cells: elucidation of the primary site of radiation damage. *Current topics in radiation research quarterly*. 12:389-407.

Watanabe, T., Y. Totoki, A. Toyoda, M. Kaneda, S. Kuramochi-Miyagawa, Y. Obata, H. Chiba, Y. Kohara, T. Kono, T. Nakano, M.A. Surani, Y. Sakaki, and H. Sasaki. 2008. Endogenous siRNAs from naturally formed dsRNAs regulate transcripts in mouse oocytes. *Nature*. 453:539-543.

Watson, R.L., A.C. Spalding, S.P. Zielske, M. Morgan, A.C. Kim, G.T. Bommer, H. Eldar-Finkelman, T. Giordano, E.R. Fearon, G.D. Hammer, T.S. Lawrence, and

E. Ben-Josef. 2010. GSK3beta and beta-catenin modulate radiation cytotoxicity in pancreatic cancer. *Neoplasia*. 12:357-365.

Wei, W., J. Jin, S. Schlisio, J.W. Harper, and W.G. Kaelin, Jr. 2005. The v-Jun point mutation allows c-Jun to escape GSK3-dependent recognition and destruction by the Fbw7 ubiquitin ligase. *Cancer cell*. 8:25-33.

Weller, M., U. Malipiero, A. Aguzzi, J.C. Reed, and A. Fontana. 1995. Protooncogene Bcl-2 Gene-Transfer Abrogates Fas/Apo-1 Antibody-Mediated Apoptosis of Human-Malignant Glioma-Cells and Confers Resistance to Chemotherapeutic Drugs and Therapeutic Irradiation. *J Clin Invest*. 95:2633-2643.

Welsh, G.I., and C.G. Proud. 1993. Glycogen-Synthase Kinase-3 Is Rapidly Inactivated in Response to Insulin and Phosphorylates Eukaryotic Initiation-Factor Elf-2b. *Biochem J*. 294:625-629.

Werner, A., S. Cockell, J. Falconer, M. Carlile, S. Alnumeir, and J. Robinson. 2014. Contribution of natural antisense transcription to an endogenous siRNA signature in human cells. *BMC genomics*. 15:19.

West, C.M., S.E. Davidson, S.A. Roberts, and R.D. Hunter. 1993. Intrinsic radiosensitivity and prediction of patient response to radiotherapy for carcinoma of the cervix. *Br J Cancer*. 68:819-823.

West, C.M., S.E. Davidson, S.A. Roberts, and R.D. Hunter. 1997. The independence of intrinsic radiosensitivity as a prognostic factor for patient response to radiotherapy of carcinoma of the cervix. *Br J Cancer*. 76:1184-1190.

Wick, W., F.B. Furnari, U. Naumann, W.K. Cavenee, and M. Weller. 1999. PTEN gene transfer in human malignant glioma: sensitization to irradiation and CD95L-induced apoptosis. *Oncogene*. 18:3936-3943.

Winkler, B.S., N. DeSantis, and F. Solomon. 1986. Multiple NADPH-producing pathways control glutathione (GSH) content in retina. *Experimental eye research*. 43:829-847.

Wold, M.S. 1997. Replication protein A: A heterotrimeric, single-stranded DNA-binding protein required for eukaryotic DNA metabolism. *Annu Rev Biochem*. 66:61-92.

Woodgett, J.R. 1990. Molecular-Cloning and Expression of Glycogen-Synthase Kinase-3 Factor-A. *Embo J*. 9:2431-2438.

Wu, L., and I.D. Hickson. 2003. The Bloom's syndrome helicase suppresses crossing over during homologous recombination. *Nature*. 426:870-874.

Yang, E.S., S. Nowsheen, T. Wang, D.K. Thotala, and F. Xia. 2011. Glycogen synthase kinase 3beta inhibition enhances repair of DNA double-strand breaks in irradiated hippocampal neurons. *Neuro-oncology*. 13:459-470.

Yano, K., and D.J. Chen. 2008. Live cell imaging of XLF and XRCC4 reveals a novel view of protein assembly in the non-homologous end-joining pathway. *Cell Cycle*. 7:1321-1325.

Yano, K., K. Morotomi-Yano, K.J. Lee, and D.J. Chen. 2011. Functional significance of the interaction with Ku in DNA double-strand break recognition of XLF. *FEBS letters*. 585:841-846.

Yano, K.I., K. Morotomi-Yano, S.Y. Wang, N. Uematsu, K.J. Lee, A. Asaithamby, E. Weterings, and D.J. Chen. 2008. Ku recruits XLF to DNA double-strand breaks. *Embo Rep*. 9:91-96.

Yi, R., Y. Qin, I.G. Macara, and B.R. Cullen. 2003. Exportin-5 mediates the nuclear export of pre-microRNAs and short hairpin RNAs. *Genes Dev*. 17:3011-3016.

Yin, J., E. Iakhiaeva, E. Menichelli, and C. Zwieb. 2007. Identification of the RNA binding regions of SRP68/72 and SRP72 by systematic mutagenesis of human SRP RNA. *RNA biology*. 4:154-159.

Yook, J.I., X.Y. Li, I. Ota, C. Hu, H.S. Kim, N.H. Kim, S.Y. Cha, J.K. Ryu, Y.J. Choi, J. Kim, E.R. Fearon, and S.J. Weiss. 2006. A Wnt-Axin2-GSK3beta cascade regulates Snail1 activity in breast cancer cells. *Nature cell biology*. 8:1398-1406.

Yoshioka, K. 1984. Some properties of the thiamine uptake system in isolated rat hepatocytes. *Biochimica et biophysica acta*. 778:201-209.

Zamore, P.D., T. Tuschl, P.A. Sharp, and D.P. Bartel. 2000. RNAi: Double-stranded RNA directs the ATP-dependent cleavage of mRNA at 21 to 23 nucleotide intervals. *Cell*. 101:25-33.

Zastre, J.A., B.S. Hanberry, R.L. Sweet, A.C. McGinnis, K.R. Venuti, M.G. Bartlett, and R. Govindarajan. 2013a. Up-regulation of vitamin B1 homeostasis genes in breast cancer. *The Journal of nutritional biochemistry*. 24:1616-1624.

Zastre, J.A., R.L. Sweet, B.S. Hanberry, and S. Ye. 2013b. Linking vitamin B1 with cancer cell metabolism. *Cancer & metabolism*. 1:16.

Zeng, J., D. Liu, Z. Qiu, Y. Huang, B. Chen, L. Wang, H. Xu, N. Huang, L. Liu, and W. Li. 2014a. GSK3beta overexpression indicates poor prognosis and its inhibition reduces cell proliferation and survival of non-small cell lung cancer cells. *Plos One*. 9:e91231.

Zeng, J., D. Liu, Z.X. Qiu, Y. Huang, B.J. Chen, L. Wang, H. Xu, N. Huang, L.X. Liu, and W.M. Li. 2014b. GSK3 beta Overexpression Indicates Poor Prognosis and Its Inhibition Reduces Cell Proliferation and Survival of Non-Small Cell Lung Cancer Cells. *Plos One*. 9.

Zhang, G.J., I. Kimijima, M. Onda, M. Kanno, H. Sato, T. Watanabe, A. Tsuchiya, R. Abe, and S. Takenoshita. 1999a. Tamoxifen-induced apoptosis in breast cancer cells relates to down-regulation of bcl-2, but not bax and bcl-X(L), without alteration of p53 protein levels. *Clin Cancer Res*. 5:2971-2977.

Zhang, J.H., T.D.Y. Chung, and K.R. Oldenburg. 1999b. A simple statistical parameter for use in evaluation and validation of high throughput screening assays. *J Biomol Screen*. 4:67-73.

Zhang, Z.M., W.D. Hu, L. Cano, T.D. Lee, D.J. Chen, and Y. Chen. 2004. Solution structure of the C-terminal domain of Ku80 suggests important sites for protein-protein interactions. *Structure*. 12:495-502.

Zheng, M., S.E. Morgan-Lappe, J. Yang, K.M. Bockbrader, D. Pamarthy, D. Thomas, S.W. Fesik, and Y. Sun. 2008. Growth inhibition and radiosensitization of glioblastoma and lung cancer cells by small interfering RNA silencing of tumor necrosis factor receptor-associated factor 2. *Cancer research*. 68:7570-7578.

Zhu, Z., W.H. Chung, E.Y. Shim, S.E. Lee, and G. Ira. 2008. Sgs1 helicase and two nucleases Dna2 and Exo1 resect DNA double-strand break ends. *Cell*. 134:981-994.

Zhuang, W., B. Li, L. Long, L. Chen, Q. Huang, and Z.Q. Liang. 2011. Knockdown of the DNA-dependent protein kinase catalytic subunit radiosensitizes glioma-initiating cells by inducing autophagy. *Brain research*. 1371:7-15.

Zielinska-Dawidziak, M., K. Grajek, A. Olejnik, K. Czaczyk, and W. Grajek. 2008. Transport of high concentration of thiamin, riboflavin and pyridoxine across intestinal epithelial cells Caco-2. *Journal of nutritional science and vitaminology*. 54:423-429.

Zopf, D., H.D. Bernstein, A.E. Johnson, and P. Walter. 1990. The Methionine-Rich Domain of the 54 Kd Protein Subunit of the Signal Recognition Particle Contains an Rna-Binding Site and Can Be Cross-Linked to a Signal Sequence. *Embo J*. 9:4511-4517.

APPENDIX

Appendix 1: Screening data tables

Table A1

Gene	Rank Product	PFP	R-score Run1	R-score Run2
PRKDC	17.54992877	0.112	-2.77248913	-2.87254
CLK3	25.78759392	0.195	-2.04204307	-2.91376
CHEK1	28.4956137	0.2375	-2.486693582	-2.74961
ATM	28.56571371	0.230862	-2.635472343	-2.43795
CSNK2B	30.85449724	0.252097	-2.058988782	-2.78619
ATR	34.05877273	0.304688	-2.372951047	-2.09122
CKS2	34.87119155	0.312121	-1.904632817	-2.59912
PKMYT1	35.4964787	0.313971	-2.012726169	-2.41409
TAF1	36.33180425	0.317429	-1.755511813	-2.65153
TAF1L	41.82104733	0.399861	-1.541934118	-2.52179
HAK	41.98809355	0.391351	-1.799665558	-2.07109
SMG1	42.14261501	0.383421	-1.690170264	-2.3331
GAK	44.72135955	0.408974	-1.869937535	-1.70943
EPHB2	45.57411546	0.4105	-2.266227599	-1.36282
ACVR2	49.74937186	0.464268	-1.738005255	-1.484
PIK3C2A	49.95998399	0.457381	-1.54611734	-1.75791
SRP72	51.75905718	0.477907	-1.702904033	-1.46401
GCK	52.47856705	0.478636	-1.573846592	-1.49582
TPK1	53.24471805	0.479222	-1.391169382	-1.88296
PCK2	54.08326913	0.483152	-1.879877227	-1.31326
PRKCL2	57.91372894	0.540106	-1.170481113	-2.12681
STK32A	58.49786321	0.537708	-1.460019936	-1.42668
MAP4K3	59.14389233	0.535714	-1.389058206	-1.49693
PFKL	59.24525297	0.5266	-1.518674315	-1.38102
CDC2	60.21627687	0.532451	-1.246492279	-1.74517
MARK3	64.93073232	0.598077	-1.361577689	-1.40574
XYLB	66.09084657	0.604717	-1.21539149	-1.48272
TGFBR3	66.1135387	0.594259	-1.125924174	-1.78053
IPMK	67.15653356	0.599	-1.827956225	-0.90456
ACVR2B	69.97856815	0.628214	-1.436206058	-1.18402
PRKCH	70.74602462	0.629035	-1.506981303	-1.07179
MARK2	80.42387705	0.763017	-1.092206653	-1.37926
WNK4	83.9761871	0.809492	-0.682898127	-1.952
DYRK1A	84.90583019	0.809917	-1.14002598	-1.2

TLK1	85.97674104	0.812049	-1.172556148	-1.11406
TRPM7	88.65664104	0.842339	-1.399208051	-0.73944
BRD4	91.86402996	0.878254	-1.145784169	-1.01432
PSKH2	92.0597632	0.86625	-1.239067752	-0.81041
DGKD	94.13819629	0.887846	-1.824127273	-0.39851
PRKCZ	95.36770942	0.893864	-0.98857154	-1.15397
BRAF	95.43584232	0.881418	-1.130059723	-0.99371
CLK4	95.66608594	0.871985	-1.144889798	-0.9501
EFNA3	95.74445154	0.86058	-1.036987123	-1.08134
HUS1	96.95875412	0.865286	-1.210794527	-0.8012
KCNH8	97.11848434	0.854718	-0.293824597	-2.34667
ROCK2	98.01785552	0.855	-0.708600341	-1.41367
PAK7	100	0.872945	-1.590901876	-0.44772
DTYMK	101.1978261	0.875068	-1.653210154	-0.40321
EFNA5	103.4891299	0.891333	-0.653920709	-1.40496
CAMK4	103.9230485	0.885855	-1.073825832	-0.9208
COL4A3BP	104.1633333	0.877013	-0.714603325	-1.33615
TOPK	104.2688832	0.867244	-1.327319257	-0.65417
DGKA	104.297651	0.856582	-0.747358426	-1.31684
CHKA	104.4126429	0.84775	-0.801698825	-1.21771
BRDT	105.2330746	0.851173	-0.960186323	-1.00414
LOC390226	106.5833008	0.858537	-0.705824826	-1.32977
GUCY2C	109.5810203	0.886566	-1.224332153	-0.61018
PACE-1	111.0315271	0.894167	-0.840759291	-1.06674
PRKCQ	112.4055159	0.900412	-0.861523967	-1.06466
PLK3	113.8419958	0.905988	-1.197441442	-0.59751
CDK9	115.0217371	0.910632	-0.885447191	-0.94758
IHPK3	116.3829884	0.91733	-0.708600341	-1.14811
SNARK	117.5755077	0.920449	-0.984683702	-0.74443
PLK4	119.9208072	0.940444	-0.547684887	-1.32128
VRK3	120.218551	0.935055	-1.396835552	-0.30031
CSNK2A1	121.8605761	0.946141	-2.084296665	0.201201
CDKN2B	122.6784415	0.945376	-1.349782721	-0.38488
PTK6	122.7191917	0.935745	-0.319437898	-1.4214
ILK	126.1427762	0.967842	-0.932968194	-0.72912
AK3L1	127.0826503	0.967865	0.125261707	-2.26812
PKM2	130.4607221	0.994536	-1.715856746	0.00629
SRMS	132.7026752	1.007653	-2.349398602	0.526766
SPHK2	134.3130671	1.017071	-0.469500307	-1.19564
MAPK7	135.7865973	1.0237	0.148765661	-1.97574
NTRK1	137.5027272	1.032079	-2.012573074	0.332392
INSRR	141.2515487	1.055631	-0.949894927	-0.54299
STK35	142.1126314	1.055673	-0.719360871	-0.73735
MAP3K13	142.1829807	1.046048	-0.275760788	-1.26284
DMPK	142.821567	1.043726	-0.47745247	-1.06514
CSF1R	142.8845688	1.034953	-0.138974863	-1.40276
SCAP1	144.0138882	1.038102	-0.907636903	-0.55626

PIK3R3	144.1873781	1.029495	-0.255744323	-1.21907
BRD3	146.355731	1.043455	0.115806812	-1.57715
AMHR2	146.4308711	1.03509	-1.337414807	-0.13891
PDK3	148.7749979	1.050357	-0.396224124	-1.06627
BTK	153.205744	1.086681	-0.765557734	-0.58534
NEK1	154.0649214	1.087325	-1.351887436	-0.04714
MAPK10	156.2561999	1.103217	-0.978450855	-0.33717
CKM	160.3995012	1.137284	-1.390450096	0.063312
FRAP1	160.9316625	1.134017	-1.102599508	-0.21066
C9ORF96	161.0434724	1.125636	-1.389772306	0.051945
PAK6	161.4249051	1.120756	-0.524540043	-0.74295
EFNB3	164.1219059	1.140542	-1.026915985	-0.23919
MAPK13	164.2071862	1.131901	-0.1252858	-1.17978
TNK2	164.5357104	1.126557	-1.104596482	-0.17853
CDKN2D	164.6815108	1.119024	-0.447990009	-0.79834
CDKL2	165.3360215	1.11621	-1.042545661	-0.20594
MAP3K14	165.8432995	1.11236	0.030113805	-1.32863
PIK3CD	166.4992492	1.110913	-0.667775578	-0.57257
ERBB3	167.4096771	1.110157	-0.688714966	-0.53847
MGC45428	168.1963139	1.108164	-1.191000543	-0.0462
BUB1	168.6416319	1.104729	-0.145316259	-1.07612
CAMK2A	168.9260193	1.099192	0.286083815	-1.46068
ANKRD3	171.0263138	1.109542	-0.868798857	-0.33348
MARK4	171.119841	1.102197	-0.908668716	-0.28399
MAPKAPK3	172.8930305	1.11203	-0.603247459	-0.60889
ULK2	175.0542773	1.125373	-0.685162295	-0.47613
BMX	175.3225599	1.118889	-1.114010212	-0.09175
CALM2	175.7668911	1.107883	-0.254526555	-0.8069
PRKCSH	175.7839583	1.099964	-0.159517077	-0.99213
NTRK2	177.5161964	1.11018	-0.150906432	-0.99213
VRK1	178.2806776	1.109071	-0.802249368	-0.30853
C9ORF12	178.8658715	1.107376	-0.196464401	-0.93059
MAP2K1	179.1926338	1.102324	-1.109845207	-0.06601
PIK3C2B	179.5550055	1.097832	-1.20821034	0.066547
RPS6KC1	179.6580084	1.090903	-0.001329759	-1.12204
PIK3R4	182.0631758	1.103897	-0.643848791	-0.46718
CRK7	183.3112108	1.108014	0.270007694	-1.33762
MAP3K1	183.6518445	1.104082	0.295159052	-1.34726
SYK	184.7593029	1.107128	-0.810873384	-0.25136
ACVR1B	185.1512895	1.104094	-0.204175611	-0.80186
FLJ10761	185.2565788	1.097367	-0.679677628	-0.40791
COASY	187.6166304	1.111093	1.660130434	-1.95061
MAP2K7	187.6459432	1.104145	-0.207184863	-0.79469
GALK2	189.9894734	1.114967	-0.782114466	-0.24729
MYO3B	191.2328424	1.119968	1.57698245	-1.86769
IGF1R	192.4993506	1.12329	-0.582491861	-0.45379
CCRK	193.4476673	1.117325	-0.199615139	-0.75056

GRK4	195.9642825	1.131329	-0.493011035	-0.50785
KSR	196.2956953	1.126289	1.195676873	-1.53662
AKT1	197.4841766	1.129156	-0.325630547	-0.62261
PRKCD	197.90907	1.125342	0.084512274	-1.01965
LATS1	197.9898987	1.119105	-0.961209364	-0.03812
CDC42BPA	198.1035083	1.113067	-0.410852516	-0.56813
URKL1	198.3607824	1.102667	-1.32710416	0.37625
EPHA4	198.8089535	1.099608	-1.171162572	0.235716
PANK4	199.7498436	1.100958	-1.463715696	0.916178
LMTK3	201.1019642	1.105387	-0.238598444	-0.68035
TNIK	201.6184515	1.103136	-0.729688559	-0.20368
PRKCG	201.9108714	1.099618	-0.008047999	-0.83002
RIPK3	202.2325394	1.096637	-0.373606214	-0.55866
NRBP	203.2043307	1.097616	-0.901160059	-0.07821
IKBKG	203.5951866	1.093873	-1.396835552	0.786809
MLCK	204.2302622	1.092443	-0.484224355	-0.45281
CHEK2	207.9975961	1.110938	-0.317958361	-0.55428
FRK	208.0552811	1.104915	-0.166183383	-0.70213
NME3	209.3800373	1.107669	0.424068988	-1.21156
SAST	209.8928298	1.105531	-1.091637231	0.185048
PDK1	210.8648856	1.100276	-1.475055661	1.626886
ANKK1	211.4142852	1.098462	-0.722494313	-0.14741
PRKX	212.3864402	1.099672	-0.318869437	-0.52496
ICK	213.6164788	1.103071	-0.004022341	-0.75233
MAPKAPK5	213.8223562	1.097892	-0.881214078	-0.01563
CDK11	213.850415	1.092204	0.166444669	-0.97128
CSNK1G1	214.368841	1.090856	-0.511527508	-0.35728
ULK4	215.9629598	1.096888	0.150466152	-0.93752
FLJ34389	216.062491	1.091852	-0.340708309	-0.4757
STK32B	217.3464976	1.096211	0.085393337	-0.80448
MUSK	219.0091322	1.096198	-0.617496433	-0.2114
MGC8407	219.0616352	1.090933	-0.298855851	-0.48521
MELK	220.027271	1.093144	-0.550000684	-0.27006
AK2	220.0499943	1.084987	-0.081040972	-0.70052
DLG1	220.0499943	1.084987	-0.779144814	-0.05121
EEF2K	221.5581188	1.081843	-0.919948212	0.092661
SGK	222.6207537	1.083794	-0.916290369	0.084422
MAPK9	223.6515146	1.080647	-0.167723932	-0.58096
CDKN1A	225.3397435	1.087574	0.762353282	-1.21796
RIPK1	227.3279569	1.094236	-0.547322314	-0.22868
RAF1	227.4335068	1.089583	0.21814808	-0.88349
NLK	228.195092	1.088927	-0.64561731	-0.14227
MYO3A	229.3948561	1.091748	-0.674839129	-0.10637
NME6	229.8347232	1.089034	-0.488882394	-0.26133
PIK3CA	230.2976335	1.087091	-1.180734658	0.67413
EPHB4	232.1637353	1.094306	-0.793677546	0.028914
KIAA1811	232.383304	1.090786	-1.366473056	1.878123

MAPK3	232.4930106	1.086114	-0.586402757	-0.17833
AATK	232.6606972	1.081745	0.082087499	-0.73257
EIF2AK3	232.7337535	1.077324	-0.952178732	0.252387
FLJ23356dup	232.7659769	1.0725	-0.182211652	-0.52074
ARAF1	232.8733561	1.068256	-0.209265408	-0.4791
NME2	234.0512764	1.071644	-0.864356052	0.091246
NME5	234.499467	1.070184	-1.136433677	0.593834
ACVR1C	234.9957446	1.06789	-0.076169535	-0.59678
MARK1	235.8134856	1.068356	-0.662665822	-0.08032
DYRK2	237.3646983	1.072773	-0.216945809	-0.44929
PHKG2	237.802439	1.070792	0.136780625	-0.74062
HK3	237.9957983	1.067005	0.167854486	-0.74616
PRKG2	238.1554114	1.063318	0.090202521	-0.72467
PI4K2B	238.6461816	1.061518	-0.082983621	-0.56337
DGKH	238.8660713	1.058244	0.288416804	-0.80448
TRIO	239.2488244	1.054084	-0.989132914	0.377946
RPS6KA3	239.2488244	1.054084	-0.624956371	-0.10521
RIOK1	239.7394419	1.050241	-0.500702707	-0.19077
PRKAB2	241.1223756	1.055328	0.025684768	-0.64312
MGC4796	241.6195356	1.053696	0.099016654	-0.71691
CDK10	242.1363252	1.048384	0.089816964	-0.69082
STK4	247.2286391	1.076502	0.300071958	-0.79318
CSNK1A1	247.4712104	1.073355	-0.06691045	-0.52737
IHPK2	249.3431371	1.075339	0.057543079	-0.61264
PRKWNK2	251.6525382	1.085169	0.5143837	-0.90638
UCK1	251.6783662	1.080777	0.671048675	-0.97386
GRK1	251.7081643	1.076444	0.132500255	-0.66972
MYLK2	254.0964384	1.086479	-0.608789153	-0.04109
BLK	254.1653005	1.08222	-0.72171976	0.118386
CHUK	254.3580154	1.078967	0.355825936	-0.77181
MGC42105	255.4407955	1.081543	-0.45093431	-0.15933
STK17B	256.7761671	1.085369	-0.464645996	-0.14663
CKS1B	256.9163288	1.082041	-0.954217818	0.515986
PDK4	257.2236381	1.079167	-0.237113905	-0.29604
MAPK12	259.1524648	1.085891	-0.754483208	0.224583
BAIAP1	259.4937379	1.079116	-0.209680338	-0.30408
CDKL5	260.5225518	1.081	-1.044405147	0.783589
MAP3K6	261.2470096	1.081315	-0.494997929	-0.09407
RPS6KB2	262.4404694	1.083651	-0.760159802	0.258286
PFKM	262.9429596	1.078287	-0.918726149	0.518836
MAP3K7	264.9433902	1.08166	0.30816664	-0.72092
LMTK2	265.7856279	1.077946	-0.660158478	0.093678
ERN1	265.879672	1.074266	-0.242476839	-0.24311
KDR	266.9269563	1.076288	0.232040686	-0.65558
PRKY	267.787229	1.077816	-0.040954552	-0.43935
MAGI-3	269.2805229	1.078289	-0.516703773	-0.03577
PIM3	269.8777501	1.078087	-0.539392186	-0.00513

KHK	270.5549852	1.073891	0.06284939	-0.49712
IRAK1	270.6159641	1.070187	-0.396504263	-0.12553
MAP2K2	271.064568	1.06461	-0.41106615	-0.11766
NEK9	273.3623968	1.068155	-0.020897713	-0.41147
YES1	273.7736291	1.066397	-0.061900587	-0.38345
STK17A	273.9653263	1.063223	0.054610171	-0.46718
EPHB3	274.226184	1.06073	-0.528943859	0.01004
FGFR2	274.4193871	1.057673	0.276135029	-0.62972
CRKL	276.1485108	1.054317	-0.614513921	0.100651
SLK	276.2607464	1.051004	-0.139730914	-0.2918
MAP3K3	279.7731224	1.065536	-0.046923249	-0.34138
PRKWNK3	280.1017672	1.063594	0.533296412	-0.73219
ITPKC	280.2748651	1.06078	-0.013491718	-0.37953
INSR	280.3408639	1.057367	-0.527184957	0.03494
UMP-CMPK	281.6806703	1.060845	-0.411575754	-0.04917
DGKI	284.1302518	1.061899	-0.071731394	-0.30343
CAMKK1	284.7279403	1.061493	-0.970081333	1.098992
MAP2K3	284.9385899	1.058997	-0.41574513	-0.03453
PTK2	286.3354676	1.063362	0.062565594	-0.41498
MAP3K11	286.9146214	1.062715	-0.202532973	-0.18364
RIOK2	288.1527373	1.065548	-0.486245855	0.030285
COMMD3	288.3747562	1.062952	-0.993069542	1.601991
TESK1	289.0415195	1.063112	0.396184566	-0.6292
FUK	289.6515148	1.06239	-0.635441198	0.255856
BMPR1A	289.843061	1.059561	-0.905353974	0.834096
CDK5R2	290.9347006	1.060976	0.030130204	-0.36374
BRD2	292.5064102	1.065302	-0.157001153	-0.18913
CDKL3	292.6174978	1.062191	0.920944409	-0.75114
RPS6KA6	294.0833215	1.0652	-0.044061829	-0.27636
ZAK	294.3976902	1.062807	-0.823877834	0.677243
LOC91461	294.4995756	1.059967	1.170854774	-0.80153
ETNK1	294.7269923	1.057442	-0.629389737	0.281479
PDGFRA	295.4285023	1.057105	-0.176990087	-0.15941
IKBKAP	295.7566567	1.055016	0.296252589	-0.52874
NEK3	295.7752525	1.051667	-0.008129919	-0.2876
ERBB4	297.7263845	1.054221	0.155942888	-0.44009
TTBK2	298.1140721	1.052994	-0.693639117	0.402388
MAP2K6	299.8132752	1.058032	0.123274641	-0.39695
ROCK1	299.9733321	1.055482	0.557746737	-0.64902
CKMT2	301.4249492	1.055431	-0.375224255	0.01268
PSKH1	302.2267361	1.055064	0.203173896	-0.44837
PIM2	302.4070105	1.052603	-0.201179765	-0.12409
TK2	308.0178566	1.073044	-0.886831814	1.2165
AK1	308.6357076	1.072642	0.04459173	-0.28308
DAPK1	309.2183694	1.071755	0.030646386	-0.25613
RIPK2	309.6320397	1.070016	-0.457854749	0.138174
DLG3	310.0104837	1.06866	-0.596867916	0.330621

PIK3R1	310.3191905	1.066553	0.399445171	-0.52671
TNK1	310.4979871	1.06418	-0.420502359	0.109484
CDKN2C	311.2699793	1.064367	0.022624665	-0.24526
TRIB1	311.3165591	1.061262	0.449204616	-0.53504
DUSTYPK	311.6191586	1.059356	0.381876301	-0.51171
KUB3	311.9038313	1.05737	-0.270942802	-0.01088
SIK2	312.7618903	1.057896	-0.205243601	-0.07337
PAK1	313.3560275	1.05734	-0.168306275	-0.10158
PRKACA	314.6426545	1.060258	0.299323184	-0.44857
CDC2L5	314.6982682	1.057281	0.912719996	-0.68251
GSG2	314.8174074	1.054819	-0.286063174	0.008552
MAPK11	315.1713819	1.053213	-0.219630741	-0.03724
CPNE3	315.3252289	1.050928	-0.109738774	-0.13346
CAMK2D	317.1435006	1.056448	0.22792206	-0.3935
MST1R	317.348389	1.054033	0.010996497	-0.20375
PMVK	317.9308101	1.053338	-0.227149782	-0.01438
EPHB1	318.0172951	1.050651	-0.6281807	0.442682
AURKB	318.405402	1.048997	-0.005609272	-0.18795
DCK	319.1238004	1.049191	-0.092890473	-0.1359
LCK	319.1394679	1.046232	0.51784538	-0.53096
FGFR4	319.4119597	1.044415	-0.474500036	0.242205
RPS6KB1	319.9812495	1.043878	-0.031942636	-0.17127
PGK1	320.1749522	1.041599	-0.649964973	0.559006
PRKAR2B	320.3185914	1.03913	0.191892286	-0.32279
PRKAB1	321.6208948	1.041416	-0.379447188	0.145563
ITK	323.2460363	1.044784	0.995526225	-0.66682
NEK6	323.4176866	1.042557	-0.304652116	0.071711
RPS6KA2	323.8981321	1.041433	0.396174684	-0.45274
PHKA1	323.9614175	1.038786	0.339087032	-0.41999
PAK4	324.9615362	1.039915	0.429807847	-0.46294
PFKFB1	325.5272646	1.039205	-0.200093221	-0.02002
RET	326.9418909	1.03904	-0.799721689	1.322739
SBK1	327.1926038	1.037042	1.569248809	-0.73127
BCR	327.2842801	1.034607	0.508572061	-0.49303
MAST3	327.7834651	1.030656	-0.31653954	0.113417
GTF2H1	328.1950639	1.029485	-0.604398063	0.509252
STK33	328.686781	1.02608	0.355935569	-0.41498
PNKP	328.9832823	1.024489	0.054973019	-0.1923
PRKCA	329.1443452	1.022383	-0.360124489	0.184229
STK38L	329.8029715	1.021676	1.131107166	-0.65939
NEK4	331.0755201	1.022158	-0.652985019	0.675444
IGF2R	331.5056561	1.021076	-0.427920475	0.26658
CHKB	332.2920402	1.02106	-0.415332201	0.264622
HIPK2	332.9864862	1.020989	-0.641447492	0.645261
STK3	333.9221466	1.019245	-0.239799226	0.070151
RPS6KL1	335.2670577	1.021841	0.28797295	-0.3175
KIT	335.5845646	1.020134	0.034869519	-0.15926

IRAK2	336.1428268	1.018797	-0.046160438	-0.10269
CAMKK1dup	338.0606454	1.0236	-0.218522047	0.061394
EPHA6	342.9110672	1.04008	-0.387690667	0.297023
PRKAA1	346.6641026	1.049061	-0.523115203	0.550669
PRPS1L1	347.9784476	1.051372	-0.459750354	0.382674
TRPM6	348.3819743	1.050526	0.36011853	-0.31597
PRPS2	350.0114284	1.051296	0.296307793	-0.27532
PRKR	351.1125176	1.052611	0.850600688	-0.49541
ROS1	352.2570084	1.054271	0.093694133	-0.14444
LIMK2	354.5504195	1.053669	0.490690578	-0.37606
MAP3K8	355.2801711	1.053814	-0.117859222	0.039191
ADCK2	355.4166569	1.051799	0.374960275	-0.29676
C10ORF89	356.2583332	1.05209	-0.093658238	0.019878
NPR2	357.7708764	1.055166	-0.137023732	0.060486
BMPR1B	358.6474592	1.055944	1.570704574	-0.59448
RFK	358.6767347	1.053333	-0.613554134	0.923247
PRKCB1	359.3744565	1.053198	-0.353268048	0.360775
ITPKA	359.7999444	1.05219	-0.235426161	0.23156
RFP	361.0900165	1.054621	-0.604748623	0.916345
CDK3	361.6490011	1.054156	-0.51857062	0.67204
STK31	361.7098285	1.051809	0.102772204	-0.11934
RELA	362.3009798	1.051391	0.045671659	-0.07426
PASK	364.7437457	1.054638	-0.080388536	0.031036
FGR	365.4805056	1.054851	0.474910501	-0.2987
HUNK	365.7512816	1.053226	-0.140926659	0.110292
DDR1	366.9822884	1.054777	-0.295467696	0.341684
MAPK1	367.1157856	1.052617	0.125626882	-0.10944
PKIB	367.4152964	1.050998	-0.198685868	0.203939
STK10	367.559519	1.049066	-0.05044239	0.029675
TBK1	367.7662301	1.047279	0.814317354	-0.41869
CLK1	367.9211872	1.045183	0.208056508	-0.15462
SSTKdup	369.1747554	1.047524	0.543415775	-0.31417
ERK8	369.5186058	1.046399	-0.253185702	0.31658
AKT3	369.6484817	1.044126	0.452753799	-0.27788
DGKB	370.867901	1.045811	0.070845055	-0.04799
MAST2	370.9339564	1.043527	0.980689719	-0.44956
ERBB2	373.1353642	1.04853	-0.167414034	0.206599
NAGK	374.0427783	1.046223	-0.033642345	0.041334
FN3KRP	376.4518562	1.049308	-0.219605632	0.311214
CAMKK2	377.3963434	1.049679	-0.09811781	0.138922
FLT4	378.153408	1.049893	0.761539962	-0.36922
PACSIN1	378.4441835	1.048294	0.031564897	0.007446
MAP3K4	379.0659573	1.047955	0.717088411	-0.31939
EFNA4	380.462876	1.050425	0.820380555	-0.37725
JAK2	382.6238362	1.055576	0.343364827	-0.18217
STYK1	383.1866386	1.054859	0.062602898	0.003653
MPP1	384.4450546	1.054019	-0.032635734	0.08937

CDC42BPB	384.8129416	1.052634	0.060521198	0.008527
BCKDK	384.9363584	1.050581	-0.089973169	0.181265
AURKC	385.9987047	1.051462	-0.146088339	0.25502
CERK	386.3159329	1.050174	0.195198526	-0.09168
CDK7	386.3871116	1.047921	0.446013558	-0.20584
PFKFB3	387.5732189	1.049044	-0.153193729	0.267709
KIAA1765	390.1486896	1.054966	-0.492471742	1.00208
FLJ23356	390.3844259	1.053383	0.322389828	-0.14396
GUCY2D	391.1725962	1.053638	-0.335721837	0.608818
ALS2CR7	395.4023268	1.059477	-0.411479643	0.779536
DYRK1B	396.8626967	1.061882	0.709890816	-0.2553
PIP5K1B	397.2404813	1.060656	0.590713077	-0.22164
SPEG	397.3310962	1.058352	0.310251322	-0.11996
PFKFB2	397.3650714	1.056081	-0.471288469	1.018657
LYK5	397.67449	1.054472	-0.558693594	2.013898
NYD-SP25	399.1240409	1.057063	-0.194620417	0.365509
SGK2	401.1882351	1.061063	-0.404501951	0.831766
PINK1	402.8721882	1.061915	0.027488807	0.125138
CIB2	404.6924758	1.062816	0.125626882	0.026559
ITPK1	405.5514764	1.063418	0.67865244	-0.21187
PRKCN	406.5599587	1.06404	0.209190217	-0.02426
IKBKE	407.8565924	1.063736	0.425670768	-0.13602
ADRBK1	408.8520515	1.064452	1.597859846	-0.4024
TEC	409.3910111	1.063895	0.252501712	-0.0457
DGKQ	409.4874845	1.061878	0.740173178	-0.22523
TRIB2	409.756025	1.060359	0.492179949	-0.15853
DLG2	411.8154927	1.064326	-0.074309493	0.298094
ALS2CR2	414.5370912	1.070933	1.077419655	-0.2929
CAMK2B	418.4973118	1.078359	0.956257461	-0.2499
PIK3CB	419.2994157	1.078825	0.586380069	-0.15248
CDKL1	419.4412951	1.076753	0.64491793	-0.16647
DGUOK	419.5414163	1.074742	0.380264517	-0.08751
EPHA5	421.0605657	1.073974	0.971100315	-0.24913
KIAA2002	421.2837524	1.072505	-0.313966368	0.90448
PRPS1	421.3241033	1.070404	0.044086723	0.204396
PRKG1	421.594592	1.068811	0.278713841	-0.012
STK36	422.5695209	1.069576	0.302017749	-0.0303
DCAMKL1	424.1650622	1.067747	-0.057335805	0.342599
TSKS	424.2640687	1.065809	-0.213369814	0.632425
HIPK3	424.5291509	1.064539	-0.2714747	0.792008
JAK3	425.0058823	1.064111	0.078840659	0.191967
FYN	427.9158796	1.063091	0.021036774	0.280537
PAK2	428.1354926	1.061553	-0.295806204	0.936891
DUSP21	429.3436852	1.060412	-0.226875158	0.713566
FLT1	431.4510401	1.064588	-0.005844401	0.331644
PRKCM	433.0958324	1.066561	0.08059073	0.229689
TGFBR2	433.5666039	1.065738	1.084769588	-0.23386

RIOK3	436.8523778	1.070878	-0.004519031	0.350004
STK16	437.1978957	1.06943	-0.095307977	0.484035
PFTK1	439.6817031	1.074583	-0.023644905	0.374007
PRKAR1B	442.6962841	1.080588	0.236881515	0.07751
PRKACG	445.2527372	1.083343	-0.110178928	0.592859
STK11	447.2940867	1.087026	0.456317473	-0.02871
IRAK3	447.3969155	1.085131	0.647609068	-0.09303
CDK4	447.7175449	1.083936	-0.109391797	0.60026
GSK3A	449.5564481	1.086613	-0.168580349	0.766018
STK22Ddup	453.4754679	1.092824	0.035429713	0.364023
MOS	453.667279	1.091155	0.252099998	0.128404
SRC	456.335403	1.093492	0.093383944	0.320043
MAP3K15	456.683698	1.092228	-0.105876356	0.656985
PKLR	457.8908167	1.092875	0.09565242	0.324175
CALM3	460.5659562	1.097761	-0.296281157	2.701992
HSMDPKIN	461.0249451	1.0969	-0.109117005	0.69049
MAP4K2	462.4283728	1.098124	-0.286689684	1.991781
MAP2K4	462.8174586	1.09701	0.97481092	-0.12876
PTK9	463.2407581	1.095714	0.238794403	0.195775
GRK6	463.6830814	1.094609	0.03388053	0.415141
LTK	468.2392551	1.101284	1.387923971	-0.17626
PIP5K2C	469.7446115	1.10266	0.015191032	0.538954
PDPK1	470.6399898	1.102946	0.071744883	0.402228
PRKAR1A	471.06369	1.101586	-0.116919359	0.84559
DYRK3	471.2769886	1.100039	0.201413081	0.27295
PTK7	474.5576888	1.105925	0.662693414	-0.00575
NEK5	475.2567727	1.105538	-0.214811642	1.500588
PTK2B	475.4702935	1.103896	0.660901718	-0.00407
GOLGA5	475.6469279	1.102232	0.996393647	-0.10276
ROR1	477.080706	1.103652	0.719110344	-0.01637
PRKCE	477.3730198	1.102137	0.568727282	0.022874
HSPB8	478.2760709	1.102143	0.94678738	-0.08003
DDR2	478.3513353	1.100323	0.87502795	-0.05551
EPHA2	481.1901911	1.103011	0.091898817	0.434098
MAP3K2	481.2691555	1.101115	-0.149269337	1.125591
GUCY2F	481.3408356	1.099189	0.159083587	0.353598
THNSL1	483.0900537	1.101318	0.15697001	0.361871
PRKCL1	484.3862095	1.102688	0.559361829	0.045921
MAPK6	486.1944056	1.104296	0.337222423	0.223903
MAK	489.1012165	1.109223	0.39922925	0.184103
PNCK	490.1897592	1.109953	0.025108354	0.66463
FER	490.2570754	1.108032	0.209546915	0.345197
EPHA3	490.6444741	1.106946	1.203248131	-0.09898
ADCK1	491.4600696	1.106877	0.11856601	0.466737
NRBP2	491.8536368	1.105603	0.132765601	0.42971
AXL	493.0314392	1.10414	0.228227531	0.341056
JAK1	493.5098783	1.10322	0.337879752	0.252673

CASK	497.0553289	1.107592	1.021627801	-0.0457
CDKL4	499.5738184	1.111358	-0.099457084	1.193164
LRRK2	500.665557	1.11196	1.724797894	-0.12024
FASTK	501.4578746	1.111755	0.798551965	0.019947
LOC340156	502.0906293	1.111186	0.724572483	0.047665
FGFR1	502.5186564	1.110419	0.354698921	0.266045
TYRO3	503.4580419	1.110709	0.3253729	0.306261
RNASEL	504.3193433	1.11049	0.340761751	0.29366
CRIM1	506.415837	1.112935	1.319206737	-0.07046
NEK8	507.9192849	1.114159	0.147863402	0.529043
PAPSS1	509.0432202	1.114422	0.952248952	0.009699
GALK1	510.4762482	1.115486	0.218697691	0.415875
MAPK14	510.4870224	1.113525	1.254724226	-0.0457
SPHK1	511.6277944	1.114013	0.590423315	0.168542
CAMK1G	512.3475383	1.11388	0.691626608	0.108074
AAK1	512.5553629	1.112317	0.115376905	0.638161
DKFZP761P0423	514.8300691	1.115241	0.215314178	0.466285
MAPK4	515.7324888	1.113221	0.003628487	0.977701
CSNK1D	517.1537489	1.11389	0.075931966	0.737428
KCNH2	518.4322521	1.114415	0.810865207	0.071215
MGC4796dup	518.8188509	1.113221	0.543024407	0.213831
KIAA1811dup	519.4997594	1.112862	0.342959281	0.348739
CALM1	521.7470652	1.115212	0.03765592	0.908112
LATS2	522.4538257	1.112636	0.223976163	0.519656
MAP4K1	523.5647047	1.113325	0.166628354	0.605095
MAP3K5	523.8625774	1.111909	0.331997511	0.371855
PDGFRL	524.22705	1.110769	0.695011128	0.177264
MVK	525.0904684	1.110541	0.63767482	0.2038
RPS6KA4	525.1161776	1.108641	0.141371964	0.649214
PIM1	526.3078947	1.108974	0.442629685	0.313178
TP53RK	526.3952887	1.107205	1.064331806	0.029722
NME4	530.6241608	1.113839	0.116502084	0.770001
PRKAR2A	530.9237233	1.112561	0.757984319	0.164071
MERTK	531.2626469	1.111235	0.540727767	0.264856
LRRK1	531.3275826	1.109466	0.900555601	0.093444
CAMK2G	535.1448402	1.114079	0.834973008	0.139313
LYN	536.1865347	1.114167	0.25378283	0.554431
ABL1	539.5164502	1.118559	0.228126847	0.609921
MAP3K9	540.2295808	1.117877	1.327506357	0.020904
PFKFB4	540.8992512	1.117453	0.260711234	0.573426
PANK2	541.6142539	1.116945	1.405165026	0.01574
HIPK4	541.8440735	1.115434	0.357961349	0.409165
PAK3	542.566125	1.114651	0.180735855	0.707488
BMP2K	542.9079112	1.113396	0.435209217	0.366703
MPP3	544.9770637	1.113037	0.292412556	0.56919
TYK2	545.4310222	1.112061	0.59147349	0.301352
MAP3K10	545.5712602	1.110481	0.690722638	0.262544

C14ORF20	545.8058263	1.109074	0.133516031	0.85832
ACVR1	547.64861	1.110538	0.03758588	1.333458
NRK	548.4806286	1.110327	0.1684207	0.785195
ADRBK2	550.3580653	1.1099	0.458359218	0.376201
FLJ32685	551.1288416	1.109282	0.520850666	0.35187
CDK2	551.3710185	1.10785	0.130565699	0.93788
SCYL1	551.5541678	1.106356	0.301825151	0.578809
PDIK1L	551.8876697	1.105033	0.256149456	0.64472
STK38	551.9112247	1.103234	0.505951507	0.361405
CSNK1E	554.5151035	1.106175	0.835124558	0.228413
ABL2	555.1162041	1.105298	0.630646763	0.330416
HRI	555.3458382	1.103903	0.207791177	0.777042
AK7	555.5069757	1.102471	1.246220769	0.083857
CSK	559.2566495	1.107064	1.086523607	0.149242
EPHA1	559.7713819	1.106034	0.494891963	0.383964
PI4KII	560.9367166	1.106336	1.102065791	0.154138
BMPR2	560.983957	1.104583	0.786491634	0.264626
CARKL	561.0632763	1.102884	1.079720957	0.168009
SRPK2	561.4730626	1.101892	0.475364666	0.410257
CDADC1	566.2225711	1.105626	0.945147585	0.236664
SNF1LK	566.5897987	1.104318	0.357051352	0.586248
MINK	567.3473363	1.102055	1.522437487	0.074149
DGKK	567.5737837	1.100654	0.09319235	1.388293
MAP4K5	567.7534676	1.099032	1.899387601	0.047247
MAPKAPK2	567.9084433	1.097424	1.163050265	0.17969
CKB	568.928818	1.097235	0.408705262	0.558128
STK24	569.8420834	1.096798	1.07758212	0.20351
HIPK1	570.3051815	1.095761	0.17062678	1.032468
EPHA7	570.9308189	1.095088	0.421533949	0.559577
RAGE	570.9570912	1.093371	1.659081271	0.072697
PHKB	571.6712342	1.090764	0.379591341	0.597827
NME7	574.202055	1.091111	0.44852695	0.551326
FGFRL1	574.4893385	1.088054	0.485948644	0.515592
VRK2	575.0165215	1.087125	0.709909879	0.356621
AK3	575.7343137	1.08642	0.343982277	0.6672
PIK4CB	578.7521058	1.089465	0.172551744	1.149757
PIP5K3	581.3449922	1.092264	0.229306404	0.96571
STK25	581.7516652	1.091287	0.472131857	0.565919
GK	584.6451915	1.094459	0.829774444	0.340807
GRK7	584.9418775	1.093177	1.185777585	0.230586
EGFR	585.9249099	1.092961	1.141921442	0.249902
AK5	586.4588647	1.092122	1.359455972	0.201067
PANK3	588.2686461	1.093217	1.056086474	0.270409
KIAA1361	592.748682	1.096724	0.956079371	0.330604
FLJ25006	594.4072678	1.097395	0.530370818	0.578442
TJP2	596.0939523	1.098166	0.956249073	0.339109
RPS6KA5	598.980801	1.100456	0.348065024	0.844467

CAMK1	599.2119825	1.099151	1.009687377	0.326726
TEX14	599.764954	1.098428	1.065501681	0.315568
SGKL	599.7666213	1.096738	0.206777444	1.413267
GNE	601.5280542	1.097481	0.914465681	0.363806
NEK11	601.9792355	1.096457	0.583559953	0.581455
MAST4	602.3603573	1.095314	1.197690777	0.292331
PIK3C3	602.4997925	1.09393	0.180735855	1.806385
TESK2	604.4071475	1.095038	0.88928409	0.382329
UHMK1	606.301905	1.094247	0.672563819	0.541275
PDXK	606.9332748	1.093495	0.487966824	0.679701
RP6-213H19.1	607.7499486	1.09283	0.335492671	1.011667
PGK2	608.3568032	1.091917	1.003822018	0.35305
PRKACB	609.5244048	1.092073	0.244505478	1.343509
HCK	610.0311467	1.091073	0.321510356	1.084048
PAPSS2	611.959966	1.091765	0.619263582	0.613459
PRKD2	614.0114005	1.092831	0.363330173	0.958906
PRKAG3	615.6362562	1.09214	0.859982929	0.440115
DAPK3	616.5387255	1.091754	0.908811293	0.425708
SNRK	617.9344625	1.091467	0.701438601	0.590023
EPHB6	619.7580173	1.092332	0.845244611	0.485926
ACVRL1	621.0104669	1.09073	0.73771257	0.573574
CSNK1A1L	622.1286041	1.090379	0.750494753	0.572541
DAPK2	624.3268375	1.091813	0.581817908	0.711355
MAP3K12	624.6471004	1.089044	0.619204676	0.68905
KIAA1804	624.9559985	1.08787	0.995152257	0.405022
STK29	625.7075994	1.087031	0.277299039	1.729993
NTRK3	625.7411605	1.08545	0.363573509	1.09267
PANK1	625.9257144	1.08405	0.906819188	0.513474
ITPKB	626.348146	1.082926	0.433660866	0.964926
ADK	627.3802675	1.081144	0.550043444	0.764797
DGKG	629.4886814	1.082108	0.271420232	2.029034
MET	631.5623485	1.081431	0.453440632	0.962302
MKNK1	631.9018911	1.080168	1.107195415	0.400899
NME1	632.2032901	1.078981	1.513899777	0.330621
PDK2	633.5897726	1.076217	0.997770155	0.454139
FLT3	634.4982269	1.075615	0.730201451	0.664077
ROR2	635.3109475	1.075029	0.665386296	0.693962
SSTK	636.7456321	1.07518	0.663440893	0.71173
JIK	638.0556402	1.074957	0.412627919	1.16323
ALK	639.7030561	1.075173	1.195432243	0.403345
MAP4K4	640.4998048	1.07444	0.740986869	0.674553
LAK	641.6774891	1.074175	1.249136157	0.39934
DLG4	642.2810911	1.073338	0.482523784	1.032154
P101-PI3K	643.4656168	1.071414	0.630272007	0.818826
CSNK2A2	644.2903072	1.069259	0.624267249	0.843856
RPS6KA1	646.3497505	1.069836	0.663253117	0.802441
PFKP	646.9969088	1.069162	0.751554194	0.69057

PCTK2	648.2900585	1.069078	0.710170251	0.753931
FRDA	648.3795185	1.067741	0.802698058	0.667843
NEK2	651.4982732	1.067839	0.771905635	0.693252
KIAA0999	653.4125802	1.068406	0.460662624	1.200273
TGFBR1	654.266001	1.064747	1.120244471	0.527348
CDK6	656.2895702	1.065231	1.274314582	0.474307
MATK	659.1213849	1.066232	0.533296412	1.130824
CAMKIINALPHA	659.1813104	1.064811	1.336068664	0.454384
TNNI3K	660.9515867	1.065056	0.846988714	0.709687
N4BP2	660.9969743	1.063584	0.797806134	0.741527
MAPK8	664.6690906	1.064395	0.559070048	1.145797
MAP3K7IP1	664.800722	1.062986	1.320214188	0.51628
STK23	665.1856884	1.061893	0.475882387	1.385692
ADCK5	665.8468292	1.061011	1.853202121	0.390947
PRKCI	668.2963415	1.060338	2.026965652	0.398482
IHPK1	669.3429614	1.060055	0.780112705	0.843785
MKNK2	671.3240648	1.058941	1.167123638	0.600908
EPHA8	672.2945783	1.058338	1.125216835	0.615311
TTBK1	675.1066582	1.056717	1.672156438	0.455933
PIP5K1A	676.2603049	1.0564	1.752664977	0.452865
ADCK4	677.5455704	1.056153	0.70479201	1.062502
AKT2	678.1799171	1.055191	0.592591606	1.264119
CSNK1G2	678.1887643	1.053755	0.511313	1.613837
HK1	678.6434999	1.052717	0.975272182	0.717002
PCK1	679.0655344	1.05156	0.485107139	1.984336
MGC16169	680.4983468	1.051233	0.910428842	0.816272
IRAK4	682.4031067	1.051475	0.852298302	0.901518
FGFR3	682.5423064	1.050149	0.788145214	0.953495
PCTK1	683.3681292	1.04915	1.263271169	0.61897
PIP5K2A	683.9736837	1.048086	0.949806094	0.814616
PIK3C2G	685.9271098	1.048499	1.276833443	0.62847
OSR1	691.4998192	1.045842	0.955825008	0.870394
HK2	692.3763428	1.04502	0.610189547	1.676041
SRPK1	694.7387998	1.044115	1.232663596	0.689858
CDK8	695.2021289	1.042952	0.776703271	1.107697
GRK5	696.5881136	1.039828	0.648641537	1.540502
CAMK1D	696.9648485	1.038598	1.172001795	0.718934
CDKN1C	697.3922856	1.037556	0.639026677	1.679109
CDK5	698.5470636	1.037124	2.102085568	0.564987
PIP5KL1	700.5883242	1.037181	0.644090077	1.752233
TAO1	710.1711061	1.039678	1.322100685	0.726653
PCTK3	713.4619822	1.040223	0.90046128	1.189024
PIP5K2B	714.0420156	1.039202	0.905030593	1.185893
ADP-GK	716.8612139	1.038238	1.362544739	0.779177
NUCKS	719.6394931	1.038644	0.731494548	2.048695
DYRK4	721.0055478	1.038151	0.760322549	1.741993
LIMK1	722.2565334	1.03736	0.73771257	2.25354

ERN2	725.2406497	1.038234	2.196426696	0.678647
MAP2K5	726.7165885	1.036658	1.676329306	0.717252
PDGFRB	728.381768	1.036391	0.757704504	3.060716
PRKAG2	731.108747	1.032439	1.717923602	0.749949
STK39	731.1908096	1.031144	0.782058023	2.134393
PLK2	731.9603814	1.030257	0.927840186	1.392219
RBKS	735.2744386	1.027903	2.281916268	0.717252
STK32C	737.1254981	1.026135	1.036132523	1.244021
RYK	739.2685574	1.024644	1.079113091	1.211031
MPP2	741.5787214	1.024485	1.064956569	1.281195
CSNK1G3	742.8694367	1.023718	0.986681014	1.459818
DKFZP434C131	743.0679646	1.022497	0.890669628	2.365611
TLK2	743.7129823	1.021506	2.166787659	0.805973
IKBKB	749.2736483	1.019956	1.480275865	0.991849
PKIA	750.29994	1.019144	1.834046919	0.903786
PHKA2	751.1923855	1.018239	1.401201922	1.055739
CDC7	755.3224477	1.018555	1.531166952	1.023233
PHKG1	756.4522457	1.01793	1.237575376	1.274557
TEK	757.0046235	1.015594	0.9940632	2.13164
PIK3CG	757.4707915	1.014413	1.637323374	1.005111
C7ORF2	760.0171051	1.014095	1.777014856	0.976668
UMPK	761.9291306	1.013248	1.567216865	1.080691
ASK	767.9583322	1.012799	1.316304191	1.353234
FLJ23074	768.3814157	1.011727	1.476266829	1.196717
PIP5K1C	769.9350622	1.010868	1.452395717	1.229444
PKN3	771.499838	1.010062	1.381790576	1.333983
ARK5	772.8984409	1.009121	1.682485408	1.139877
KSR2	775.7157985	1.008677	1.278749266	1.682164
ZAP70	778.8632743	1.007004	1.835840963	1.168529
NEK7	780.4921524	1.006182	1.48371359	1.35524
PXK	783.4960115	1.004533	1.457817471	1.478215
STK22C	786.326904	1.003798	1.677679072	1.328342
FN3K	790.838163	1.002105	1.418911155	1.935526
FLJ13052	792.3673391	1.001247	1.749874964	1.381724
MULK	792.4645102	1.000049	1.500078469	1.737182
CLK2	811.969827	1.000927	2.222881931	1.812384
CDK5R1	820.4998477	1	2.249091726	3.204973

Table A1. Primary high-throughput colony formation assay screen List of radiosensitivity scores (R-score) for the two primary screen runs of the 709 Dharmacon Kinome ON-TARGET*plus* siRNA library. Genes ordered by rank product analysis using R-score values. Radiosensitising siRNAs shown by R-scores <0. Abbreviations: Percentage of false prediction (PFP).

Table A2

Screen	Screen Run	Library Plate	Mean siNT SF after 7 Gy	% CV
Primary Screen	1	1	0.065	19.81%
		2	0.074	16.62%
		3	0.070	33.54%
		4	0.078	15.78%
		5	0.073	19.29%
		6	0.070	22.70%
		7	0.083	30.87%
		8	0.100	33.77%
		9	0.084	15.07%
	2	1	0.079	13.65%
		2	0.079	8.98%
		3	0.098	14.33%
		4	0.089	20.64%
		5	0.092	15.73%
		6	0.092	18.35%
		7	0.101	14.59%
		8	0.093	15.51%
		9	0.092	16.16%
Secondary Screen	1	1	0.092	12.29%
	2	1	0.080	8.02%

Table A2 Intra-assay variability.

Mean un-normalised surviving fraction (SF) for non-targeting siRNA (siNT) following 7 Gy irradiation and corresponding coefficients of variation (CV) across the primary and secondary screen library plates are shown. CV calculated by dividing the standard deviation of siNT SF_{7Gy} by the mean siNT SF_{7Gy}.

Table A3

Gene	Rank Product	PFP	R-score Run1	R-score Run2
ATM	3.301927	0.015	-7.43373	-7.3684
PRKDC	5.313293	0.04	-6.13342	-5.77834
CDC2	7.113787	0.110833	-5.17802	-6.64324
TAF1	7.883735	0.124286	-5.75644	-4.45539
MARK2	7.958114	0.109375	-5.61649	-5.62891
CLK3	10.39117	0.25	-5.78792	-4.06633
GAK	11.47759	0.2985	-5.5476	-4.22583
MULK	11.88784	0.310909	-5.07646	-4.30879
MAP4K3	12.14636	0.299167	-4.97033	-4.95304
PIK3C2A	13.27614	0.353846	-5.37506	-4.29703
XYLB	15.13217	0.476786	-4.58231	-4.32119
PRKCL2	15.62678	0.483	-4.13955	-3.99355
DGKD	16.6803	0.53	-4.86016	-3.76176
TLK1	17.83177	0.582941	-4.78866	-4.11414
FLJ13052	18.29155	0.587778	-2.70328	-4.62765
GCK	19.42134	0.655789	-5.10971	-3.66074
TAF1L	20.65811	0.70975	-4.66111	-4.09631
EPHB2	22.64743	0.828095	-4.30628	-3.62874
BRAF	24.9353	0.956364	-4.19997	-2.04878
PKM2	27.15593	1.086957	-3.41142	-3.91335
SRMS	27.30518	1.052708	-3.68874	-2.96704
TPK1	28.09492	1.0724	-5.2426	-1.68947
DTYMK	28.67371	1.074615	-2.66619	-3.32043
SRP72	28.95991	1.054444	-4.27162	-2.22763
GUCY2C	30.80769	1.124643	-3.00206	-1.62136
ROCK2	30.9684	1.096897	-3.22927	-3.80346
GSK3B	31.33932	1.088333	-4.60453	-2.94799
CSNK2B	31.96807	1.089355	-2.41152	-3.73965
SMG1	33.65805	1.15625	-3.50315	-2.48566
IHPK3	33.68451	1.12303	-2.75491	-2.04861
DYRK1A	33.70917	1.091176	-3.74989	-1.80467
TOPK	34.48834	1.100571	-4.13955	-1.87718
CSF1R	35.84605	1.1375	-2.08907	-2.81433

ACVR2B	38.05831	1.221081	-5.01352	-0.10764
IPMK	38.21302	1.1975	-1.54822	-2.49463
CLK4	38.27865	1.168718	-2.94173	-1.72851
CSNK2A1	39.83473	1.204875	-2.53106	-1.26796
CAMK4	40.62195	1.214146	-1.60862	-1.28517
PLK4	42.19224	1.25	-2.96735	-0.85416
NTRK1	43.52801	1.271628	-1.50445	-1.17824
COL4A3BP	44.42832	1.249222	-1.68497	-2.73072
AK3L1	44.74756	1.232174	-4.15339	-0.94117
PRKCH	46.01638	1.255851	-2.57579	-1.74323
PTK6	47.62203	1.28875	-1.96441	-1.31368
PSKH2	48.14798	1.28102	-1.77198	-1.74998
EXOSC10	48.72342	1.2763	-1.80249	-1.11097
PFKL	49.10459	1.261275	-0.95252	-1.34857
VRK3	49.52075	1.248654	-2.52551	-1.29567
HUS1	49.6103	1.227736	-2.82138	-1.25323
PLK3	50.53088	1.23	-1.22563	-2.31428
TRPM7	51.13051	1.224818	-1.90366	-0.56925
BRD3	51.16937	1.204286	-0.78051	-1.8718
BRDT	52.44029	1.214912	-1.66772	-0.86293
BRD4	52.50688	1.195776	-0.4954	-1.28761
MYLK	57.29609	1.282373	-2.2162	0.840643
PRKAA2	58.93971	1.298333	-1.83883	-0.46761
PKMYT1	59.2856	1.281475	-1.65985	-0.64197
ACVR2	60.70863	1.283468	-3.31506	-0.06882
HAK	61.15218	1.270794	-1.59182	-1.23295
TGFBR3	62.18329	1.27	-0.95823	-0.34569
CHKA	62.69797	1.258923	-2.81349	2.867491
EFNA3	63.46891	1.233731	-0.71686	-0.34815
CDKN2B	64.96361	1.235294	-1.03714	-0.40168
STK22C	66.21418	1.232246	-1.40855	-0.46255
CLK2	67.29343	1.229286	-1.59182	-0.27177
FES	68.07072	1.220141	-1.1039	0.055213
CDK5R1	69.6939	1.205	-1.44101	-0.02328
CKS2	70.0136	1.192568	-0.48181	-1.01794

KCNH8	72.88617	1.185395	1.107199	0.04329
PRKCQ	76.75958	1.164051	-0.87558	2.649254
EFNA5	77.95263	1.141728	0.061556	0.788593
WNK4	78.38697	1.130488	-1.19197	4.447382
MARK3	79.89016	1.110476	0.772705	-0.05686
PCK2	81.74664	1.103647	1.042937	-0.30339
PRKCZ	85.16917	1.072955	1.324428	-0.16389
PAK7	85.32425	1.061124	0.289948	0.535149
MAPK7	88.66168	1.030652	1.200119	1.046589
DGKA	91.97439	1.021075	3.00651	1.515868
STK32A	92.31759	1.010213	3.272219	2.846899
PACE-1	93.30321	0.999737	3.320649	2.339296

Table A3 Secondary colony formation assay screen

Top 76 genes chosen based on rank product from primary screen were re-run twice in 96-well plate colony formation assay using Dharmacon siGENOME siRNA. Rank product scores were calculated based on R-score. Radiosensitising siRNAs shown by R-scores <0. Abbreviations: Percentage of false prediction (PFP).

Appendix 2-Manuscript: Identification of vitamin B1 metabolism as a tumor-specific radiosensitizing pathway using a high-throughput colony formation screen.

Identification of vitamin B1 metabolism as a tumor-specific radiosensitizing pathway using a high-throughput colony formation screen

Gaganpreet S. Tiwana[1,*], Remko Prevo[1,*], Francesca M. Buffa[1], Sheng Yu[1], Daniel V. Ebner[2], Alison Howarth[2], Lisa K. Folkes[1], Balam Budwal[1], Kwun-Ye Chu[1], Lisa Durrant[1], Ruth J. Muschel[1], W. Gillies McKenna[1] and Geoff S. Higgins[1]

[1] Cancer Research UK/MRC Oxford Institute for Radiation Oncology, Gray Laboratories, Department of Oncology, University of Oxford, Oxford, UK

[2] Target Discovery Institute, Nuffield Department of Medicine, University of Oxford, Oxford, UK

[*] These authors contributed equally to this work

***Correspondence to**: W. Gillies McKenna, **email**: gillies.mckenna@oncology.ox.ac.uk*

*Correspondence to: Geoff S. Higgins, **email**: geoffrey.higgins@oncology.ox.ac.uk*

Keywords: Tumor radiosensitivity, High-throughput screening, Thiamine, TPK1

***Received**: November 24, 2014* ***Accepted**: January 22, 2015* ***Published**: February 28, 2015*

This is an open-access article distributed under the terms of the Creative Commons Attribution License, which permits unrestricted use, distribution, and reproduction in any medium, provided the original author and source are credited.

ABSTRACT

Colony formation is the gold standard assay for determining reproductive cell death after radiation treatment, since effects on proliferation often do not reflect survival. We have developed a high-throughput radiosensitivity screening method based on clonogenicity and screened a siRNA library against kinases. Thiamine pyrophosphokinase-1 (TPK1), a key component of Vitamin B1/thiamine metabolism, was identified as a target for radiosensitization. TPK1 knockdown caused significant radiosensitization in cancer but not normal tissue cell lines. Other means of blocking this pathway, knockdown of thiamine transporter-1 (THTR1) or treatment with the thiamine analogue pyrithiamine hydrobromide (PyrH) caused significant tumor specific radiosensitization. There was persistent DNA damage in cells irradiated after TPK1 and THTR1 knockdown or PyrH treatment. Thus this screen allowed the identification of thiamine metabolism as a novel radiosensitization target that affects DNA repair. Short-term modulation of thiamine metabolism could be a clinically exploitable strategy to achieve tumor specific radiosensitization.

INTRODUCTION

To identify novel clinically exploitable targets for radiosensitization, we aimed to develop a high-throughput assay that closely reflected the clinical use of radiation. Surrogate markers and viability assays evaluating tumor cell survival following radiation have previously been used in radiation sensitivity screens [1-3] but have several limitations. In particular cell viability assays such as the 3-(4,5-Dimethylthiazol-2-yl)-2,5-diphenyl tetrazolium bromide (MTT) assay, which measure the number of cells in active metabolism are unreliable for radiation studies for several reasons. Radiation induces cell cycle arrest slowing proliferation, without altering overall survival to the same extent [4, 5]. Cells that ultimately show clonogenic failure often temporarily continue to proliferate for several generations yielding false negatives [6]. Moreover, cell viability assays can be affected by non-proliferating yet metabolically active senescent cells. Viability assays adapted for long term growth assessment such as the Sulforhodamine B colorimetric assay have been shown to be comparable to the CFA, but still lack the ability to assess a single cell's replicative potential [7]. Alternative surrogate markers of cell death following ionizing radiation include DNA damage assays such as γH2AX foci quantification. Although we have successfully used this approach previously [8], it may only be suitable for identifying targets that directly interfere with DNA repair.

The gold standard for assessing cell radiosensitivity

is the colony formation assay (CFA) as it evaluates the true clonogenic potential of a cell following irradiation and is thus the closest *in vitro* equivalent to the clinical use of radiation. We adapted this assay so it can be performed in 96-well plates, enabling us to screen for novel radiosensitizing targets in a high-throughput approach. Using this technique we screened a siRNA library targeting 709 kinases. In addition to known expected targets, we identified a series of novel targets including thiamine pyrophosphokinase-1 (TPK1), a key component of the thiamine metabolism pathway. The discovery that thiamine metabolism is associated with tumor radiosensitivity was an unanticipated finding, and may represent a new clinical strategy for augmenting radiotherapy.

RESULTS

A high-throughput colony formation screen identifies TPK1 as a radiosensitizing target

HeLa cells were chosen for adaptation of the clonogenic assay to a 96-well format because they form distinct, tight and countable colonies even after irradiation in 96-well plates (Fig. 1A). By optimizing cell seeding density and colony growth times, we obtained colonies that were large enough to accurately assess clonogenic survival yet small enough to fit up to 100 colonies per well so that a surviving fraction (SF) could be calculated reliably and reproducibly. The 7 Gy radiation dose provided a maximal difference between surviving fractions for the positive and negative controls. We used this assay to screen a siRNA library containing 709 siRNAs against protein kinases on two separate occasions. The average plating efficiency for non-targeting (NT) siRNA treated wells was 28% (+/- 9.45) with an average SF at 7 Gy of 0.084 (+/- 0.019). Knockdown of DNA-PK*cs* was used as positive control and had a SF of 0.0038 (+/- 0.003) at 7 Gy. This yielded a Z-factor of 0.13 for the first run and 0.46 for the second run, demonstrating a good dynamic range between siNT (negative) and siDNA-PK*cs* (positive) controls with robust reproducibility between replicates. A radiosensitization score, R-score, was calculated for each target, with low values indicating greater radiosensitization. The coefficient of determination (R^2), a measurement for inter-assay variability, comparing the R-score values between the two runs was 0.38. Targets from the primary screen were ordered using rank product analysis, minimizing variability in R-scores between screening runs. The validity of the screening protocol was confirmed by the identification of known modulators of radiosensitivity including DNA-PK*cs* (PRKDC), CHEK1, ATM and ATR (Fig. 1B). A full list of the targets with radiosensitivity scores and heatmap can be found in Table S1 and Supplementary Figure S2, respectively.

A secondary screen of the top 76 targets was performed, using siGENOME SMARTpool rather than ON-TARGET*plus* siRNA, to avoid off-target effects (Fig. 1C). The Z-factor of the secondary screen was 0.55 for the first and 0.62 for the second run. The R^2 coefficient comparing the R-scores between the two runs was 0.58. Of the chosen targets from the primary screen, 89% had R-scores< 0, indicating high reproducibility. Coefficients of variation (CV), a measurement for intra-assay variability, for siNT SF_{7Gy}, across the library siRNA plates for the primary and secondary screen can be found within Table S2. Targets from the secondary screen were ordered by rank product. Targets ranked within the top 40 from the secondary screen (Table S3) were selected for further evaluation based on the following criteria: novelty in the context of radiosensitivity, differential expression in tumor cells compared to normal tissue based on Oncomine data [9], and availability of reagents for expanded study. One of these novel targets was TPK1, a key component of the thiamine metabolism pathway, which converts thiamine into active thiamine pyrophosphate. Other candidate genes identified in the screen are still being investigated.

TPK1 knockdown causes radiosensitization in tumor but not normal tissue cells

We confirmed that the identification of TPK1 was not due to off-target effects of the library siRNA by depleting TPK1 using two siRNAs from a third vendor. Knockdown of TPK1 using either of two Ambion Silencer Select siRNA strands radiosensitized HeLa cells in a standard colony-forming assay (Fig. 2A). The survival enhancement ratio at a surviving fraction of 0.10 (SER_{10}) for siTPK1-1 and siTPK1-2 was 1.33 and 1.30, respectively. TPK1 knockdown also caused significant radiosensitization in the highly radioresistant SQ20B head and neck tumor line (SER_{10} of 1.14; p <0.001) and the breast ductal carcinoma cell line BT-549 (SER_{10} of 1.19; p<0.001; Fig. 2A). In contrast, TPK1 knockdown did not radiosensitize the normal tissue lung fibroblast cell lines MRC5 and HFL-1 (Fig. 2B). Knockdowns were confirmed by immunoblotting (Fig. 2A, B, insets). Together these data suggest that TPK1 could represent a target for tumor specific radiosensitization.

Disruption of thiamine metabolism causes enhanced radiosensitization

Next we sought to establish whether depletion of other members of the thiamine metabolism pathway would also radiosensitize tumor cells. Knockdown of thiamine transporter 1 (THTR1), the main carrier transporting thiamine into the cells, radiosensitized HeLa cells to a similar degree as TPK1 knockdown (Fig. 3A). Double

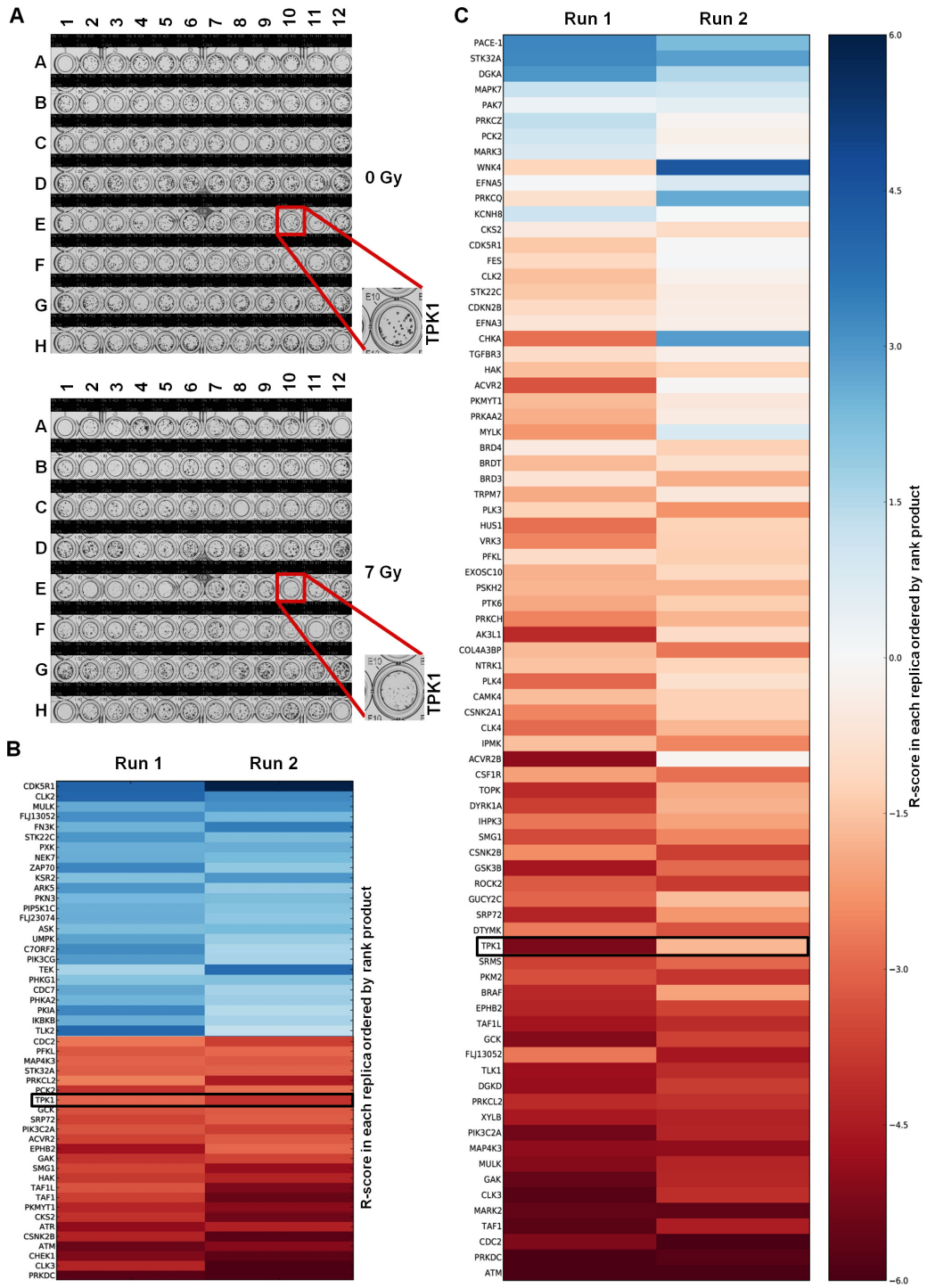

Figure 1: High-throughput colony formation screen identifies TPK1 as novel radiosensitizer. A) Crystal violet stained 96-well plates following 0 Gy and 7 Gy irradiation. The TPK1 siRNA containing well is indicated. Representative plates of quadruplicate repeats are shown. Plate layout can be found in Supplementary Figure S1. B) Heatmap of the R-scores of the primary screen of 709 Dharmacon Kinome ON-TARGET*plus* siRNA library. Screen was carried out twice and rank product scores were calculated based on R-score. Radiosensitizing siRNAs shown by R-scores <0. Top 25 lowest and highest ranked siRNAs are shown. siRNAs that reduced plating efficiency below 5% were excluded from analysis. C) Heatmap of secondary screen of the top 76 targets from primary screen using Dharmacon siGENOME siRNA. Screen was performed twice and ordered based on rank product.

knockdown of TPK1 and THTR1 together resulted in sensitization with an SER_{10} comparable to TPK1 and THTR1 knockdown alone, consistent with the same pathway being affected (Fig. 3A). In contrast, knockdown of mitochondrial pyrophosphate carrier (TPC) did not cause radiosensitization (Fig. 3B). Knockdown for all genes was confirmed by qRT-PCR (Fig. 3).

To test whether pharmacological inhibition of TPK1 had similar effects to TPK1 or THTR1 knockdown, we incubated cells with pyrithiamine hydrobromide, PyrH, a thiamine analogue which competes for the binding of thiamine to the active site of TPK1 [10]. As shown in Fig. 4A, HeLa cells pre-incubated with PyrH were significantly more sensitive to radiation (SER_{10}: 1.3, p<0.001) than untreated cells. A representative panel of cell lines derived from histological sites typically treated with radiotherapy was assembled and treated with PyrH. Figure 4A shows significant radiosensitization of CAL-51 breast carcinoma (SER_{10} of 1.76; p <0.001), H460 lung carcinoma (SER_{10} of 2.09; p <0.0001), HCT-116 colorectal carcinoma (SER_{10} of 1.64; p <0.00001), PSN-1 pancreatic adenocarcinoma (SER_{10} of 1.19; p <0.0001) and BT-549 breast carcinoma (SER_{10} of 1.24; p <0.0001). Similar to knockdown of TPK1, PyrH treatment did not radiosensitize normal tissue lung fibroblast cell lines HFL-1 and MRC5 (Fig. 4B). In addition, we demonstrated that significant radiosensitization could be achieved with clinically relevant doses following TPK1 and THTR1 knockdown or PyrH treatment using a fractionated irradiation regimen of 3 x 2 Gy (Fig. 5).

Together these results suggest that depleting cancer cells of thiamine pyrophosphate by silencing components

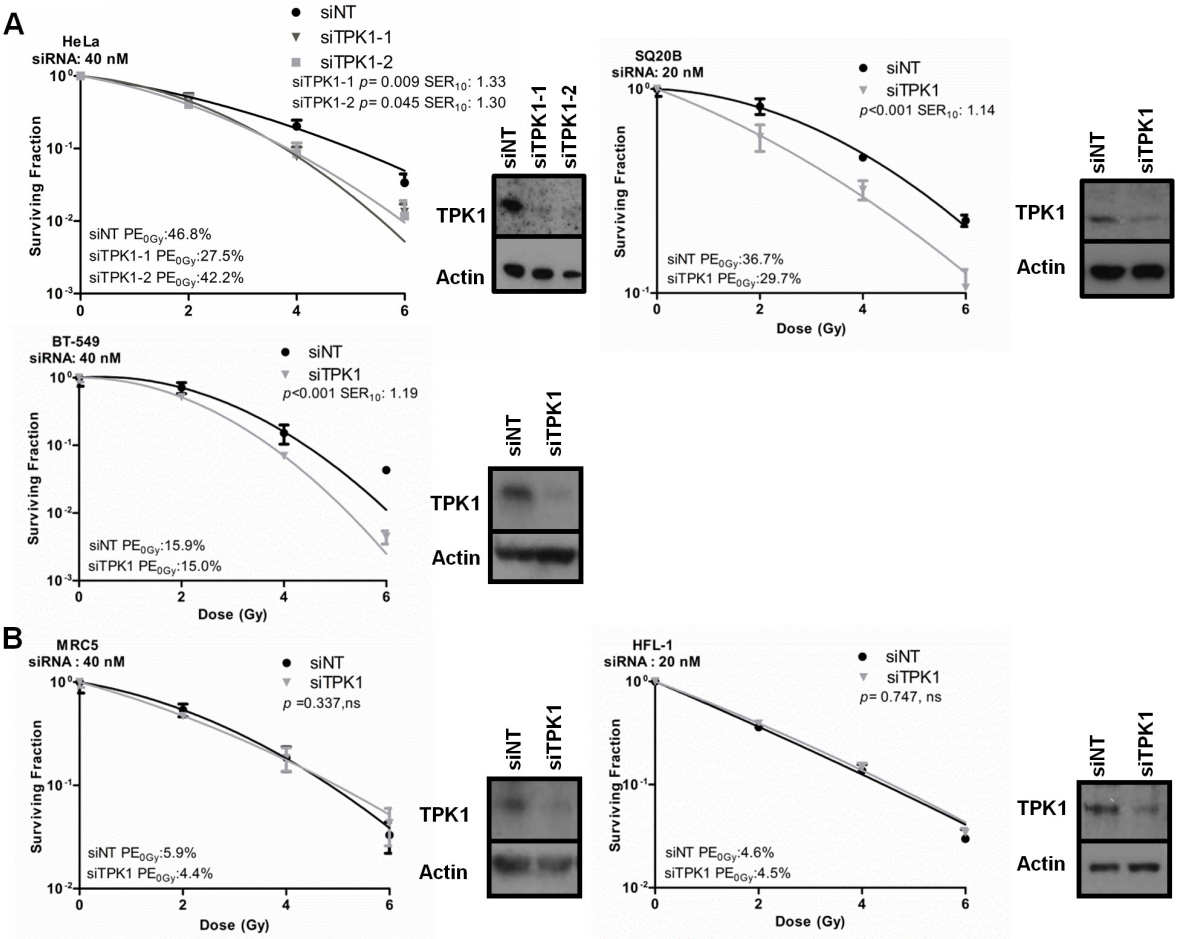

Figure 2: Validation of TPK1 as a target for tumor specific radiosensitization. A) CFA of tumor lines HeLa, SQ20B and BT-549 cells irradiated following Ambion siRNA transfection with non-targeting (siNT) and siTPK1. HeLa and BT-549 cells were transfected with 40 nM, SQ20B with 20 nM siRNA. HeLa cells were transfected with two different TPK1 siRNAs: TPK1-1 and siTPK1-2. Knockdown was confirmed by immunoblotting (insets). B) CFA of normal fibroblast HFL-1 and MRC5 cells irradiated following 20 nM (HFL-1) or 40 nM (MRC5) Ambion siRNA transfection with siNT and siTPK1. Knockdown was confirmed by immunoblotting (insets). CFA: representative of three independent experiments, data points presented as mean +/- SD from triplicate wells, p-values generated by factorial 2-way ANOVA. Sensitization enhancement ratio at 0.10 surviving fraction (SER_{10}) calculated from non-linear regression of linear quadratic model.

of the thiamine metabolism pathway or by inhibiting TPK1 causes radiosensitization.

Perturbation of thiamine metabolism results in persistence of DNA-damage foci

To investigate whether the increased radiosensitivity was due to alterations in DNA repair, we assessed the level of DNA damage foci after radiation. Knockdown of TPK1 and THTR1 in HeLa cells caused significant elevation in γ-H2AX and 53BP1 foci at 24 hrs post 6 Gy irradiation (Fig. 6A, B). Similarly, cells pretreated with PyrH prior to irradiation showed significantly more unresolved 53BP1 and γ-H2AX foci (Fig. 6A, C). Together these findings suggest that depleting cells of thiamine pyrophosphate inhibits their ability to repair DNA breaks.

As thiamine pyrophosphate is required as a cofactor for transketolase in the pentose-phosphate pathway for the production of ribulose-5-phosphate, utilized in the production of nucleotides, we tested whether cells treated with the thiamine analogue had reduced levels of cellular nucleotides. High performance liquid chromatography (HPLC) analysis confirmed that dATP, dCTP, dGTP and dTTP were all reduced in cells treated with PyrH (Fig. 6D).

DISCUSSION

To identify novel modulators of tumor radiosensitivity, we adapted the colony formation assay (CFA) for high-throughput screening. Although the adaptation of the CFA for screening purposes has been trialed by others [11, 12] , this report is the first to use CFA for a siRNA screen, which led to the identification of TPK1 as a potential radiosensitization target. We showed that TPK1 knockdown caused radiosensitization in tumor but not normal cells. The finding that tumor cells have a greater dependency on TPK1 for survival following irradiation may reflect their altered metabolism or increased levels of replicative stress.

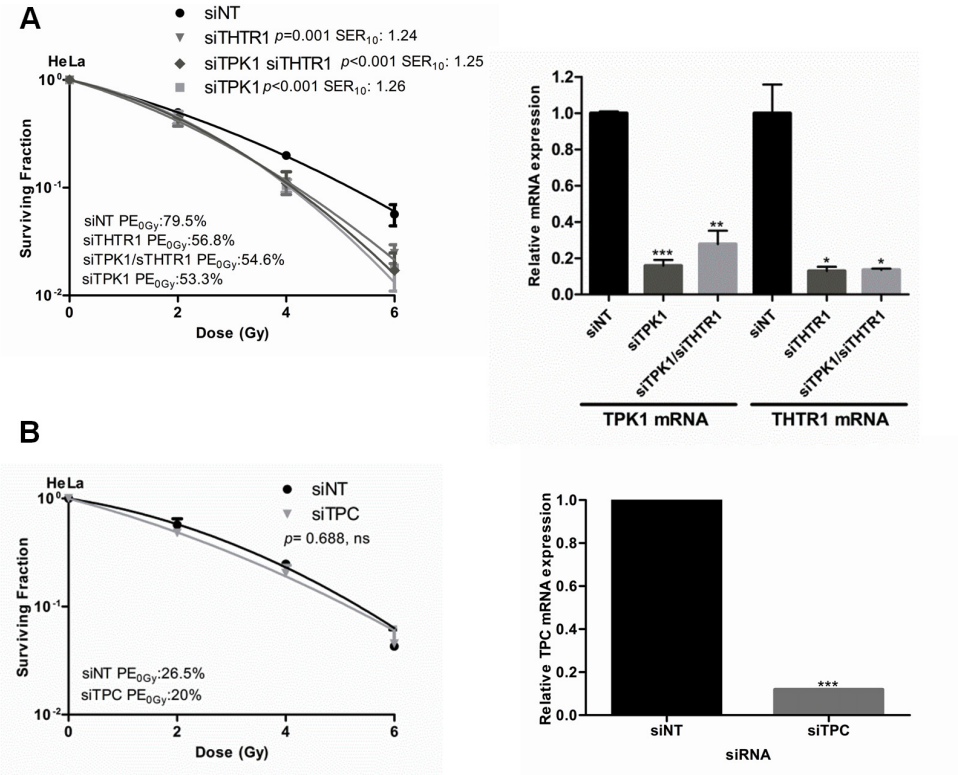

Figure 3: Thiamine metabolism pathway components evaluated for radiosensitization. A) CFA of HeLa cells irradiated following 40 nM Ambion siRNA transfection with siNT, siTPK1, siTHTR1 and siTHTR1/siTPK1. Knockdown confirmed by qRT-PCR (inset) B) CFA of HeLa cells irradiated following 20 nM Ambion siRNA transfection with siNT and siTPC. siTPC knockdown confirmed by qRT-PCR (inset). Representative of three independent experiments, data points presented as mean +/- SD from triplicate wells, *p*-values generated by factorial 2-way ANOVA. Sensitization enhancement ratio at 0.10 surviving fraction (SER_{10}) calculated from non-linear regression of linear quadratic model. qRT-PCR: Unpaired two-sided students t-test comparing siNT to candidate knockdown t-tests*p<0.05, **p<0.01, ***p<0.001.

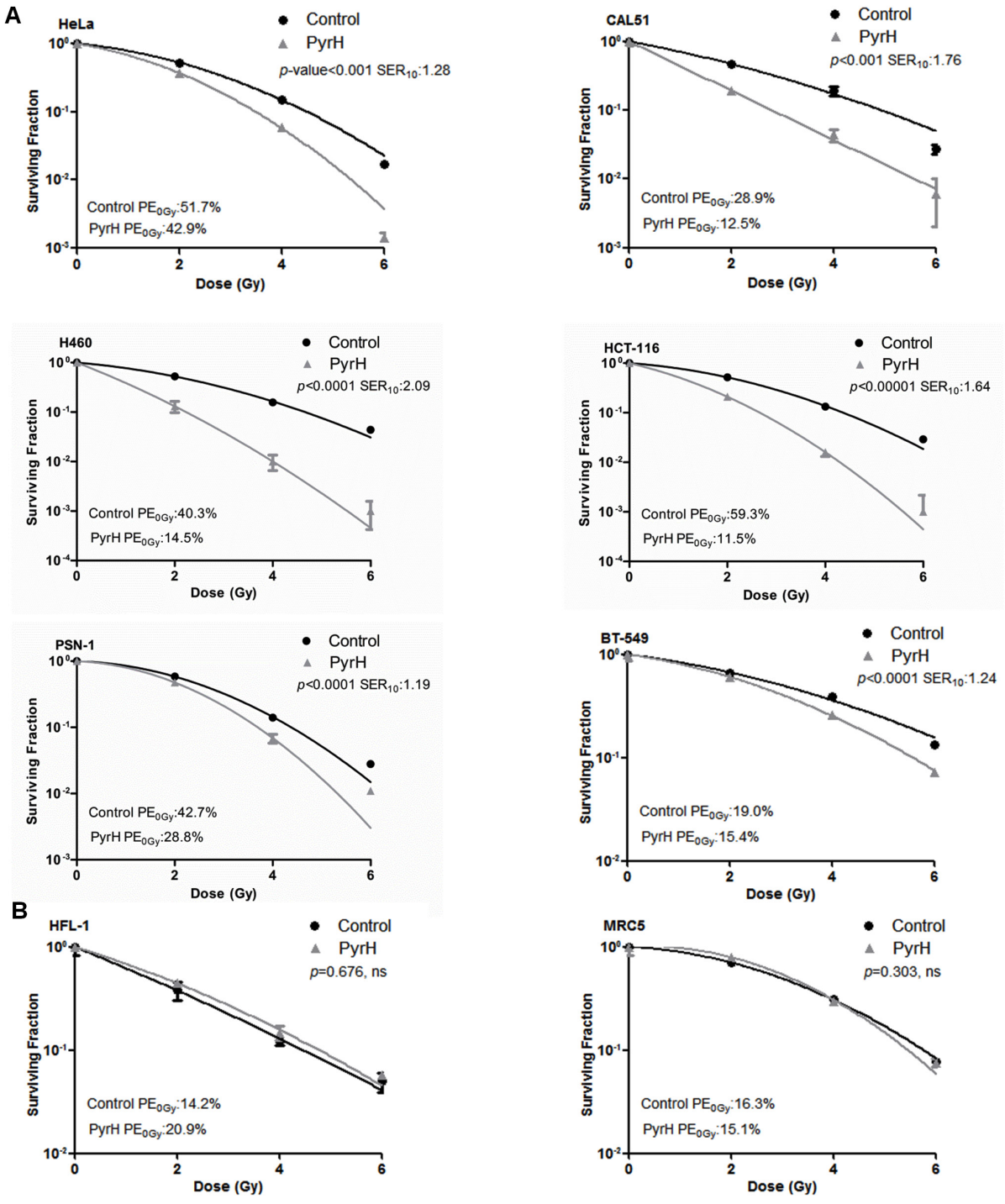

Figure 4: Thiamine metabolism is a key determinant of tumor specific radiosensitivity. A) Colony formation of the tumor lines HeLa, CAL51, H460, HCT-116, PSN-1 and BT-549 cells irradiated after 4 days incubation with DMSO (control) or 10 μM PyrH. B) Colony formation of normal lung fibroblasts lines HFL-1 and MRC5 cells irradiated after 4 days incubation with DMSO (control) or 10 μM PyrH. CFA: representative of three independent experiments, data points presented as mean +/- SD from triplicate wells, *p*-values generated by factorial 2-way ANOVA. Sensitization enhancement ratio at 0.10 surviving fraction (SER_{10}) calculated from non-linear regression of linear quadratic model.

Radiosensitivity of TPK1 knockdown is linked to the pentose-phosphate pathway

Thiamine is transported into the cell by the proteins encoded by SLC-19 family of transporters, SLC19A2/THTR1 and SLC19A3/THTR2 [13, 14]. TPK1 subsequently converts thiamine into its active form thiamine pyrophosphate (TPP), which can then be transported into the mitochondria by TPC and used as co-factor for the citric acid cycle enzymes branched chain α-ketogluturate dehydrogenase and pyruvate dehydrogenase complex [14, 15]. TPP is also a co-factor for the transketolase enzyme required for the production of ribose-5 phosphate (R5-P) in the non-oxidative arm of the pentose phosphate pathway.

TPK1, SLC19A2/THTR1 and SLC25A19/TPC have been shown to be up-regulated in breast cancer in both patients and cell lines [16]. Unlike TPK1 and THTR1 knockdown, TPC knockdown did not cause an increase in radiosensitivity (Fig. 3B), suggesting that TPK1 depletion-induced radiosensitivity is primarily brought about through the activity of TPP in the pentose phosphate pathway. Since the non-oxidative arm of this pathway is used to produce the backbone of nucleotides, R-5P [17], it could be postulated that inhibition of thiamine metabolism would result in reduction in the nucleotide pools. This was indeed found to occur when cells were treated with PyrH (Fig. 6D). This model fits with observations that inhibition of the transketolase enzyme by oxythiamine caused a reduction in R-5P, nucleotide acid synthesis and a subsequent tumor proliferation delay [18, 19].

The radiosensitization seen with PyrH treatment, TPK1 and THTR1 knockdown was accompanied by a persistence of double-strand break foci after irradiation (Fig. 6A, B, C). THTR1 knockdown was associated with a greater number of residual 53BP1 and γ-H2AX foci compared to siTPK1, but interestingly this did not translate in increased radiosensitization, which was similar for TPK1 and THTR1 knockdown (Fig. 3A). These observations could be explained by different effects on DNA repair kinetics or additional unknown roles for thiamine metabolism that contribute to tumor radioresistance.

It could be hypothesized that the increased unresolved DNA-damage breaks seen after thiamine metabolism inhibition may occur due to the low levels of nucleotides reducing the efficiency of DNA-repair leading to increased radiosensitivity. A model of radiosensitization by inhibition of thiamine metabolism has been depicted in Supplementary Figure S3.

The finding that TPK1 depletion or inhibition caused radiosensitization in tumor but not normal tissue cells suggests that inhibiting TPK1 may be a potentially useful clinical strategy to cause tumor-specific radiosensitization. The main obstacle to such an approach lies in the complications associated with thiamine deprivation. The most common clinical manifestation of thiamine deficiency is Wernicke's encephalopathy, which results from long-standing, severe alcohol abuse and can be promptly reversed by administration of parenteral thiamine [20]. Individuals with autosomal mutations in the TPK1 gene exhibit features of dystonia, lactic acidosis and retardation symptoms, typically after age one [21].

Long-term thiamine depletion is thus not a viable clinical option. However, conventional radiotherapy is typically delivered over a duration of several weeks, stereotactic ablative body radiotherapy over a period of

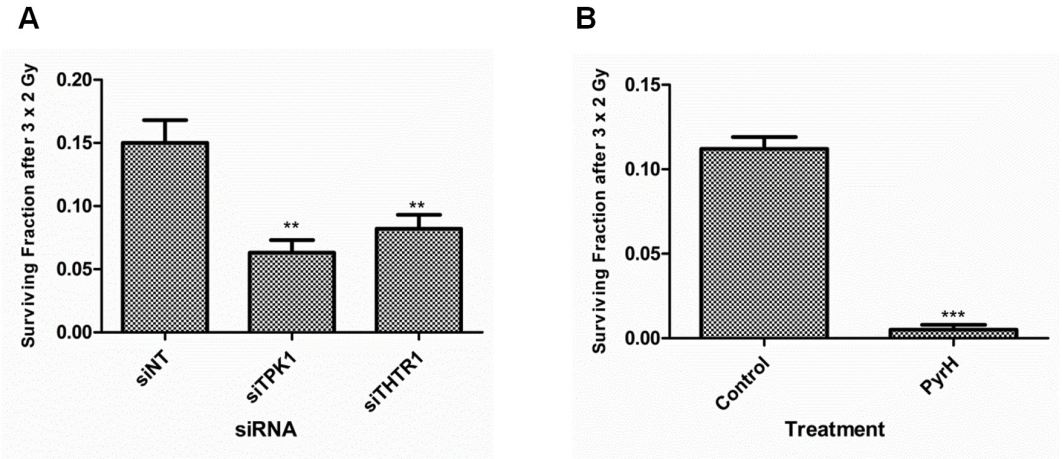

Figure 5: Fractionated irradiation treatment radiosensitizes HeLa cells after thiamine metabolism disruption. A) Colony formation of HeLa cells irradiated with three single doses of 2 Gy provided on 3 consecutive days after 48 hrs transfection with 40 nM Ambion siRNA for siNT, siTPK1 and siTHTR1. B) Colony formation of HeLa cells irradiated with a three single doses of 2 Gy given on 3 consecutive days initiated after 72 hrs of incubation with DMSO (control) or 10 μM PyrH. Colony formation assay: representative of three independent experiments, data points presented as mean +/- SD from triplicate wells. Unpaired two-sided students t-tests comparing siNT/ control to candidate knockdown/treatment $^{**}p<0.01$, $^{***}p<0.001$.

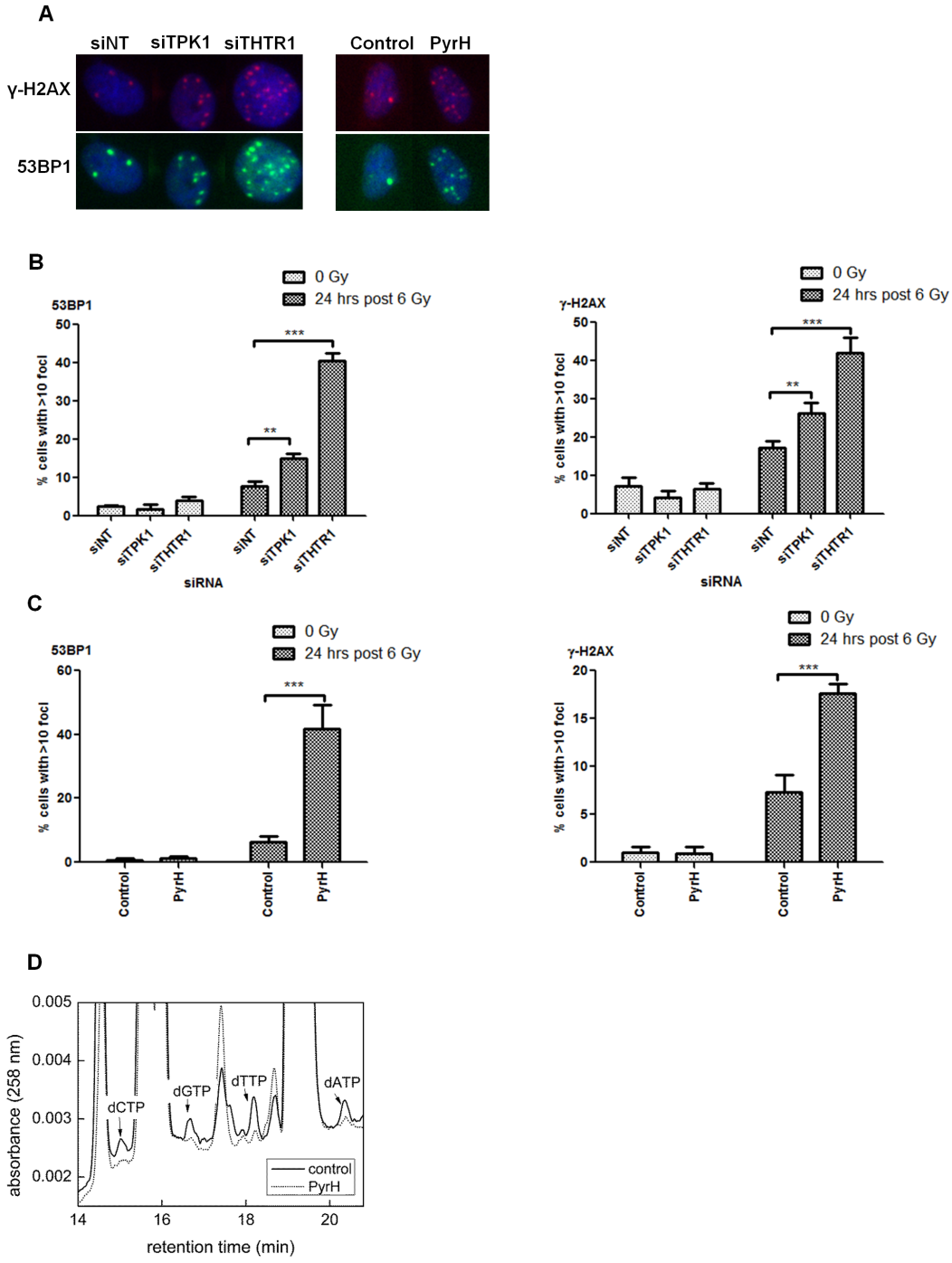

Figure 6: Perturbation of thiamine metabolism results in persistent DNA-damage and reduced nucleotide pools. A) HeLa cells were irradiated following transfection with 40 nM Ambion siRNA (siNT, siTPK1 and siTHTR1), or treatment with either DMSO (control) or 10 μM PyrH. Cells were fixed 24 hrs post-irradiation and probed for γ-H2AX (red), 53BP1 (green) and nuclei (blue). Representative images of irradiated cells treated and stained as indicated are shown. B) Quantification of DNA damage foci in HeLa cells irradiated after siRNA transfection as indicated, counting a minimum of 500 cells per well. Representative experiment of n=3 is shown, data represented as mean +/- SD from triplicate wells. Unpaired two-sided students t-tests comparing siNT to candidate knockdown $^{**}p<0.01$, $^{***}p<0.001$. C) Quantification of DNA damage foci in HeLa cells irradiated after 4 days incubation with DMSO (control) or 10 μM PyrH. Cells stained and quantified as described in B. D) High performance liquid chromatography of HeLa cells incubated with or without PyrH for 4 days. Representative of n=3.

days and brachytherapy over a few hours. It is therefore possible that temporary inhibition of thiamine metabolism may improve the efficacy of radiotherapy before clinical symptoms of thiamine deficiency become apparent. Such a rationale is similar to the use of the folic acid antagonist methotrexate in acute lymphocytic leukemia and osteosarcoma [22], which is administered at high-doses that might otherwise be fatal but this outcome is avoided by reversal with folinic acid before folic acid deficiency results in clinically apparent symptoms. Future work will require the validation of our findings *in vivo*. The use of compounds such as oxythiamine, a competitive analogue of thiamine that unlike PyrH does not cross the blood brain barrier [23], may circumvent the neurotoxicity associated with thiamine depletion.

By developing a high-throughput assay suitable for siRNA and compound screening, our study has shown that thiamine metabolism modulates radiosensitivity and provides a rationale for TPK1 inhibition as a novel clinical target for tumor specific radiosensitization.

MATERIALS AND METHODS

Cell culture

HeLa, BT-549, CAL-51, H460, HCT-116, PSN-1, MRC5 and HFL-1 cells were purchased from American Type Culture Collection (ATCC). SQ20B cells were kindly provided by Dr. Ralph Weichselbaum (University of Chicago). HeLa, SQ20B, BT-549, HCT-116 and PSN-1 were maintained in Dulbecco's modified Eagle's medium (DMEM), MRC5 in MEM and HFL-1 in F-12 Hams media. All media (Sigma) were supplemented with 10% FBS. All cell lines were tested for mycoplasma using MycoAlert (Lonza). Cell lines were never grown beyond four months after purchase. The HeLa cell line, which had been cultured for a longer period, was authenticated by LGC standards (ATCC) by short tandem repeat (STR) profiling. The SQ20B cell line was authenticated by DNA sequencing methods and has not varied over time.

High-throughput colony forming assay siRNA screen

ON-TARGET*plus* (Dharmacon) siRNA library containing 709 siRNA pools (4 strands per gene) was utilized in the 96-well CFA screen. Non-targeting siRNA (siNT) and DNA-PK*cs* (PRKDC) siRNA were used as negative and positive controls (plate layout is shown in Supplementary Figure S1). HeLa cells were reverse transfected with library siRNA at 20 nMol/L final concentration using Dharmafect1 (Dharmacon) transfection reagent. 72-hours post-transfection, cells were lifted, diluted and plated into two sets of quadruplicate repeat 96-well plates. Approximately 192 cells were plated in 0 Gy (untreated) plates and 1600 cells were transferred to plates treated with 7 Gy irradiation. Cells were left for 4-hours at 37°C (5% CO_2) and treatment plates (one quadruplicate repeat set) were irradiated as described below. Plates were stained with crystal violet at 6 days (untreated) or 8 days (irradiated) post-irradiation and counted using GelCount colony counter (Oxford Optronix).

Following rank product analysis of two separate runs of the kinome library (see below), the top-76 targets were chosen for secondary screening using a siRNA library of siGENOME siRNA (Dharmacon), and this secondary library was screened on two separate occasions using identical methods.

Screening statistical analyses

Plates were analyzed by calculating the plating efficiency (PE) for treated and untreated wells: *PE = Average Colony Number / Cells plated*. . siRNAs that had $PE_{0\ Gy} < 0.05$ were removed from further analyses. Surviving fractions (SF) for the remaining genes were calculated using the formula: $SF = (PE)_{0\ Gy} / (PE)_{7\ Gy}$. Surviving fractions were normalized to the average non-targeting (NT) SF for each plate of the library. A radiosensitization R-score was calculated on the normalized SF: *R-score = (Normalized SF – 1) / (Mean absolute deviation of normalized NT SF)*. Targets were ranked in ascending order based on R-score. Rank product analysis was carried out between replicate runs for both the primary and secondary screen [24]. The percentage of false prediction (PFP), equivalent to the false discovery rate, was estimated using the *rankprod* package in R (http://www.cran.org). The PFP estimate is based on permutation (N=100). The quality of the screening method determined by the dynamic range between the positive and negative control siRNAs, taking into account the reproducibility between replicates was determined by Z-factor calculation [25]. Z-factors were calculated based on normalized SF using the formula:

$$Z - Factor = 1 - \frac{3(\sigma_{NT_{SF}} + \sigma_{DNA-PKcs_{SF}})}{\left|\mu_{NT_{SF}} - \mu_{DNA-PKcs_{SF}}\right|}$$

siRNA transfections

Validation studies used a reverse transfection protocol for siRNA at a final concentration of 20 or 40 nMol/L Ambion Silencer Select siRNA (Life Technologies) and INTERFERin-HTS (Polyplus) transfection reagent concentrations optimized for each cell line. Cells were re-plated for clonogenic assays, immunofluorescence and knockdown confirmation by Western blotting or qRT-PCR at 72-hours post-

transfection.

siRNA sequences

Sense strand sequence for Ambion siRNA: TPK1 (TPK1-1): GGAGACUUUGAUUCUAUUA, (TPK1-2) GCCUUUGGACAACUAUUUU, THTR1: GCCUUAUUGUUACAUGGUU, and TPC: GACCAUGUAUAGGAGCGAA.

Thiamine analogue treatment

Cells were incubated for four days in 10 μM pyrithiamine hydrobromide (Sigma) in low thiamine medium (M199; Sigma) prior to irradiation. Six hours after irradiation, the medium was changed to DMEM and cells were plated for colony forming assays or immunofluorescence described below.

6-well colony formation assay

Inhibitor-treated or siRNA transfected cells were plated as single cell suspensions and left for 4-hours at 37°C (5% CO_2) prior to irradiation. Colonies were grown for 7-14 days and stained with crystal violet.

Effects of treatment on the dose survival curves were estimated using two approaches

A) Survival data was fitted using non-linear regression with the linear quadratic equation $S = \exp^{-(\alpha D+\beta D^2)}$; S denotes survival probability, D (Gy) is radiation dose and α (Gy^{-1}) and β (Gy^{-2}) are parameter constants. An indicator variable was introduced to specify targeting and non-targeting condition as described previously [26]. The sensitization enhancement ratio at a surviving fraction of 0.10 (SER_{10}) was calculated: $SER_{10} : D_{untreated} / D_{treated}$, where $D_{untreated}$ and $D_{treated}$ yield 10% survival as calculated using α (Gy^{-1}) and β (Gy^{-2}) parameters.

B) A factorial 2-way ANOVA was performed with survival as the dependent variable and dose levels (2, 4 and 6 Gy) and treatment (control, siRNA) as the two factors; interaction between dose and treatment was estimated.

Irradiation

A. 96-well plate irradiation

Plates were irradiated in batches of 24 after being placed in a 2 cm thick tissue-equivalent Plexiglas phantom and irradiated with 6MV photons using a Varian IX linear accelerator at gantry angles 0 and 180 degrees to a total dose of 7Gy. Cross-sectional film dosimetry tests confirmed the accuracy of this technique.

B. 6-well plate irradiation

Plates were irradiated at 2, 4 and 6 Gy using caesium -137 irradiator, Gamma Service: GSR D1; dose rate 1.938 Gy $min^{-}1$.

Immunoblotting

Protein lysates were prepared using RIPA lysis buffer (Thermo Scientific). Following SDS-PAGE electrophoresis and subsequent immunoblotting, bound TPK1 antibody (ProteinTech, #10942-1-AP) was detected by developing film from nitrocellulose membrane exposed to chemiluminescence reagent (SuperSignal, Millipore).

Quantitative real-time PCR (qRT-PCR)

Total RNA was extracted using GenElute kit (Sigma) and cDNA was prepared using the Affinity script cDNA synthesis kit followed by qPCR using Brilliant II SYBR Green (Agilent Technologies) and a MX3005P qPCR machine (Agilent Technologies). All amplifications were as follows: 95°C for 30 s, 58°C for 30 s, and 72°C for 60 s for 40 cycles. Primer sequences were designed using NCBI Primer-BLAST/Primer3 software and always spanned exon-exon junctions. Primer forward (F) and reverse(R) sequences 5' to 3' were: GAPDH-F:CCGCATCTTCTTTTGCGTCGC, GAPDH-R: AAATGAGCCCCAGCCTTCTCCATG, TPK1-F: TCGTGACACTGGGAGGCCTTG, TPK1-R: ACCTGTGCTTTCCTGGTTGGAGC, THTR1-F: ACCGAGAGGGAGGTCTTCAA, THTR1-R: AGCCCCTGCAGTAGAACAAC, TPC-F: GGAGCTAGAGAGAGCGGAGA and TPC-R: CATCAGTATCAAGATACGGTCTGT. Ct values were converted into relative copy number and normalized to GAPDH control.

Immunofluorescence

siRNA-transfected or thiamine analogue-treated HeLa cells were re-plated in 96-well plates, left for 4 hrs at 37°C (5% CO_2) to adhere and treated with 6 Gy irradiation. Plates were left for 24 hrs post-irradiation and fixed. Cells were probed with anti-γ-H2AX ser 139 (Upstate/Millipore, #05-636) and 53BP1 (Cell Signaling Technology, #4937S) antibodies as described before [8] and foci counted using IN Cell Analyzer (GE).

High performance liquid chromatography

PyrH treated cells were lifted and lysed in 6% TCA. Deoxynucleotide triphosphates (dNTPs) were extracted from diluted samples containing 2.6% TCA as described

previously [27].

ACKNOWLEDGEMENTS

G.S.Higgins is supported by a Cancer Research UK Clinician Scientist Award (Grant number C34326/A13092). Additional support was provided by grants from Cancer Research UK, the Medical Research Council and the National Institute for Health Research Biomedical Research Centre, Oxford.

CONFLICT OF INTEREST

There are no conflicts of interest.

REFERENCES

1. Ito E, Yue SJ, Moriyama EH, Hui AB, Kim I, Shi W, Alajez NM, Bhogal N, Li GH, Datti A, Schimmer AD, Wilson BC, Liu PP, Durocher D, Neel BG, O'Sullivan B, et al. Uroporphyrinogen Decarboxylase Is a Radiosensitizing Target for Head and Neck Cancer. Sci Transl Med. 2011; 3(67).
2. Zheng M, Morgan-Lappe SE, Yang J, Bockbrader KM, Pamarthy D, Thomas D, Fesik SW and Sun Y. Growth inhibition and radiosensitization of glioblastoma and lung cancer cells by small interfering RNA silencing of tumor necrosis factor receptor-associated factor. Cancer research. 2008; 68(18):7570-7578.
3. Lally BE, Geiger GA, Kridel S, Arcury-Quandt AE, Robbins NE, Kock ND, Wheeler K, Peddi P, Georgakilas A, Kao GD and Koumenis C. Identification and biological evaluation of a novel and potent small molecule radiation sensitizer via an unbiased screen of a chemical library. Cancer research. 2007; 67(18):8791-8799.
4. McGowan EM, Alling N, Jackson EA, Yagoub D, Haass NK, Allen JD and Martinello-Wilks R. Evaluation of Cell Cycle Arrest in Estrogen Responsive MCF-7 Breast Cancer Cells: Pitfalls of the MTS Assay. Plos One. 2011; 6(6).
5. Bjork-Eriksson T, West CML, Cvetskovska E, Svensson M, Karlsson E, Magnusson B, Slevin NJ, Edstrom S and Mercke C. The lack of correlation between proliferation (Ki-67, PCNA, LI, Tpot), p53 expression and radiosensitivity for head and neck cancers. Brit J Cancer. 1999; 80(9):1400-1404.
6. Price P and McMillan TJ. Use of the tetrazolium assay in measuring the response of human tumor cells to ionizing radiation. Cancer research. 1990; 50(5):1392-1396.
7. Pauwels B, Korst AEC, de Pooter CMJ, Pattyn GGO, Lambrechts HAJ, Baay MFD, Lardon F and Vermorken JB. Comparison of the sulforhodamine B assay and the clonogenic assay for *in vitro* chemoradiation studies. Cancer Chemoth Pharm. 2003; 51(3):221-226.
8. Higgins GS, Prevo R, Lee YF, Helleday T, Muschel RJ, Taylor S, Yoshimura M, Hickson ID, Bernhard EJ and McKenna WG. A small interfering RNA screen of genes involved in DNA repair identifies tumor-specific radiosensitization by POLQ knockdown. Cancer research. 2010; 70(7):2984-2993.
9. Rhodes DR, Kalyana-Sundaram S, Mahavisno V, Varambally R, Yu J, Briggs BB, Barrette TR, Anstet MJ, Kincead-Beal C, Kulkarni P, Varambally S, Ghosh D and Chinnaiyan AM. Oncomine 3.0: genes, pathways, and networks in a collection of 18,000 cancer gene expression profiles. Neoplasia. 2007; 9(2):166-180.
10. Liu JY, Timm DE and Hurley TD. Pyrithiamine as a substrate for thiamine pyrophosphokinase. J Biol Chem. 2006; 281(10):6601-6607.
11. Lin SH, Zhang J, Giri U, Stephan C, Sobieski M, Zhong L, Mason KA, Molkentine J, Thames HD, Yoo SS and Heymach JV. A High Content Clonogenic Survival Drug Screen Identifies MEK Inhibitors as Potent Radiation Sensitizers for KRAS Mutant Non-Small-Cell Lung Cancer. Journal of Thoracic Oncology. 2014; 9(7):965-973.
12. Katz D, Ito E, Lau KS, Mocanu JD, Bastianutto C, Schimmer AD and Liu FF. Increased efficiency for performing colony formation assays in 96-well plates: novel applications to combination therapies and high-throughput screening. Biotechniques. 2008; 44(2):ix-xiv.
13. Ganapathy V, Smith SB and Prasad PD. SLC19: the folate/thiamine transporter family. Pflugers Archiv : European journal of physiology. 2004; 447(5):641-646.
14. Hawkins CF, Borges A and Perham RN. A common structural motif in thiamin pyrophosphate-binding enzymes. FEBS letters. 1989; 255(1):77-82.
15. Danner DJ, Wheeler FB, Lemmon SK and Elsas LJ, 2nd. *In vivo* and *in vitro* response of human branched chain alpha-ketoacid dehydrogenase to thiamine and thiamine pyrophosphate. Pediatric research. 1978; 12(3):235-238.
16. Zastre JA, Hanberry BS, Sweet RL, McGinnis AC, Venuti KR, Bartlett MG and Govindarajan R. Up-regulation of vitamin B1 homeostasis genes in breast cancer. The Journal of nutritional biochemistry. 2013; 24(9):1616-1624.
17. Usmanov RA, Neef H, Pustynnikov MG, Schellenberger A and Kochetov GA. The effect of thiamine pyrophosphate modification on its coenzyme function in a transketolase-catalyzed reaction. Biochemistry international. 1985; 10(3):479-486.
18. Boros LG, Puigjaner J, Cascante M, Lee WN, Brandes JL, Bassilian S, Yusuf FI, Williams RD, Muscarella P, Melvin WS and Schirmer WJ. Oxythiamine and dehydroepiandrosterone inhibit the nonoxidative synthesis of ribose and tumor cell proliferation. Cancer research. 1997; 57(19):4242-4248.
19. Rais B, Comin B, Puigjaner J, Brandes JL, Creppy E, Saboureau D, Ennamany R, Lee WN, Boros LG and Cascante M. Oxythiamine and dehydroepiandrosterone induce a G1 phase cycle arrest in Ehrlich's tumor cells

through inhibition of the pentose cycle. FEBS letters. 1999; 456(1):113-118.

20. Blass JP and Gibson GE. Abnormality of a thiamine-requiring enzyme in patients with Wernicke-Korsakoff syndrome. The New England journal of medicine. 1977; 297(25):1367-1370.
21. Mayr JA, Freisinger P, Schlachter K, Rolinski B, Zimmermann FA, Scheffner T, Haack TB, Koch J, Ahting U, Prokisch H and Sperl W. Thiamine pyrophosphokinase deficiency in encephalopathic children with defects in the pyruvate oxidation pathway. American journal of human genetics. 2011; 89(6):806-812.
22. Cohen IJ and Wolff JE. How Long Can Folinic Acid Rescue Be Delayed After High-Dose Methotrexate Without Toxicity? Pediatr Blood Cancer. 2014; 61(1):7-10.
23. Greenwood J and Pratt OE. Comparison of the effects of some thiamine analogues upon thiamine transport across the blood-brain barrier of the rat. The Journal of physiology. 1985; 369:79-91.
24. Birmingham A, Selfors LM, Forster T, Wrobel D, Kennedy CJ, Shanks E, Santoyo-Lopez J, Dunican DJ, Long A, Kelleher D, Smith Q, Beijersbergen RL, Ghazal P and Shamu CE. Statistical methods for analysis of high-throughput RNA interference screens. Nature methods. 2009; 6(8):569-575.
25. Zhang JH, Chung TD and Oldenburg KR. A Simple Statistical Parameter for Use in Evaluation and Validation of High Throughput Screening Assays. J Biomol Screen. 1999; 4(2):67-73.
26. Chalmers AJ, Bentzen SM and Buffa FM. A general framework for quantifying the effects of DNA repair inhibitors on radiation sensitivity as a function of dose. Theor Biol Med Model. 2007; 4.
27. Moss J, Tinline-Purvis H, Walker CA, Folkes LK, Stratford MR, Hayles J, Hoe KL, Kim DU, Park HO, Kearsey SE, Fleck O, Holmberg C, Nielsen O and Humphrey TC. Break-induced ATR and Ddb1-Cul4(Cdt2) ubiquitin ligase-dependent nucleotide synthesis promotes homologous recombination repair in fission yeast. Gene Dev. 2010; 24(23):2705-2716.